AN UNCERTAINTY QUANTIFICATION AND MANAGEMENT METHODOLOGY TO SUPPORT REWORK DECISIONS IN MULTIFIDELITY AEROELASTIC LOAD CYCLES

A Thesis
Presented to
The Academic Faculty

by

Brandon J. Johnson

In Partial Fulfillment
of the Requirements for the Degree
Doctor of Philosophy in the
School of Aerospace Engineering

Georgia Institute of Technology
May 2017

AN UNCERTAINTY QUANTIFICATION AND MANAGEMENT METHODOLOGY TO SUPPORT REWORK DECISIONS IN MULTIFIDELITY AEROELASTIC LOAD CYCLES

Approved by:

Professor Dimitri Mavris, Advisor
School of Aerospace Engineering
Georgia Institute of Technology

Professor Stephen Ruffin
School of Aerospace Engineering
Georgia Institute of Technology

Professor Daniel Schrage
School of Aerospace Engineering
Georgia Institute of Technology

Dr. Frode Engelsen
Boeing Research & Technology
The Boeing Company

Dr. Neil Weston
School of Aerospace Engineering
Georgia Institute of Technology

Date Approved: March 27, 2017

To my parents,

thank you for your love, support, and inspiration.

ACKNOWLEDGEMENTS

First I would like to thank my advisor, Professor Dimitri Mavris, for being such a great advocate for me from the very beginning of when I started in the Aerospace Systems Design Laboratory (ASDL) and all the way until the very end. I would not have been able to complete this without his support and belief in me.

I would to thank all of my thesis committee for all their guidance. In particular, I must thank Dr. Frode Engelsen for his tireless effort in helping me develop and refine this thesis topic. Dr. Engelsen was always honest and fair and continued to push me to achieve engineering excellence. He has been a wonderful teacher during this project.

I also must thank Dr. Zhimin Liu from ASDL for his advice and continued support throughout the entire process. Sharing his own experiences in graduate school was invaluable to me. I would like to acknowledge the instrumental and timely help of Matt Bopp from the Aerothermodynamics Research and Technology (ART) Laboratory with the CFD analysis in this work. I would also like to thank the Boeing Company along with the National Science Foundation and Sloan Foundation for their support of me and this research.

Finally, above all I must thank my parents, Drs. Anthony and Adrienne Johnson, whom this dissertation is dedicated to. They paved the way and provided the best example possible for me to strive to complete my own doctorate. I only hope I can achieve the success they have, both professionally and in life.

TABLE OF CONTENTS

LIST OF TABLES

LIST OF FIGURES

SUMMARY

Cost overruns and schedule delays have plagued almost all major aerospace development programs and have resulted in billions of dollars lost. Design rework has attributed to these problems and one approach to mitigating this risk is reducing uncertainty. Failing to meet requirements during flight test results in one of the most significant and costly rework efforts. This type of rework is referred to as *major* rework and the main purpose of this thesis is to reduce this risk by improving the loads analysis process.

Loads analysis is a crucial part of the design process for aerospace vehicles. Its main objective is to determine the worst-case loading conditions which will realistically be experienced in normal and abnormal flight operations. These conditions are called critical loads. With this information, a structure is designed and optimized to withstand such loads and certify the design. Observing the current approach to loads analysis has revealed some shortcomings related to uncertainty and the allocation of load and structural margins. The fields of uncertainty quantification and uncertainty management were chosen to address these limitations and a framework was proposed to support decisions for rework in loads analysis.

Key aspects of the framework include utilizing a Bayesian network for modeling the loads process as well as propagating various uncertainty sources to the system response. Bayesian-based resource allocation optimization is another key aspect and used to reduce and manage uncertainty. Finally, the goal of the framework is to determine the optimal tradeoffs between aerodynamic fidelity and margin allocation to minimize the risk of major rework while considering their respective costs under a

finite budget. Assigning costs related to fidelity and margins are intended to reflect the users' prioritization of uncertainty, computational cost and performance degradation through weight penalties.

The demonstration model is the undeformed Common Research Model (uCRM) wing, which is representative of a transonic wide-body commercial transport. The modeling and simulation environment is multidisciplinary and anchored in three software programs to perform various analyses: NASCART-GT for computational fluid dynamics; NASTRAN for doublet-lattice method aerodynamics, structural analysis and aeroelastic analysis; and HyperSizer for failure analysis and structural optimization.

Four experiments were conducted related to epistemic uncertainty quantification, uncertainty propagation and sensitivity analysis via Bayesian network, developing an uncertainty management system based on resource allocation for loads analysis and finally experiments to optimize and evaluate the overall framework against seven design scenarios to explore a potential decision makers' varying priorities and against a baseline model representing the current approach. Key findings reveal the structural required margins are the dominant factor in reducing the risk of rework but the aerodynamic fidelity and load margin are important for balancing performance and uncertainty when considering financial implications within a finite budget.

The contributions of this thesis to the aerospace engineering community include; an integrated modeling and simulation environment for the load analysis process and structural design, uniquely applying and developing a Bayesian network for efficient uncertainty modeling and propagation and a viable cost-based uncertainty management system for loads analysis, among others.

CHAPTER I

MOTIVATION

1.1 Introduction

The commercial airline market is poised to double in size over the next three decades in terms of number of aircraft in service [33]. This growth is met by many challenges for the relatively few companies in this market to gain a competitive advantage. Analyst from Strategy& (Formerly Booz & Company)[47] four major challenges for the industry: increasing production rates, growing demand for more efficient aircraft, digitization of the industry and unsustainable development cost and value distribution. When looking at the airplane lifecycle, all of these challenges can be addressed in part by the design process within the development phase. The last challenge may be the most pressing and is evident in new development programs being notoriously long, expensive and riddled with uncertainties which poses substantial risks to the manfacturer and the customer. For example, the average cost for recent large commercial wide-body aircraft development is more than US $19 billion and has made new development programs nearly a "bet-the-company" move [47]. Program delays can result in billions of dollars from factors such as rework, disruptions in supply chain and production, and compensation to airline customers, to name a few. When these risks are associated with the design, this is referred to as design risk.

To meet the market challenges, design risk must be systematically reduced. Design risk is at its highest during flight and ground tests conducted on full-scale test articles which serve to validate the design. Failing to meet the requirements of these tests can be catastrophic because of the money invested in the test articles and the need to fix the design and repeat the test programs. Thus flight and ground test failures

can lead to profit loss, delays, damaged reputation and significant redesign. From an engineering perspective the redesign, i.e. rework, is the most important and the focus of this work.

An effective design process will, as much as possible, get it right the first time and minimize excess time and resources to fix a design after failure. Rework is more damaging, in terms of costs and schedule disruption, the later it occurs in a development program. Improving the design process is no easy feat given the size and complexity of aircraft systems. Failures can occur in many different systems of the aircraft but structural failures are particularly important given its impact on safety and certification. Thus structural design is a prime target for improvement to address rework.

One of the most important aspects of the structural design process is the analysis of loads because of the uncertain nature of loads and the costly consequences of failing to predict them accurately and design to these specifications. Loads analysis is a critical step in aerospace design in general because of its impact on structural weight, which directly affects aircraft performance. Figure 1 depicts a schematic of loads analysis which is composed of several load cycles. Each cycle represents stages in the design process.

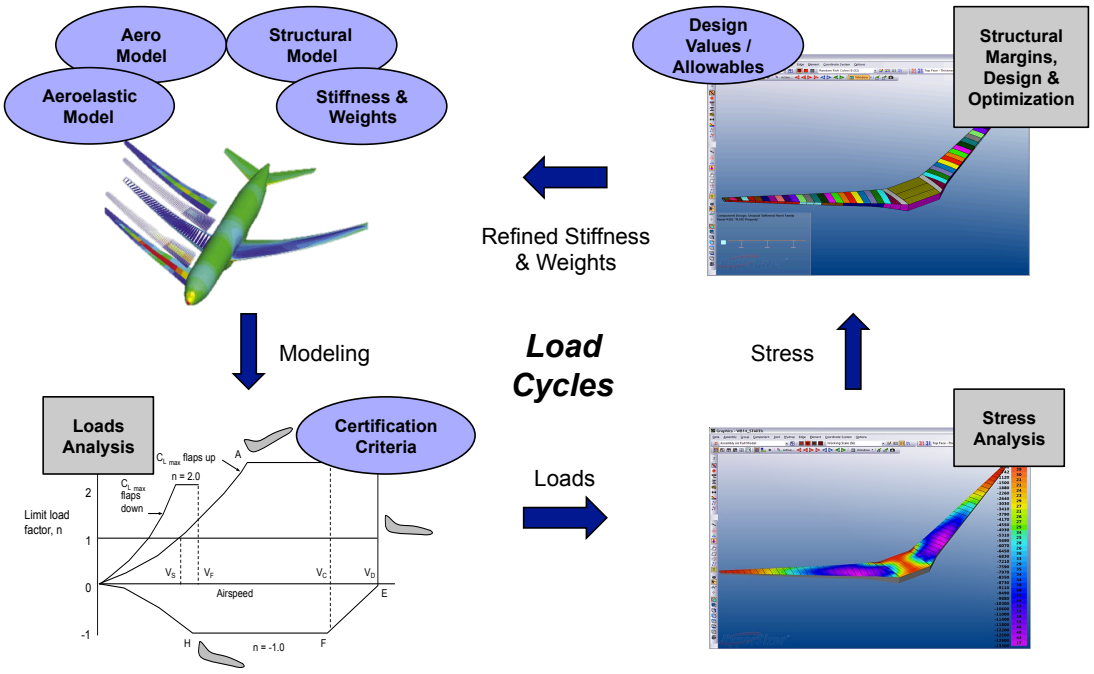

Figure 1: Schematic of loads analysis

Loads analysis is very multidisciplinary and involves analyzing a large number of load cases, defined by certification criteria, in which the loads are calculated for each case. The subset of largest loads are deemed critical and are translated into internal stresses. These stresses, along with other structural responses, are used to calculate margins of safety of several failure analyses based on predetermined allowables, also known as design values. The selection of failure methods are also driven by regulations. The lowest margins drive the structural design during optimization to meet certification and other requirements.

The structural stiffnesses assumed initially are not known precisely and are a function of the internal structural design (internal layout, component definition, materials etc.). The stiffnesses must be updated as the design is finalized in the load cycles. When analyzing the load cases, a coupling exists between aerodynamics and structures due to an aircrafts' elasticity. Consequently the loads and stiffnesses are

interdependent. When the stiffness is updated the loads also change so iteration is required to stabilize both and mature the design. The loads process generally referred to here as the series of analysis cycles, where each represents an iteration between loads and structures. Multiple cycles are conducted to mature the design and converge the stiffness, afterwards leading to flight and ground testing for validation.

The combination of load uncertainties, stiffness and sizing iterations are significant sources of rework in the structural design process [39]. Removal of uncertainty can help reduce the risk of rework. Uncertainty quantification (UQ) aims to calculate the effects of error or inaccuracies in our experiments and analysis methods [27]. As will be discussed, little work has been done in the literature in regards to quantifying and mitigating the uncertainty in the loads process itself [160]. Increasing the fidelity in analysis methods can reduce specific sources of uncertainty, but will also increase the computational expense. Increasing load and structural margins can reduce the risk of rework but at the cost of increased weight and diminished performance.The methodology presented in this thesis is an optimization framework to trade the aerodynamic fidelity, load margins and structural margins to minimize the risk of rework in loads analysis while also managing uncertainty and costs related to these analysis and design decisions.

An important aspect of this framework is the consideration of fixed resources. Here the term "resources" is used to describe the overall budget and schedule of a design program. The main factors under consideration which impact these resources are uncertainty, computational time and effort, weight, and redesign. Each factor can and will be assigned a cost and the aforementioned analysis and design decisions will be made under a fixed budget. The magnitude of both the costs and budget are subjective and are primarily meant to convey the priorities of the user rather than attempt to assign a specific dollar amount. Though some efforts have been made in the literature to do assign such costs [6] and will be used for benchmarking.

This thesis will discuss potential methods to construct the rework decision framework for loads analysis, analyze results from experiments to explore and improve the framework and finally evaluate the framework against rework in the current loads analysis approach.

1.2 Problem Statement & Structure of Dissertation

From the motivation an initial literature search to address design risk was conducted. Some strategies to mitigate design risk emerged. Prominent researchers such as Professor Willcox from the Massachusetts Institute of Technology and others have focused on a "life cycle" approach to design [110][117]. which is a holistic view of the entire life of an aircraft from cradle to grave and includes financial implications and long term costs as opposed to simply designing to maximize performance [90]. One such work from Peoples and Willcox (2006) [117] states:

> *"... eliminating design uncertainty earlier is more beneficial than producing a suboptimal designdespite the larger impact of incurring the cost of design changes earlierdue to heavier discounting of later cash flows."*

Their findings and the initial literature search speak to both uncertainty and intentionally including and planning for rework (design changes) when mitigating design risk and thus a potential strategy to do so involves: reducing uncertainty as early as possible, include financial metrics in optimization to improve life cycle design and proactively consider rework. Thus a problem statement was developed to guide the development of the thesis:

> ***Problem Statement:*** *Develop a decision making framework to reduce design risk in aerospace structures by considering rework, uncertainty, and financial*

implications

The structure for the remainder of this thesis is described in the following. Chapter 2 discusses how the problem addressed in this thesis was formulated. Chapter 3 will review the background concepts which will form the theoretical foundation for the proposed framework. Chapter 4 introduces and summarizes the proposed framework. Chapter 5 will detail the modeling and simulation environment and experimental setup. Chapter 6 discusses the experimental plan to address the research questions and validate the initial hypotheses. Finally, Chapter 7 will summarize the body of work from this thesis and discuss the contributions and future work.

CHAPTER II

PROBLEM FORMULATION

2.1 Problem Scope & Model Formulation

The problem statement is a broad one so the scope must be defined to feasibly address the problem within this thesis. Naturally to address rework and design risk we must focus on the design portion of the development program. Though there are multiple design phases; i.e. conceptual, preliminary, detailed, etc.; the conceptual phase involves design of the configuration and planform shape which was deemed to be out of scope for this work given the focus on higher fidelity analysis methods, and specifically aerodynamic fidelity. This focus also narrowed the scope to loads analysis in order to study the effects of aerodynamic uncertainty on structural design and rework.

The loads analysis process typically consists of a number of load cycles over the course of the overarching design process. Although estimation of loads is done even at the earliest stages of conceptual design, here "loads analysis" is defined as occurring after the outer-mold-line (OML) of the aircraft has been fixed and preliminary wind tunnel experiments have been performed on a subscale test model. Thus this thesis methodology assumes any given design is beyond the early conceptual phase where the planform and configuration have been selected and frozen. After wind tunnel testing, loads are analyzed; on the order of 1,000 cases for the initial cycle based on feedback from experts. Prior to that, only a handful of cases are chosen to determine initial structural weight and definition. Subsequent load cycles ramp up the number of cases to increase accuracy and accompany higher fidelity methods as the design detail increases resolution. After the loads analysis is complete a flight test demonstrator is

built where one of its primary objectives is to validate the predicted loads. Although both flight and ground tests are equally important and necessary after the loads process, only the flight load survey will be considered in this work. The loads process is depicted in Figure 2 and 3.

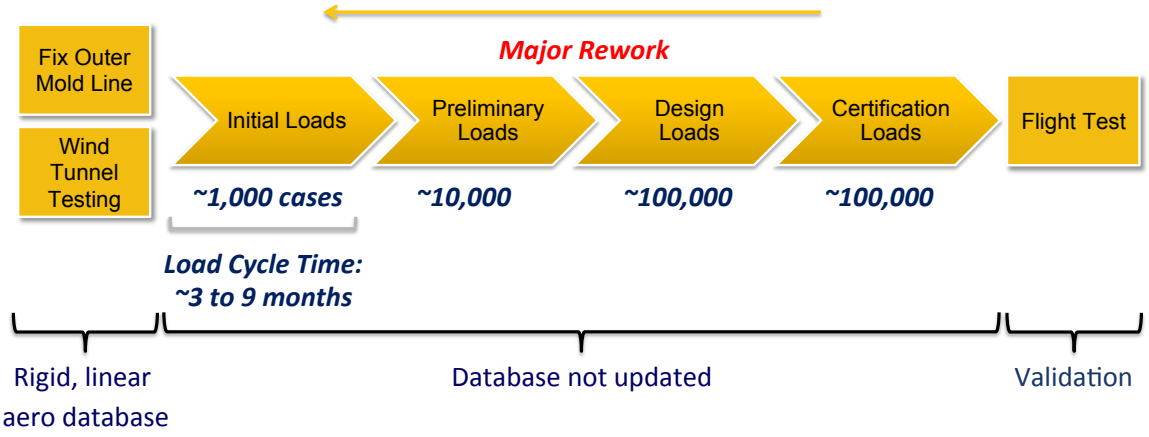

Figure 2: Loads Process with Major Rework

With an understanding of the loads process and its impact on flight test, the modeling environment and test case could be formulated to further refine the scope. The design risk discussed in motivation applies equally to both commercial and military applications, but work in the Aerospace Systems Design Laboratory which preceded this thesis focused on the former, in collaboration with the Boeing Company, and so only commercial transports were considered here. Thus an appropriate model and test case should be representative of a commercial transport. The emphasis on loads analysis and structural design allude to aeroelastic analysis, which imposes additional requirements on any potential model.

Three important modeling requirements include a planform shape for aerodynamic analysis and an internal primary structure for structural analysis. Additionally both the aerodynamic and structural models must be undeformed for aeroelastic analysis.

A full aircraft model could be utilized, but all these requirements can be satisfied by only considering the wing. This simplifies the analysis for the initial development of the framework. It is also appropriate because the aeroelastic effects are greatest on the wing relative to any other major aircraft component.

The general problem statement developed from the motivation will be applied specifically to a commercial transport wing and consider aeroelastic analysis and design after the conceptual phase. Although still general, the scope is appropriate enough to fully formulate the problem, which will be done in the remainder of this chapter. Next, the specific sources of rework addressed in this work will be discussed.

2.2 Sources of Rework in Loads Analysis

There are two sources of design rework targeted in this work. The first type, referred to as *major* rework, occurs when the actual loads are greater than expected and cause structural failure during flight test, also called flight load survey. Initial wind tunnel tests result in simplified (linear and rigid) aerodynamics used throughout the load analysis cycles. When the actual loads (nonlinear and aeroelastic) are validated during flight test it may reveal that these simplifications underestimated the simulated loads. If failures occur the flight tests are suspended or canceled and significant rework is necessary to fix the design. Additionally, by this time significant investments have already been dedicated to implementing the flight test program and building test articles which may have to be repeated.

In reference to Figure 2, flight test validation is a critical check point for major rework. Wind tunnel experiments are carried out in the beginning of the loads process to create an aerodynamic database of surface pressures. Although wind tunnel testing is viewed as an accurate aerodynamic approach, it is based on a semi-rigid test model. The model is intended to be rigid but does have some flexibility. Therefore the

measured pressures need to be corrected for the rigid assumption. Both the correction and the rigid assumption itself introduce uncertainty. The rigid assumption is not representative of real aircraft structures which are elastic and subject to aeroelastic effects. In addition, the aerodynamic data is often linearized to accompany efficient low to mid fidelity aerodynamic analysis. This is common practice in commercial transports where the high-fidelity methods such as computational fluid dynamics are deemed unnecessary given tried and true airplane configurations and the typical operational flight envelope. But advancements in computation, composites, technology, etc. may soon require higher-fidelity aerodynamics for more unconventional designs.

Nevertheless linearization adds uncertainty to the loads given the aerodynamics experienced by the aircraft are nonlinear. The rigid linear database from wind tunnel testing is used in subsequent load cycles to correct the aerodynamic analysis methods. In Figure 2 these cycles are labled as *Initial, Preliminary, Design and Certification Loads*, where the names imply the types of load cases utilized in the loads analysis and their increasing maturity. Even though the calibrated analysis reduces certain uncertainty sources (e.g. compressibility, 3D effects, etc.), it introduces the aforementioned sources. Given the expense of wind tunnel experiments the aerodynamic database is not updated throughout the loads process. The predicted loads are only validated at the conclusion of the load cycles through flight testing. If the actual loads and structural response are significantly greater than those predicted during loads analysis, major rework can occur.

Improving or repeating wind tunnel experiments could reduce uncertainty, but this is out of the scope of this thesis and would have significant costs associated with them. An alternative method of reducing the risk of major rework is to adjust the fidelity of the analysis methods used during the load cycles. The calibration data is only effective if the analysis has similar fidelity to utilize all the information. For an extreme example, a 2D airfoil code can only use a small (if any) amount of

wind tunnel data because they have vastly different fidelity, but a 3D CFD analysis could potentially benefit from all the wind tunnel calibration data. At the other extreme, a viscous CFD code with mesh deformation capabilities could potentially overcome the linear rigid wind tunnel assumptions and reduce the effect of uncertainty in using the calibration data. The benefits of such analysis decisions must quantified and appropriately weighed against factors such as computational costs and increased modeling complexity. One of the objectives of this thesis is to depart from the common practice of using low to mid fidelity aerodynamics and explore the impact of higher fidelity methods during load cycles to reduce the risk of rework, but account for limited resources.

Conversely the second type of rework, referred to here as *minor* rework, corresponds to any redesign effort required between load cycles and prior to any flight or ground test validation. This rework is "minor" because the cost relative to major rework is substantially less, primarily because of when the rework occurs. Unlike major rework, not all minor rework is bad, which was alluded to in the motivation and the work of Peoples and Willcox [117]. Design changes frequently happen prior to certification as new information and requirements are introduced and rework can be intentionally done to reduce weight and increase performance. Unintentional minor rework can occur when insufficient structural margins cannot cover potential increases in loads when both the stiffnesses and design are updated between cycles. Increasing the margins can reduce such rework, but at the cost of increasing the structural weight and degrading aircraft performance. A schematic of unintentional minor rework is shown in Figure 3. This minor rework may be exacerbated when loads are intentionally increased in load analysis to prevent unconservative designs. Whether intentional or not, decision makers need to weigh the costs and benefits explicitly in order to make the best analysis and design decisions for a given scenario. The framework developed in this thesis has the potential to aid in these decisions.

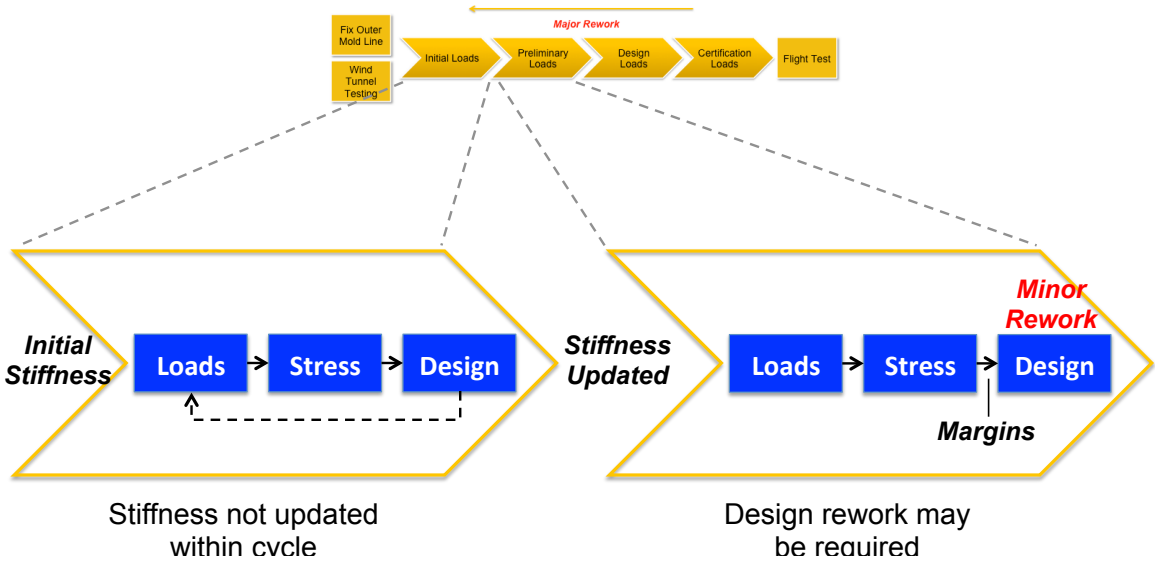

Figure 3: Loads Process with Minor Rework

The organizational structure of a typical aerospace company plays a role in minor rework. Loads analysis is usually done by a specific group and described as such [165];

> *"...in aircraft design projects, [the] loads group lies at the heart of the design cycle. It receives inputs from various design groups such as aerodynamics group, structures group, weight and balance group, systems groups, airworthiness group, and so on. Not only receiving these inputs, but [the] load[s] group also provides outputs to various groups, mainly structural design and analysis. Those interactions make aircraft loads one of the most multidisciplinary subjects in aircraft design and analysis."*

The multidiscipline nature and importance of loads in an aerospace organization is captured in the following schematic describing the interactions of the loads group:

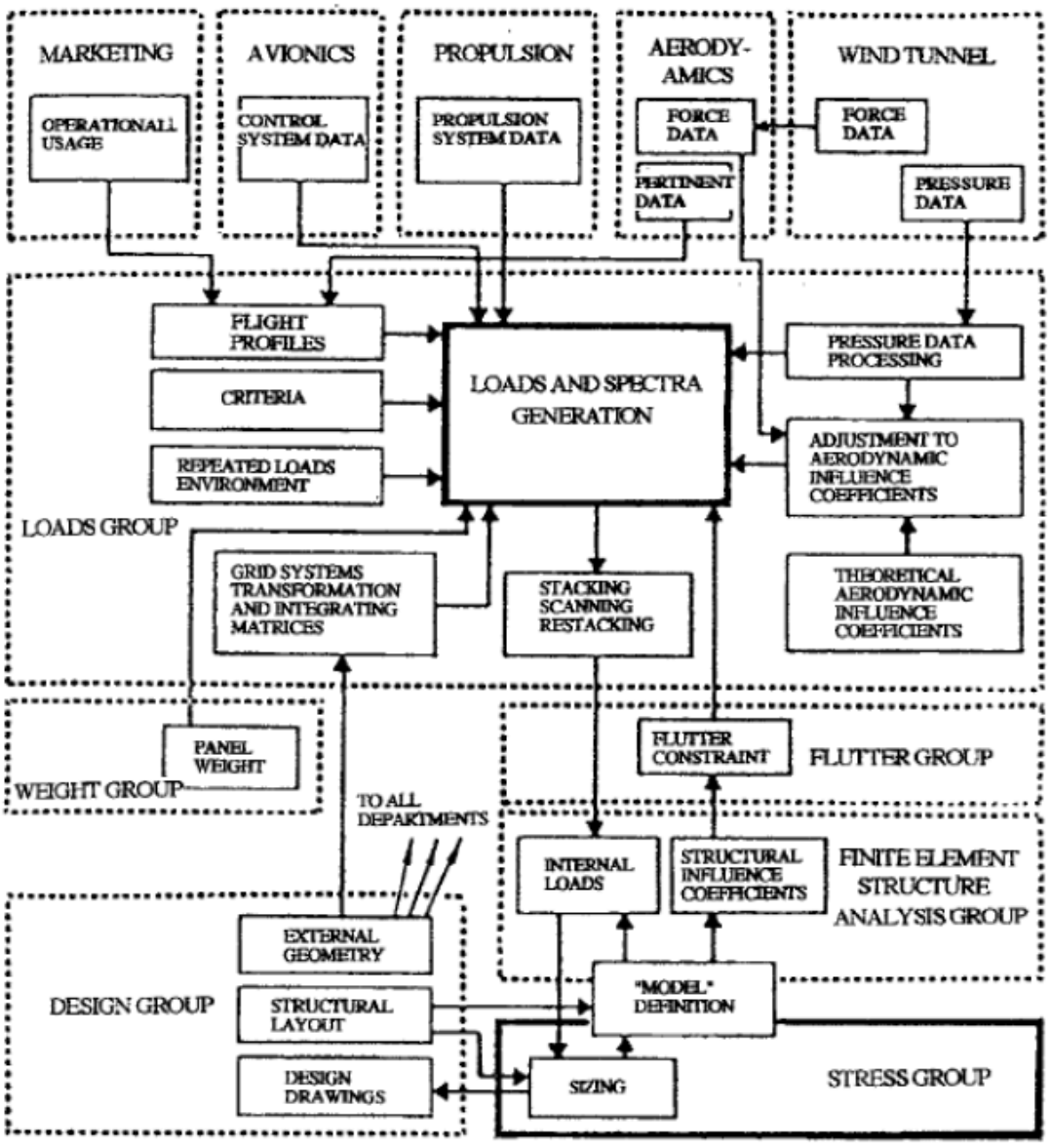

Figure 4: Interactions of Loads Group in Aircraft Design Organization [109]

Figure 4 also visualizes the separation of the loads group from the stress, structural analysis and design groups. Any change in the design or analysis of any group can change the loads. Even in a small organization there will be iterations due to the people and processes involved. In the thesis, these three latter groups are considered

one consolidated *stress* group. The size and complexity of the interactions between the loads and stress group are the reasons why the stiffness is not updated within a given cycle as mentioned in Section 1.1. For example, 1,000 load cases may be analyzed by the loads group in the initial load cycle as shown in Figure 2. The resulting internal loads are based on initial stiffness estimates and are given to the stress group to perform structural analysis and design. This cycle can take three to nine months. The stress group will calculate updated stiffness values for the new structural design which affects the loads. But the loads group does not update their load calculations in the initial load cycle. Instead, the new stiffness is used in the following preliminary load cycle when the loads group analyzes 10,000 load cases. The fact that neither the stiffness nor the loads are allowed to converge within a load cycle adds uncertainty to the design solution produced in that cycle. There cannot be an indefinite number of cycles, so a stopping criteria is used. Typically four cycles are enough to converge the design as shown in Figure 2 based on subject matter experts.

Any realistic loads analysis will assume a non-rigid structure and therefore will be concerned with the interactions between the fluid and flexible structure, i.e. aeroelasticity. Most numerical aeroelastic methods are iterative. Although the loads have been updated in the preliminary load cycle, the structural margins used by the stress group have not been. Those margins may have been adequate previously, but insufficient if the new loads have significantly increased, thus resulting in failure in the structural analysis. The failed systems or components will then be redesigned to meet safety requirements, which is rework. This rework is considered minor in this thesis because it causes additional work within a load cycle but typically does not require any previous cycles to be repeated.

The structural margins are implemented to account for uncertainty but they are typically decided based on experience and expert opinion. Insufficient margins will cause minor rework, but increasing margins will ultimately cause excess structural

weight. The same can be said for load margins. The other objective of this thesis is to determine the optimal balance of allocating load and structural margins and structural weight to reduce the risk of rework under constrained resources.

An overview of the traditional approach to loads analysis has been given. Some of the weaknesses of this approach have been alluded to in the discussion of rework and the complex, iterative and uncertain nature of this process. The latter characteristics could potentially equate to significant uncertainty. The following section discusses these weaknesses and their consequences in more detail.

2.3 Limitations of the Current Approach

2.3.1 Quantifying and Mitigating Uncertainty

New aircraft development programs have a historical precedent for high risks in terms of cost and schedule. Up until 2009 the total acquisition cost overrun for major defense programs, the majority for aircraft[1], was estimated at $296 billion. Research, development, test and evaluation (RDT&E) costs increased by 42% over initial estimates and expected deliveries were delayed 22 months on average [144]. In 2011, Collopy et al [32] extrapolated these results to completion and reported the total loss due to delay, overruns, and reductions in material (generally caused by overruns) to be $55 billion per year, or $150 million each day. The 2009 Government Accountability study examined 47 defense programs in-depth and found at key decision points "most programs proceeded with far less technology, design, and manufacturing knowledge than best practices suggest and faced a higher risk of cost increases and schedule delays". Increasing design knowledge is equivalent to decreasing design uncertainty, a core component of the proposed framework.

[1]Seven out of the top ten largest acquisition programs were for aircraft; the other three programs were for a submarine, missile and aircraft carrier.

Analogous trends and challenges are seen in the commercial aircraft realm. Although not all of the cost overruns and delays are attributed to the design process, there have been several high-profile examples where structural design flaws due to loads resulted in significant delays and cost implications. Two recent examples include the Airbus 380 and Boeing 787 development programs [112]. By the time the first A380 aircraft was complete the development cost increased from \$9.43 billion[2] (€8.8) [113] to an estimated \$11.78−15.00 bilion[2] (€11−14) [2] and the first delivery was delayed two years. One of the launch customers for the A380, Qantas Airways, reported in its 2005−2006 annual fiscal report that it has "brought to account \$100 million AUD (\$76 million US) compensation from Airbus for delayed delivery of its initial and subsequent aircraft" [73].

In 2006 the A380 wing was undergoing ultimate static load testing when it failed prior to the mandated ultimate load and resulted in program delays. It has been documented that detailed, high-fidelity structural analysis was a prime contributor to identifying the root cause and developing the solution: "straps along the stringer feet on both sides were implemented to avoid separation and rivets were replaced locally with bolts" [111]. Based on this, uncertainty quantification and management of fidelity potentially could have helped avoid the failure and rework which ultimately added to costs, delays and weight. Both uncertainty quantification and uncertainty management are key aspects of the proposed method called the Rework Decision Framework (RDF).

The Boeing 787 risks and setbacks have been well-documented and highly publicized. By the time of first delivery in 2011 the program cost had swelled to an estimated \$32 billion [55] and four years of delay. Although the primary cause of these setbacks was due to the simultaneous introduction of radically new technology and supply chain strategies, there were also costly delays and rework due to

[2]Using average exchange rate from 2000 [148]

structural flaws resulting in increased weight [159]. Similar to the A380, structural failure occurred during static load testing of the wing in May 2009. Delamination of the stringers on the upper skin occurred at the side-of-body interface between the fuselage and wing. The failure occurred just beyond the limit load which meant a redesign was be necessary to increase the structural integrity to withstand the mandated ultimate load [54].

The rework to design the side-of-body fix was estimated to cause a three month delay in the flight test program and added to the already delayed first delivery [1]. According published sources [53] engineers with knowledge of the issues claimed the "retrofit will be tremendously difficult to implement on the [flight test aircraft] already built because the mechanics will have to do the tedious and meticulous work inside the confined space of the wing." These reports, although very speculative, speak to difficulties which arise from rework and retrofitting. The source also claimed the area showed up as a "hot spot" in Boeings analysis prior to the wing delamination but it was never addressed. It may not have been the case that critical loads were missed, but instead it is possible the impact of such loads were underestimated. Uncertainty quantification can help better quantify this impact and clearly show decision makers where areas in the design need to be addressed to mitigate risks. As of July 2009, Barclays Capital analyst Joe Campbell estimated the total cost overrun of the Dreamliner program due to "extra startup and engineering costs, penalties owed to customers for delivery delays and contractual obligations to suppliers for engineering changes [to be] in the vicinity of $11 billion" [54].

Real-world aircraft development pitfalls show the necessity of efforts to avoid major rework due to test failures. Increasing knowledge as early as possible could improve these symptoms which plague nearly all new development programs. Examples of this principle from academia include the previously cited work of Peoples and Willcox [117] who conclude that decreasing uncertainty early in design is critical for

mitigating business risk. Specifically they emphasize that "incurring costs early in a program to ensure a successful design represents a safer strategy than going to market with a design that has missed performance goals" [117]. Incorporate this approach into all aspects of the design process could potentially reduce risk in the development program.

The current approach to loads analysis accounts for uncertainty through classic approaches such as margins and safety factors. But these approaches do not reduce uncertainty, instead they compensate for it. Uncertainty reduction efforts in the current approach are largely dependent on physical experiments, such as wind tunnel tests, which can be very expensive. Although compensation is necessary, without rigorous assessments of uncertainty relying solely on these approaches can inevitably lead to over-design and less performance. Safety factors and margins can be supplemented with measurements of confidence, which comes directly from uncertainty quantification. Once measured, confidence can be systematically increased in order to reduce uncertainty and mitigate rework risk.

2.3.2 Empirically-based Decisions on Fidelity and Margins

As stated previously, in a given load cycle a large set of cases are run in conjunction with a chosen fidelity for each of the multidisciplinary analyses. Both the number of cases and fidelity are selected, in part, to attempt to reduce uncertainty. The number of cases is primarily dictated by regulations and other safety practices. So this begs the questions; how much fidelity is enough? Based on subject matter experts, computational fluid dynamics are more commonly used for designing military aircraft where supersonic flight regimes and extreme maneuvers are necessary and require advanced aerodynamic analysis but not typical in designing commercial transports. Could benefits related to rework be achieved with higher-fidelity methods?

Prior knowledge and empirical data can help answer these questions, but they both quickly become unavailable or unreliable for novel designs. Analysis fidelity decisions are often made as a function of time available to carry out the analysis and the phase in the design program which dictates qualitatively how accurate the solution should be. Poor decisions for analysis methods can result in inefficient use of resources and potentially wasted time and money or unacceptable levels of uncertainty and too much risk. Analysis fidelity decisions should be made with quantified metrics relating the uncertainty reduction benefits, and potential costs, rather than simply doing what has worked in the past.

A similar argument can be made for allocating design margins. As has been mentioned, structural margins are typically empirically-based and an "if it ain't broke, don't fix it" approach taken. Although there is a growing amount of research on reliability-based and other probabilistic methods to effectively replace empirical margins [61][96], such approaches are not utilized in the proposed Rework Decision Framework. Such advanced methods could be incorporated into the framework for future work. The choice to develop this framework around classically defined, i.e. deterministic, margins and safety factors was to demonstrate a decision system which could be applied to existing aircraft development programs. Although probabilistic-methods are popular in academia, they are far from becoming common practice or approved for certification purposes by regulatory bodies. Instead of fixing the margins to their historical levels, both the structural and load margins are varied in this framework to assess their impact on rework and optimized based on constrained resources.

2.3.3 Reactive Approach to Rework

In the current approach to the loads process, of course every effort is made to avoid flight and ground test failures and these failures are not normal occurrences by

any means. But new concepts and technology in the future will posed additional risk because designers will be in new territory. Therefore one could argue that the lack of integrating uncertainty quantification and management into normal design practices and the reliance on empirically-based margins make it difficult to proactively plan for major and minor rework for novel concepts. One only needs to look at some of the 787 development issues which occurred when various new technologies were infused on the same platform and introduced new uncertainties which may have never been considered because they were unproven on any previous aircraft [40].

It is thus assumed, and agreed upon by some industry experts, that the current approach treats rework in a reactive rather than proactive manner [12]. In other words, design rework is handled as it becomes necessary to fix a problem or reduce weight, which is reactionary. An alternative approach would be to simulate when both major and minor rework might occur when decisions are made on specific analysis and design choices. In this work, those decisions are related to aerodynamic fidelity and margin allocation. Therefore this thesis seeks an alternative, proactive approach to decisions which affect design rework. Next, the key features of the proposed alternative will be discussed.

2.4 Rework Decision Framework: A New Approach to Aid Loads Analysis

Some limitations in the current approach to loads analysis and design have been discussed. In order to address these limitations two focus areas for this thesis have been identified; uncertainty quantification and uncertainty management. These two areas are utilized together in the overarching framework to aid in specific analysis and design decisions which could reduce the risk of major rework and potentially improve loads analysis. An overview of the framework is discussed here.

It has been shown that uncertainty quantification can potentially improve loads

analysis and design in general. Overcoming subjective or empirical assessments of risk is an important first step before attempting to mitigate such risks. In terms of major rework risk, several sources of uncertainty exist in loads analysis, but this thesis focuses on aerodynamic uncertainty because of the emphasis on loads. Once identified, the impact of the uncertainty on the desired responses in the system must be quantified. The field of uncertainty quantification and sensitivity analysis have numerous approaches which will be discussed in Chapter 3.

Reducing uncertainty once it has been quantified requires unique methods, especially because some uncertainty sources by definition cannot be reduced. Several of these methods will be discussed, but the literature often only focuses on *how* to reduce uncertainty but less on *if* certain sources should be reduced. Identifying important reducible uncertainty points back to sensitivity analysis. But to truly answer this question we turn to uncertainty *management*. In a realistic airplane development program there is limited time, money, and computational resources to employ often-expensive experiments and numerical methods to reduce uncertainty. Approaches to determine how much uncertainty should be reduced given constrained resources will be explored.

Treating uncertainty directly can potentially reduce uncertainty associated with the prediction of failure but in the context of current practices, we must also address the allocation of margins. To counteract unconservative loads, a margin may be directly applied to the loads to artificially increase them. This practice is regularly employed in engineering by implementing safety factors. Past failures in aerospace programs have shown designing to the "ultimate" historically defined by a 1.5 safety factor is not always enough to avoid major rework [112]. Instead of making the loads more conservative, another approach to avoid major rework is to increase the required minimum margin of safety in the structure. The margin of safety is defined for a specific failure analysis so it will have a different effect on the structure than

the load margin which impacts all failure analyses dependent on the force.

Both the load and structural margins are applied to make the structural design more conservative and are well established methods. This thesis proposes a third, unique approach to addressing major rework: increasing analysis fidelity. In addition to decreasing uncertainty, adjusting the fidelity can affect the conservativeness of the loads as well. But unlike margins, more fidelity comes with more computational costs. The overarching rework decision framework utilizes uncertainty quantification and management in conjunction with optimization to trade aerodynamic fidelity, load margins and structural margins to reduce the risk of rework while taking into account the relative costs associated with these decisions.

In order to address rework proactively different scenarios and decisions need to be evaluated to assess their impact. An example of such a scenario can be notionally depicted by looking at the wing bending moment on the conceptualized model described in Section 2.1. The wing bending moment is an integrated load which generally can tell us about the state of internal stresses as shown in the simple beam equation:

$$\sigma = \frac{My}{I} \tag{1}$$

where σ is the bending stress, M is the bending moment, y is the distance from the neutral axis and I is the moment of inertia. Two scenarios are portrayed by plotting a notional bending moment curve shown in Figure 5.

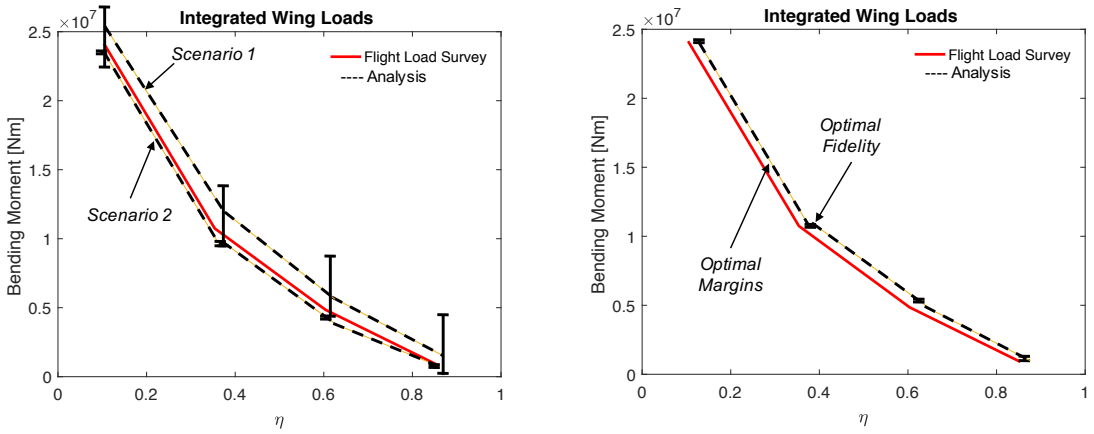

(a) Scenarios 1 and 2

(b) Optimal solution

Figure 5: Analysis uncertainty and load margin for notional wing bending moment compared with true loads from flight load survey

The red curve in Figure 5 is the true bending moment derived from the flight load survey and the dashed curve is the analysis prediction as a function of the span location, η where 0.0 is the wing root and 1.0 is the wing tip. The error bars represent the magnitude of uncertainty (exaggerated for illustrative purposes only). In the context of the bending moment a positive margin would indicate the mean value of the analysis loads are greater than the true loads, i.e. more conservative. This is beneficial because underpredicting the loads, i.e. unconservative, increases the risk of flight test failure.

In the first scenario there is a positive margin, but a large amount of uncertainty means there is a chance the positive margin will not be realized. In the second scenario there is a small negative margin but low uncertainty so there is a high degree of confidence in the prediction. How can a decision maker proactively plan for rework with these two scenarios? The proposed decision framework allows the decision maker to optimize to see if there is a solution which has both a positive mean margin and low uncertainty which can be achieved with a combination of the right aerodynamic fidelity level and margin allocation.

This simplified example shows us a few things: first, the problem statement is multiobjective because both the mean and variance of the responses are important. Secondly, analysis fidelity is important because it realistically shows how close we are to the "true loads" and it impacts the uncertainty. But higher fidelity means more computational costs. Thirdly, if a more conservative design is preferred to avoid major rework margins can be added to the load directly, which has a different affect than the structural margin. Finally, the aforementioned scenarios speak to different priorities the decision maker might have. For example, the may value a lower uncertainty in some situations more than others. Thus a scenario-based framework would be beneficial.

Results will show that the fidelity, load margin and structural margin influence the mean and variance (uncertainty) in the bending moment. With this information a decision maker can proactively plan for rework as they choose analysis methods and allocate margins.

To complete the problem formulation for the Rework Decision Framework we must address who will use it, how will it be used and when will it be used. For *who*, the framework will be most beneficial for managers and technical leaders in the aerospace industry who make decisions or are responsible for the outcomes of the loads group, stress group, design group or other engineering groups related to the loads process. To review the *how*, the Rework Decision Framework can be utilized for:

- Simulate various analysis fidelity, load margins and structural margins to estimate potential impacts on rework and costs
- Trade performance, rework, uncertainty and computational cost for a given scenario based on the decision-makers priorities
- Use the results of the framework to make more informed decision for analysis methods and margins

Finally for *when*: the Rework Decision Framework can be utilized throughout the load cycles, but the earlier the better in terms of being proactive. The framework should as be used as events occur which change the decision makers priorities which are captured in the simulated design scenarios.

2.5 Research Objective & Primary Hypothesis

With problem formulated the research objective of this thesis is the following:

> ***Research Objective:*** *Develop a methodology for loads analysis to quantify and manage uncertainty related to aerodynamics and load case parameters in order to improve decision making for rework by optimizing fidelity, load margins and structural margins*

From the objective, two research goals were developed which drove the background and literature review:

> ***Research Goal 1:*** *Develop a methodology to quantify uncertainty due to aerodynamic analysis fidelity and load case parameter uncertainty*

> ***Research Goal 2:*** *Develop a methodology to improve decision making for design rework in loads analysis*

The first hypothesis is the overarching hypothesis which concerns the entire thesis. Therefore it is consider the primary hypothesis:

> ***Primary Hypothesis:*** *For a given design scenario, the proposed framework*

involving uncertainty quantification and management will lead to improved decisions regarding rework and performance compared to the current approach

The literature review will be discussed in the next chapter and focuses on uncertainty quantification and management methods to accomplish the two research goals. Additionally the review will develop research gaps, research questions and secondary hypotheses to address them.

CHAPTER III

RESEARCH DEVELOPMENT & BACKGROUND

3.1 Rework in Design

Research for decreasing rework and redesign often fall under the field of operations research, which is ultimately concerned with improving decisions in an industrial system using advanced analytics and optimization. These fields span to most engineering disciplines and applications, but the focus on aeroelasticity and the unique aspects of the airplane development in the problem formulation narrowed the literature search to the aerospace field. A review of the aerospace research regarding rework and redesign have focused heavily on it from a production or operations perspective [39]. In other words, rework which occurs after the system has been designed, certified and has begun production or even entered service. This type of rework is often tied with repair and servicability [156]. The problem formulation for this thesis is primarily concerned with design rework, and therefore redesign which occurs in the pre-production phase. The body of applicable research is thus smaller but there are some notable works which will be briefly highlighted.

There is a significant amount of design rework research previously done which stems from Professors Taiki Matsumura and Raphael T. Haftka from th University of Florida [96][94][95][172][171][120][119]. In general these papers focus on reliability-based structural design optimization methods which are concerned with balancing redesign and performance through added weight. Of particular interest is the work of Villanueva et al. [172][171] and Price et al [120][119]because of their treatment of epistemic uncertainty, i.e. a lack of knowledge (see Section 3.3.1) and the use of Bayesian methods which are utilized in this work and discussed in more detail in

Section 3.4. Other related design rework research has been done by Arundachawat et al from Cranfield University [11][12] which combines both structural analysis and operations and logistical approaches to predict failure modes under uncertainty and reduce rework.

Although the methods from University of Florida are very useful and similar in scope, their focus on reliability is one major differentiator from this work. As was stated, deterministic structural margins are utilized here so the Rework Decision Framework can be applied to existing development programs. Additionally some of these works consider epistemic uncertainty along with aleatory, but they do not focus on analysis fidelity as a mechanism for improving rework. To the author's knowledge, no such work in aerospace has this specific focus. Finally, none of the aforementioned papers differentiate and consider both load and structural margins. The papers from Arundachawat et al do not specifically focus on the allocation of structural margins.

3.2 Introduction to Loads Analysis

The aerospace loads process generally describes a multidisciplinary design, analysis and optimization (MDAO) process which results in structural sizing and definition. The structure is discretized into sections or components where each is subjected to numerous loading scenarios. The external forces and moments which constitute the loads come from a variety of different sources and flight conditions so the analysis requires many disciplines such as aerodynamics, structures, propulsion and controls. These external loads are translated to internal loads and their response is determined through structural analysis. When critical loads are identified, structural design and optimization will size and define each component to achieve a favorable objective, which in many cases is weight and cost.

The loads process is a fundamental step in the overall design process. Typically

the loads analysis is divided into cycles and supports the design phases of the overall airplane development. These cycles can be described as initial loads, preliminary loads, design loads and certification loads, see Figure 2.

When the conceptual design phase is complete the general configuration and outer mold line (OML) is frozen. Wind tunnel models can then be built and tested. The resulting data helps formulate the loads used throughout load cycles. A relatively modest amount of load cases are analyzed ($\sim$ 1000 cases) and with subsequent cycles the set of cases increases in size and complexity. This ramp up is associated with finer detail in the design and more advanced tools. The final load cycles consist of approximately 100,000 cases. The initial and preliminary loads generally correspond to the preliminary design phase. Design and certification loads generally correspond to the detailed design phase. At the completion of the design phase a version of the airplane is manufactured specifically for flight testing to verify the analysis and wind tunnel model. After the OML has been frozen for a commercial transport design the loads process, including all cycles, can typically take three to nine months[1].

Structural design is a critical step in the overall design process of any physical system. The objective of structural design is to "develop a structure that fulfills requirements with regard to serviceability and safety in a cost-effective manner" [51]. In aerospace, this primarily involves defining the internal layout, component sizing and material definition. These three characteristics are optimized to withstand a predetermined maximum amount of stress or deformation resulting from the expected loads experienced by the aircraft during operations. An aircraft's state defines its configuration, weight, maneuver, flight condition, ground condition, etc. at any given instant in time. All the loads cannot be precisely known for a given aircraft state because the environment to which it operates isn't precisely known. In addition,

[1] All magnitudes for the number of load cases and duration of load cycles are derived from feedback from subject matter experts involved in this work

there are an infinite number of states the aircraft could realize during its lifetime. Load cases are essentially the combinations of airspeeds, altitudes, temperatures and flight and ground conditions [165]. Thus a load case defines a set of conditions which will determine all the loads the aircraft will experience in a single state. Therefore analysts will evaluate thousands of load cases to account for these unknowns and various states.

The goal of loads analysis is to find the loads which will control, or drive, the structural design. This special subset of load cases is referred to as the controlling or critical load case set. This set will determine the size, shape and material properties of the structure so all failure modes analyzed will theoretically be avoided. Often times the critical load set is determined by calculating the envelope of the summed external loads or by plotting the internal forces and moments. The internal loads which envelope all others are the critical loads. Another mechanism for determining critical loads is through failure analysis. For example, the load cases resulting in the lowest margin of safety from a particular failure method can be viewed as critical. The critical load set is used in this thesis as the driving factor of the overall structural design and weight. Aircraft performance and costs can directly tied to weight [81] so the loads process is crucial. Details on the individual disciplines in loads analysis will be discussed in the experimental setup in Chapter 5.

3.3 Uncertainty in Loads Analysis

The need for uncertainty quantification (UQ) in the loads analysis process has been discussed in Chapter 1. This section discusses some background information to aid in the understanding of the UQ discipline. In general UQ can be thought of a series of steps to quantitatively determine the uncertainty (or error) in a system response due the uncertainty in it's inputs and noise factors. Visually these steps are

depicted in Figure 6:

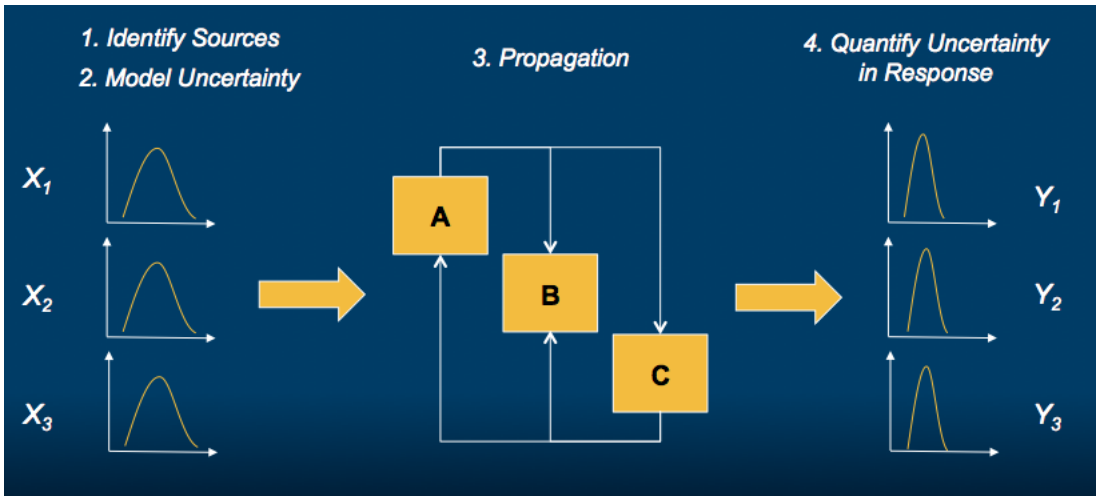

Figure 6: Notional depiction of uncertainty quantification process

In reference to Figure 6, Section 3.3.1 addresses Step 1 and discusses several uncertainty sources related to loads and those considered in this work; namely aerodynamic analysis fidelity and load case parameter uncertainty. Section 3.3.2 addresses Step 2 and discusses how the two sources will be modeled. Section 3.3.3 addresses Steps 3 and 4 and discusses several propagation methods from the literature and how the response uncertainty will be represented. The knowledge base for UQ has grown exponentially due to the reliability on computer models for design and analysis and its applicability to nearly every discipline in applied science and engineering. Thus there is a plethora of methods and terminology, but a small, relevant subset will be discussed and considered here. The methods discussed in this section will serve as candidate methods in the experimental plan to represent uncertainty in proposed framework.

3.3.1 Uncertainty Sources in Loads Analysis

Former U.S. Secretary of Defense Donald Rumsfeld said on February 12, 2002,

> *"There are known unknowns. That is to say, there are things that we now know we dont know. But there are also unknown unknowns. There are things we do not know we dont know"*

The "unknown unknowns" means there are an infinite number of sources of uncertainty in any real system making it impossible to attempt to identify and model all sources. Even if it were possible, the result would be useless because the response uncertainty would be infinite. Thus a major step, arguably the most important and most difficult, is to identify what are the most significant sources in a system which are useful to a study, the "known unknowns". Some difficulty lies in the fact that the system must be understood to even identify where variability and noise may occur [152]. But it often requires expert system knowledge to distinguish these sources from each other and determine which significantly impacts the response and which are relevant. The relevancy of a source can refer to how controllable the uncertainty is or how likely it is to occur in the system during a given time period. The latter is one of the primary concerns of reliability engineering [68]. Expert knowledge for identifying significant and relevant sources for loads analysis was acquired through literature review and industry experts.

Two major categories exist in the UQ field for sources of uncertainty; aleatory and epistemic. Aleatory uncertainty represents natural variability inherent in a system. This type of uncertainty is also called *irreducible* because, as the name suggest, it cannot be eliminated in the sense that variability will always exist in the system. Though the effects of this uncertainty can be reduced, which is the approach taken by robustness methods. Epistemic uncertainty characterizes a lack of knowledge about a system. This knowledge can be supplemented and increased so epistemic uncertainty is called *reducible*. Both these types are important and will be utilized in this thesis.

Analysis fidelity represents a type of epistemic uncertainty which can represent

model form error relative to reality. Given the problem fomrulation this would be a prime candidate for an uncertainty source, but does it have a significant impact on loads? To answer this we must look at the literature. For load uncertainty in commercial transport aircraft, a large portion of the research focuses on dynamic gust loads due to their complexity and difficulty in prediction [72][60][29][10]. The purpose of this thesis is to develop a framework which could apply to virtually any uncertainty source in the realm of loads analysis. As stated in Section 5.3.1 static load types are much simpler and computationally less expensive to analyze than dynamic loads. Thus gust load analysis were not considered in this initial development.

Epistemic uncertainty due to analysis fidelity has been studied often in aerodynamics and aeroelasticity [26][42][66][97], though not often with respect to the loads analysis process utilized in industry. It is hypothesized that aerodynamic fidelity will have a significant impact on the external loads in this work. For example, the baseline aerodynamic method used in this thesis cannot capture shock formation due to it's linearized compressibility assumption, but computational fluid dynamics (CFD) can so there will be significant differences in pressure distributions in transonic flight. Feedback from industry experts involved in this work also confirmed aerodynamic fidelity is a novel, significant and relevant source for loads analysis so it was chosen as one of two uncertainty sources to evaluate the proposed framework.

The parameters which define a load case are intended to represent different operational states of the aircraft, tor example, its speed and altitude. Of course it is impossible to precisely know all the states an aircraft will experience during its lifetime so there is some variability in these parameters which represents aleatory uncertainty. This type of uncertainty if fairly common in studying aerodynamics but still is an important consideration and therefore will be included as the second source of uncertainty.

Besides the two aforementioned uncertainty sources there are many others which

are also significant and relevant to loads analysis, especially given its multidiscipline nature. For example, uncertainty due to analysis fidelity could be applied to other disciplines such as structural analysis, aeroelastic analysis and control theory, although control laws are not explicitly modeled in this environment. High fidelity methods have been explored for dynamic aeorelasticity and flutter prediction [16], although only static analysis is considered here. The choice of varying fidelity for only aerodynamics was primarily made to limit the scope of the work and take advantage of the analysis tools integrated into the modeling environment, which is discussed in detail in Chapter 5.

In terms of parameter aleatory uncertainty, aerospace structural design offers a few common uncertainty sources in the literature. Material properties have always been popular choices for parameter uncertainty in UQ applications [34][76][104]. It has become even more popular with the expanding use of composites, and consequently the material definition design space has also expanded. The flexibility offered by composites also brings many more sources of uncertainty when compared to traditional metals. Non-heterogeneous material properties, directional stiffness, layup configurations, manufacturing considerations are some examples where variability can occur [177][65][99][175]. Chapter 1 mentioned the importance of stress allowables and margins of safety in structural design and risk. In fact margins of safety were created for this very purpose, to account for the uncertainty before UQ became a commonly used design and analysis tool, but mostly limited to research. They are typically predesignated by subject experts but there is a great deal of uncertainty in the values themselves [167][158]. Many argue there is too much conservatism in their use, especially given the same values have been used for decades in some applications.

Although the other uncertainty sources mentioned have been shown to be both significant and relevant in the literature, they do not directly result in variability in

the external load calculations. Thus the final choices for uncertainty sources considered in this thesis are related to aerodynamic fidelity and load case parameters. Due to the novelty in applying these sources to loads analysis, it's not clear how significant they will be in terms of response uncertainty. But the beauty in UQ is that it supplements or sometimes even circumvents expert knowledge by quantifying the significance and relevancy through sensitivity analysis which will be discussed in more detail in Section 3.5.2.

3.3.2 Modeling

The uncertainty sources to be examined in this work were identified. The next step is to determine how the uncertainty will be represented in a modeling environment. Probability-based methods have long since dominated the field of UQ [157] for aleatory sources. Dealing with uncertainty and error is the basis behind probability and statistics so it is natural that many methods are based on its theories. Epistemic uncertainty on the other hand has not received a general consensus on how to represent it. Thus two general categories exist for modeling epistemic uncertainty; probabilistic and non-probabilistic.

Probabilistic methods are based on the theory of probability, or the analysis of random variables. Two key assumptions are made when using probability in most UQ methods; the uncertainty in question is indeed random and it can be accurately represented by a distribution function. Most often a probability density function (PDF) is chosen to model the uncertainty source. Probability density functions are mathematical functions of continuous random variables which represent the likelihood of an event to occur. The integration of the PDF over a range of values gives the probability of the random variable falling within the given range. An expert who is very familiar with a given system and uncertainty source will assign a distribution

which most reflects the variation or physical nature of the error. Because this assignment is subjective and the resulting response error is highly dependent on the choice of distribution, probabilistic methods have received some skepticism [145], though it is still widely accepted and used in the UQ community.

One probability-based approach for modeling epistemic uncertainty has received wide acceptance in the UQ community: Bayesian methods. Their view on probability differs from the traditional frequentist view and instead take a subjective view [139], which has led to its acceptance. These methods also avoid the aforementioned pitfalls of relying on assumed probability distributions because these distributions are updated when new data becomes available. Bayesian methods will be discussed in more detail in Section 3.4.

The aforementioned reliance on choosing the "right" input distribution has fueled non-probabilistic methods. Also, probabilistic methods are well suited for studying parameter uncertainty because they are inherently concerned with the effects of variation. In contrast, model uncertainty is concerned with the effect of knowledge, or the lack there of, in a model, simulation or analysis. Some would argue that probability cannot capture the knowledge of a model due to its fundamental definition [157]. This idea has also caused non-probabilistic methods to become more popular, given the increasing importance weighted to epistemic uncertainty. The most widely used non-probabilistic methods are interval analysis, possibility theory, evidence theory and fuzzy logic. Each of these have fundamental differences between each other and some have been shown to be generalizations of probability theory [147]. They primarily deviate from probability because they are based on the concept of incomplete information where probability assumes complete information [20] about the problem and its modeling. For example, possibility theory provides a mathematical foundation to quantify the notions of "possibility" and "necessity" and to combine opinions of different experts which led to the concept of fuzzy sets [180]. Evidence theory provides a

mathematical foundation to quantify the notions of "plausibility" and "belief" which is based on Dempster-Shafer theory of evidence [146].

Another type of non-probabilistic model is deterministic uncertainty, where the uncertainty parameters are modeled as constants which may change. All aforementioned models were nondeterministic. Deterministic uncertainty is modeled in the following form:

$$\mathbf{f} = \mathbf{f}(\mathbf{x} + \boldsymbol{\gamma}, \boldsymbol{\alpha}) \tag{2}$$

where $\mathbf{f}$ is a function dependent on $\mathbf{x}$ control variables, $\boldsymbol{\gamma}$ represents uncertainty related to production tolerances or sensor and actuator imprecision, $\boldsymbol{\alpha}$ represents uncertainty related to a changing environment and operating conditions [20]. Some have argued and demonstrated that non-probabilistic methods can still be utilized in conjunction with probability [157]. For example, utilizing probability for parameter uncertainty and evidence theory for model uncertainty for the same system.

The purpose of this work is not necessarily to advance the theory of any UQ method. In the literature many argue about the fundamental theory behind many of the non-probabilistic methods and how they compare to probability. Though important, these nuances are not critical to the development of the proposed methodology. Therefore the ease of understanding and implementation of the chosen method are of paramount concern given its computational expense is feasible. Probability is much more utilized and easily understood by the general aerospace community than it's non-probabilistic counterparts. The ability to assign a mean, variance, and confidence interval to the structural weight response which can be immediately comprehended by a user without further background knowledge is of great importance. As discussed in Section 3.2 both uncertainty sources lend themselves well to probability. Therefore the modeling of aerodynamic fidelity and and load case parameter uncertainties will

be done using a probabilistic approach.

3.3.3 Propagation

The modeling method influences the propagation method, for example a probabilistic approach to uncertainty modeling calls for probabilistic propagation methods. Only probabilistic uncertainty propagation methods will be discussed here.

As the name describes, propagation methods transfer the uncertainty in the input through the system and onto the response. Probability-based methods sample the input probability density functions and propagate these distributions to the system outputs. The resulting response data is collected and fit to a PDF. Depending on the type of distribution, the uncertainty is quantified by the parameters of the PDF or by calculating statistical confidence intervals.

The propagation method is applied to the system, so for computer experiments this may involve calling a mathematical function or software representing an analysis method. Some of the propagation methods to be discussed require a large number of sample points to accurately fit the response distribution and thus prohibit expensive function calls. This leads to the question of which sampling subject should be used for the propagation. Instead of calling the analysis method itself, a surrogate model can be sampled instead and significantly reduce the computational cost because it is an analytical function. As usual, the tradeoff for speed is accuracy. This begs the question, how accurately can a surrogate model represent the actual analysis? If an accurate surrogate can be created, this is usually the preferred method over directly calling an expensive analysis. There are several types of surrogate models which have been shown to be quite accurate for certain systems. The most widely used are response surface equations (RSE's), artificial neural networks (ANN's), and Kriging (Gaussian Process Models) [151].

As discussed, the sampling subject often enables certain propagation methods. If an accurate surrogate model can be used or the analysis itself is computationally inexpensive, one of the simplest and most popular methods is Monte Carlo. Monte Carlo involves sampling one or more input distributions many times until enough response data is collected to fit a probability density function. The response of a deterministic analysis can be treated as non-deterministic, and thus it's uncertainty can be assessed in a probabilistic sense. The shear number of samples required to fit the response data makes Monte Carlo infeasible for even moderately expensive analysis methods in many situations. But with enough data points the response distribution can be very accurately resolved, which justifies its wide use.

A class of methods derived from Monte Carlo are referred to as Quasi-Monte Carlo methods. Instead of sampling a probability distribution with a sequence of pseudorandom numbers, these methods use low-discrepancy sequences. Halton and Sobol sequences are examples of low-discrepancy sequences, the latter will be used in this work for sensitivity analysis. These are not random and result in more evenly space samples which lead to lower convergence rates compared to Monte Carlo [13]. Due to the fact that the method is deterministic it can be more difficult to estimate the error or variance, which is of utmost importance in UQ.

The expense of Monte Carlo methods and its derivatives have led to methods which attempt to approximate a distribution at the cost of accuracy. In the field of reliability several methods exists: First Order Second Moment (FOSM), First Order Reliability Method (FORM), and Second Order Reliability Method (SORM). Other methods include Fast Probability Integration, Point Estimation Method, and Global Sensitivity Equations. Stults (2009) [157] gives a qualitative comparison of these methods for a multifidelity analysis selection problem framework which is repeated here in Figure 7. The criteria used in this comparison are: the amount of time needed to use the method, ability to handle non-monotonic models, ability to handle higher

order problems, and scalability of the method in terms of time required and quality of result. Although a different set of criteria would be used in this work, these figures of merit are still important so this qualitative study can be used as a starting point for evaluating different propagation methods.

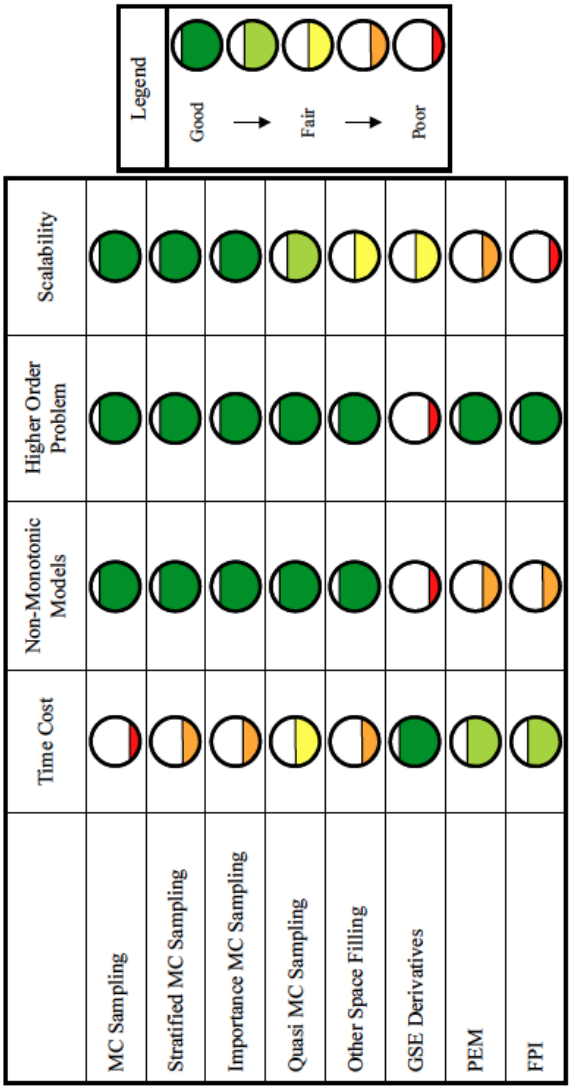

Figure 7: Qualitative Comparison of Uncertainty Propagation Methods [157]

3.3.4 Uncertainty Reduction and Management

In the problem formulation one of the limitations of the current approach to loads analysis is relying on expensive experiments such as wind tunnel tests to provide calibration data as a form of uncertainty reduction. Physical experiments are thus a classic method for uncertainty reduction. Other similar practice include calibration, verification and validation. To provide high quality data which can maximize uncertainty reduction these experiments must be done on full scale systems which accurately simulate the systems' environment. This is difficult and costly for aerospace systems and so computationally-based methods will be pursued instead in this work.

Based on a review of the literature on uncertainty reduction one way to classify these methods is based on the source of uncertainty. If the uncertainty source is due to variability, i.e. aleatory uncertainty, then specific methods are usually applied. It was mentioned earlier that aleatory uncertainty is irreducible. Though true, the resulting system response uncertainty can be made to be less sensitive to the variability in the inputs. These types of approaches are classified as robustness methods [176]. If instead, a criteria is set in which a solution must achieve a minimum probability of success in the presence of variation then this approach is considered a reliability method [68]. Although these are both popular forms of design optimization under aleatory uncertainty, the nature of epistemic uncertainty has spawned other approaches to uncertainty reduction.

Another broad category of uncertainty reduction approaches can be classified as multifidelity methods. As the name suggests, these methods utilize varying levels of fidelity or the inclusion of information and data to reduce uncertainty. A popular multifidelity approach is to represent a computationally expensive system or analysis with an approximation or surrogate model which can be orders of magnitude quicker to solve and still capture the main effects of the underlying analysis. An example of this is using polynomial chaos to construct the low fidelity model [10]. Another

approach stems from information theory and seeks to determine where in a system there is a lack of information or data. A popular technique is the treatment of entropy as a measure of uncertainty with the goal of maximizing it to decrease uncertainty [24]. One of the more common multifidelity approaches is to use Bayesian methods to incorporate data from varying fidelity analyses in order to reduce uncertainty [82].

Reducing uncertainty can be accomplished with one of the aforementioned approaches but none of them alone focuses on if uncertainty sources should be reduced. The *if* depends on the magnitude of the impact of the source on the responses of interest and what resources are available to reduce the uncertainty. The impact can be assessed with sensitivity analysis which is standard practice in UQ but the consideration of resources is typically overlooked in the literature. Uncertainty management thus involves both the reduction of uncertainty and decision-making [101]. Uncertainty management is already a much smaller research area in UQ, but uncertainty management approaches in engineering which also involve financial considerations is even smaller. A promising approach which will be discussed in more detail is resource allocation and stems from Quantification of Margins and Uncertainty (QMU). QMU methods were first developed out of Sandia National Laboratory to design nuclear reactors but has grown and been applied to other fields [61][167] [168]. The resource allocation methodology is Bayesian-based and will be discussed in Section 3.5.

3.3.5 Conclusion

The research goal for uncertainty quantification given in Chapter 1 is to develop a methodology to quantify epistemic and aleatory uncertainty due to aerodynamic fidelity and load case parameters respectively. UQ in conjunction with sensitivity analysis enables the user to see which sources affect the uncertainty in the response the most. Thus the impact of analysis choices is quantified with respect to uncertainty.

In addition, UQ will help determine where to focus analysis resources in downstream load cycles and design phases. For example, load cases which are critical and also cause large variability should be explored with higher fidelity tools during detailed design.

An overview of UQ methods was given in this chapter. Although aerodynamic fidelity has been explored, its effect on loads analysis has not been. This gap will be addressed by applying existing UQ methods to loads analysis. Existing methods consist of techniques to model uncertainty and to propagate it to system responses. Probability-based propagation techniques were discussed; Monte Carlo, Quasi-Monte Carlo and distribution approximation methods. Some propagation methods are exhaustive require surrogate modeling to be computationally feasible. Popular surrogate models were listed. Bayesian methods offer accepted probabilistic approaches for epistemic uncertainty and easily integrate with aleatory uncertainty. Therefore Bayesian methods will be explored in this work and discussed in the next two sections.

3.4 Bayesian Methods for Uncertainty Quantification and Reduction

Several candidate methods were previously explored to reduce epistemic uncertainty. Bayesian methods were a natural choice because of their use of probability which aligns well with the probabilistic aleatory uncertainty sources. Their ease of understanding has led to their popularity and use in numerous fields, including aerospace engineering. Having a large body of published work on such methods also makes them an ideal choice. In the section some basic concepts are introduced and the Bayesian methods utilized in this thesis are discussed, specifically Bayesian inference and Bayesian networks.

3.4.1 Bayesian Inference

All Bayesian methods and theory are related to the work developed by Reverend Thomas Bayes and expounded upon and originally published by Richard Price in 1763 [19]. Bayes' theorem (or Bayes' rule) takes advantage of the law of conditional probability and is used to determine the probability of an event based on prior knowledge of evidence related to the event:

$$P(A|B) = \frac{P(B|A)P(A)}{P(B)} \tag{3}$$

where the probability of event A is calculated with the condition that event B occurs.

Such a simple formulation has developed into a entire field of probability and statistics with wide-ranging applications. Bayesian statistics utilizes one interpretation of probability in which evidence about an event are assigned probabilities which reflect their degree of belief. This degree of belief can be altered when new evidence becomes available, which is known as Bayesian inference [139]. Bayesian inference is one of the most powerful and popular applications of Bayesian methods because it allows us to make initial assumptions about the uncertainty of quantity and then update this uncertainty based on new data. Such data can be based off of experimental tests, numerical analysis, simulation, survey, etc. For an uncertain continuous random variables θ, Bayesian inference can be expressed as:

$$f''(\theta) = \frac{L(\theta)f'(\theta)}{\int L(\theta)f'(\theta)d\theta} \tag{4}$$

$f'(\theta)$ is known as the prior probability distribution of θ and expresses all the current knowledge available about the variable. $f''(\theta)$ is known as the posterior probability distribution and is conditioned on the existence of evidential data related to θ. $L(\theta)$ is known as the likelihood of θ and is proportional to the probability of the evidence

conditioned on θ.

In the context of loads analysis, the uncertainty in a given aerodynamic parameter is assumed prior to the load cycles and may be based on past airplane development programs or wind tunnel calibration data, the latter is explored in this work. The uncertain parameters are also dependent on the aerodynamic analysis using during the load cycles. Initially we assume a certain aerodynamic fidelity level but then may wish increase the fidelity in order to reduce uncertainty. If the higher fidelity analysis is run the resulting data can be used in Bayesian inference to update the prior distributions and calculate the parameters' posterior distributions.

The likelihood function is an important consideration in using Bayesian inference. Although a similar concept, *likelihood* is different from *probability* in statistics. In the context of parameters, probability describes potential future outcomes of a fixed parameter prior to having data to fully determine the outcome. Likelihood describes how likely a parameter describes an outcome after some evidential data is available. The concept of likelihood has been informally used for centuries until a rigorous formulation was described by Fisher in 1922 [48]. The integration of the likelihood function does not equal one so it does not follow the laws of probability. Because of this the magnitude of the function is only important in a relative sense.

The most widely used aspect of likelihood is the maximum likelihood estimation (MLE) of a parameter. But unlike MLE, the entire function is utilized in Bayesian inference to construct the entire posterior distribution, not simply the maximum value. For a given response function $\boldsymbol{y}$ which is dependent on input variables $\boldsymbol{x}$ and uncertain parameters $\boldsymbol{\theta}$, observed data for the response $\boldsymbol{y_D}$, and an assumed Gaussian observational error with zero mean, the likelihood function can be written as:

$$L(\boldsymbol{\theta}) = P(D|\boldsymbol{\theta}) = \prod_{i=1}^{n} \frac{1}{\sigma\sqrt{(2\pi)}} exp - \left[\frac{(\boldsymbol{y_{D,i}} - \boldsymbol{y_i}(\boldsymbol{x_i}, \boldsymbol{\theta})^2}{2\sigma^2}\right] \tag{5}$$

where σ is the standard deviation of the observation error and can be assumed or treated as an uncertain parameter and updated using Bayesian inference.

The denominator of Equation 4 is a normalizing constant which ensures the posterior distributions integrates to unity. The posterior distribution, like the likelihood function, is only known up to a proportionality constant which in this case is equal to the integral function [141]. If there are multiple uncertain parameters this integration can be computationally intensive. Thus numerical methods such as Markov Chain Monte Carlo can be utilized to draw samples and construct the posterior distribution. This numerical approach is discussed in the next section.

3.4.2 Markov Chain Monte Carlo Sampling

Markov Chain Monte Carlo (MCMC) sampling methods are class of algorithms which are specially suited for constructing probability distributions known only up to a proportionality constant, which is the case for Bayesian inference. The algorithm is used to construct a Markov chain whose equilibrium distribution fits the intended posterior distribution. The chain evolves after a number of steps and when converged can be used to sample the posterior. Increasing the number of steps size increases the quality of the fit for the posterior distribution. MCMC are popular methods for Bayesian inference by drawing samples of the posterior distribution by numerically approximating Equation 6.

$$f''(\boldsymbol{\theta}) \propto L(\boldsymbol{\theta}) f'(\boldsymbol{\theta}) \tag{6}$$

A Markov chain is a type of discrete Markov process. A Markov process is a random process where the future independent, in a stochastic sense, of its past behavior. Thus the process in the future is only predicted based on the current state and not the past. [57]. The process moves through a sequence of random variables which

is called a "chain". Markov processes are named after Andrey Markov who studied such processes as a doctoral student in Russia and published a foundational paper in 1906 [91]. The *Monte Carlo* in MCMC refers to the sampling method used to draw samples from the Markov Chain after it has converged to approximate the desired distribution.

There are number of algorithms classified as MCMC. Two popular methods are implemented into MATLAB's Statistics and Machine Learning Toolbox; the *Metropolis-Hasting* and *Slice* sample algorithms. MATLAB documentation [161] summarizes the two approaches and excerpts are included here. For the Metropolis-Hastings algorithm:

> "Random numbers are generated from a distribution with a probability density function that is equal to or proportional to a proposal function... To produce quality samples efficiently with the Metropolis-Hastings algorithm, it is crucial to select a good proposal distribution. If it is difficult to find an efficient proposal distribution, use the slice sampling algorithm without explicitly specifying a proposal distribution."

In this work MCMC will be used to construct the posterior distributions of uncertain aerodynamic parameters which are NASTRAN's empirical adjustment factors. It is unclear what the posterior distributions will look like, so the advantage of not specifying a proposal distribution in the Slice sample method is very attractive. The algorithm is summarized as:

> "In instances where it is difficult to find an efficient Metropolis-Hastings proposal distribution, the slice sampling algorithm does not require an explicit specification. The slice sampling algorithm draws samples from the region under the density function using a sequence of vertical and horizontal steps.

First, it selects a height at random from 0 to the density function $f(x)$. Then, it selects a new x value at random by sampling from the horizontal 'slice' of the density above the selected height. A similar slice sampling algorithm is used for a multivariate distribution... Slice sampling can generate random numbers from a distribution with an arbitrary form of the density function, provided that an efficient numerical procedure is available to find the interval $I = (L, R)$, which is the 'slice' of the density."

The implementation of the Slice sample method used in MATLAB is summarized and quoted below [107] [161]:

"For a function $f(x)$ proportional to the density function is given, then do the following to generate random numbers:"

Step 1: "Assume an initial value $x(t)$ within the domain of $f(x)$."

Step 2: "Draw a real value y uniformly from $(0, f(x(t)))$, thereby defining a horizontal 'slice' as $S = x : y < f(x)$."

Step 3: "Find an interval $I = (L, R)$ around $x(t)$ that contains all, or much of the 'slice' S."

Step 4: "Draw the new point $x(t + 1)$ within this interval."

Step 5: "Increment $t \rightarrow t + 1$ and repeat steps 2 through 4 until you get the desired number of samples."

After sampling, the posterior distribution is constructed using a nonparametric Kernel density estimation approach [130]. In general MCMC methods have been a key enabler for Bayesian inference for large problems which may include hundreds of uncertain quantities. When expensive "black box" analyses are dependent on these uncertain quantities, surrogate modeling is almost a prerequisite to implement Bayesian

methods. Surrogate modeling techniques used in this thesis will be discussed in more detail in Section 6.3.1.

3.4.3 Bayesian Networks

In uncertainty quantification the propagation of uncertainty from inputs to outputs is referred to as the *forward problem*. Propagation techniques such as Monte Carlo were introduced in Section 3.3.3. The process of inferring the uncertainty of an input is known as the *inverse problem*. Such techniques include Bayesian inference discussed in the previous section. In some applications both the inverse and forward problems are solved and utilized to quantify uncertainty. When such applications are large, complex or include multiple sources of uncertainty Bayesian networks are often employed.

A Bayesian network is a probabilistic directed acyclic graphical (DAG) model which represents the conditional dependencies, in a statistical sense, between variables or parameters which are uncertain [139]. Each uncertain quantity is a random variable and represented as a node. The links, or edges, represent conditional dependencies. As with other DAG's the edges in a Bayesian network are unidirectional (*directed*) and thus there is no way to start at a particular node and end up back at the beginning (*acyclic*). Disconnected nodes represent quantities which are conditionally independent.

A probability density function (PDF) is assigned to each uncertain node and affects the subsequent distributions of all other nodes dependent on it (i.e. its *child* nodes). These assigned probability distributions are viewed in the Bayesian interpretation of probability and therefore can be updated with new or simulated evidence. The term "Bayesian network" was first coined by Judea Pearl in 1985 [116]. Since their inception, Bayesian networks have become quite popular and used in wide-ranging

fields and applications.

Bayesian networks often carry our the inverse and forward problems to accomplish three main goals: inference, parameter learning and structure learning. The first has been already been discussed in Section 3.4.1 and can efficiently be employed in Bayesian network software to update many unobserved nodes with data from other observed nodes based on approaches such as MCMC and others. A node is referred to as *observed* if evidential data exists for the quantity. *Parameter learning* is used to estimate an unknown parameter based on other observed nodes. Parameter learning differs from inference because it is intended to estimate a finite value for a parameter while inference determines the new uncertainty of the parameter. In other words, learning maximizes some statistical quantity, such as maximizing the probability or likelihood, to estimate the parameter and inference constructs the posterior distribution given new evidence. Often methods such as maximum likelihood estimation are used to learn a parameter. Finally, *structure learning* uses algorithms to determine the conditional dependencies, i.e. the structure, of a Bayesian network given data [122]. For extremely large and complex problems it would be intractable for a human to construct an appropriate network, especially because there are many ways to define the same problem using such networks.

There a several types of Bayesian networks used to carry out the three aforementioned tasks. The choice of type depends on the system being represented by the network. If a system changes with time dynamic Bayesian networks (DBN) can be used to model it and relate variables over adjacent time steps. A DBN uses a state-space model representation and utilizes specific algorithms to carry out inference and learning between states for dynamic systems. Popular types of DBN's are Hidden Markov Models (HMM) and Kalman filters. In fact, DBN's were first developed by Paul Dagum in the early 1990's to unify and extend these popular methods in a general probabilistic graphical representation and be able to carry out inference [37].

3.4.4 Conclusion

In Section 3.3 several approaches were discussed to quantify and reduce epistemic uncertainty. Bayesian methods were selected for their probabilistic nature and popularity in statistics and machine learning. In this section an overview of Bayesian methods was given and particularly Bayes' theorem, Bayesian inference and Bayesian networks were discussed. Bayesian inference will be utilized in the proposed approach to reduce epistemic uncertainty in aerodynamic empirical adjustment parameters by updating the parameters' prior distributions using data from simulated higher fidelity aerodynamic analysis. Two algorithms were briefly discussed to draw samples from the posterior distribution based on Markov Chain Monte Carlo sampling. Slice sample is the more attractive method because it does not require a proposal distribution to approximate the posterior. Some drawbacks are the performance of the algorithm is highly dependent on certain parameters which can be difficult to intuitively estimate apriori. Nevertheless Slice sample will be the default approach used in the experimental plan.

Both the inverse and forward problems are necessary in the proposed approach. The epistemic uncertainty will be reduced in the inverse problem and the updated posterior distributions of the empirical adjustments will be used to propagate uncertainty to the rework response in the forward problem. A Bayesian network will be used to carry out the inverse and forward problems and quantify uncertainty in the system-level response based on all aleatory and epistemic sources. Bayesian networks are commonly used to carry out the tasks of inference and parameter learning. Only inference will be of importance in this work because we are more interested in the effect of the empirical adjustments on rework than explicitly specifying their values. In large complex systems it can be difficult to determine the conditional dependencies

required for a Bayesian network. In these cases the structure can be *learned* using data and appropriate algorithms. In this work, the dependencies are simple enough to characterize beforehand so structure learning won't be employed.

In reality the design environment changes in each cycle of the loads process. As the design matures in the cycles, for example, the structural definition becomes more refined, additional load cases are added to the analysis, customer requirements may change, etc. Thus the loads process is a dynamic process. For simplicity a static environment will be assumed to develop the rework decision framework. Thus the use of dynamic Bayesian networks is not necessary in this work. For future work, the dynamic design environment will be included and DBN's or other Bayesian methods for dynamic systems should be explored further.

3.5 Resource Allocation Optimization for Uncertainty Management

Uncertainty reduction is an important part of the rework decision framework. To properly address rework, accurate assessments of failure need to be obtained. With numerous sources of uncertainty it is not feasible to target all sources when resources are limited. In Section 3.3.4 several candidate methods for uncertainty management were discussed to reduce epistemic uncertainty under constrained resources. Resource allocation optimization was chosen as a promising uncertainty management method because of its use of Bayesian methods which were previously selected for uncertainty reduction, flexibility for various types of problems, simple problem formulation and ease of implementation. In this section the details of the resource allocation approach are outlined.

3.5.1 Resource Allocation Methodology

The term "resource allocation" has been applied to a number of fields including economics, strategic planning, computer engineering and information technology. Often in these contexts resource allocation deals with scheduling and assigning resources as they become free from doing certain tasks. But generally, resource allocation deals how best to assign or distribute available resources to accomplish some goal. In this thesis *resource allocation* refers to a specific methodology for reducing epistemic uncertainty in engineering design problems via constrained optimization. To the authors knowledge, the methodology utilized in this framework is based off of the original work of Urbina et al (2010) [167] and further developed by Sankararaman [137], both from Vanderbilt University under Dr. Sankaran Mahadevan.

The work of Urbina et al came out of efforts from Sandia National Laboratories to perform quantification of margins and uncertainty (QMU) and focused on optimizing experimental tests to reduce uncertainty. Multiple parameters across multiple levels of models and tests were not calibrated in this work. Sankararaman generalized the approach to hierarchical systems by using "all available component-level models and data to quantify the uncertainty in the system level performance prediction" [141]. This is important because physical tests can be expensive at higher levels in the system hierarchy due to increased complexity. It may not be feasible to perform tests at the system level so data from tests at lower levels must be incorporated into the uncertainty assessment at higher levels. Sankararaman et al was able to apply the resource allocation method to several types of problems including multidiscipline, mult-level, and feedback-coupled problems which are all applicable to the loads analysis.

The methodology attempts to answer two questions: First, what type of test or experiment should be conducted to reduce the uncertainty (e.g. wind tunnel test of a specific load case)? and secondly, how many repetitions of each type should be

conducted (multiple repetitions creates more calibration data and accounts for experimental errors)? To answer these questions an optimization is done to determine the distribution of tests to minimize the variance in the system level response. Each type of test has an associated cost and so the optimization is constrained based on a fixed budget. The method relies on Bayesian networks for inference and propagation of various sources of uncertainty in complex systems. Due to the expense of performing tests, experimental data for inference is simulated with multiple realizations. The general steps for the methodology are described below:

Step 1: Design and construction of Bayesian network

Step 2: Sensitivity analysis and dimensionality reduction

Step 3: Bayesian inference

Step 4: Resource allocation optimization

Both Bayesian networks and Bayesian updating were discussed in Section 3.4. For resource allocation the Bayesian network must include observed nodes which supply the evidence to update the uncertain nodes. For example in Figure 8 the square nodes represent observed data for the subsystem responses Y_1 and Y_2. D_{Y_1} and D_{Y_2} will be used in Bayesian inference to update the uncertain parameters Θ_1 and Θ_2. In this figure Z is the system-level response and X_1 and X_2 are design variables.

As with all Bayesian networks all uncertain quantities must be identified and their relationships to component-level, subsystem-level, and system-level responses established. In addition, the Bayesian network allows for integration of other uncertain sources such as model errors, measurement errors, surrogate modeling errors etc. and these must be included in the structure of the network. As was mentioned, if systems are particularly large and/or complex structure learning algorithms can be used to aid in designing the structure.

The actual construction of the Bayesian network is heavily software dependent. There are number of software specifically for designing, building and executing inference and learning for various types of Bayesian networks. Capabilities have also been added in well-known programs to handle them. In this work the construction was done in MATLAB to fit into the overall design environment. Although some 3rd-party toolboxes have been developed for Bayesian networks in MATLAB, these were not utilized here. Instead the Bayesian network is implemented by linking several surrogate models together to represent subsystem and system level responses in loads analysis. The inverse problem is solved with the MATLAB MCMC methods previously discussed and the forward problem is solved with Monte Carlo sampling of the surrogate models. More details on the specific types of surrogate models used in this framework will be discussed in Section 6.3.1 of the Experimental Plan and Results chapter.

Steps 2 and 4 will be discussed in more detailed along with other important aspects of the methodology in the following sections.

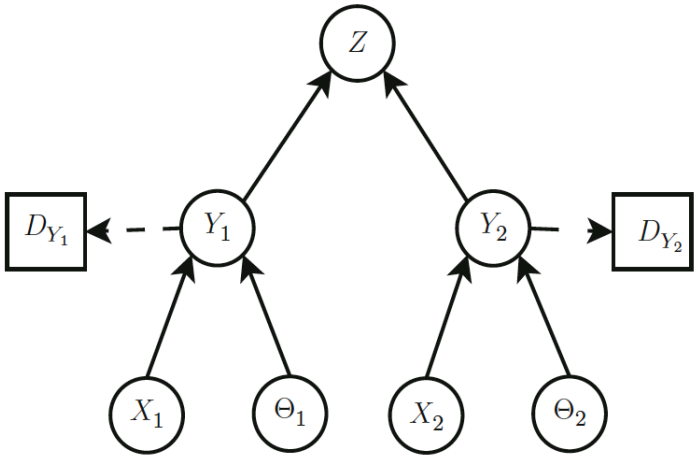

Figure 8: Example Bayesian network [139]

3.5.2 Sensitivity Analysis and Dimensionality Reduction

Bayesian inference is carried out at each step in the optimization in order to evaluate the system response uncertainty. This can be expensive even for problems with only a few uncertain parameters. Thus Step 2 is important to identify which types of tests should be conducted to maximize uncertainty reduction. Sensitivity analysis can accomplish this. Traditional derivative-based sensitivity methods only calculate local sensitivity which cannot capture the effects of uncertainty from multi-level sources at the system level. *Global* sensitivity analysis (GSA) on the other hand can appropriately apportion variance at the system level in such systems and provide information for identifying significant sources of uncertainty and the corresponding tests to mitigate them [135].

GSA is based on the second moment and calculates the effect of each input on the variability of the output, which is a measure of uncertainty [84]. For a given response $Y = G(X_1, X_2, ...X_n)$, with X_i inputs the first order sensitivity indices are given by:

$$S_i = \frac{V[E(Y|X_i))}{V(Y)} \tag{7}$$

where V and E are the variance and expectation respectively. The sum of first-order indices of all variables is always less than or equal to unity. The first-order index represents the main effect contribution of each input factor to the variance of the output.

Interactions between inputs can have significant impacts on the response itself and its uncertainty [176], so higher order sensitivity indices can be calculated which measure the impact of uncertainty caused by the interactions of two or more variables. It is necessary to specify each interaction to calculate higher-order indices, which can be cumbersome for large problems. Instead the *total* effects index can be calculated

and measures the sum of the main effect plus all other higher order interaction terms involving the variable. The total effects indices are given by:

$$S_{T_i} = 1 - \frac{V[E(Y|X_{\sim i}))}{V(Y)} \tag{8}$$

Saltelli et al (2008) suggest an efficient approximation to calculating Equations 7 and 8, otherwise Monte Carlo can be used but may require multiple loops and become quite expensive. The suggested approximation is utilized in the experimental plan. The useful properties of these indices are summarized by the authors and quoted here [135]:

- "Whatever the strength of the interactions in the model, S_i indicates by how much one could reduce, on average, the output variance if X_i could be fixed; hence, it is a measure of main effect."
- "By definition, S_{T_i} is greater than S_i, or equal to S_i in the case that X_i is not involved in any interaction with other input factors. The difference $S_{T_i} - S_i$ is a measure of how much X_i is involved in interactions with any other input factor."
- "$S_{T_i} = 0$ implies that X_i is noninfluential and can be fixed anywhere in its distribution without affecting the variance of the output."
- "The sum of all S_i is equal to 1 for additive models and less than 1 for nonadditive models. The difference $1 - \Sigma_i S_i$ is an indicator of the presence of interactions in the model."
- "The sum of all S_{T_i} is always greater than 1. It is equal to 1 if the model is perfectly additive."

It should also be noted that the indices can be negative using this formulation. The authors mention negative indices are a result of numerical error and occur when analytical sensitivity indices are approximately zero. Therefore variables with negative values are deemed unimportant. Increasing the sample size when evaluating Equations 7 and 8 reduces the chances of producing negative indices.

Sensitivity analysis identifies significant uncertain inputs which influence outputs. What the user does with this information is problem dependent but often it is used to reduce the size of a problem or model. For resource allocation this is important because although Bayesian networks represent a wholeistic approach to uncertainty modeling and quantification, the inverse and forward problems can be expensive for large problems. Even when surrogate modeling is used to drastically improve the computational cost, fitting large amounts of surrogates can still require sampling of expensive analyses. Minimizing the size of the Bayesian network can help improve efficiency and surrogate modeling.

Reducing the problem can be achieved in the realm of machine learning and data mining, and is referred to as dimensionality reduction [131]. Machine learning generally describes a field in computer science and statistics which gives computers the ability to learn without being explicitly programmed through algorithms which can learn from data to make predictions [136][75]. Dimensionality reduction differs from typical sensitivity analysis techniques because it utilizes training data to learn and the predicted responses to determine important inputs by analyzing the accuracy of the prediction with separate test data.

The dimensionality reduction process can usually be segmented into reducing the number of factors (features), called feature selection or transforming higher dimensional problem into a lower dimensional space, called feature extraction [121]. Feature selection can be achieved with variable screening techniques from statistics such as ANOVA, normal quantile plots, Lenth's Method and stepwise regression [176].

In machine learning, feature selection is the combination of a search technique for proposing a new subset of features, along with an evaluation measure to score the different subsets. Three categories of feature selection algorithms are wrappers, filters and embedded methods which are distinguished by the evaluation measure [59].

In wrapper methods a predictive model is used to evaluate the score and determine the feature subset. The model is built on a subset of the data and an error rate based on the number of misclassified points. The misclassification (error rate) is calculated from hold-out data within the subset and is the subset score. Statistical stepwise regression is a type of wrapper method where a regression model is built by systematically adding and removing factors from the model. Filter methods use a proxy measure as the evaluation criteria to capture essential information of the feature subset without the computational cost compared to wrapper methods. Common proxy measures are based on mutual information, correlation coefficients and significance tests [179]. Embedded methods generally describe models which embed feature selection into how the original model is constructed. A commonly used embedded method is the LASSO method (least absolute shrinkage and selection operator) in which certain coefficients of a linear model are penalized and reduced to zero so only a subset of non-zero coefficients remain [163]. Feature selection will be utilized to reduce the number of uncertain empirical adjustment parameters in the aeroelastic analysis to improve surrogate modeling.

Feature extraction essentially involves mapping a group of features to a new smaller set of features. The new feature set is intended to retain the relevant information from the original features. The problem dimension reduction should improve computational efficiency and sometimes improve interpretation by using the simpler model. The most common example of feature extraction for linear models is principle component analysis [43]. Feature extraction will be used to reduce the number of

coupling variables in the Bayesian network representation of the loads analysis process. Sensitivity analysis and dimensionality reduction will be important methods to improving the rework decision framework and making it computationally feasible to implement for real-world large and complex problems.

With a combination of global sensitivity analysis and dimensionality reduction the significant tests are identified and included in as compact a Bayesian network as possible to improve efficiency and maximize uncertainty reduction. Step 2 is critical to making the resource allocation optimization feasible for realistic problems.

3.5.3 Objective Function and Constraints

Sankararaman et al suggests two formulations of the optimization problem; one uses the system-level response variance as the objective function and test budget as the constraint and the other minimizes the test cost subject to a constraint on the variance reduction. The former is utilized in this work. The problem is posed as the following:

$$\begin{aligned} \underset{N_{test}}{Minimize:}\ & E[Var(R)] \\ s.t.:\ & \Sigma_{i=1}^{q}(C_i N_i) \leq TotalBudget \\ & N_{test} = [N_1, N_2, ...N_q] \end{aligned} \tag{9}$$

where $E[Var(R)]$ is the expecation of the varaince of the system-level response R, N_i is the number of tests conducted for the ith test, C_i is the cost of the ith test.

As stated previously, the tests and resulting test data are simulated and thus require multiple realizations. For each realization, Bayesian inference will be done based on N_{test} at a given step in the optimization and updated epistemic uncertainty along with aleatory uncertainty will be propagated to R. As such, R will be a distribution and the variance will be calculated for each realization. The expectation of

the variance will then be calculated from the aggregate of realizations for each step and minimized by the optimizer.

No rigorous definition for test costs is given in any of the work of Sankararaman related to resource allocation. The original work of Urbina applied the resource allocation method to an existing experiment which allowed them to use realistic cost estimates. The cost estimates themselves was never the focus in these publications which intentionally allows flexibility into how the user defines them. This is beneficial but also makes the total budget and test costs highly subjective. Comparing one test to another, only the relative cost is of importance and how those cost constrain the maximum allowable number of tests for a given budget.

3.5.4 Optimization Approaches

The resource allocation optimization is an integer problem with objective function which can be expensive given Bayesian inference is done for multiple realizations at each step. Thus Sankararaman et al suggest two approaches to decrease the computational burden. The first involves breaking the problem into multiple stages. Within each stage the optimal test distribution is found using an exhaustive search based on a portion of the total budget. The best solution of a given stage is used as a starting point in the following stage. Optimizing on the smaller budget limits the variable ranges for the integer problem and thus reduces the search space compared to the single large problem. Using the optimal previous stage results is equivalent to a greedy search between stages and in theory should allow the same optimal solution to be found after the final stage. The system response variance is reduced after each stage and there is typically diminishing returns as the number of stages increases. Thus the optimization problem can be terminated before the entire budget is exhausted which may result in some computational savings compared to a single exhaustive search.

Given a total budget for potential tests, the optimization problem is divided into j stages and each stage is allocated a budget of ϕ^j such that $\Sigma\phi^j = \textit{Total Budget}$. The multi-stage resource allocation optimization problem is posed as the following for the first stage:

$$\begin{aligned} &\underset{N^1_{test}}{Minimize:}\ E[Var(R)] \\ &s.t.: \Sigma^q_{i=1}(C_i N_i) \leq \phi^1 \\ &N^1_{test} = [N^1_1, N^1_2, ...N^1_q] \end{aligned} \tag{10}$$

where ϕ^1 is the budget allocation for stage 1, and N^1_{test} is the optimal experiment combination for the stage 1 budget ($= \phi^1$). For subsequent stages the search depends on the solution from the previous stage. For the jth stage, given budget allocation ϕ^j, the problem is posed as:

$$\begin{aligned} &\underset{N^j_{test}}{Minimize:}\ E[Var(R)] \\ &s.t.: \Sigma^q_{i=1}(C_i N^{j,new}_i) \leq \phi^j \\ &N^j_{test} = N^{j-1}_{test} + N^{j,new}_{test} \\ &N^{j,new}_{test} = [N^{j,new}_1, N^{j,new}_2, ...N^{j,new}_q] \end{aligned} \tag{11}$$

where the superscript new refers to the new test combination at the jth stage.

The second approach to increasing efficiency in this problem is to create a system level surrogate model for the response variance as a function of the N_i. To accomplish this a design of experiments (DoE) would be used to sample the test design space and then the surrogate model would be fit on the sample data. Optimization on the surrogate model would significantly decrease the computational cost of the problem. The accuracy of the solution would be subject to the quality of the surrogate model. Given the fact that surrogates may already be used to replace analysis methods, using a surrogate model of surrogate models can lead to large errors if care is not taken in

the fitting process. The design of exmperiments and surrogate modeling techniques used in this work will be discussed in Section 6.3.1.

The integer problem in resource allocation presents unique challenges for optimization algorithms so several potential methods will be briefly discussed. Discrete problems often eliminate gradient-based methods which can be very efficient. But such methods suffer from only finding locally optimal solutions and are highly dependent on the initial value. These algorithms are also ill-suited for stochastic problems which have random variations in the objective functions, also known as "noisy" functions. Stochastic problems are common in optimization under uncertainty but all uncertain systems are not stochastic.

Special algorithms have been developed specifically for noisy functions and also do not rely on analytic gradient information. Such methods can be categorized as direct search methods [20]. Stochastic approximation methods are in this category and use approximations to the Jacobian (gradient) and Hessian matrices of f along with an iterative update formula to find the next point which converges to the minimization of the expectation of some utility function [126].

Pattern search methods are a subset of direct search but use no derivative information, analytical or approximate. Instead these methods generate a set of search points based on a pattern, evaluate each of these search points in terms of the robust measure, than accept those points which are deemed improvements over the previous search points. The most popular pattern search method [17] is the simplex strategy developed by Nelder and Mead [108]. This classic method has been modified for noise by the works of D. Humphrey et al [62] and E. Anderson et al [8]. Metahueristic optimization is also in the category of direct search methods. They are designed to efficiently explore a large design space rather than search one path to the optimum. Some of the most popular metaheuristics are based on nature and evolutionary principles, such as genetic algorithms (GA).

Typically a genetic algorithm consists of the following procedures; initialization, selection, genetic operations and termination [174]. An initial "population" is set which represents the search space. The size of this population stays constant throughout the search so for the Inside-Out Method this population size can be determined based on how large the user expects the significant set to be. Because the size is an indicator of the level of risk or conservatism of the solution it can be determined in other ways as well. Each candidate solution has a set of properties which can be mutated and altered; traditionally, solutions are represented in binary strings of 0's and 1's which are its "chromosomes". In selection a fitness function will determine which members of the population are most fit and will survive to the next generation. The fitness function is akin to the objective function and will be based on the lowest margin of safety for each load case. The design space is explored via genetic operations which produce a new generation of the population. Two commonly used genetic operations are crossover and mutation. During crossover two members of the population will "mate" and produce a child solution which have some characteristics of both parents. During mutation one or more chromosomes are flipped in randomly chosen members of the population. If implemented each chromosome would represent a the number test conducted of a specific type. New generations are successively created until a termination criteria is met. There are many different modifications to genetic algorithms in the literature.

3.5.5 Conclusion

Uncertainty management allows the proposed framework to offer insight into decisions which may reduce uncertainty and lessen the probability of rework while under constrained resources. Of all the candidate approaches the resource allocation methodology suggested by Sankararaman et al [137] was chosen because of its use of

Bayesian methods, flexibility, published results with problems related to loads analysis and relative ease of implementation. The basics of this approach were discussed in this section. The general steps for resource allocation include the construction of the Bayesian network, sensitivity analysis, Bayesian inference and solving the resource allocation optimization problem. Each of these steps were discussed here or in previous sections.

The resource allocation methodology will be modified to apply to loads analysis in order to address rework. Sankararaman et al was only interested in minimizing the system-level variance because they were only trying to answer the questions of which experimental tests should be run and how many repetitions of each type. For starters, this work is not concerned with physical experiments but rather disciplinary analyses at increased fidelity who's data can be used to improve the accuracy of lower fidelity methods. In order to address rework properly, the load and structural margins must also be included in the uncertainty management system, but they do not impact the uncertainty in the rework response directly. Therefore the single objective of system-level variance will not be adequate. Despite this, the basic principals of the resource allocation method are still applicable.

Given the modified objective function, the approaches to solving the resource allocation problem may differ from the two methods originally suggested, namely the multi-stage approach and the system-level surrogate approach. The inclusion of load margin and structural margin variables in the optimization does not lend itself well to partitioning the budget for multiple stages. This approach works for number of tests because there is a cumulative effect on reducing the variance. Such a cumulative effect does not exist for the margins, even if they are treated as discrete. The system-level surrogate approach will be explored for loads analysis.

The modified resource allocation method requires gradient-free optimization just

as the original method so direct search algorithms will be explored. The optimization problem for rework may be posed as an integer problem if only discrete margin levels were assumed. A more natural approach would be to have the margins continuous and the fidelity level discrete. This would require an algorithm able to handle mixed-integer problems. MATLAB's Global Optimization Toolbox (R2016b) includes pattern search and genetic algorithm, but the former can only handle integer problems while the latter can handle integer and mixed-integer. These and potentially other algorithms will be explored further during experimentation.

In general, the resource allocation methodology offers a good starting point to for uncertainty management and building the rework decision framework for loads analysis. An overview of all the relevant background information has been presented in this chapter and the framework will now be posed in Chapter 4.

3.6 Conclusion & Research Gaps

The background and literature review for uncertainty quantification and management revealed several observations. These observations then led to research gaps which will be addressed in the experimental plan to contribute to the aerospace and scientific community. These research gaps are summarized below:

1. ***Loads Analysis***

   A comprehensive MDAO environment is not readily available for modeling load cycles in loads analysis and structural design

2. ***Uncertainty Quantification***

   A standard procedure does not exist for estimating the epistemic uncertainty in linearized lift curve slope due to compressibility

3. ***Uncertainty Management***

An established correlation between aerodynamic fidelity and design rework does not exist

4. ***Rework Decision Framework***

   A proactive rework mitigation strategy does not exist involving aerodynamic fidelity, load margins and structural margins for aeroelastic loads analysis which can be implemented in design phase

CHAPTER IV

PROPOSED APPROACH

The uncertainty quantification and uncertainty management system (UMS) are key components to the overarching methodology and its structure, from a conceptual standpoint, is referred here as "the framework". A description of the modeling and simulation (M&S) environment will be given in the next chapter to fill in the specific details of the framework. The upcoming section discusses an overview; one of the principal components of the framework, the Bayesian network; followed by important elements of the optimization problem and finally conclusions for the proposed approach.

4.1 Introduction to Rework Decision Framework

A conceptual schematic for the framework is given in Figure 9 and depicts how the uncertainty quantification and management research areas interact with the modeling environment of the aeroelastic loads process.

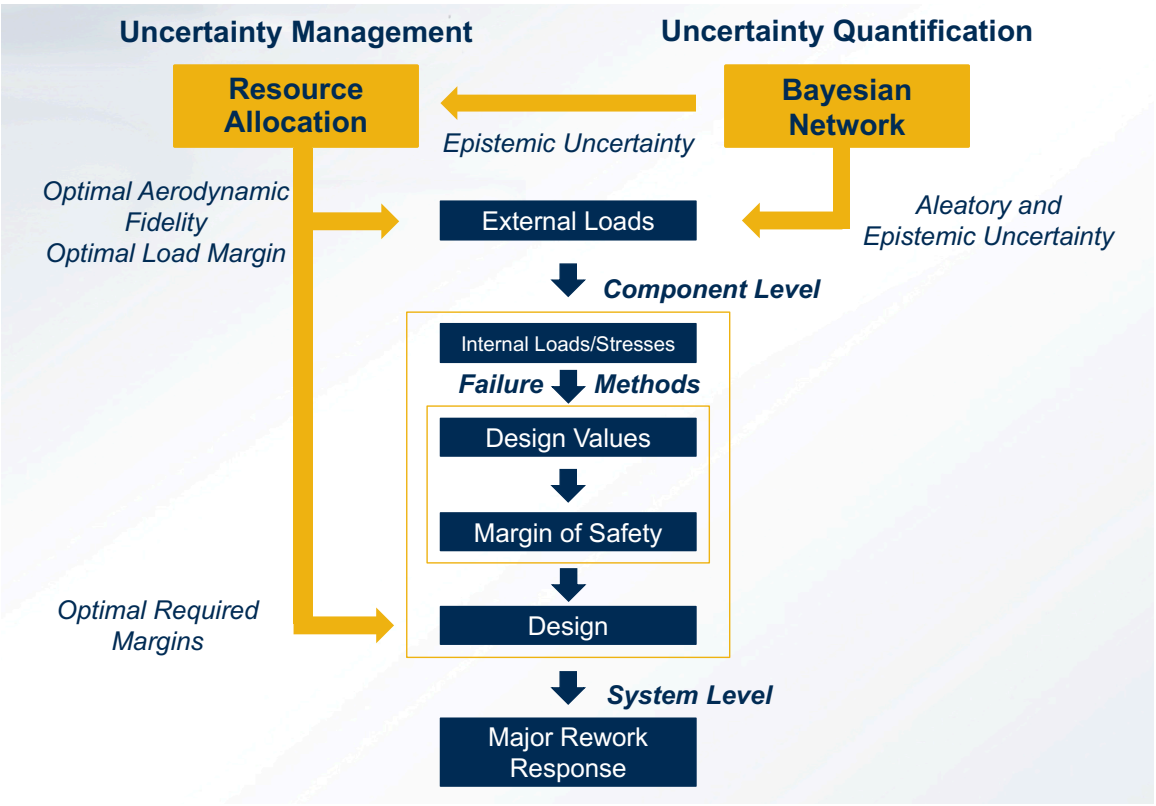

Figure 9: Proposed framework for uncertainty management system

This figure shows why uncertainty quantification and uncertainty management are key components of the framework. The uncertainty quantification component estimates the various sources of uncertainty and propagates them to the other parts of the system where required. The two sources of uncertainty modeled are from aerodynamic analysis fidelity and load parameter uncertainty. The arrows indicate all sources are propagated directly to the external loads, which are applied to the structure for each load case. The load parameter uncertainty are the only sources of aleatory uncertainty in this environment.

The aerodynamic fidelity is modeled with NASTRAN correction factors, where the epistemic uncertainty is represented by probability distributions for each factor. The uncertainty management system simulates and controls this fidelity which impacts the external loads. The external loads from the load cases are transferred to each

structural component and then into internal loads and stresses. At the component level, failure analysis is done and margins of safety calculated.

The uncertainty in each component's critical margin of safety due to fidelity, load parameters is assessed and aggregated over the wing. The UMS will simulate variations in fidelity, load margin and structural margins to determine their impact on the system level major rework response. Through resource allocation optimization the UMS will determine the optimal inputs based on their costs and the total budget constraint. The key components in the UQ and UMS areas will be discussed in the next two sections.

4.2 Bayesian Network for Loads Analysis

All of the uncertainty quantification and propagation in this environment is carried out using a Bayesian network. As mentioned before, Bayesian networks (BN) provide a systematic framework for characterizing uncertainty in a system by use of directed acyclic graphs which describe conditional dependence of uncertain variables and observed data. The experiments in Section 6.3 deal with the construction and design of the Bayesian network utilized in this framework. A simplified Bayesian network for aeroelastic loads analysis is shown in Figure 10. Loads analysis is a coupled, multi-level, multidiscipline problem and an appropriate network must be designed to reflect each of these aspects.

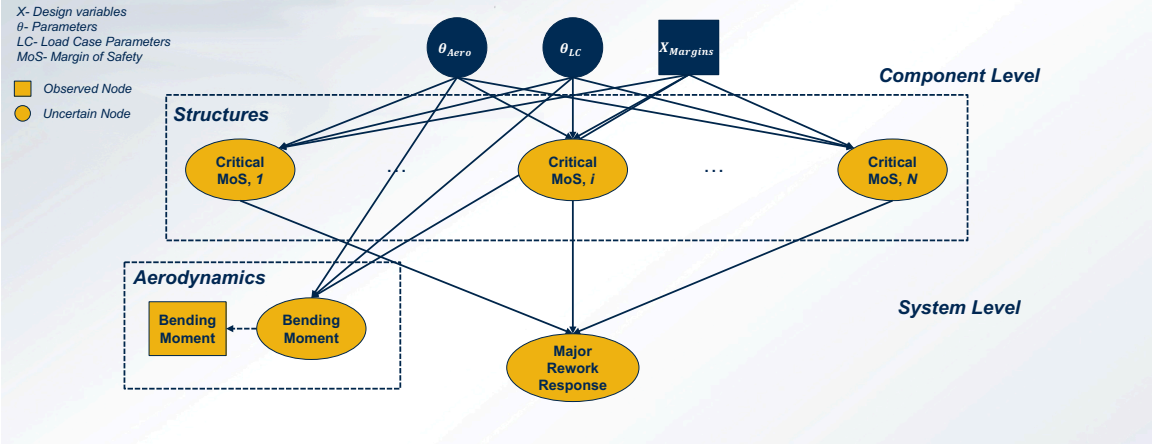

Figure 10: Generic Bayesian network for uncertainty quantification in loads analysis

In Figure 10, square nodes are observed data or deterministic variables while non-square nodes represent uncertain quantities. θ are parameters and X are analysis or design variables controlled by resource allocation optimization. Ovular nodes represent subsystem and system responses from computational models. The load case parameters (e.g. Mach number, altitude, etc.) include aleatory uncertainty ($\boldsymbol{\theta_{LC}}$). The uncertain aerodynamic model parameters $\boldsymbol{\theta_{Aero}}$ are the aforementioned correction factors which represent epistemic uncertainty and are influenced by the chosen fidelity. $X_{Margins}$ represent the load and structural margins.

The Bayesian network will be used for parameter calibration via the inverse problem and uncertainty propagation via the forward problem as described in Section 3.4.3. In the inverse problem $\boldsymbol{\theta}$ is calibrated using the bending moment response data from simulated higher fidelity aerodynamic analysis. The aerodynamic empirical adjustment (correction) factors are updated by simulating an increase in aerodynamic fidelity. In the context of Bayesian statistics, calibration data is treated as observed data, thus they are square nodes. In the forward problem, the uncertainty from the newly calibrated aerodynamic model parameters, along with all other uncertainty, are propagated to each component's critical margin of safety and in turn to the major rework response which is used by the UMS as discussed next.

4.3 Resource Allocation Optimization Problem

The underlying method in the uncertainty management system is the optimization based on a modified version of the resource allocation problem discussed in 3.5.1. The principal modifications are the type of tests simulated, their cost and the objective function. Each of these modifications is discussed in further detail here.

In the works of Sankararaman et al [140][137][141][139] a "test" typically represented a physical experiment in which the output was used as calibration data. Experimental tests are simulated using computational models and multiple realizations of the test are needed in the resource allocation method. In this work, the tests are not physical and instead are *computational* experiments. For example, in the loads process computational experiments are needed to see how changing the fidelity of an analysis impacts the responses of interest and their uncertainty. These experiments are deterministic so uncertainty sources related to experimental error are not of interest here as they were in previous work. But computational experiments can be applied in the same manner as physical ones in the resource allocation problem because each has a measurable impact on the response variance and a cost to conduct this test. The experiments of interest are related to aerodynamic fidelity, load margins and structural margins.

The cost of an experiment is another differentiator of the proposed approach. In the previously cited work the cost of a test is associated with the dollar value necessary to conduct the test, e.g. material cost to run a stress test to determine the Young's Modulus of a new material. In this sense the cost of an experiment may be relatively easy to estimate because such tests are often done in reality. In this work the cost of a computational experiment is more generic and subjective. For example, the cost of increasing the aerodynamic fidelity accounts for factors

such as computational cost (e.g. increased runtime which could lead to schedule delays) and additional resources needed to handle increased modeling complexity (e.g. skilled labor, access to high-performance computing cluster, etc.). Such costs are more difficult to estimate. Additionally, the only benefit to the aforementioned physical experiments was the reduction of uncertainty in the system-level response. Here, other benefits are considered and taken into account in the overall cost of an experiment. For example, the experiments associated with redesigning a component at a certain required margin can lead to weight penalties or savings. Historically in the aerospace community there are direct correlations between weight and financial quantities such as direct operating cost [81].

Thus the net cost (or benefit) of each experiment from various factors is expressed and used in the optimization problem. Although using currency makes the evaluation of an experiment much more useful to the user, assigning such units accurately would take a great deal of effort and most likely very subjective. Instead, the user assigns costs which reflect their prioritization of how important factors such as uncertainty and weight are to them. In this sense, only the relative costs of each experiment and their relation to the total budget is important in this framework. Priorities change in different scenarios depending on where in the development process they occur so varying the experiment costs will be a part of the experimental plan.

In the aforementioned resource allocation studies the system response variance was the single objective function. The system response of interest in this work is related to the occurrence of major rework so it is beneficial to simultaneously optimize the mean of the response along with its variance.

4.4 Summary of Framework

The framework for the proposed approach is summarized in the following steps:

Step 1: *Construct Bayesian Network*

Determine structure of Bayesian network (BN) and assign prior distributions to all uncertain inputs and parameters.

Step 2: *Sensitivity Analysis*

Perform global sensitivity analysis to identify important load case parameters and W_{KK} parameters which contribute significant uncertainty to the system-level response.

Step 3: *Choose X*

For each step in optimization select potential fidelity level, load margin and required margin.

Step 4: *Update Aerodynamic Parameters*

Simulate aerodynamic analysis based on X. Use Bayesian inference to update selected θ_{Aero} parameters using bending moment response data for calibration.

Step 5: *Calculate Costs, System Response*

Calculate expected mean and variance of system-level response R from multiple realizations by propagating uncertainty from updated θ_{Aero} and load case parameters.

Step 6: *Find X^*,*

Complete optimization to solve resource allocation problem and determine the optimal combination of fidelity, load margin, and structural margin based on total budget.

Some considerations of the first two steps of the framework will be discussed. Steps 3-6 will depend on the specific methods chosen during the experimental plan and will be discussed in more detail there.

The preliminary steps for this framework are to construct the Bayesian network and perform sensitivity analysis. As discussed in the background there are methods to learn the structure of a network if the relationship between nodes is complex. Assigning prior distributions can also be difficult if variables and parameters are unknown in a system. In the literature there are several techniques for assigning probability distributions if necessary [24]. Parameters with epistemic uncertainty have to take special consideration due to probability theory and methods for assigning probability to these parameters was discussed in [**?**]. In this work the calculation of prior distributions for the uncertainty in the empirical adjustment factors was an extensive part of this thesis and is detailed in 6.2.

As part of Step 1, it is most likely necessary to construct surrogate models to accompany the Bayesian network. Given the computational demands of the Bayesian inference and uncertainty propagation, surrogate modeling may be a key enabler to the proposed framework. In this work several surrogate models are needed to define the relationship between inputs and outputs of various analysis software and is discussed further in 6.3.1. Additional uncertainty caused by using surrogate models can be included in the network and updated accordingly, although this additional error is not considered in this work.

Sensitivity analysis is another critical step to making this framework computationally feasible. It is possible to assign uncertainty to almost every aspect of a system but typically only a few sources are relevant in terms of the quantities of interest. Global sensitivity methods were discussed in 3.5.2. Such methods are used here to pinpoint which aerodynamic model parameters, load cases, load case parameters and margins are important to the rework response mean and variance.

4.5 Conclusion

The proposed approach to address rework in aeroelastic loads analysis consists of uncertainty quantification and uncertainty management. A general framework for carrying out both these tasks was outlined. Primarily the uncertainty quantification is done using a multi-level, multi-discipline Bayesian network to represent the conditional dependence between uncertain quantities and responses in the M&S environment. The calibrated parameters of interest are related to the aerodynamic fidelity. The calibration data is produced by simulating multifidelity aerodynamic analysis and using the bending moment response. After update, the effects of the new aerodynamic parameter uncertainty and load case parameter uncertainty on the system-level response is measured and inputted into the uncertainty management system. The system response of interest here is related to major rework but will be specified from several candidates later.

The UMS is based on the modified resource allocation optimization problem. The mean and variance of the response are optimized. The output of the UMS is the optimal set of fidelity and margins to reduce the risk of major rework subject to a constrained budget.

The proposed framework is a general one and many methods and techniques are available in the literature as discussed in Chapter 3 which could be applied to the UQ and UMS components. The goal of the experimental plan is to try candidate methods in this framework, assess their performance against the current approach to loads analysis and narrow down the selection. It is unlikely there is one framework which is best for all scenarios, but good candidates will be suggested for a select set of important scenarios in aeroelastic loads analysis.

CHAPTER V

EXPERIMENTAL SETUP

5.1 Demonstration Model

Some of the requirements for the demonstration model were discussed in the Problem Formulation. To recap, the chosen model must represent a commercial transport and be capable of performing aeroelastic analysis. Such analysis dictates the must be an aerodynamic shape, i.e. planform, to perform aerodynamic analysis. There also must be a primary structure, i.e. wing box, to perform structural analysis and design. The structural model must also be undeformed for aeroelastic analysis.

In the literature there are a few popular aeroelastic models which fit these requirements, typically they focus on the wing as is done in this work. Some examples include the AGARD models [178] and the BAH models from Bisplinghoff, Ashley, and Halfman (1955). Both represent classic models used as standards for validation of aeroelastic problems. Because CFD will be utilized in this work for high fidelity aerodynamic analysis, it would be beneficial if the chosen model had been used in CFD studies. Although CFD models exist which are treated as standards because of their wide-use, such as the ONERA M6 wing [142], not all of them have also been used for aeroelasticity. For example, many of the CFD models are in their cruise configuration, i.e. deformed, or do not include any internal structural definition. Fortunately some models do exist which have been used for both CFD and aeroelasticity, including the ONERA M6 [28] and the NASA Common Research Model (CRM).

The demonstration model used to evaluate the framework is based on a modified version of the CRM. It was chosen primarily because it fit all the model requirements,

is well-known, has publicly available wind-tunnel data and most importantly a fully-functioning NASTRAN aeroelastic model existed and was provided by the Boeing Corporation for this work. This NASTRAN model was accompanied by an existing IGES model of the wing planform suitable for CFD analysis and developed at the University of Michigan [71]. Details of the model and its development will now be discussed.

The CRM was developed in response to recommendations out of the NASA Subsonic Fixed Wing (SFW) Aerodynamics Technical Working Group (TWG) in 2007. Industry and government leaders in aerospace met and discussed the need for "common, publicly-available contemporary experimental databases for the purpose of validating specific applications of CFD" [170]. The detailed aerodynamic design of the CRM was primarily done by the Boeing Company while the physical model was primarily designed, fabricated and tested by NASA. Since its inception, the CRM has been used in numerous aerodynamic analysis validation studies because of a relatively large collection of published CFD and wind tunnel data. A photograph of the wind tunnel model is depicted in Figure 11.

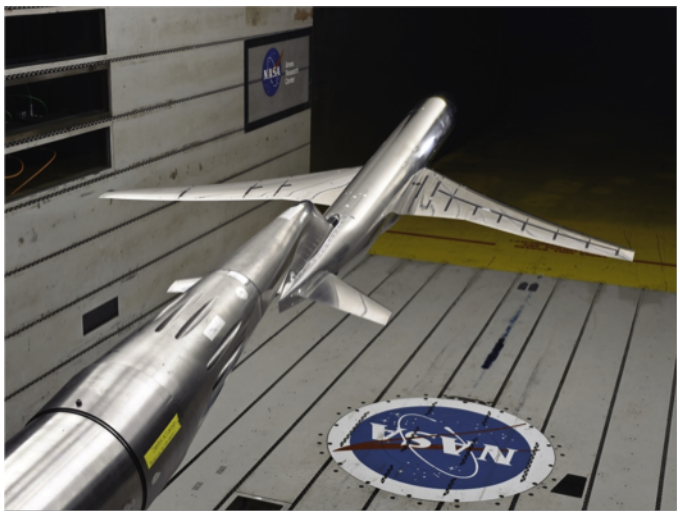

Figure 11: Common Research Model in wind tunnel test.

The original CRM model is representative of a transonic, wide-body commercial transport. It is designed to fly at a cruise Mach number of 0.85 with a nominal lift coefficient of 0.50, and at a Reynolds number of 40 million per reference chord. The TWG specified the wing have an aspect-ratio of 9.0, and a taper-ratio of 0.275. The CRM is a complete airplane configuration but in this study the wing design is of most interest. Components of the fuselage and empennage are only included in the model when necessary for boundary conditions and stability and control purposes. The resulting full-scale wing design specifications are depicted in Table 1.

Table 1: Reference Quantities for CRM [170]

Specification	***Value***
Wimpress Wing Area, Sref	4,130.0 ft^2
Trap-Wing Area	4,000.0 ft^2
Reference Chord, Cref	23.0 in
Wing Span	192.8 ft
Xref	110.5 ft
Yref	39.1 ft
Zref	14.8 ft
Taper Ratio, λ	0.275
Wing Sweep, $\Lambda_{C/4}$	35^o
Aspect Ratio, AR	9.0

The CRM was intended for CFD validation so the wing configuration is in the cruise condition and deformed relative to the jig-shape. This presents problems for aeroelastic design and analysis so a modified version was created by the Multidisciplinary Design Optimization Laboratory at the University of Michigan, Ann Arbor led by Joaquim R. R. A. Martins [71]. This model, called *uCRM*, is the undeformed, or jig-shape, wing configuration and is utilized in this work. The original CRM was designed to resemble the Boeing 777-200ER but does not include any structural model. The uCRM wingbox also resembles that of the 777-200ER as shown in Figure 12 and includes two spars and forty-six ribs. The uCRM has been used in several aeroelastic studies which have also incorporated CFD [71][89].

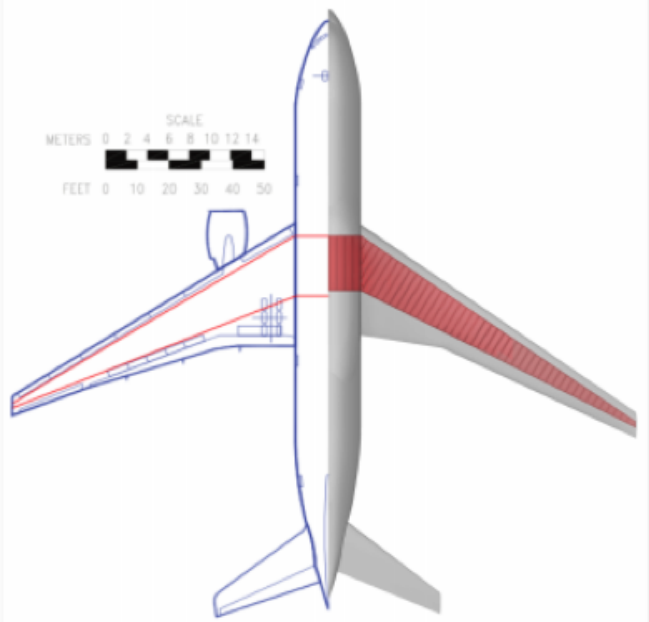

Figure 12: uCRM Comparison to B777-200ER

5.2 Modeling and Simulation Environment Overview

5.2.1 Requirements & Development

Requirements for the modeling and simulation environment emerged from the problem formulation, research development and proposed approach. These requirements can be categorized into those which are dictated by the multidisciplinary analysis of aeroelastic load cycles and those dictated by the uncertainty quantification and management to construct the rework decision framework.

An integrated environment is needed which includes aerodynamic analysis, structural analysis, aeroelastic analysis and structural design. Some of the challenges for constructing such an environment are related to linking the various analysis methods together so they can communicate and share data. This is often a non-trivial task, especially for legacy analysis codes which may not have been originally designed to work

with external methods. The linking is even more critical in feedback coupled systems where large amounts of data need to be transferred and translated between codes after each iteration. Two feedback loops exist here, the first is the coupling between the aerodynamics and structures for aeroelastic analysis. The second is the coupling between the structural design and aeroelastic analysis. Details on these feedback loops will be discussed in detail later in this chapter. A final challenge comes from the identified research gap for modeling load cycles in loads analysis and structural design. Because of this gap, there aren't readily available modeling environments in the literature to base this work off of.

The integrated analysis environment is the core of the rework decision framework as shown in Figure 9. The uncertainty quantification and management components have separate requirements. Surrogate modeling is an essential requirement for feasibly carrying out Bayesian inference, uncertainty propagation, sensitivity analysis and optimization. As has been discussed for the selected methods in this work Bayesian inference requires Markov Chain Monte Carlo simulation and uncertainty propagation requires Monte Carlo simulation. Sensitivity analysis and optimization subsequently can re quire both. In addition, sensitivity analysis can be carried out with machine learning methods for feature selection.

A single system must be able to serve as the "wrapper" to integrate all the analysis methods and include the functionality for the decision framework. Fortunately MATLAB (R2016b) has the ability to satisfy all these requirements. Other programming environments and languages exist which could meet these requirements but arguably at steeper learning curves. Thus MATLAB was chosen to build the M&S environment. Details of the M&S environment, analysis methods and models will now be discussed. The details of the uncertainty quantification and management will be discussed in Chapter 6.

5.2.2 Modeling Environment Overview

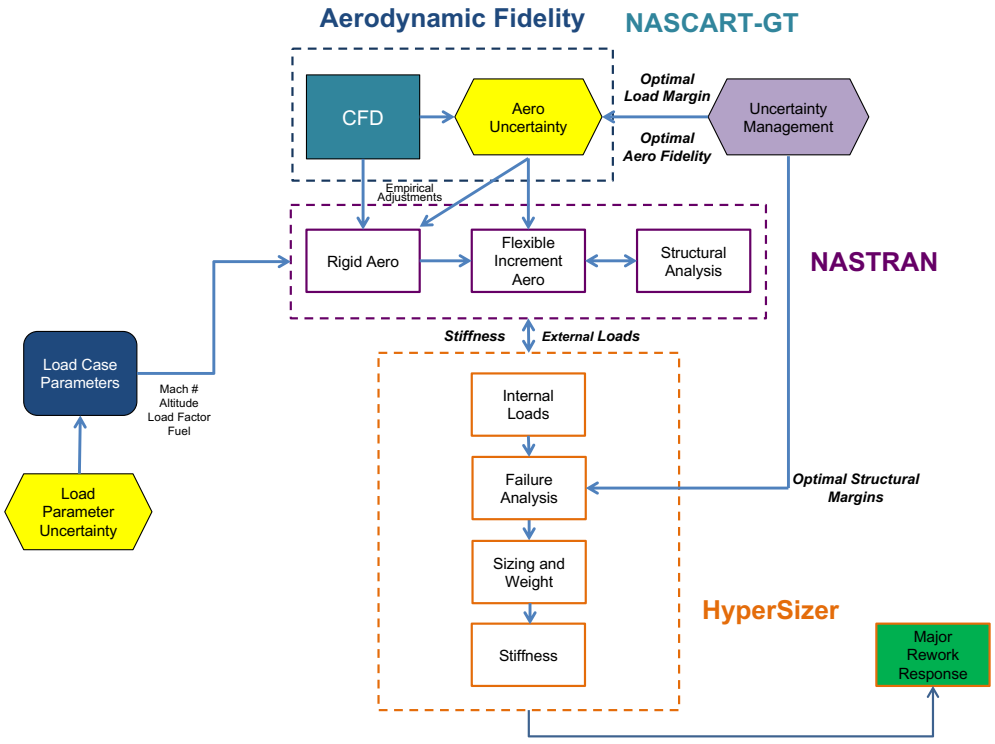

Figure 13: Modeling and simulation environment for loads analysis

Figure 13 depicts the modeling and simulation (M&S) environment used in this work. The environment consists of analysis methods which represent different disciplines related to loads analysis and structural design. The environment also describes the system inputs and outputs as well as the linkages between analysis methods. The system-level inputs consist of load case variables, aerodynamic fidelity variables. The two sets of variables are related to the two sources of uncertainty examined in this thesis; aerodynamic fidelity and load parameter uncertainty (marked in yellow). The load case variables define each load case and are Mach number, altitude, load factor and fuel weight.

As will be discussed, two aerodynamic analyses are used in this environment; NASTRAN's Doublet-Lattice Method (DLM) and CFD with NASCART-GT. CFD data is used to define empirical adjustments which are implemented in DLM and

correct the aeroelastic equations to supplement the DLM with higher fidelity external aerodynamic data. For each simulated fidelity level there will be a prescribed mean and standard deviation to the adjustment factors. The magnitude of the standard deviation will be an approximation of the error of the analysis with respect to the truth data represented by CFD analysis. It is assumed the uncertainty is normal (in statistical terms). More details on the empirical adjustments and their associated uncertainty will be provided in Section 6.2.

The core of the aeroelastic analysis is done using MSC NASTRAN 2014. The external aerodynamic data is imported from NASCART-GT for CFD analysis. Finite-element analysis (FEA) loads are transferred from NASTRAN to HyperSizer where internal stresses are calculated and failure analysis and structural design are carried. There are iterations between NASTRAN and HyperSizer due to the component stiffnesses which are initially assumed and subsequently updated along with the structural design until convergence or the maximum number of iterations is reached. Thus each NASTRAN-HyperSizer iteration represents a load cycle and an iteration between the loads and stress groups.

The green box represents the system-level response for major rework and is calculated within HyperSizer after four load cycles (i.e. iterations). Four iterations were chosen to mimic the initial, preliminary, design and certification load cycles in a real development program. Typically these four cycles are enough to converge the loads and stiffness and produce a mature structural design for flight test and evaluation. Due to the assumptions and limitations of the model, it may not always be the case that the loads and stiffness converge after four iterations between NASTRAN and HyperSizer in all components.

Surrogate models are utilized to represent the interactions between the aforementioned analysis methods. These same surrogates constitute the Bayesian network for

carrying out the inverse and forward uncertainty problems. Thus the Bayesian network can be viewed as a system-level surrogate for the entire M&S environment. The uncertainty management system (purple) selects the aerodynamic fidelity, load margin, and structural margin via the resource allocation optimization. Those variables are introduced into the Bayesian network to ultimately calculate the major rework response. The interaction between the M&S environment, Bayesian network and resource allocation optimization form the rework decision framework. Next, important aspects of the M&S environment and applicable theory will be discussed further.

5.3 Load Cases

5.3.1 Load Case Types

The design of all aircraft must be certified by the Federal Aviation Administration (FAA) before it can be operated. The FAA establishes Federal Aviation Regulations (FAR's) to govern all aviation activities including the design of aircraft. FAR 25 applies to the airworthiness of transport category aircraft, which is defined as any "jet with ten or more seats and any propeller-driven aircraft with greater than nineteen seats or over 19,000 lb maximum takeoff weight (MTOW)" [4]. FAR 25 is broken into hundreds of sections and several of them pertain to the structural integrity which is of interest in this work. Most of the loading scenarios (cases) used in the analysis are derived from FAR requirements in order to ensure the safety of the design. Airplane manufacturers also supplement these requirements with their own, often proprietary, loading scenarios based on historical experience. Load cases can be grouped into categories or types based on their physical nature and the aircraft state which produced them. This section discusses the major load case types as depicted in Figure 14 and details those which will be used in this thesis.

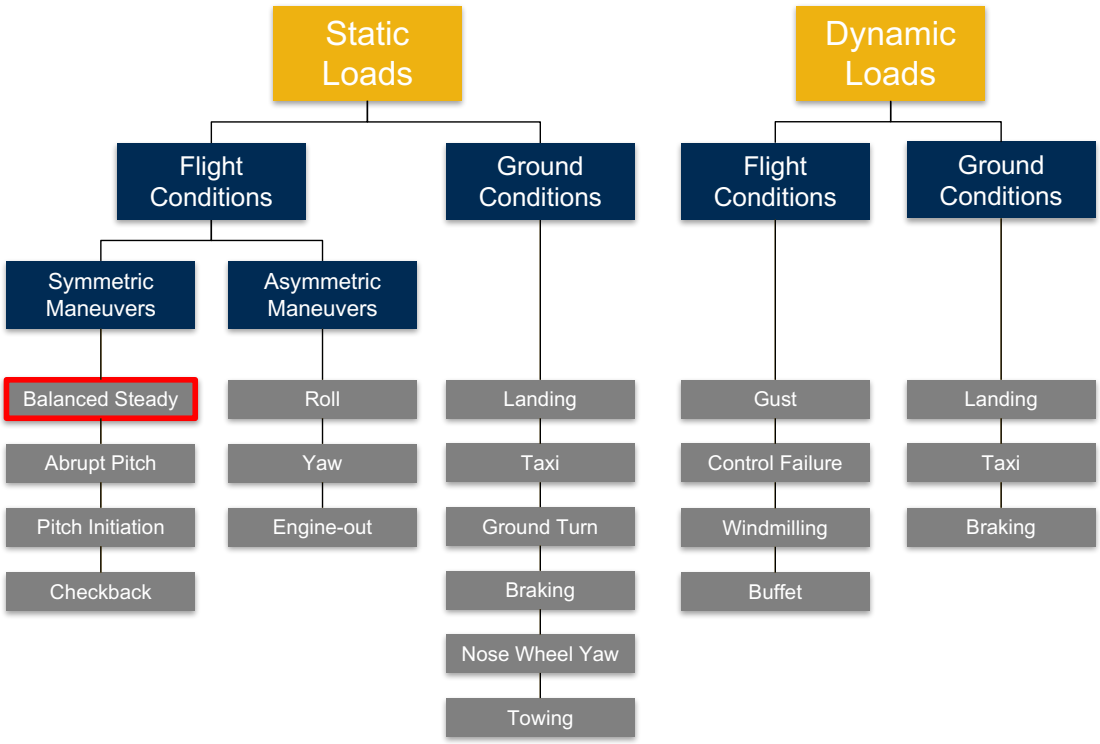

Figure 14: Types of load cases. Balanced steady (highlighted in red) will be analyzed in experimental plan

The most broad category of loads are static versus dynamic. Static loads occur when the aircraft is in a state of static or quasi-static equilibrium and thus the forces and accelerations are independent of time. Referring to the aeroelastic triangle later shown in Figure 26, these loads do not result from vibratory inertia forces. Dynamic loads occur when the aircraft state results in forces and accelerations which vary with respect to time. Analysis of dynamic loads require more complex disciplines such as flight dynamics and control theory which are not integrated into this modeling environment and are out of the scope of this work at this time. Thus only static loads will be explored. Under each of these categories are flight conditions and ground conditions resulting in different types of loading scenarios. Flight conditions are more pertinent to the structural sizing of wings and so only these conditions will be used

here. Flight conditions can be further categorized into symmetric and asymmetric maneuvers. Symmetric maneuvers maintain symmetry of the aircraft about the longitudinal axis throughout the maneuver and therefore are limited to cruise and pitch maneuvers. Asymmetric maneuvers do not maintain this symmetry with respect to the configuration and loading. In order to limit the scope of this work, the more general balanced steady cases will be utilized for symmetric maneuvers. Although the provided uCRM model was previously used for asymmetric load cases, there was not enough time to modify the model as necessary for this environment for both symmetric and asymmetric. Thus only symmetric cases are considered.

Balanced steady maneuvers refer to maneuvers where the lift is balanced by the weight and side force so there is zero acceleration. For symmetric maneuvers, this results in zero pitch acceleration. Two symmetric balanced steady load case types will be analyzed in this work: positive 2.5 g pull up and -1 g push down. The cruise load case is commonly analyzed, but was ignored here because it is rarely a critical load case in terms of structural design. The load factor is defined as the ratio of the amount of load imposed on an aircraft structure to the weight of the structure itself. Load factors are expressed in terms of the gravitational constant, g. The maximum maneuver load factor is dictated by FAR's and for commercial transports is +2.5 g and -1 g [4].

5.3.2 Load Case Parameters

For each load case type there are numerous individual load cases analyzed. A load case prescribes all the factors which define a unique state of the aircraft. Each aircraft state results in different external loads experienced by the structure. These factors cab be referred to as parameters. Any change in a parameter results in a new load case. Many factors influence the state of an aircraft but historical perspective

tells us certain factors are more influential to certain load case types for traditional configurations [87]. For example, wind speed on a given day would have a large influence on a dynamic gust load case but not necessarily on a static taxi load case. Given the chosen load case types and focus on wing design, the variable parameters considered are Mach number, altitude load factor and fuel density.

In a typical loads analysis parameter ranges and levels are determined and a full-factorial design experiment is utilized to determine the internal load envelope for shear, bending and torsion [87]. Several specific speeds are required to be analyzed by the FAA and are called design speeds [4]. These speeds are based on structural integrity considerations and empirical data. These design speeds are visually depicted in a "V-n Diagram" as shown in Figure 15. The diagram shows different design speeds as a function of load factor. The load factors will dictate which maneuver and gust conditions should be analyzed. The subscript letters refer to different speeds and conditions dictated by FAR's. For example, V_D refers to the design speed which is typically regulated to be 1.15 times the design cruise speed V_C for transport aircraft [79] and should be evaluated at the ultimate load factor, $n = 2.5$ to determine the appropriate envelope. The letters on outside edge refer to other conditions which must be evaluated to determine the required flight envelope.

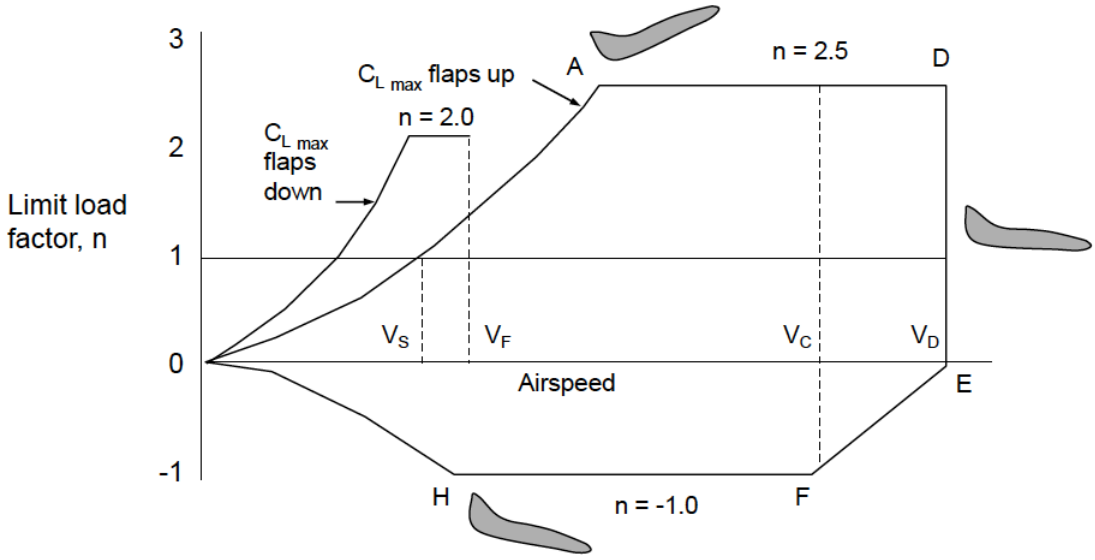

Figure 15: Notional V-n diagram, Frode Engelsen 2015

The altitude primarily affects aerodynamic loads because of air density. Altitude contour lines are often imposed onto the V-n diagram but similar information can be derived from a placard or speed-altitude diagram. These plots visually display the design speed for a given structural design altitude. The altitude is chosen for operational considerations and in conjunction with required design speeds, the design Mach numbers are imposed. This information is used to select altitude ranges for loads analysis [87]. A generic speed-altitude plot is depicted in Figure 16.

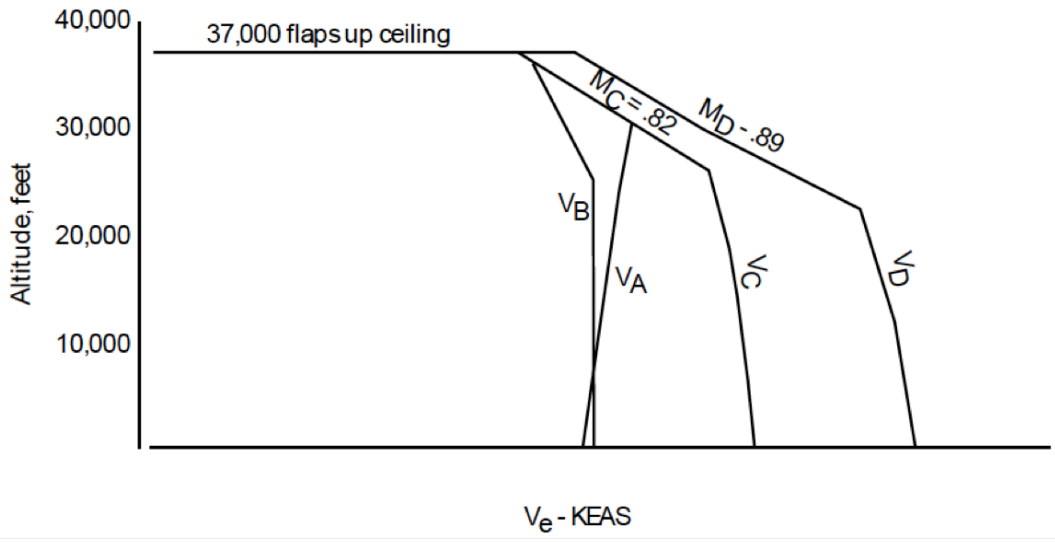

Figure 16: Notional speed-altitude diagram, Frode Engelsen 2015

The fuel weight is an important consideration for inertial loads [87]. Fuel is constantly being burned so consequently the center of gravity (c.g.) is constantly shifting. Its location is essential for any force analysis as well as stability and control considerations. An aircraft will initially begin operations equal to or less than the maximum fuel weight. Fuel is burned in order to reach cruise altitude so in-flight load cases are not typically analyzed assuming full fuel. If max fuel was assumed during flight the resulting structural design would be too conservative and overweight. In commercial transport aircraft there are fuel tanks in the center body and in each wing. The fuel is burned from the center tank first so the wing weight provides inertia relief from bending for as long as possible. The c.g. location shifts differently when fuel is burned from the different tanks. Thus the fuel density parameter also dictates the fuel c.g. location. Several fuel densities will be analyzed in the loads process and the ranges can be determined visually from fuel burn curves on a c.g. diagram. An example of a c.g. diagram (without the fuel burn curves) is shown in Figure 17. The payload weight and distribution obviously affect the c.g. location as well. For commercial

transports the luggage plays an important role. In the underbelly of the fuselage the payload can be packed to intentionally shift the c.g. in favorable ways. The purpose of loads analysis is to find the critical loading scenarios so the payload weight and c.g. will be fixed to their most extreme values for wing design: as far forward as possible and equal to the max design payload weight.

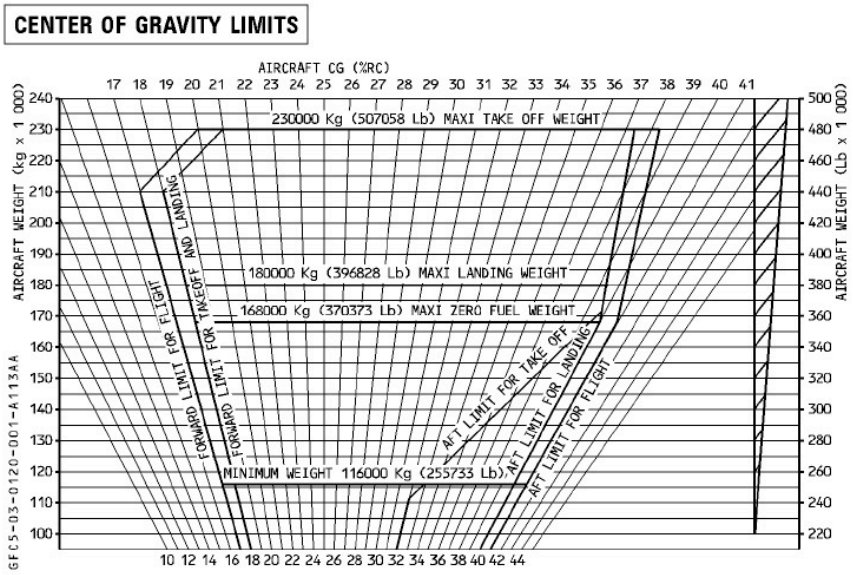

Figure 17: Generic center of gravity diagram [166]

5.3.3 Critical Load Cases for Environment

To simplify the modeling, only steady symmetric load case types are considered in this work. Based off of literature on the uCRM model, public data on the Boeing 777-200, and the flight envelope in Figure 16 an envelope was assumed for the demonstration model and is shown in Figure 18. Thirty-eight load cases were initially used for downselection and are represented by circular points on the plot. The maneuver, rough gust, and cruise speeds were tested at 2.5 and -1.0G load factors and the dive speed was only tested at 2.5G's as per regulations. It should be noted that no gust analysis was used in this thesis, but the speed and altitude for a gust scenario as recommended in FAA regulations was used to specify these cases [4]. These load cases

were used in the M&S environment and HyperSizer determined the critical load case in each structural component based on the minimum margin of safety. More details of the failure analysis and selection of critical cases will be discussed in subsequent sections. From the initial set, four were critical in at least one component and selected as the final set. These four cases are indicated by dashed circles in Figure 18.

Four parameters are used to specify a load case in this work; Mach number, altitude, load factor and fuel density. The first three are dictated by regulations and can be visually selected from flight envelope and Vn diagrams. The fuel density uncertainty in this work is based on variances in jet fuel production. For the baseline (deterministic) load cases the nominal fuel weight included in the uCRM model is assumed and designated as 100%, while uncertainty can cause this value to be greater than or less than the nominal value. Table 2 lists the baseline (deterministic) load case parameters for the four critical load cases.

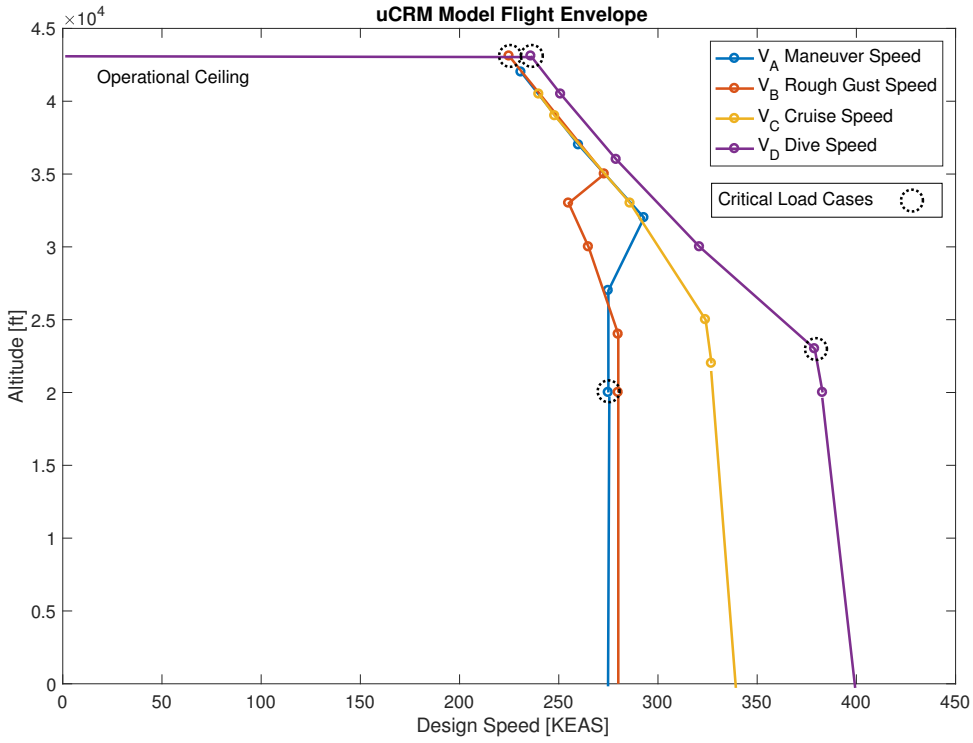

Figure 18: uCRM model flight envelope and critical load cases

Table 2: Critical Load Case Parameters

Load Case	***Mach***	***Altitude***	***Load Factor***	***Fuel***
1	0.85	43100 ft	2.5G	100%
2	0.90	23000 ft	2.5G	100%
3	0.60	20000 ft	2.5G	100%
4	0.89	43100 ft	2.5G	100%

5.4 Aerodynamic Analysis

5.4.1 Aerodynamic Analysis Overview

The atmosphere imparts pressure on an aircraft and result in forces and moments applied to the skin. The environmental conditions and aircraft maneuver will change the pressure distribution and ultimately change these loads. When an aircraft executes a maneuver it actuates control devices to purposefully change the aerodynamic loads in order to alter it's orientation, lift or drag. Air-breathing engines increase the velocity of intake air through combustion and exhaust it to create thrust. Thrust and the effects of propulsion will directly or indirectly add or change the aerodynamic loads on other parts of the aircraft. All the aforementioned physics require aerodynamic analysis to quantify the resulting forces and moments. There are many methods to support such analysis and these can be categorized into experimental, numerical and analytical. Analytical methods refer to closed form, exact solutions which do not require numerical approximations or discretization to solve. Popular methods within each category will be discussed.

Although there may be other experimental aerodynamic methods, the two readily used for commercial transport design are wind tunnel testing and flight testing.

Although no experiment is without error, flight testing is the most accurate because aerodynamic data is measure during actual flight operations. In the earliest days of aviation design this was the only method to collect such data. In modern design, a full scale test vehicle is built with integrated sensors to measure various data, including aerodynamic pressure, over numerous parts of the aircraft [124]. The pressure is generally measured using Bernoulli's Principle:

$$\frac{v^2}{2} + \int_{p1}^{p} \frac{d\tilde{p}}{\rho(\tilde{p})} + \Psi = \text{constant} \quad \text{(along a streamline)} \tag{12}$$

Equation 12 depicts the compressible flow version [31] where v is the flow velocity, p is the pressure, ρ is the density and Ψ is the potential associated with the conservative force field. The pressure at the surface of the aircraft can be calculated by a manometer or other similar device by the change in fluid velocity relative to the free-stream or vehicle velocity. Flight test experiments are only typically done after a detailed design has been fully defined. A flight test program will be used for validation of previous analysis and is required for certification by the FAA [143]. Building a test article can be quite expensive and time-consuming so wind tunnel testing is used as an alternative experimental method.

The first enclosed wind tunnel was developed by Francis Herbert Wenham in 1871 [14]. Wind tunnels utilize a fixed model with a controlled fluid moving over the model surface. Similar measurement devices used in flight testing are also used in wind tunnels and utilize Bernoulli's Principle. Other common measurement methods include pressure-sensitive paint, smoke, bubbles and beam balances to determine the pressure distribution [88]. Wind tunnel testing is viewed as more accurate than numerical or analytical methods because they measure the aerodynamic forces directly rather than assume a model [58]. But there are significant simplifying assumptions compared to

flight testing. Some of the most important are related to scaling and rigidity. Wind tunnels can also be expensive to maintain and operate and it is often infeasible to use one large enough to fit a full-scale model, though it has been done. Thus models are geometrically similar but scaled down to fit into smaller wind tunnels. The scaling has important effect on aerodynamics and requires the Mach number and Reynolds number, among others, to be kept constant to accurately compare results to the full scale design [86]. Both are dimensionless parameters which describe the velocity relative to the speed of sound and the inertial forces relative to the viscous forces respectively. Wind tunnel models are often made of different materials than those of the production aircraft. The model is typically much more stiff but not completely rigid [153]. Therefore wind tunnel testing is used for rigid-body aerodynamics and the results require removal of any elastic effects. Although aeroelastic wind tunnel models have been developed to reflect the full scale flexibility, this can be complicated [23] and thus avoided. Wind tunnel analysis is commonly done prior to load cycles, so this analysis is simulated using CFD on a rigid (undeformed) model.

Numerical methods were developed based on aerodynamic theory to calculate loads on a computer in order to save time and money relative to experimental methods. Aircraft aerodynamic theories are numerous but nearly all are derivatives of the Navier-Stokes equations which is a statement of the balance of momentum [106]:

$$\rho\left(\frac{\partial \boldsymbol{u}}{\partial t} + \boldsymbol{u}\cdot\nabla\boldsymbol{u}\right) = -\nabla p + \mu\nabla^2\boldsymbol{u} + \frac{1}{3}\mu\nabla(\nabla\cdot\boldsymbol{u}) + \rho\boldsymbol{g} \tag{13}$$

where $\boldsymbol{u}$ is the flow velocity, p is the pressure, μ is the dynamic viscosity, and $\boldsymbol{g}$ is the body acceleration. There are broad categories which describe aerodynamic theories which include compressible or incompressible; subsonic, transonic or supersonic; and viscous or inviscid. The first category refers to wheter the density of the fluid has

constant density (incompressible) or not (compressible). The second category refers to the flow speed regime being below, near, or above the speed of sound respectively. The third category refers to whether viscous effects will be considered in the flow. Viscosity is primarily concerned with the drag force [9]. This work will focus on transonic flow, which is by definition compressible, due to the commercial transport aircraft demonstration model. Although drag is a fundamental aerodynamic force, this work will assume an inviscid flow. The baseline aerodynamic method in this modeling environment is inviscid and neglects drag, therefore all other methods will assume the same for compatibility. This neglection will be discussed later in this section.

Generally there are two major classes of numerical aerodynamic methods: computational fluid dynamics (CFD) and panel methods. CFD methods discretize and numerically solve the Navier-Stokes equations. Often the discretization is done with the finite-volume method where a solution to the conservation of mass, momentum (Navier-Stokes) and energy as well as turbulence equations are found on discrete control volumes [46]. When an inviscid flow is assumed the Navier-Stokes equations reduce to the Euler equations. The governing equations for the finite-volume methods are:

$$\frac{\partial}{\partial t}\iiint \boldsymbol{Q} dV + \iint \boldsymbol{F} d\boldsymbol{A} = 0 \tag{14}$$

where $\boldsymbol{Q}$ is a vector of conserved variables, V is the volume of the control volume element, $\boldsymbol{F}$ is the flux vector and $\boldsymbol{A}$ is the surface area of control volume element [114]. Although CFD is less expensive in terms of time and resources than wind tunnel testing, it still has a high computational cost for large meshes and complex geometries. But more powerful computers have allowed CFD to be utilized more

readily in design, but less for commercial transports based on subject matter experts.

Similarly to wind tunnel data, CFD will be utilized in this thesis for validation and to help calculate the effects of uncertainty due to analysis fidelity. The CFD software used here is called NASCART-GT and was developed by Professor Stephen Ruffin in the Aerothermodynamics Research and Technology Lab (ARTLAB) at Georgia Institute of Technology. NASCART-3D is a viscous solution-adaptive Cartesian grid flow solver [133]. It is capable of solving the Euler equations, Navier-Stokes equations, or a hybrid method with Euler and integral boundary layer equations for viscous flows. Including the integral boundary layer equations with the inviscid Euler equations allows the viscous effects of the boundary layer to be approximated near the surface without solving the full Navier-Stokes, thus increasing efficiency at the cost of some accuracy.

There are different kinds of meshing schemes used by CFD in the "tessellation of Euclidean space" which represent the flow and body surfaces [162]. Two broad mesh categories are structured and unstructured. A structured mesh tessellates the space with congruent element shapes in a regular pattern. An unstructured mesh is more flexible and allows for tessellation with various shapes, but in an irregular pattern. A comparison of the two mesh types is shown in Figure 19. An unstructured mesh requires a connectivity list to describe how vertices form elements and thus can require additional computational storage. A subdivision of these categories are Cartesian meshes where the normal of each element aligns with the directions of a Cartesian coordinate system.

NASCART-GT utilizes an unstructured Cartesian grid so all elements are either unit squares (for 2D) or unit cubes (for 3D). The elements can vary irregularly, depending on the flow features. The quality of a mesh is critical for achieving accurate solutions and so refinement is an important step in finding an appropriate mesh. In practice this was done manually and required extensive experience until automatic

mesh adaptation techniques were developed. NASCART-GT implements a mesh refinement algorithm which looks at specific aspects of the solution to determine where a finer mesh resolution is needed [164] and is shown in Figure 20. The solution parameters available for mesh adaptation include divergence, vorticity, entropy, magnitude and turbulence gradients. NASCART-GT was chosen for this work due to its industry acceptance, ease of use, previous work done with fluid-structure interaction and convenient access to the development team at the Georgia Institute of Technology. Specifically NASCART-GT can capture nonlinear compressibility effects such as shock formation to correct the baseline aerodynamic method which will be discussed.

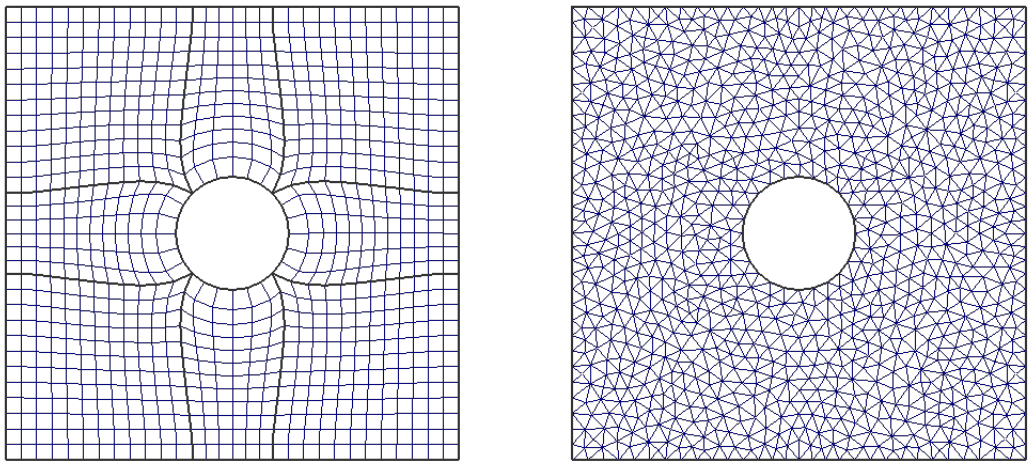

Figure 19: Different mesh types of a 2D cylinder. Left; structured grid, right; unstructured grid [3]

The inviscid Euler equations can be further simplified and have led to numerical methods which are less computationally expensive than CFD. An irrotational flow is one that has zero vorticity everywhere, $\nabla \times \boldsymbol{v} = 0$. Under the inviscid, irrotational and steady assumptions, the flow field is conservative and can be represented as the gradient of a scalar function called the velocity potential [18]. When the flow is also incompressible the governing equations reduce to the Laplace equation, $\nabla^2 \varphi = 0$, where φ is the velocity potential. Solutions to the Laplace equations can be superimposed to solve the velocity flow fields of many common aerodynamic problems,

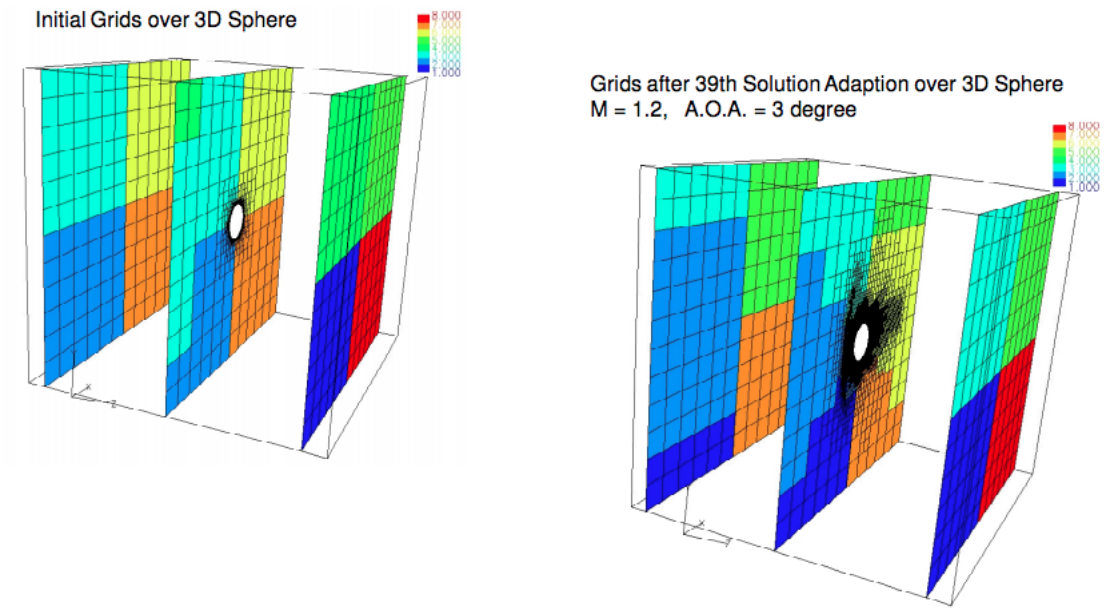

Figure 20: Solution-adaptive mesh refinement in NASCART-GT [134]

thus leading to potential flow theory. In panel methods a geometry is discretized into panels and potential flow solutions (singularities) are imposed on each panel. The pressure distribution can be resolved from the calculated velocity flow field. The assumptions limit potential flow to low subsonic speed regime without modification. Since their development in the 1960's more advanced panel codes have been adapted to handle unsteady and compressible flows [92]. The savings of computational time in panel methods come at the cost of accuracy compared to CFD or experimental methods.

MSC NASTRAN (2014) is a widely-used structural finite element analysis solver developed by NASA in the late 1960s [105]. In addition to structural analysis it has aeroelastic capabilities as well. Embedded in the aeroelastic analysis are several internal aerodynamic methods and the capability to import external methods such as CFD. Both internal and external aerodynamic capabilities will be utilized in this work. The internal method used here is the Doublet-Lattice method (DLM) and is an unsteady panel code. DLM was selected over other aerodynamic methods in NASTRAN because of its industry use and the chosen demonstration model; a commercial

transport wing, i.e. transonic flow, high aspect-ratio and a wing-only model[1].

The MSC Nastran aeorelastic users' guide describes the DLM theory [36]. DLM is based on linearized aerodynamic potential flow theory and thus ignores any viscous effects such as skin friction drag. Though lift-induced drag can be derived from lift, DLM doesn't account for drag due to D'Lambert's Paradox [38] and so no drag will be considered here. A lifting surface is modeled as a collection of trapezoidal flat-plate panels with side edges parallel to the free stream. Small-angle approximation is also assumed so the incidence of any panel with respect to the flow cannot be large. For each panel the unknown lifting pressure is assumed to be uniformly concentrated across the 1/4 chord line. This pressure is represented by imposing a string of singularities based on theoretical solutions to potential flow. The DLM imposes constant-strength oscillating doublets as singularities on each panel. DLM attempts to model unsteady aerodynamics by allowing each panel to oscillate out-of-plane in harmonic motion about a chosen control point. The control point is located at the 3/4 chord point and centered spanwise. It is the location where the normalwash boundary condition is satisfied. "The normalwash (or downwash) is the normal velocity induced by inclination of the finite-span lifting surface to the free stream" [128][56]. A schematic of the DLM formulation is depicted in Figure 21:

[1]The demonstration model only includes the empenage for required stability and control. The fuselage is not fully modeled and represented as a beam for mass and boundary condition purposes. See the Section 5.4.2 for more details

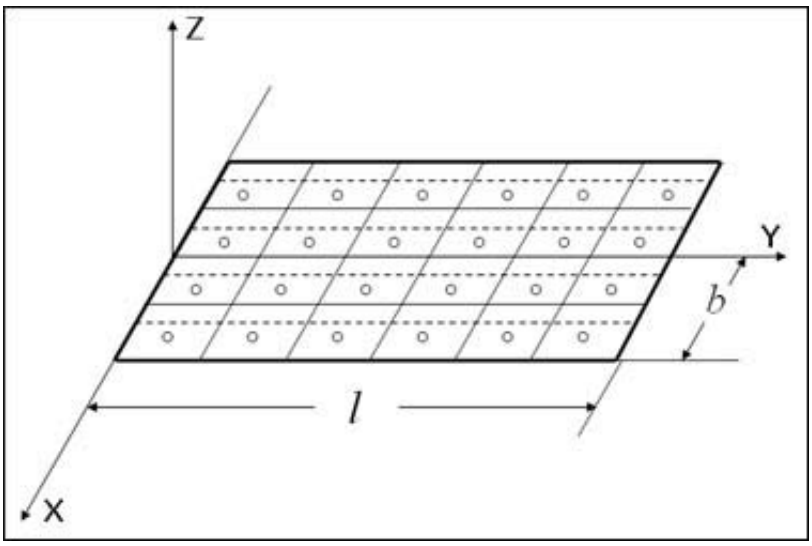

Figure 21: Panel discretization schematic of Doublet-Lattice Method [36]

where Y is the spanwise direction, X is the flow direction, open circles indicate control points and dashed lines indicate the 1/4 chord for each cell. Some limitations for DLM include its limitation to small deformations and problems where "in-plane kinematics are not important" [25][169] and "inability to capture all relevant steady aerodynamics in flight dynamics" [15]. DLM has been used widely in the aeroelastic community and leads to relatively efficient and reliable solutions [103]. DLM will be the baseline aerodynamic method used in this thesis.

The last category of aerodynamic analysis are the analytical methods. Closed-form expressions for aerodynamic forces require significant simplifications and thus have the lowest accuracy relative to the previously discussed categories but can be solved almost instantaneously. Such methods include thin airfoil theory and lifting-line theory. These methods are not compatible with the chosen model and modeling environment so will not be considered further. This thesis utilizes three aerodynamic analysis methods: panel codes via NASTRAN's Doublet Lattice Method, simulated wind tunnel testing and simulated flight load survey. The wind tunnel testing is simulated with rigid CFD analysis and the data is used to correct NASTRAN's DLM. The

flight load survey is simulated with CFD on a nonrigid model to incorporate aeroelastic effect and again used to correct NASTRAN, see Figure 22. All CFD analysis is done via NASCART-GT. The first two methods represent different fidelity levels and thus have different uncertainties while the flight load survey is treated as "truth" in this context. Details on their implementation will be discussed in the experimental setup in Chapter 5.

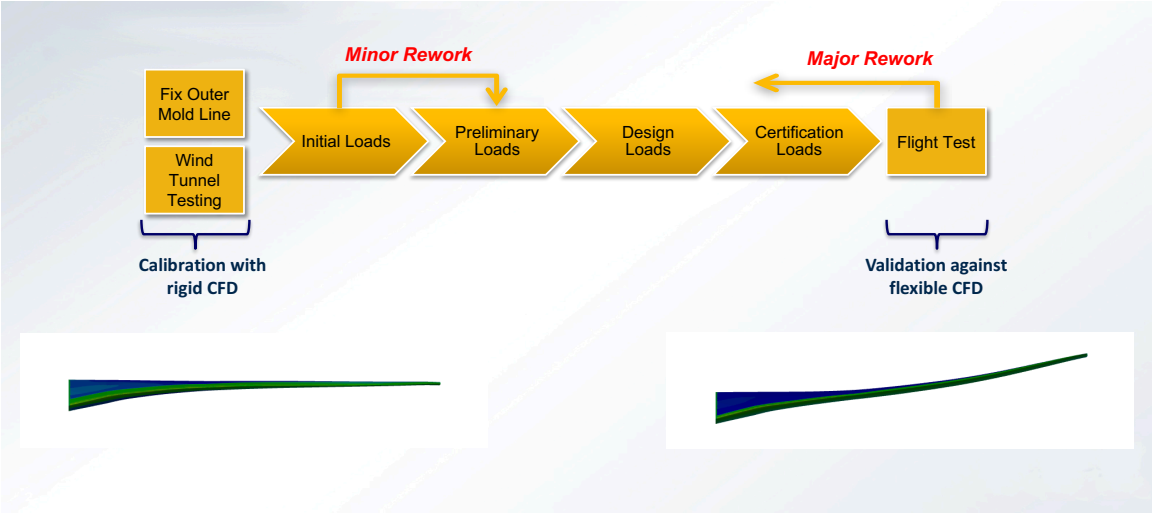

Figure 22: Schematic of integrating rigid and flexible CFD into loads analysis

5.4.2 Doublet-Lattice Method Model

A complete uCRM NASTRAN model was provided by The Boeing Company to serve as the demonstration model and was developed in collaboration with NASA. The development and original purpose of the model were not fully disclosed so only the aspects of the model relevant to this work will be discussed. Although the model was fully-functioning, significant modifications were necessary to implement it into the loads analysis M&S environment and will be discussed in the remaining sections of this chapter. The model included a half-span DLM aerodynamics model with wing,

fuselage, empenage and engine nacelles. The aerodynamics model is has infinitely thin surfaces and subject to the requirements of DLM discussed in Section 5.4.1. The DLM model is shown in Figure 23. The "engines" are modeled as lifting surfaces, no propulsion analysis is utilized in this environment.

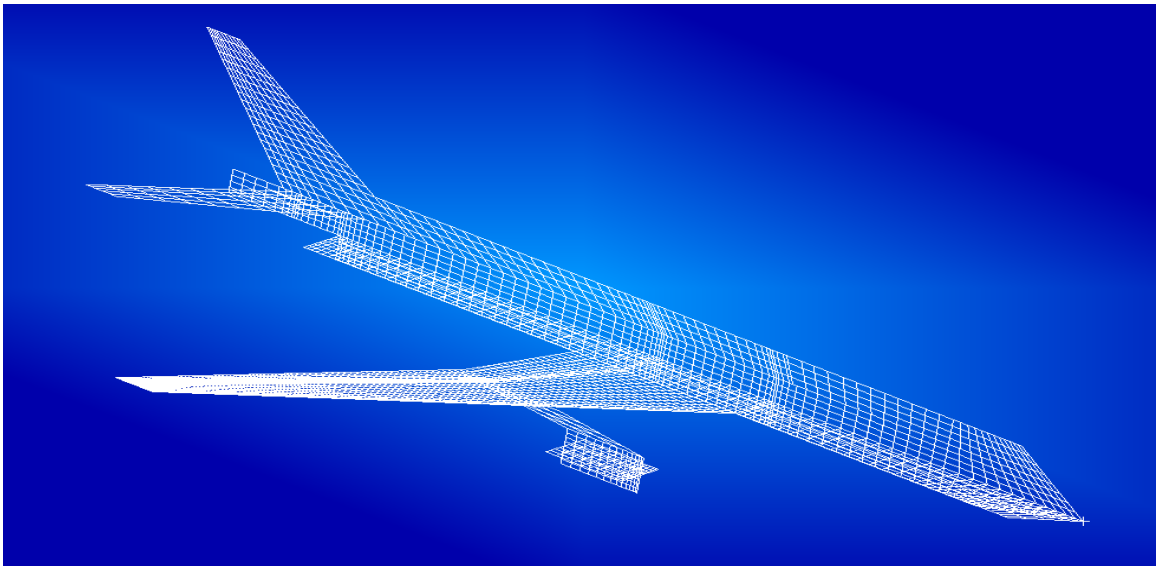

Figure 23: uCRM NASTRAN DLM aerodynamic model

For the demonstration model, this work focuses on the wing and only utilizes the other components as necessary. The wing mesh consists of 2,323 quad elements (referred to as aerodynamic boxes) and 101 chordwise strips along the span which are aligned with the flow direction as required by DLM. This will be important because the aerodynamic empirical adjustment factors representing epistemic uncertainty are treated as constant along each strip. For trimming purposes, control surfaces are defined in NASTRAN for the ailerons (inboard and outboard), elevator and rudder.

The aerodynamic model is connected to the structural model with splines for aeroelastic analysis. In NASTRAN the DLM mesh is primarily used to calculate aerodynamic pressure and transfer to the finite element mesh. Thus the normal modeling requirements of FEA such as mass, material properties, boundary conditions etc. are not applied directly to the DLM mesh. Several splining options are available

but this model utilizes "infinite plate" splines. See Section 5.5.2 for more details.

5.4.3 Computational Fluid Dynamics Model

The CFD data used for calibration with NASTRAN is an integral part of the M&S environment and uncertainty quantification. Some of the CFD theory pertaining to NASCART-GT has been discussed in Section 5.4.1 and the process and results of coupling between CFD and NASTRAN is detailed in Section 6.2. This section focuses on important aspects of developing the uCRM CFD model in NASCART-GT. NASCART-GT consists of four primary input files; *stl* file with mesh definition, general input file, geometry configuration file and post-processing file.

The mesh is inputted with a stereolithography (stl) file format which is common for CAD programs. Luckily, MSC Patran (the post-processor for NASTRAN) has the ability to export a finite-element mesh into an stl file. In addition to the uCRM NASTRAN model a 3D aerodynamic was developed and made publicly available by original developers at the University of Michigan [71]. The file is in an Initial Graphics Exchange Specification (IGES) format, but can be imported into Patran. Once imported, surface geometries were created and meshed with 205,910 triangular elements (CTRIA3). Typically CFD requires a finer resolution mesh than FEA, which is the case here.

The main input file for NASCART-GT contains a number of user-defined parameters to control the CFD analysis. Some key parameters will be discussed, an example input file for the uCRM model is included in Appendix A. The Mach and altitude load case parameters determine the freestream condition inputs for Mach number, pressure and temperature. The effects of load factor and fuel weight are not captured in the static modes of NASCART-GT used here, but there is a dynamic model capability which could potentially model these effects. Although not explicitly a load

case parameter, the angle of attack is dependent on the load case and this is modeled in NASCART-GT. The angle of attack is one of the most important parameters for coupling CFD to NASTRAN as will be shown later. Although capable of handling small 2D viscous problems, it would be intractable for a viscous analysis of the uCRM model so these features are turned off.

Several parameters exist for defining the surface boundary conditions, flowfield grid and gas properties among others. A major advantage of NASCART-GT is its mesh adaptation which reduces the modeling effort significantly which often plague CFD analysis. Nevertheless there are parameters which control the simulation and grid adaptation which had to be adjusted for the uCRM model and are listed in Table 3.

Table 3: uCRM NASCART-GT Settings

NUMBER_OF_ITERATIONS	10000
ADAPTION_FREQUENCY	500
ADAPTION_START	500
ADAPTION_STOP	8000
GRID_RESOLUTION	256

The number of iterations and adaptation settings were selected based on convergence plots of the integrated loads which are calculated in NASCART-GT. An example of such a plot is shown in Figures 24 and 25. As in this example, the solution converges prior to the maximum number of iterations. In Figure 24' legend F refers to force components and M refer to moment components, starting from 0 (e.g. the x component is the zeroth component) which aligns with NASCART-GT's convention. The spikes in the residuals occurs every 500 iterations when the mesh

adaptation occurs. A higher frequency and higher stopping iteration causes the mesh to refine more which typically results in more accurate solution but increased computational cost. The GRID_RESOLUTION turned out to be a very important setting for the uCRM model. It was discovered that the resolution had to be increased from the default settings due to the wing geometry and mesh in order to avoid errors in the cell slicing functionality of the mesh adaptation. This substantially increased the number of cells after refinement and the computational cost. Runtime varied from case to case but some took on the order of 72 hours to complete on a single 24-core supercomputer cluster node. Such runtimes are common for CFD, which is why accounting for the computational cost in this thesis is so important.

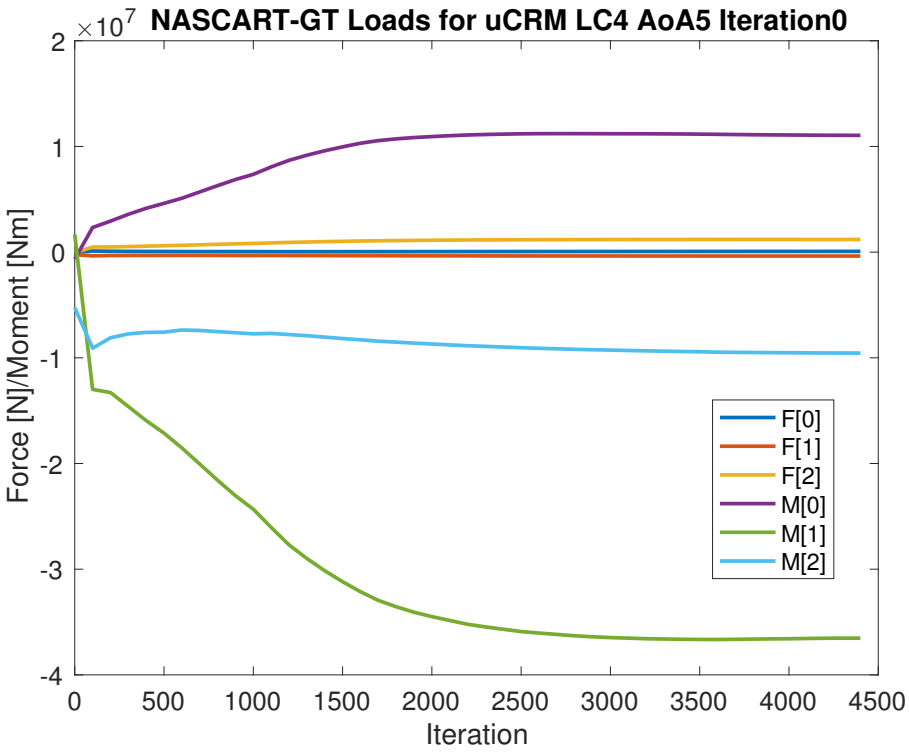

Figure 24: NASCART-GT integrated load convergence

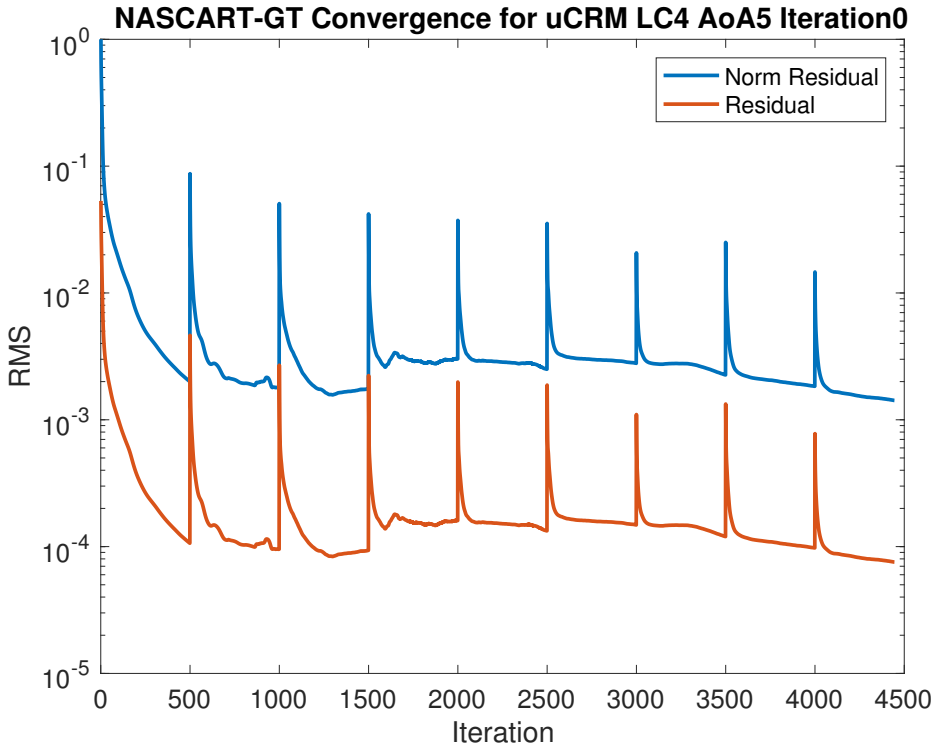

Figure 25: NASCART-GT residual error

5.5 Structural Analysis & Design

5.5.1 Structural Analysis Overview

Loads experienced by an aircraft come from sources other than aerodynamics. The weight of the structure, payload, fuel and subsystems cause inertial loads. The structure is non-rigid so elastic loads occur. If in a landing or crash configuration, impact loads will also occur. Structural analysis calculates stresses, strains and deformation due to these loads using three sets of equations [21]. The equations of motion can be posed as the equilibrium equations for a differential volume in the material to determine the internal stresses due to applied forces and moments:

$$\nabla \boldsymbol{\sigma} + \rho \boldsymbol{b} = \rho \boldsymbol{a} \tag{15}$$

where $\boldsymbol{\sigma}$ is the stress tensor, $\boldsymbol{b}$ is the vector of body forces and $\boldsymbol{a}$ is the acceleration of the differential volume. The constitutive laws, i.e. stress-strain relations, are used to determine the strains given stresses:

$$\sigma_{ij} = C_{ijkl}\epsilon_{kl} \tag{16}$$

where C_{ijkl} is the elasticity tensor and is the strain tensor in index notation. Finally the strain-displacement relations are used to determine the deformation from the strains:

$$\epsilon_{ij} = \frac{1}{2}\left(\frac{\partial u_i}{\partial x_j} + \frac{\partial u_j}{\partial x_i}\right) \tag{17}$$

in index notation where u is the deformation vector and x is the Cartesian coordinate vector. Together with the appropriate boundary conditions, these equations form the governing equations to solve an elastic deformation problem. More complicated problems, such as involving heat or crack propagation, can be solved with modified or more general forms of these equations.

Similar to aerodynamics, structural analysis methods can vary in complexity and accuracy based on the physical assumptions of the theory. There are also experimental, numerical and analytical methods. Experimental methods include tests such as fracture, fatigue or crack propagation to determine different properties of a material or system. Typically coupons composed of material used in the actual system are subject to loading and strain gauges determine the strain measurements. Through these

measurements the resulting stress and deformation can be backed out. For aerospace applications the usual limitation in these experiments is the equipment size because of their inability to properly test the actual components in the environments they will experience once assembled. Only after detailed design are full-scale test vehicles built to undergo static tests, fatigue and vibration tests which are very costly. On the other end of the spectrum, analytical methods require significant assumptions to reach an equation which can be solved exactly and without numerical methods. An example would be the Euler-Bernoulli beam equations in one-dimension [44]. Most, if not all, of these methods are inappropriate for aerospace structures beyond the very beginning conceptual phase of design. Neither experimental nor analytical methods will be used in this work due to their expense and low accuracy respectively.

Numerical methods are widely used in structural analysis. In aerospace the numerical methods are often validated experimentally via ground and flight test. The most prominent numerical method is finite element method (FEM) used in finite element analysis (FEA) software. The finite element method is a discretization method like that of CFD to solve structural mechanics problems for complex systems. A body is discretized into elements on a structural mesh and the boundary conditions and governing equations, called a boundary-value problem (BVP), are imposed and solved at each element. The global BVP is "rephrased into its weak form in order to approximate it locally on each element using chosen basis functions" [123]. Similar consideration for meshing occurs for FEM as previously discussed for the finite-volume method in CFD. NASTRAN will be the FEA solver used for structural analysis in this work.

The constitutive laws require material properties in order to determine strains from stresses or vice versa. Thus the material definition is an important design and analysis problem which becomes more complex if considering composites instead of metals in aerospace. A composite material is any material composed of two or more

constituent materials with distinct physical or chemical properties which when combined produce different characteristics than the individual constituents. These materials, specifically carbon-fiber-reinforced polymers, have been used widely in recent aerospace designs due to their lightweight and high strength-to-weight ratio compared to conventional metals [155][41]. The flexibility in designing composites allow them to take advantage of directional stiffness but also introduce more design variables such as parameters related to ply orientation and layup [69].

A commercial software program called HyperSizer is utilized to facilitate the material definition and structural sizing. HyperSizer includes an extensive database and advanced analysis capabilities for composite design. In this work, the material definition will be fixed and metallic so many of these design features will not be utilized. The primary use of HyperSizer will be for determining critical loads via failure analysis and structural sizing. Although these fall in the realm of structural design, these methods will be discussed separately in Section 5.5.4.

5.5.2 Aeroelastic Analysis Overview

The coupling of aerodynamic and structural phenomena has been well-studied, but not entirely well-understood, since the earliest fixed-wing flight. In fact, the Wright Brother's are viewed by some as the first experimental aeroelasticians with their wing-warp (twist) method of control [125]. Aeroelasticity is the study of the coupling between aerodynamic, inertial and elastic forces which occur when a flexible body is subjected to fluid flow. Aerodynamic loads deform the structure of an aircraft, but this deformation also changes the lift distribution which subsequently changes the aerodynamic load. The complexity and cyclical nature of this coupling requires additional analysis methods to determine aeroelastic effects, such as iterative methods [98]. The introduction of thermodynamic effects and control surface forces are deemed

aerothermoelasticity and aeroservoelasticity respectively, but won't be considered in this work. Aeroelastic analysis is divided into two fields: static and dynamic. The "Collar Triangle" is often used to describe the attributing disciplines under static and dynamic aeroelasticity:

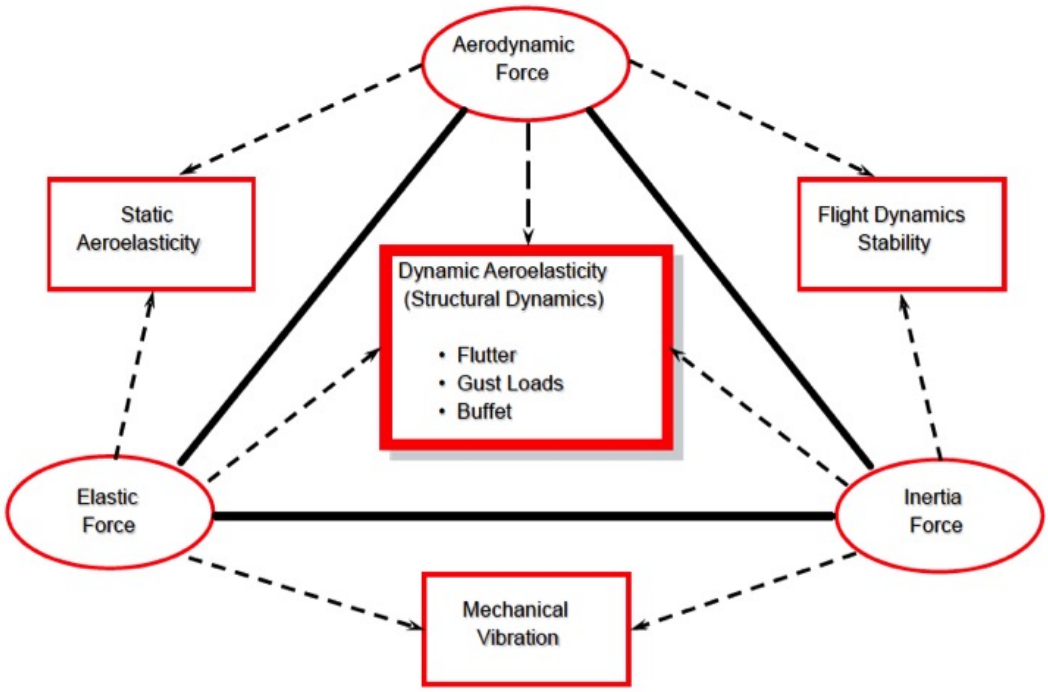

Figure 26: Variation of Collar Triangle, Frode Engelsen 2015

Under dynamic aeroelasticity the adverse physical phenomena of gust loads, flutter, buffeting and transonic effects are studied with the usual intent of avoiding them [52]. Due to the complexity and available computational resources, this work will focus only on static aeroelasticity and consequently only the coupling between aerodynamic and elastic forces.

Static aeroelastic analysis is predominantly used to analyze maneuver loads, but also to study the phenomena of divergence and control reversal. Divergence occurs when the elastic structural response is unbounded given a finite external force input. Typically this occurs when an aircraft reaches a certain velocity and its wings twist or bend uncontrollably to the point of catastrophic failure [100]. The speed at which this

occurs is called the divergence speed and the goal of this analysis is to calculate this speed. Traditional aeroelastic design seeks to alter this divergence speed so it does not occur within the operating conditions of the aircraft. Control reversal occurs when the deflection of an aircraft's control surface results in either loss of control or the opposite response than intended [118]. Typically this occurs when the wing deforms to the point when the lift vector caused by the aileron deflection is zero or reverses direction.

In addition to avoiding adverse phenomena, both static and dynamic aeroelasticity are used in design to take advantage of an aircraft's flexibility. A commonly used definition for aeroelastic tailoring is [150]:

> *"the embodiment of directional stiffness into an aircraft structural design to control aeroelastic deformation, static or dynamic, in such a fashion as to affect the aerodynamic and structural performance of that aircraft in a beneficial way,"*

Aeorelastic tailoring has been studied since late 1960's and many benefits have been explored including weight minimization, flutter, divergence, stress, roll reversal, control effectiveness, lift, drag, skin buckling and fatigue [30]. Composite materials are a natural enabler for aeroelastic tailoring because of their ability to achieve directional stiffness. Other enablers include "smart materials" which actively change their configuration or properties when exposed to an external stimuli [41]. In this work the material definition will be fixed throughout the analysis so aeroelastic tailoring will not be considered explicitly though aeroelastic analysis will be a central component.

Static aeroelastic analysis will be carried out using MSC NASTRAN. The aerodynamic and structural analysis theories have been previously discussed. NASTRAN couples these analysis by interpolating between the aerodynamic and structural grids

and the theory is described in the aeroelastic users' guide and summarized here [36]. The aerodynamic grids are flat-panel lifting surfaces from DLM and the structural grid is 1, 2, or 3-dimensional array of grid points from the finite element mesh. The interpolation method used is called splining. Several splining methods are available including linear, surface and user-defined splines. These methods transform the deflections and forces between aerodynamic and structural models. A matrix describes this transformation:

$$\{u_k\} = [G_{kg}]\,\{u_g\} \tag{18}$$

$$\{F_g\} = [G_{kg}]^T\,\{F_k\} \tag{19}$$

where the subscripts g and k describe the aerodynamic and structural property respectively, u is the deflections, F is the force and G_{kg} is the transformation matrix defined by the chosen splining method. Splines allow dissimilar aerodynamic and structural grid points to be connected, and also allows the grid sets to be chosen independently to better suite the aerodynamic and structural theories respectively.

NASTRAN performs static aeroelastic analysis by calculating the aircraft trim conditions, with "subsequent recovery of structural responses, aeroelastic stability derivatives, and static aeroelastic divergence dynamic pressures" [36]. The basic set of equations for static aeroelastic analysis in NASTRAN is:

$$[K_{aa} - \bar{q}Q_{aa}]\,\{u_a\} + [M_{aa}]\,\{\ddot{u}_{aa}\} = \bar{q}[Q_{ax}]\{u_x\} + \{P_a\} \tag{20}$$

where K_{aa} is the stiffness matrix, M_{aa} is the mass matrix, P_a is the vector of applied loads, $\bar{q}$ is the flight dynamic pressure, u_x is the vector of aerodynamic "extra" points

used to describe aerodynamic control surface deflections and overall rigid body motions, $\ddot{u}_{aa}$ is the vector of translational accelerations, Q_{aa} is the aerodynamic influence coefficient matrix, and Q_{ax} is a matrix "providing forces at the structural grid points due to unit deflections of the aerodynamic extra points" [36]. The subscript a refers to the structural analysis-set. The splining matrix of Eq 18 and 19 is used to transfer all the aerodynamic properties to the corresponding grid points on the structural mesh.

5.5.3 Finite-Element Analysis Model

The uCRM model also includes a FEA structural model of the wingbox. The DLM and FEA models are coupled through the aforementioned splines and together they form the complete model for NASTRAN's static aeroelastic analysis, known as solution sequence 144. The FEA model is shown in Figure 27. The main component of the model is the mesh defining the wingbox which is highlighted in green. Other components include the fuselage modeled as a rigid beam, horizontal tail and inboard and outboard ailerons. This particular model is intended for symmetric maneuvers, i.e. pitch, so only the horizontal tail is necessary for trimming. Concentrated mass elements (CONMN2) are added to simulate the weight and inertial effects of the aircraft and are shown in magenta triangles. The mass elements model fuel weight and are influenced by the fuel density load case parameter. Rigid body elements (RBE's) connect nodes from different component meshes and the concentrated masses. RBE's are depicted with magenta lines and circles.

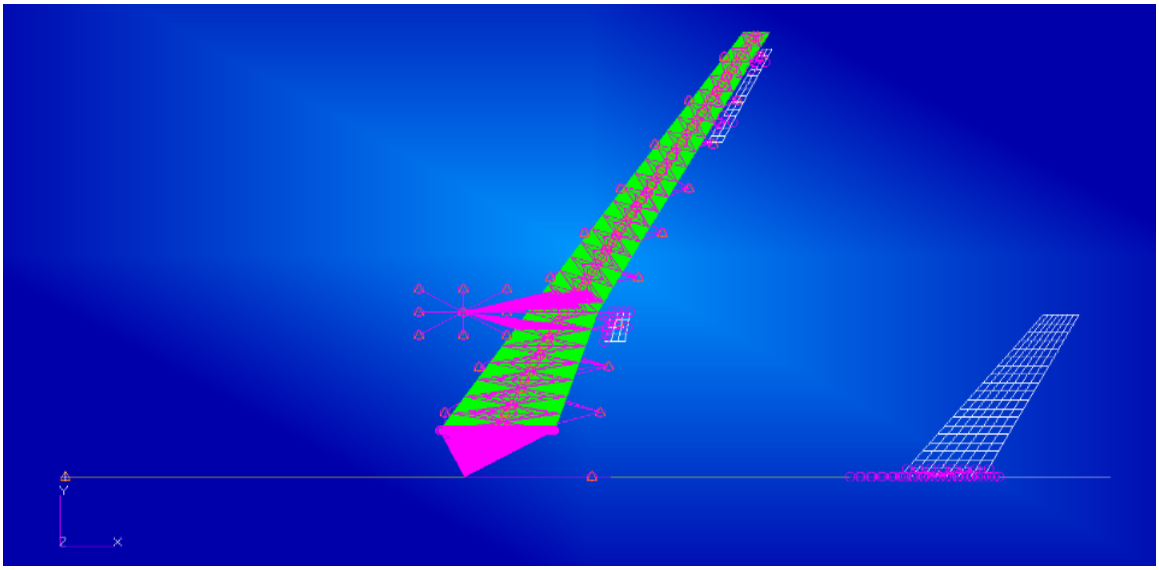

Figure 27: uCRM NASTRAN structural model

Unlike the aileron and tail meshes, the wing box mesh is significantly finer than the DLM mesh. This is primarily due to the requirements of FEA to achieve an accurate solution. The wingbox mesh has 51,702 quad elements (CQUAD4). The original model had triangular elements (CTRIA3), but those were incompatible with HyperSizer at the time. Creating the quad mesh took a significant amount of effort, primarily due to redefining numerous other model entities to the new quad mesh nodes. The original wingbox contained a front and rear spar, fifty-two ribs[2], and upper and lower wing skins with stringers. The main advantages of HyperSizer stems from its ability to efficiently analyze various component types with the "smeared stiffness" approach (see Section 5.5.4). Therefore the discrete stiffeners included in the original FEA model would undermine the component design in HyperSizer and so they are removed from the FEA model. The fuselage, tail and control surfaces are retained in the FEA model but are excluded from the HyperSizer model. Given the focus of this framework, it is only necessary to size the wingbox components.

[2]The uCRM model published in [71] had only 46 ribs, so it is assumed additional ribs were added to the model by The Boeing Corporation

Although HyperSizer modifies the stiffness and material definitions of FEA model, an initial set of properties must be assigned prior to the first iteration. These initial properties can be thought of as initial assumptions of loads group in the first load cycle, when there is a large degree of uncertainty because detailed structural analysis has yet to be done. Such assumptions may come from previous conceptual design studies and will impact the convergence through the load cycles and the final design for certification and flight testing. Table 4 lists some of the initial properties of the FEA wing model, some have been modified from the original model. The wingbox is assumed to be entirely composed of a generic aluminum metal. All FEA mesh elements are shell elements with the exception of the fuselage which uses bar elements. The bending moment of inertia ratio $12I/T^3$ is a NASTRAN shell property for the "ratio of the actual bending moment of inertia of the shell, I, to the bending moment of inertia of a homogeneous shell, $T^3/12$" [105].

Table 4: Summary of Wingbox Initial FEA Properties

Young's Modulus E	70.0 GPa
Shear Modulus G	26.9231 GPa
Poisson's Ratio ν	0.3
Thickness T	0.02 m
$12I/T^3$	5.0

In NASTRAN, each mesh element must have an associated property set (PSET). For example, all of the properties shown in Table 4 are assigned to shell elements via PSHELL entries. A convenient way to group components is to assign them the same property set. Such groupings needed to be modified for integration into HyperSizer

as will be discussed. Therefore it was necessary to redefine the property sets in NASTRAN from the original model.

5.5.4 Failure Analysis and Critical Loads

In the context of an aircraft manufacturer, determining the critical values to design a structure can be approached from two perspectives. The typical aerospace organization has a loads group and stress group [109]. This section will explore some of the details behind both the perspectives as well as how they will be viewed in this thesis.

The ultimate goal of the loads group is to produce the internal loads in each structural component which will be used for structural design by subsequent analysis and design groups. The analysts will evaluate a large set of load cases consisting of different types and parameters to calculate the external loads. These loads and appropriate boundary conditions will be imposed in the equilibrium equations (Equation 15) and will be solved by a structural solver, such as FEA, to produce the resulting internal loads. For preliminary wing analysis, the important external loads are the three-dimensional shear force, bending moment and torsional moment distributions in the primary structure [87]. The locus of these forces and moments will form an envelope where the outer edge represents the highest loading. To the loads group this envelope represents the critical loads [165].

The loads group would then give the subset of critical loads to the stress group. The stress group, which is typically much larger than the loads group, will determine the stress, strain and deformation due to the provided internal loads [165]. To do this they will evaluate the constitutive (Equation 16) and strain-displacement equations (Equation 17) using a structural solver. The process of determining critical loads is more involved from the stress perspective because it involves failure analysis. Failure

analysis is the process of determining when a structure will "fail" and how it will fail by any number of physical failure modes [68]. For example, a simple failure mode is necking of a linear-elastic ductile material under tensile load in the axial direction. The member will undergo plastic deformation when the yield stress is reached and fail under ultimate stress. If a component were analyzed where plastic deformation was unacceptable, the highest normal stress would be compared with the material's yield stress. The comparison would determine a margin of safety for the component. An example calculation is shown in Equation 21.

$$Margin\,of\,Safety = \frac{\sigma_y}{\sigma_{applied}} - 1 \tag{21}$$

where σ_y is the yield stress.

The larger the margin of safety, then presumably the safer the component is from that failure mode. Failure does not necessarily mean something physically breaks, it can be defined as not meeting a requirement. There are commonly published material properties for metals. Other forms of Equation 21 are used for the calculation of margins where an "allowable" stress (or load) is used instead of the applied stress for design purposes. A classic, but some view as conservative, factor of safety used in aerospace is 1.5 [80][120]. A factor of safety is a similar concept to margin of safety. Equation 21 can be modified slightly to be put in terms of safety factors (FOS):

$$Margin\,of\,Safety = \frac{Allowable\ stress}{Calculated\ stress * FOS} - 1 \tag{22}$$

There are numerous failure analyses for failure modes related to bending, shearing, torsion, buckling, crack propagation, cyclical loading, impact, etc. The stress group uses such failure analysis in conjunction with predetermined allowables and margins

of safety to evaluate the structural response. Every load case is analyzed by a set of failure methods in every component under consideration. The load case resulting in the lowest margin of safety for a particular component (or section) is viewed as critical by the stress group and is different from the loads group. Even though both are appropriate, in this work critical load cases are selected based on the margin of safety as was discussed in Section 5.3.3. Clearly the values for the allowables and margins have a large influence on the structure because they are a measure of how conservative the design will be. High margins may produce overly conservative designs which are overweight and result in lower performance even though they will be safer in terms of structural failure. Margins which are too small are risky and susceptible to failure even though they may be light weight.

Once identified, the critical cases will drive the design to ensure the structure will satisfy all safety requirements during operation. The structural design procedure optimizes the component size, shape, material definition and topology to ensure all required margins are met while reaching some objective. The classical structural design objective in aerospace is to minimize weight, but advances in MDAO have allowed other objectives such as manufacturing and lifecycle costs to be included as well [32][50].

In the proposed approach aeroelastic analysis is used to determine external and internal loads for each component. This information is passed to an analysis program called HyperSizer to carry out the failure analysis and structural design. HyperSizer is a structural design software from the Collier Research Corporation and;

> *"...is used throughout the design process–including certification–to quantify all critical failure modes, reduce structural weight, and sequence composite laminates for fabrication to avoid unexpected design problems and weight*

growth as the design matures. It provides a complete CAE software interface that is used from preliminary design to final analysis." [35]

HyperSizer specializes in composite design and has a large database of composite material properties and structural failure methods. Although the proposed framework could incorporate composite materials into the structural design by taking advantage of HyperSizers' unique capabilities, this will be left for future work. To simplify, develop and evaluate the framework, only traditional metals will be considered in this work.

HyperSizer utilizes a "smeared stiffness" approach to efficiently analyze component shapes when performing structural optimization. Smeared stiffness is a modeling technique to transform local stiffness from discrete subcomponents to a single global stiffness representation of a structural component. For example, in Figure 28 four strategies are presented for modeling a stiffened panel. Strategies 2, 3 and 4 model the stiffeners as discrete subcomponents of the stiffened panel. The smeared stiffness method is utilized in strategy 1 and visualized in Figure 28. Instead of discretely modeling these subcomponents, their individual stiffness are "smeared" into the global stiffness. This modeling approximation allows HyperSizer to represent numerous component designs and material definitions accurately and efficiently by avoiding the need to remodel or remesh in FEA [7]. After structural design optimization, HyperSizer updates the FEA input files with the appropriate stiffness and material definitions so that structural analysis can be done on the new design.

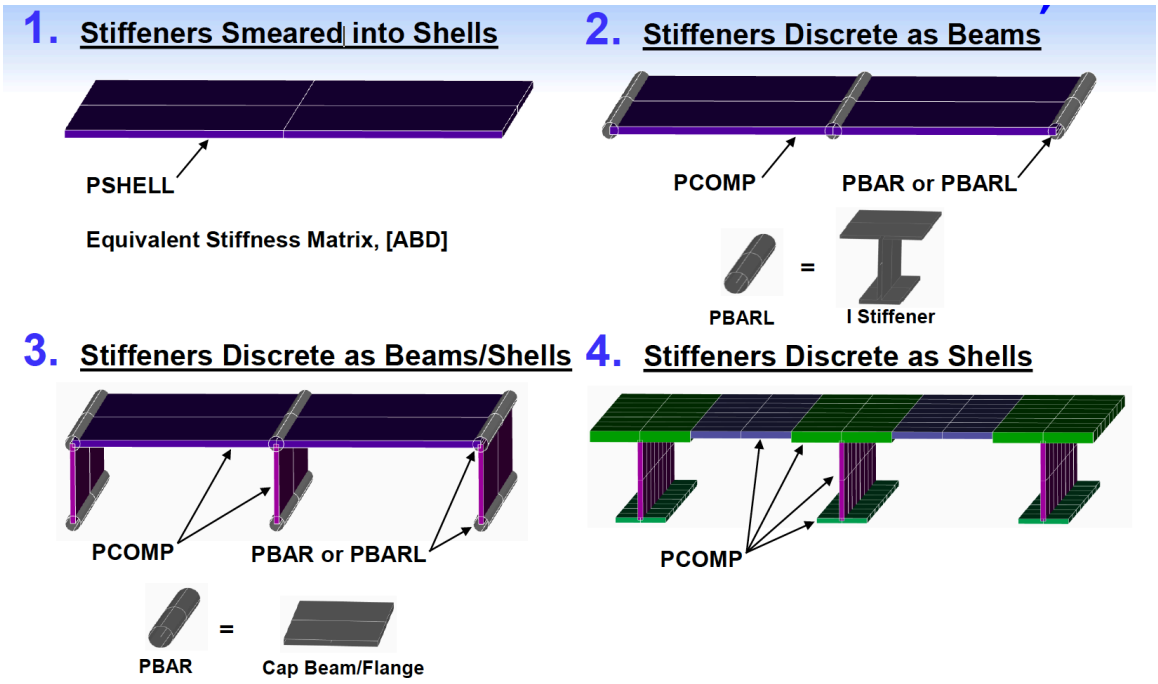

Figure 28: Stiffener modeling approaches using NASTRAN terminology [7]

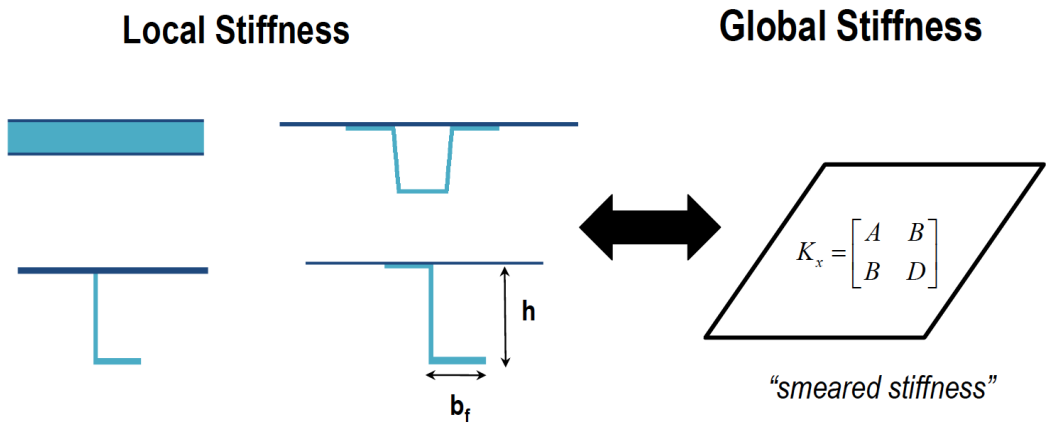

Figure 29: HyperSizer smeared stiffness method [7]

5.5.5 Structural Design Model

The HyperSizer model used for structural design optimization will be briefed in this section. At the core of the HyperSizer model is the FEA (or FEM) model itself. Data is automatically transferred from the FEA input and output into the HyperSizer database and outputted back to FEA after optimization. A summary of the relevant data imported and exported (updated) is shown in Figure 30. As discussed, only the wingbox is included in the HyperSizer model which is composed of shell elements in NASTRAN.

FEM Entity	Imported	Updated
Grids	✓	
Shell Elements		
- Grid Connectivity	✓	
- Offsets	✓	✓
- Orientation	✓	✓
- Property ID	✓	✓
- Stacking Sequence/Thickness	✓	✓
Materials		
- Material IDs	✓	✓
- Stiffnesses and allowables	✓	✓

Figure 30: FEM data transfered to and from HyperSizer [35]

The property ID entity in Figure 30 is very important to modeling in both NASTRAN and HyperSizer. HyperSizer has two main levels of abstraction for model features; assemblies and components. At the higher level, assemblies are intended to group features which share similar properties or are manufactured as single entities while components describe discrete features. HyperSizer uses the property ID's from the FEM model to define components. As was alluded to in Section 5.5.3, the original uCRM NASTRAN model had property ID's which needed to be redefine to integrate appropriately with HyperSizer's component and assembly definition. In the current

HyperSizer model there are 50 assemblies consisting of 86 components in total. The upper and lower skins, front and rear spars and 46 ribs are all separate assemblies. The ribs were treated as separate assemblies because each rib geometry differs in a discontinuous fashion and could not be manufactured with the same mold per se, unlike the skins and spars.

An assembly in HyperSizer will have the same material definition and compatible component designs. For simplicity and better tractability of results, only a single material was used for all assemblies. The material is an aluminum with similar elastic properties to the original NASTRAN models but HyperSizer requires a more detailed definition. Table 5 lists the properties of the aluminum used in the HyperSizer model.

Table 5: uCRM HyperSizer Material Properties

Form	*Plate*
Spec	*AMS 4206*
Temper	*T7751*
Basis	*B*
ρ	0.1004339 lb/in^3
T_{ref}	32° F
α	12.77778 μin/in/F
F_{tyL}, F_{tuLT}	88 ksi
F_{tuL}	91.00001 ksi
F_{tyLT}	86.99998 ksi
F_{tuLT}	91.00002 ksi
F_{su}	48 ksi

where F are design allowables for the material and the subscripts t and c refer to tensile and compressive, y and u for yield and ultimate (1.5 safety factor), L and LT

for longitudinal (parallel to grain) and long traverse directions (longest dimension perpendicular to grain, i.e. width) and s for shear, respectively.

All the components within an assembly should have the same design space of component concepts for the optimization to choose from. There are numerous concepts available in HyperSizer, for example I-stiffened, Z-stiffened, sandwich panel, etc. For similar reasons as the material, only one concept was considered; unstiffened panel. Although not realistic given many of the wingbox components on commercial transports are stiffened, this concept has only one dimension; thickness. This significantly simplifies the sizing results and allows better tractability of the margin of safety throughout the load cycles. A schematic of the component concept is pictured in Figure 31.

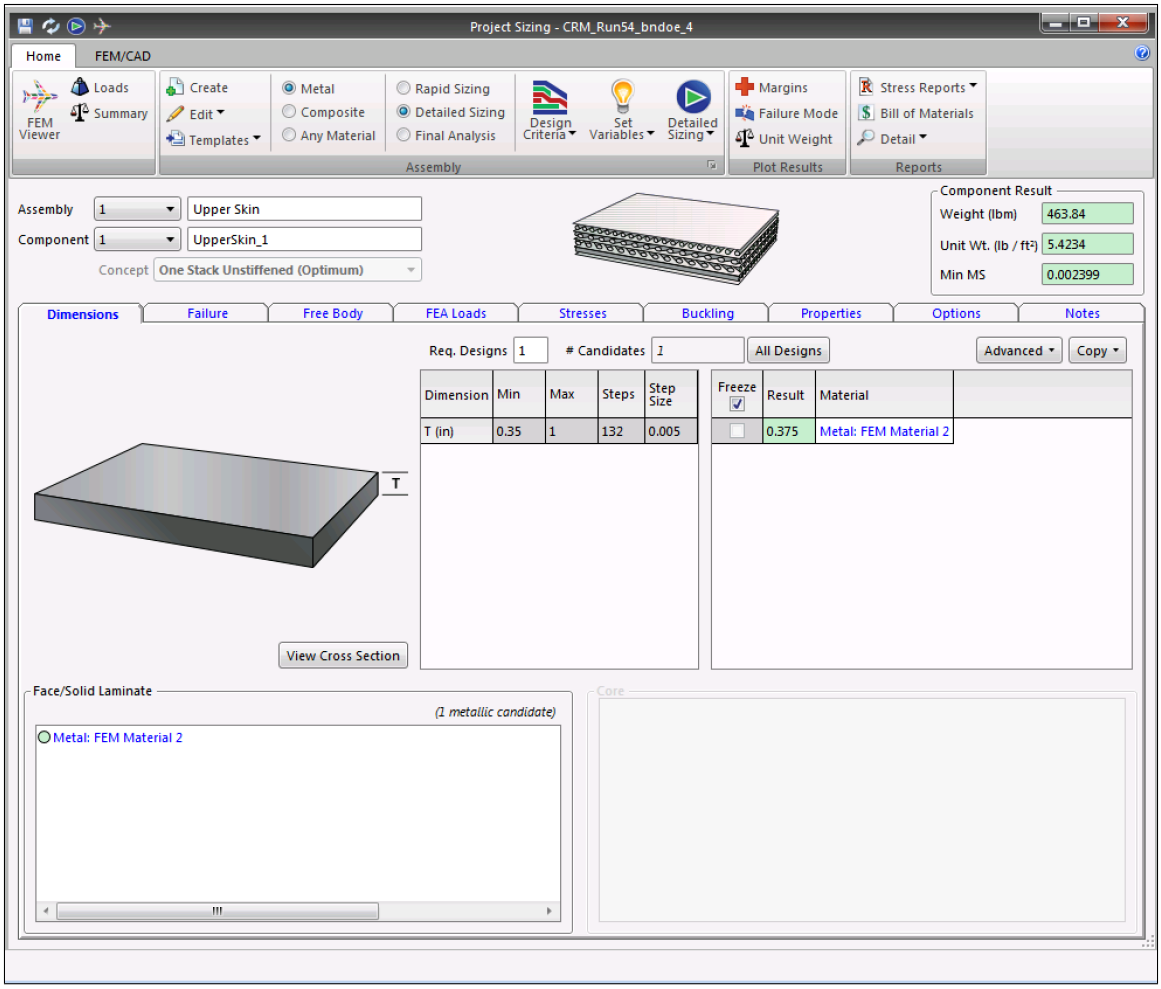

Figure 31: HyperSizer unstiffened panel component concept

The last pertinent feature of the HyperSizer model is the failure analysis. Only one failure method was utilized; von Mises yield stress criterion. This method was chosen because of its wide-use in structural analysis which will allow some intuition in interpreting the margin of safety results. According to the HyperSizer documentation on the von Mises criterion [35]:

> "...also called maximum-distortion-energy criterion, theorizes that a component is safe as long as the maximum distortion energy per unit volume in a material is smaller than the distortion energy required to cause a yield in a

tensile test specimen of the same material (Beer and Johnston 1981)"

Under this criteria all panels are as plane stress. The theory was originally developed for limit load but HyperSizer has modified it for ultimate load. A comparison of the von Mises and well-known Tresca criterion is depicted in Figure 32.

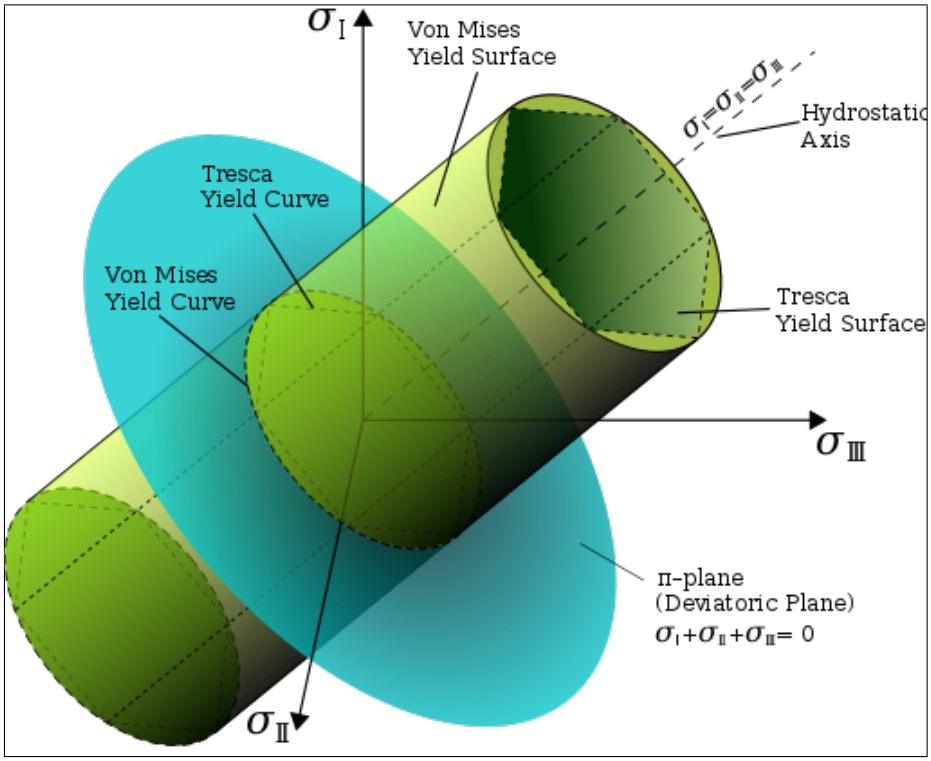

Figure 32: von Mises and Tresca yield surfaces in the principle stresses coordinates, including the Deviatoric Plane and the Hydrostatic axis [132]

Using this criteria we can directly attribute failure and the margin of safety to several physical quantities, namely the distortion energy. The distortion energy can first be derived from the Cauchy stress tensor which is composed of the hydrostatic stress tensor and deviatoric stress tensor [21]:

$$\sigma_{ij} = \frac{\sigma_{kk}}{3}\delta_{ij} + s_{ij} \tag{23}$$

where δij is the kronicker delta math function, σ_{kk} is the hydrostatic tensor which causes volumetric expansion or contraction on a stressed body and s_{ij} is the deviatoric stress tensor which distorts the body. It is common to look at invariants in the (Cauchy) stress tensor to determine principal stresses, the same thing can be done with the deviatoric tensor:

$$|s_{ij} - \lambda\delta_{ij}| = -\lambda^3 + J_1\lambda^2 + J_2\lambda + J_3 = 0 \tag{24}$$

where λ is constant of proportionality associated with the eigenvalue of the stress tensor and J are the invariants of the characteristic equation. Another interpretation of the von Mises crietrion is that yielding occurs when the second deviatoric stress invariant, J_2 reaches a critical value related to the well-known yield stress, σ_y [173]:

$$J_2 = \frac{1}{6}\Big[(\sigma_x - \sigma_y)^2 + (\sigma_y - \sigma z)^2 + (\sigma_z - \sigma x)^2 + \sigma_{xy}^2 + \sigma_{yz}^2 + \sigma_{xz}^2\Big] = \frac{\sigma_y}{\sqrt{3}} \tag{25}$$

In HyperSizer the von Mises criterion for ultimate load dictates failure when:

$$\sqrt{\left(\frac{\sigma_x}{F_{(tc)uL}}\right)^2 - \left(\frac{\sigma_x\sigma_y}{F_{(tc)uL}^2}\right)^2 + \left(\frac{\sigma_y}{F_{(tc)uLT}}\right)^2 + \left(\frac{\tau_{xy}}{F_{su}}\right)^2} > 1.0 \tag{26}$$

Only the critical load cases are of concern for sizing so all components are sized to the ultimate load which includes x1.5 safety factor compared to limit loads. Equation 26 can be interpreted as the ratio of the applied distortion energy to the allowable distortion energy, $Failure\ Criteria = \frac{DE_{applied}}{DE_{allowable}}$. The allowable distortion energy is

a function of the material stress allowables shown in Table 5 for the chosen material. The margin of safety based on this failure criteria for ultimate load is calculated by:

$$MS_u = \frac{1}{\sqrt{\left(\frac{\sigma_x}{F_{(tc)uL}}\right)^2 - \left(\frac{\sigma_x \sigma_y}{F^2_{(tc)uL}}\right)^2 + \left(\frac{\sigma_y}{F_{(tc)uLT}}\right)^2 + \left(\frac{\tau_{xy}}{F_{su}}\right)^2}} - 1.0 \tag{27}$$

when $MS_u > 0$ no failure occurs and the margin of safety can thus be interpreted as $MS_u = Failure\ Criteria - 1.0$. Table 6 summarizes the relationship between the margin of safety, von Mises failure criterion and the distortion energy.

Table 6: HyperSizer von Mises Criterion Summary

Margin of Safety	***Failure Criteria***	***Distortion Energy***
0	1.0	$Applied = Allowable$
1.0	0.5	$Applied = \frac{1}{2} Allowable$
∞	0	$Applied \ll Allowable$
-1.0	∞	$Applied \gg Allowable$

In HyperSizer failure analysis based on the von Mises stress criterion is performed on every component after each iteration. In order to simulate the loads process and keep track of minor rework, a component will only be redesigned if the calculated margin of safety is below the require margin. The alternative would be to redesign every component after every iteration. Based on subject matter expects the former was viewed as the more realistic practice and employed here. More redesign would result in decreased weight which may be viewed as more important from a performance perspective than any incurred cost from redesign. Nevertheless, redesigning

only when necessary allows us to analyze how decisions related to fidelity and margins would incur more or less minor rework, which is one of the costs used in resource allocation optimization problem.

5.6 Conclusion

An overview of the demonstration model based on the uCRM model and the modeling and simulation environments were given. The uCRM was chosen because a complete model was provided by The Boeing Company and because of its use in aeroelasticity studies, in addition to the popularity of its predecessor, the NASA Common Research Model. The M&S environment consisting primarily of NASTRAN for aeroelasticity, NASCART-GT for CFD and HyperSizer for structural design was briefly discussed. All three analysis methods required modifications to the provided uCRM model, which was a not a trivial task. An overview of the development of the necessary models for the respective programs was presented.

The uCRM provides a realistic model for evaluating the rework decision framework. The experimental plan and results are detailed in the next chapter. The experiments will be used to address the hypotheses and research questions and develop the uncertainty quantification, uncertainty management and overall framework for this thesis.

CHAPTER VI

EXPERIMENTAL PLAN, OBSERVATIONS & RESULTS

6.1 Summary of Research Development

An overview of the research development up to this point will be given and completed in this chapter. Generally speaking there is top-down approach for the research development where high-level objectives lead to a primary hypotheses and through the research development end at specific research questions and secondary hypotheses to answer them. As the development advances, the scope narrows and finer levels of details are required. After the research development is sufficiently defined the experimental plan is designed and executed to validate the hypotheses and answer the research questions with results. The conclusion of the thesis then addresses the original research objective and validates the associated primary hypothesis.

The primary purpose of this thesis is to improve decision making in loads analysis regarding rework. The motivation behind this and the importance of rework in aerospace design was given in Chapter 1. After observing sources of rework and limitations in the current approach to loads analysis and structural design the overall research objective of this thesis was posed:

> ***Research Objective:*** *Develop a methodology for loads analysis to quantify and manage uncertainty related to aerodynamics and load case parameters in order to improve decision making for rework by optimizing fidelity, load margins and structural margins for new concepts*

The objective can be decomposed to two specific research goals:

Research Goal 1: *Develop a methodology to quantify uncertainty due to aerodynamic analysis fidelity and load case parameter uncertainty*

Research Goal 2: *Develop a methodology to improve decision making for design rework in loads analysis*

Accomplishing these two goals in this thesis requires focus areas to review the literature and assess alternative methods. Clearly the field of uncertainty quantification is an appropriate research area for the first goal. For the second goal it is was identified from the motivation that uncertainty should be reduced within a framework to specifically address sources of rework in loads analysis. In order to reduce uncertainty in the context of realistic airplane development programs where cost overruns and delays are frequent, the field of uncertainty management was explored to define a potential method. The research areas of uncertainty quantification and management were identified under a hypothesis directly related to the research objective and overall purpose of this thesis. This hypothesis is referred to as the primary hypothesis because to encompasses all other hypotheses:

Primary Hypothesis: *For a given design scenario, the proposed framework involving uncertainty quantification and management will lead to improved decisions regarding rework and performance than the current approach*

A review of the literature was done and summarized in Chapter 3 related to the research focus areas and other necessary areas related to loads analysis. Observations and available methods from the literature review revealed gaps in research which could potentially be addressed by this thesis and contributions to the scientific community.

A summary of these gaps are:

1. *A comprehensive MDAO environment is not readily available for modeling load cycles in loads analysis and structural design*
2. *A standard procedure does not exist for estimating the epistemic uncertainty in linearized normal force coefficient slope due to shock formation*
3. *An established correlation between aerodynamic fidelity and design rework does not exist*
4. *A proactive rework mitigation strategy does not exist involving aerodynamic fidelity, load margins and structural margins for aeroelastic loads analysis which can be implemented in design phase*

Potential methods were explored and downselected to a few candidates which would be evaluated in experiments. Specific research questions were developed based on these candidate methods and in light of the aforementioned gaps. From the literature review, hypotheses were imposed to initially answer the questions. To differentiate from the primary hypothesis which addresses the entire thesis, these are referred to as secondary hypotheses. The experimental plan serves to provide sufficient data to address the research questions and accept or reject the primary and secondary hypotheses. A summary of the research questions and associated hypotheses and experiments are given below.

Sections 3.3 and 3.4 discussed the relevant background in uncertainty quantification as it pertains to loads analysis. The number of available options for UQ and uncertainty reduction were narrowed to Bayesian methods and use of Bayesian networks for modeling the loads analysis process and quantifying uncertainty. This choice led to the following:

Research Question 1: *What are the appropriate methods for defining the prior probabilities of uncertain nodes in the Bayesian Network?*

Hypothesis 1: *Epistemic uncertainty prior probability distributions can be defined based on the fidelity level and estimated relative error compared to simulated truth data*

It is difficult to compare one method of defining uncertainty to another other than from a theoretical basis or with actual truth data, i.e. recorded observations from a system in actual operation. The truth data referenced here is only simulated and refers to CFD results from a flexible model. Extensive effort has been done to estimate the epistemic uncertainty sources and answer the first research question. But instead of a formal experiment comparing alternate uncertainty modeling approaches, Hypothesis 1 will be accepted or rejected based on subject matter experts who will evaluate the results and use previous studies of related work from Bansal and Pitt (2013) [16].

Sections 3.3 and 3.5 discussed the importance of identifying important sources of uncertainty through sensitivity analysis. As discussed in Chapter 5, the M&S environment for loads analysis is computationally intensive and will require sensitivity analysis and other techniques to reduce the size of the problem. Additionally there are multiple sources of aleatory and epistemic uncertainty being modeled but only the latter are reducible. It can take significant effort to reduce uncertainty so to effectively management it is important to distinguish and compare aleatory and epistemic uncertainty, leading to the following:

Research Question 2: *How important is epistemic uncertainty to major rework relative to other sources?*

Hypothesis 2: *Empirical adjustment parameters with epistemic uncertainty will be significant among aleatory sources relative to the major rework response*

Experiment 1: *Determine impact of uncertainty on major rework*

Out of several potential uncertainty management approaches discussed in Section 3.3.4 the resource allocation method was chosen. No published studies utilizing this method were applied directly to loads analysis so modifications may be necessary:

Research Question 3: *How should the optimization problem be posed to effectively reduce and manage uncertainty in the loads analysis process?*

Hypothesis 3: *The resource allocation methodology provides an appropriate foundation to reducing and managing uncertainty in loads analysis*

Experiment 2: *Evaluate uncertainty management optimization approaches*

Chapter 4 overviewed the rework decision framework and discussed how uncertainty quantification and uncertainty management work together within the framework. Because this is a unique approach to address rework in loads analysis, the framework could be structured in numerous ways. The final research question is:

Research Question 4: *For a given design scenario, what is the appropriate method to improve rework decisions regarding major rework in loads analysis?*

Hypothesis 4: *For a given set of costs, optimizing the aerodynamic fidelity, load margin and structural margin will improve rework decisions regarding major*

rework

Experiment 3: *Determine impact of cost functions on major rework*

Experiment 4: *Evaluate framework to support rework decisions*

Addressing the final research question and hypothesis requires multiple experiments. Experiment 3 will determine the impact of the cost functions which are subjective. It also will look at a number of design scenarios reflect changing priorities for trading performance, uncertainty, rework and computational costs. The final experiment is the most important and compares the proposed framework against a baseline which is representative of the current approach to loads analysis. The results of Experiment 4 will accept of reject the primary hypothesis.

The remaining sections of this chapter detail the experimental plan, observations and results to address the aforementioned research objective, goals, questions and hypotheses. The conclusion of the experimental plan subsequently concludes the research development for this thesis.

6.2 Epistemic Uncertainty Quantification

6.2.1 Aeroelastic Coupling Overview

6.2.1.1 Purpose of CFD Coupling

There are two main purposes to coupling CFD to the aeroelastic analysis. The first is to model various levels of aerodynamic fidelity in order to realistically quantify aerodynamic epistemic uncertainty. Epistemic uncertainty is a cornerstone to this work because it is one of the main sources of design rework in aeroelastic loads analysis, as has been discussed. This thesis proposes a framework to reduce the uncertainty in the loads analysis process which requires the prior distribution of all uncertainty sources be defined. In order to accurately assess the performance of this framework the initial epistemic uncertainty due to aerodynamics should be as realistic as possible. The coupling of high fidelity aerodynamics through CFD with the low fidelity Doublet-Lattice Method (DLM) accomplishes this.

The second purpose of coupling is to simulate the actual loads process. As was shown in Figure 2, the loads process begins with wind tunnel testing of a rigid subscale model of the airplane configuration after it has been frozen through the conceptual design process. An aerodynamic database is then created to correct the computational aerodynamic analyses used in the load cycles. On the other end, flight testing is done after the completion of the load cycles to validate the design by subjecting it to realistic operating environments. These two activities must be simulated to recreate the loads process and test the proposed framework.

The rigidity of the wind tunnel model is a very important consideration and can be very complicated to match aeroelastic behavior [23]. Therefore rigid assumptions can be used, but naturally the wind tunnels models are not perfectly rigid [153] so elastic effects are removed from the data. Although the intention of using a wind tunnel is to get a more accurate prediction of aerodynamic pressure, the rigid assumption ignores the aeroelastic effect which in turn affects the accuracy of the pressure distribution

results. Also the loads from the wind tunnel analysis can be linearized in a commercial airplane development programs [102] so the data can be applied to and correct linear aeroelastic analysis. Thus when the computational aerodynamic analysis is calibrated with wind tunnel data, uncertainty is introduced by these rigid, linear assumptions. In this work the wind tunnel test data is simulated by performing CFD analysis of the undeformed (rigid) aerodynamic model.

Flight test validation is one of the most important (and expensive) activities in the loads process. All the assumptions from computational analysis and the design itself are tested by building a full-scale version of the finalized design, called the flight test article. This article is flown by test pilots and undergoes a series of maneuvers to simulate different flight conditions in a real environment. Similar to wind tunnel testing, this activity is simulated using CFD in this work. The external loads acting on an aircraft during the flight load survey can be nonlinear and the flexible structure is subjected to the full effects of aeroelasticity. Thus CFD analysis must be run on a flexible model. The flexible CFD coupling process is discussed in detail in Section 6.2.3.1. The flexibility in the structure cannot be exactly modeled because the structural stiffness is uncertain prior to the actual construction of the test article. As will be detailed later, the flexible CFD analysis is done on a model whose stiffness has been converged through a series of load cycles in order to represent the flexibility as accurately as possible.

6.2.1.2 Aerodynamic Empirical Adjustments

The method to supplement low fidelity analysis with high fidelity data is largely dictated by the analysis programs themselves. NASTRAN has two principal methods to include high fidelity aerodynamic data: direct import of an external aerodynamic

mesh and correction factors. The former is the more accurate approach and involves defining an external mesh in the appropriate format, which is then coupled to the NASTRAN structural FEA model. The demonstration model in this work was developed and vetted by experts at The Boeing Company and NASA. Using the direct import approach would require redefining all the controllers, splines, masses, boundary conditions and other quantities which link the aerodynamic model to the structural model and appropriately constrain both. After such modifications a verification study would then be necessary to ensure the new model was built correctly and met the same quality standards as the original. It was deemed that this approach would require efforts which were out of the scope of this thesis given the timeline.

The correction factor approach allows minimal modifications to the NASTRAN model itself and instead involves defining the $[W_{KK}]$ and $[FA2J]$ empirical adjustment matrices based on external high fidelity data. A schematic to visualize the effect of the corrections is shown in Figure 33. The $[W_{KK}]$ adjustment factor is intended to correct the aerodynamic force and moment applied to an element (also referred to as an aerodynamic box) on the DLM aerodynamic mesh for incidence changes. As discussed in the background the DLM is a flat-panel method and so $[W_{KK}]$ will correct the aerodynamic forces per incidence change to account for curvature and thickness in geometry and nonlinear compressibility which are captured in NASCART-GT but not in NASTRAN.

To show how the empirical adjustments are applied in NASTRAN, Equations 28-30 are explored. They represent three matrix equations which are used to summarize the relationships required to define a set of aerodynamic influence coefficients [129]. These are the basic relationships between the pressure and the dimensionless vertical, or normal, velocity induced by modifying the angle of the surface relative to the airsteam; i.e. the downwash (or normalwash) [36],

$$\{w_j\} = [D^2_{jk} + ikD^2_{jk}]\{u_k\} + \{w^g_j\} \tag{28}$$

$$\{f_j\} = \bar{q}[A_{jj}]^{-1}\{w_j\} \tag{29}$$

$$\{P_k\} = [W_{kk}][S_{kj}]\{f_j\} + \bar{q}[S_{kj}]\{f^e_j/\bar{q}\} \tag{30}$$

where:

w_j = downwash

w^g_j = static aerodynamic downwash

f_j = pressure of aerodynamic box j

q = flight dynamic pressure

k = reduced frequency, $k = \omega b/V$

ω = angular frequency

b = reference semichord

V = free-stream velocity

$A_{jj}(Mach, k)$ = aerodynamic influence coefficient matrix

u_k, P_k = displacements and forces at aerodynamic grid points

D^1_{jk}, D^2_{jk} = real and imaginary parts of substantial differentiation matrix

S_{kj} = integration matrix

$\{f^e_j/\bar{q}\}$ = *FA2J* matrix

It should be noted that w^g_j includes the static incidence distribution that may arise from an initial angle of attack, camber, or twist and is therefore a third type of empirical adjustment which can be inputted using the $[W2GJ]$ matrix. The inclusion of $[FA2J]$ using CFD data from the uCRM model already accounts for camber and twist so it is redundant to use both adjustments. Only $[W_{KK}]$ and $[FA2J]$ will be utilized in this work.

$[W_{KK}]$ is an Nx2 matrix where each row corresponds to an aerodynamic box and the columns are the correction factor for the force and moment respectively. It is derived based on the ratio of the pressure coefficient slope for CFD and DLM for corresponding points on the two meshes. For simplicity, it is assumed the force and moment have the same correction factor because they are both derived from the aerodynamic pressure. Two important factors come about from this correction factor: how is the pressure coefficient slope calculated and how are corresponding points found on CFD and DLM meshes given they are different? Both of these details are addressed later in Section 6.2.1.3.

The second adjustment factor available in NASTRAN is the $[FA2J]$ matrix. It is used to correct for the zero lift assumption at zero-degree angle of attack in DLM. This assumption comes about because of thin airfoil theory [5]. Thus the aerodynamic pressures at zero angle of attack are imported from NASCART-GT. Unlike $[W_{KK}]$, $[FA2J]$ is only defined for the undeformed (rigid) case and therefore remains the same for both rigid and flexible CFD coupling. $[FA2J]$ is an Nx1 matrix where each row corresponds to an aerodynamic control point located on an aerodynamic box. The issue of dissimilar meshes is handled in the same way for both $[W_{KK}]$ and $[FA2J]$ and is discussed in Section 6.2.1.4. Also, it should be noted that in this work $[W_{KK}]$ is the more critical of the two adjustment factors because it differs with the rigid and flexible assumption and is the primary method of modeling epistemic uncertainty in the aerodynamics.

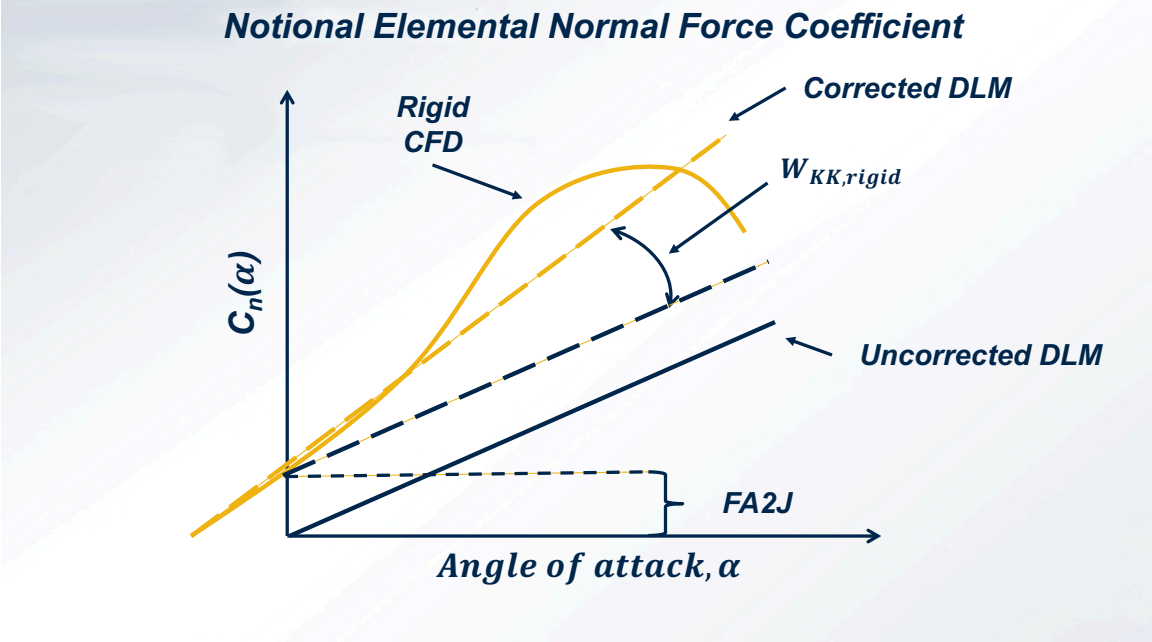

Figure 33: Corrections to normal force coefficient from NASTRAN empirical adjustments

6.2.1.3 Normal Force Coefficient

The aerodynamic data from the NASCART-GT CFD solver must be translated appropriately into the $[W_{KK}]$ and $[FA2J]$ matrices to incorporate this high fidelity data into NASTRAN. NASCART-GT produces several outputs as mentioned previously, but fthese empirical adjustments are only dependent on the coefficient of pressure, C_p, on the surface of the wing mesh (see Equation 31). $[FA2J]$ only requires C_p so this can be imported directly to NASTRAN after accounting for the dissimilar meshes. $[W_{KK}]$ is more complicated because it requires the ratios of pressure coefficient slope between NASCART-GT and NASTRAN. The slope is defined as the change in aerodynamic force divided by the change in angle of attack. All aerodynamic forces are essentially derived from pressure so C_p is used to calculate the slope.

$$C_p = \frac{p - p_\infty}{\frac{1}{2}\rho_\infty V_\infty^2} \tag{31}$$

The CFD and DLM meshes are quite different in terms of refinement, geometry and element types. The CFD mesh is much finer (205,910 elements) includes thickness and curvature and has triangular elements while the DLM mesh is coarser (3,132 elements), flat and infinitely thin and has quad elements. Thus many CFD elements will fit into a single DLM element causing non-smoothness in C_p distribution from CFD translated onto the DLM mesh. This is a discretization error and so one technique to avoid it is to use an area weighted average of the pressure coefficient, known here as the normal force coefficient, C_n instead of directly using C_p. C_n represents the force relative to the normal direction of the surface to which it acts, unlike the lift force which is perpendicular to the global flow direction. It is calculated as the area averaged pressure coefficient of M elements along the chord-wise strip of the wing mesh:

$$C_n = \frac{\sum_{\boldsymbol{i=1}}^{\boldsymbol{M}} C_{p_i} A_i}{\sum_{\boldsymbol{i=1}}^{\boldsymbol{M}} A_i} \tag{32}$$

Using C_n, each element in $[W_{KK}]$ is defined as:

$$[W_{KK}] = \frac{\left(\left(C_{n,CFD}(\alpha_1) - C_{n,CFD}(\alpha = 0)\right)/(\alpha_1 - 0)\right)}{\left(\left(C_{n,DLM}(\alpha_2) - C_{n,DLM}(\alpha = 0)\right)/(\alpha_2 - 0)\right)} \tag{33}$$

where α is the angle of attack in radians and is specified differently depending on whether rigid or flexible CFD coupling is used. Details for defining α will be discussed in their respective sections in 6.2.2.1 and 6.2.3.1.

6.2.1.4 Transferring Loads Between Dissimilar Meshes

One of the challenges of the correction factor method in NASTRAN is the data needs to be communicated between dissimilar meshes. An algorithm was developed to automatically find the corresponding elements between the two meshes and some key aspects of this method are discussed in this section. The CFD and DLM are both based on the same uCRM model [71] so the DLM model is simply a 2D projection of the uCRM model planform. This makes the translation between meshes much easier because only the vertical z direction differs between corresponding points on the meshes.

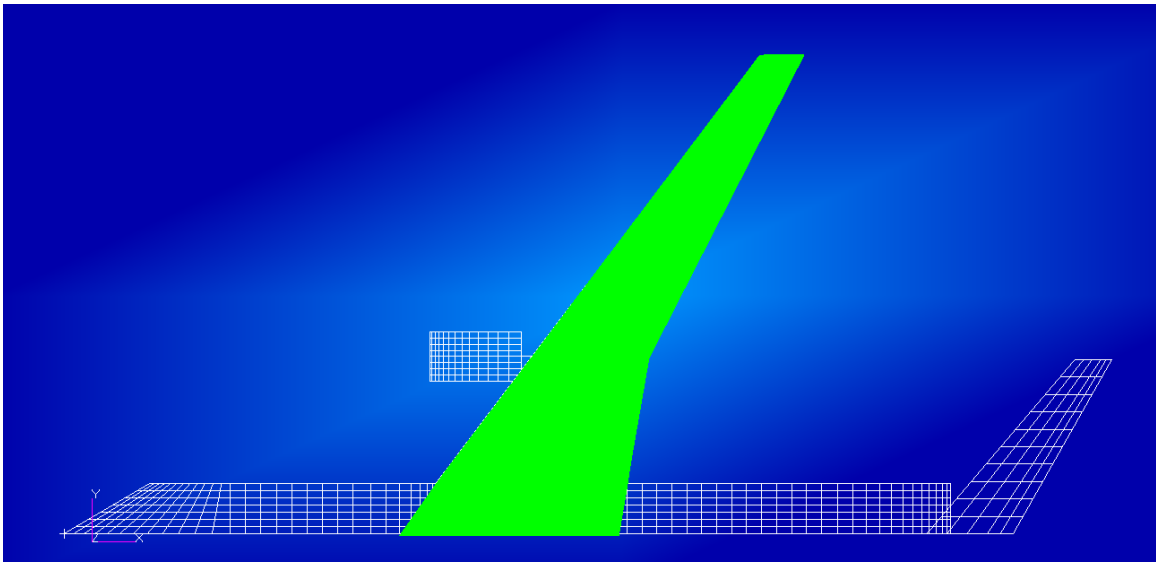

Figure 34: Alignment of planforms for CFD mesh (green) and DLM mesh (white).

The computational demands of CFD require a much finer mesh resolution than DLM, in addition to more elements needed to account for the geometry. Thus the resolution difference between the meshes is substantial. The first step of the matching algorithm is to find all the triangular CFD elements which fit into a given DLM quad element. Given the identical planform shapes, only the x and y coordinates of a given

element's centroid need to be considered.

Pressure is a function of the surface area so the C_p from NASCART-GT is dependent on the triangular element area. The topology of the meshes means there will be overlap between the edge of the DLM boxes and the projection of the CFD elements. The overlapping areas must be taken into account to correctly translate the appropriate forces. The overall matching algorithm is described in the following steps for each DLM element:

Step 1: Search entire CFD mesh and find nodes projected inside DLM element.

Step 2: Identify CFD elements associated with nodes from Step 1.

Step 3: Check each CFD element from Step 2 and find any projected intersection points with DLM element edge.

Step 4: Using intersection points, calculate adjusted projected area of each CFD element inside the DLM element.

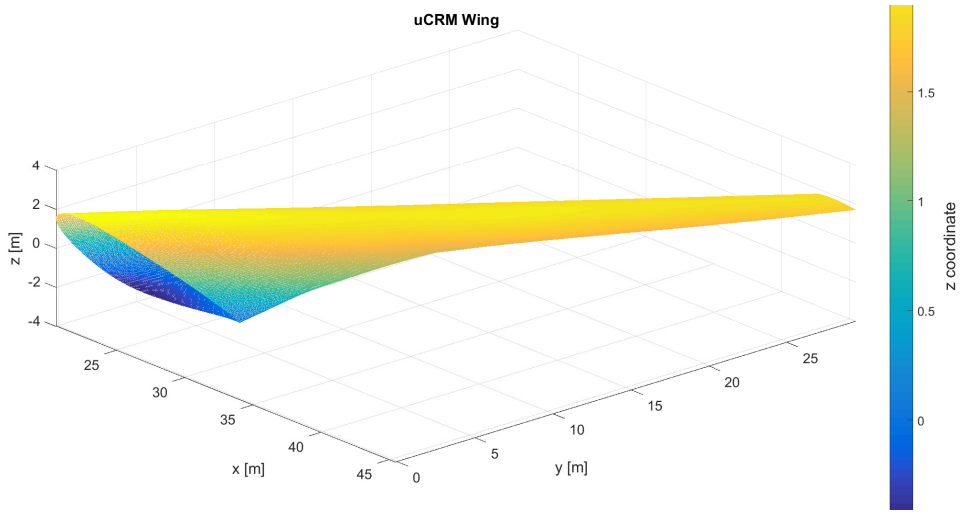

Figure 35: Triangulation of CFD wing mesh used for matching algorithm

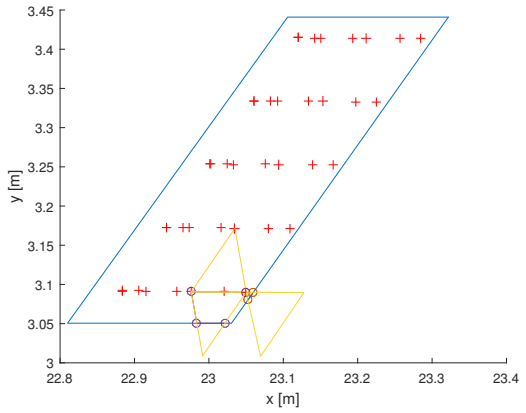

(a) Steps 1-2: Nodes (red) of CFD triangular mesh elements (yellow) matched to DLM quad element (blue)

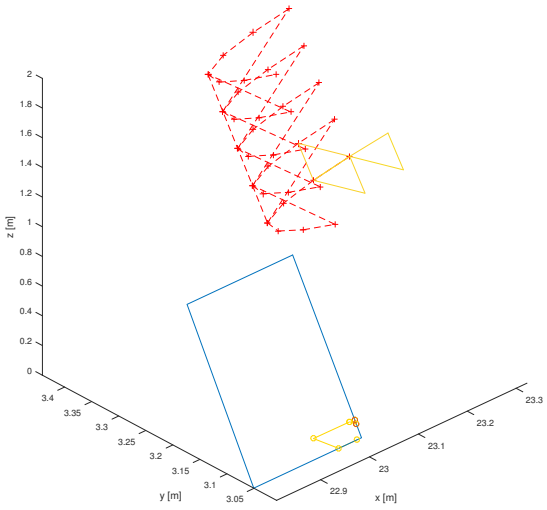

(b) Step 3: Intersection points (circles) of CFD elements on DLM element and adjusted projected area. Red dashed lines represent the 3D wing surface.

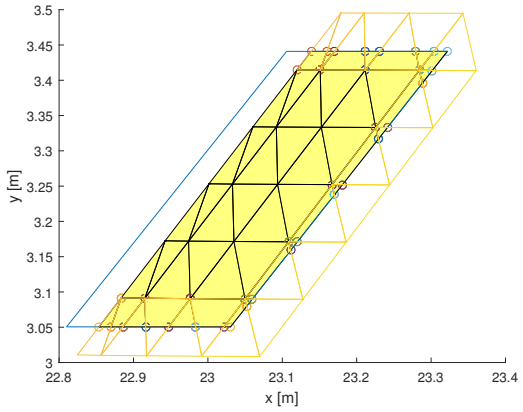

(c) Step 4: Projected area (yellow) of all matched CFD elements.

Figure 36: Example of matching algorithm for dissimilar meshes at leading edge.

Once the CFD elements have been matched for a given DLM box they are grouped by whether they are on the top or bottom surface so the correct C_P is calculated. This is easily done using the normal vector outputted from NASCART-GT for each

element. The lack of thickness in the DLM means that there are no distinct top and bottom surfaces so the difference between the top and bottom C_P is transferred to NASTRAN. Physically this makes sense because the aerodynamic lift is related to the difference in pressure between the top and bottom surface of an airfoil.

In order to preserve virtual work in the transfer of forces, the coefficient of pressure from CFD is calculated using Equation 34 for *i=1,2 ... M* CFD elements matched with DLM element j:

$$C_{p_j} = \frac{\sum_{\boldsymbol{i=1}}^{\boldsymbol{M}} C_{p_i} A_i}{A_j} \tag{34}$$

Equation 34 is used for $[FA2J]$ and is inserted into Equation 32 to find the normal coefficient, which is then used in Equation 33 to calculate $[W_{KK}]$.

6.2.1.5 Limitations of Empirical Adjustments

In comparison to the direct import method, the correction factor approach is less accurate because the latter still relies on the Doublet-Lattice Method for all aerodynamic calculations and applies the resulting forces to the structural model. NASTRAN only provides a few types of corrections which do not compensate for all physics missing in the DLM. Specifically, the $[W_{KK}]$ correction to the normal force coefficient slope assumes a linear slope. In reality the slope is not linear for viscous, compressible flow. In addition, the geometrical differences between the DLM mesh and structrual mesh causes the feedback between loads and structural response to have some error. Thus even if the empirical adjustments were exactly known, the limitations of the DLM would reduce the accuracy of the aeroelastic solution in comparison to using CFD data directly with the structural model as is done in the

direct import method. But these limitations must be weighed against computational costs, complexity and modeling effort.

The empirical adjustments are limited by the fidelity of the external aerodynamic analysis used to calculate them. NASCART-GT is primarily intended for inviscid analysis and thus cannot capture viscous effects such as viscous drag, boundary-layer interaction and flow separation. The last item is of particular interest in this work. Although incapable of accurately modeling flow separation, almost all inviscid solvers suffer from numerical viscosity which can lead to numerical (i.e. non-physical) flow separation [115]. The numerical schemes to discretize the momentum advection Euler equations and extrapolate states between mesh cells results in truncation errors. The error term mimics the diffusive nature of viscosity [49] and so a byproduct is an inviscid flow can portray viscous-like phenomena. Thus at high angles of attack the NASCART-GT flow solution can separate from the body and cause nonlinear effects in the aerodynamic properties. $[W_{KK}]$ can only be used to correct a linear slope so any numerical separation should be avoided to maintain the accuracy of the correction factors and risk adding uncertainty rather than reducing it.

Due to the nature of how $[W_{KK}]$ is calculated, the problem of numerical separation is more pertinent to flexible CFD coupling where higher angles of attack are necessary. The maneuver vertical load factor used in NASTRAN for these cases are carefully chosen to keep the trimmed wing angle of attack in the linear range and avoid this phenomena. The details of this approach are discussed further in Section 6.2.3.

6.2.1.6 CFD Coupling Summary

The goal of coupling external CFD data to the FEA solver is to quantify epistemic uncertainty and simulate the loads process in an actual development program. The correction factor approach was chosen over the direct import method in NASTRAN due to the significant modeling and verification efforts needed for the latter. This

choice does come with certain drawbacks including inherent inaccuracies due to DLM and the need to translate aerodynamic forces between the dissimilar CFD and DLM meshes. The process to do this translation and calculate the $[W_{KK}]$ and $[FA2J]$ empirical adjustment matrices was outlined.

The empirical adjustments are only as accurate as the external aerodynamic analysis used to calculate them. The choice of an inviscid CFD solver benefits from less computational cost but also comes with the inability to capture viscous phenomena in addition to nonphysical nonlinearities due to numerical viscosity which must actively be avoided. All of the methods discussed in this section are implemented in the results shown in the remainder of Section 6.2 related to aerodynamic fidelity.

6.2.2 Rigid Coupling of CFD and Doublet-Lattice Method

6.2.2.1 Rigid CFD Coupling Process Overview

In Equation 33, α_1 and α_2 are defined for rigid CFD coupling as arbitrary angles of attack greater than zero. The angles can be arbitrary because only the change in C_n is of interest. For the CFD analysis, $\alpha_1 = 0.0349066$ radian (two degrees) because the angle is small enough to avoid any numerical separation. For the NASTRAN analysis, $\alpha_2 = 1$ radian is used out of convenience so the denominator in the lift curve term is unity. Unlike in CFD, the NASTRAN analysis can be run at a high angle of attack because flow separation and other viscous phenomena aren't captured.

The general steps for calculating rigid $[W_{KK}]$ is fairly straightforward; CFD analysis is done using the undeformed mesh for each load case at $\alpha = 0, 2^o$. NASTRAN analysis is done for each load case but with the aeroelastic feedback turned off and constrained so the trimmed $\alpha = 1$ *rad*. Turning off the aeroelastic feedback is akin to running a rigid analysis so the CFD and DLM data are comparable. The results from the CFD and DLM are then used in conjunction with the previously discussed matching algorithm to calculate rigid $[W_{KK}]$, $[FA2J]$ is the same for both rigid and

flexible coupling. Next, the results for the rigid CFD coupling are presented.

6.2.2.2 Rigid CFD Results

Results from the rigid (undeformed) CFD analysis at $\alpha = 0^o$ are of particular importance because they alone define $[FA2J]$ and are used throughout all the analysis. The effects of angle of attack will be seen in the next section. It should be noted that dynamic behavior was not modeled in NASCART-GT (although it is capable) so the vertical load factor is irrelevant for all undeformed CFD results. All flowfield pressure values are in Pascals [Pa].

Load Case 1: Mach 0.85, 43100 ft

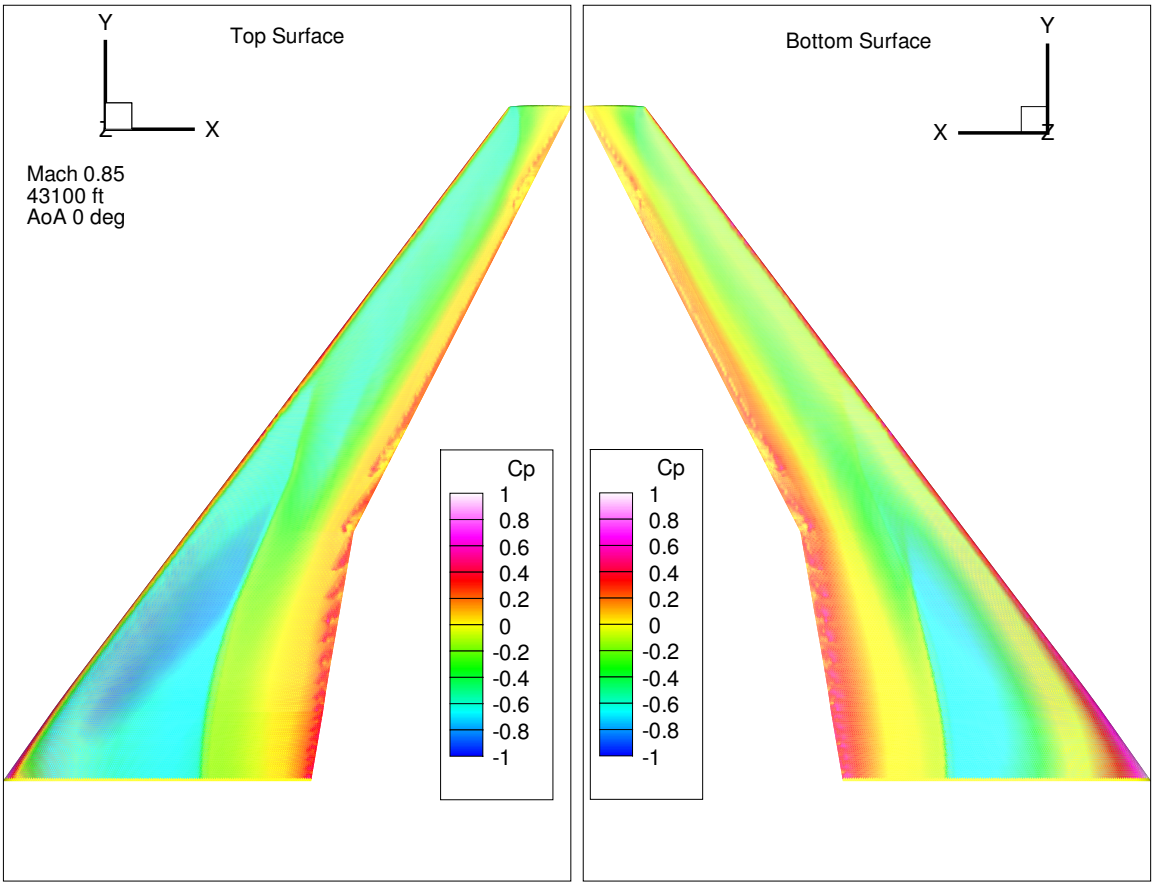

Figure 37: C_p distribution on top and bottom surfaces.

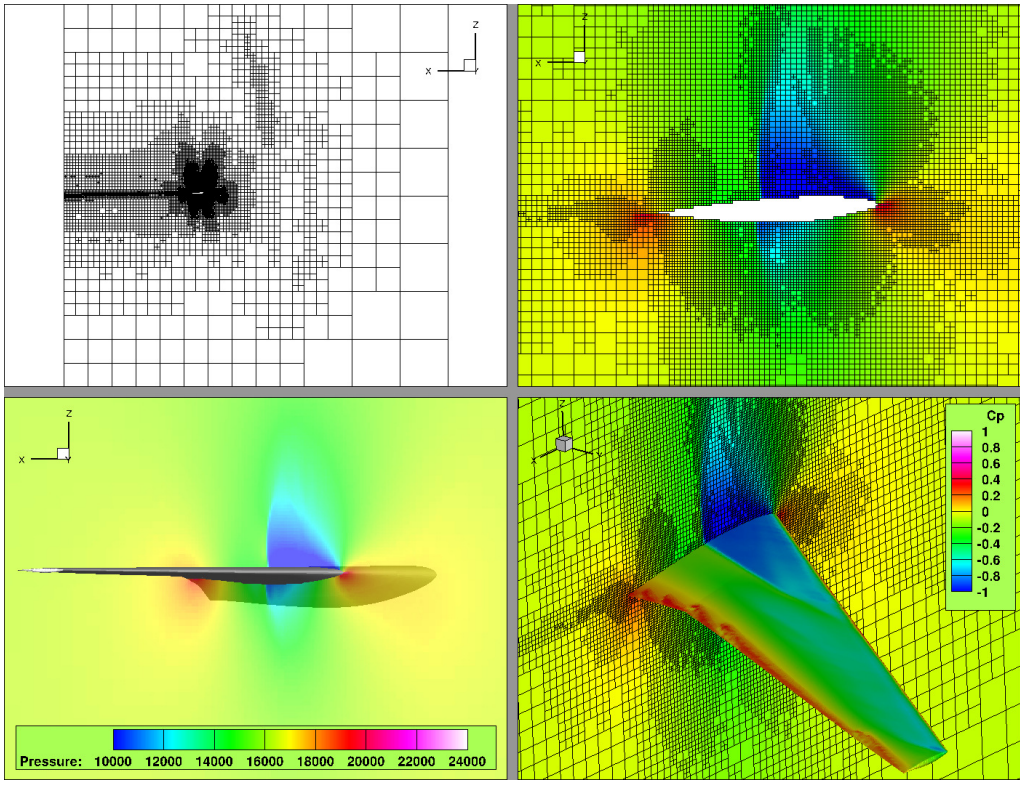

Figure 38: Flowfield mesh and pressure at 25% span and C_p on wing surface.

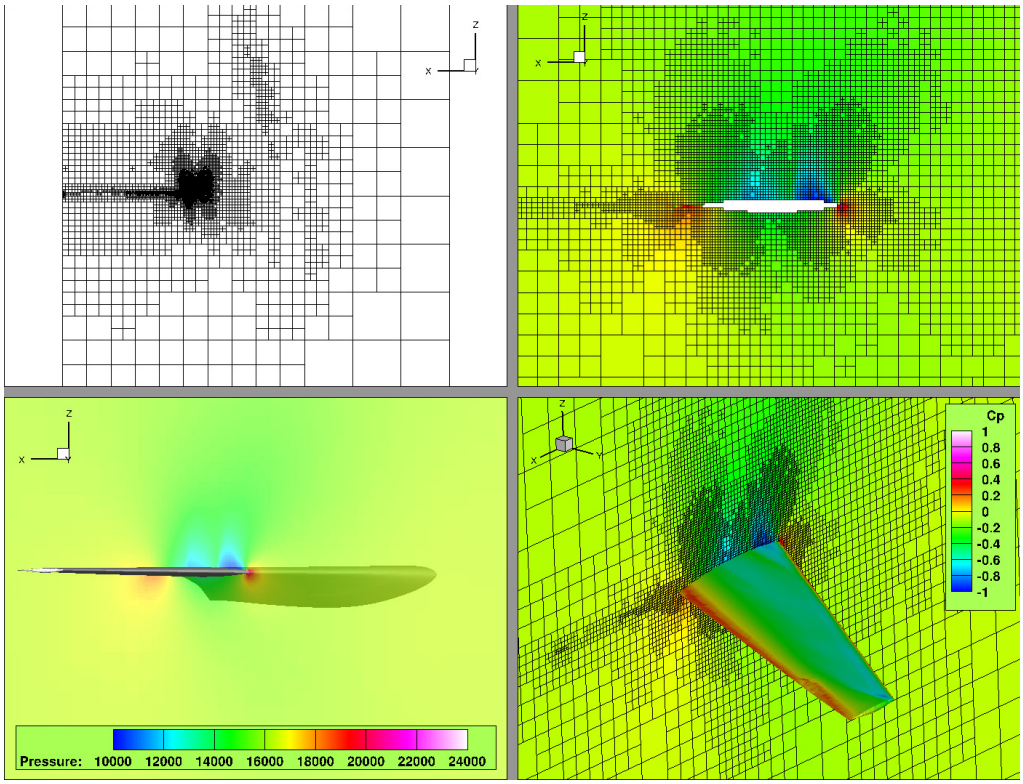

Figure 39: Flowfield mesh and pressure at 50% span and C_p on wing surface.

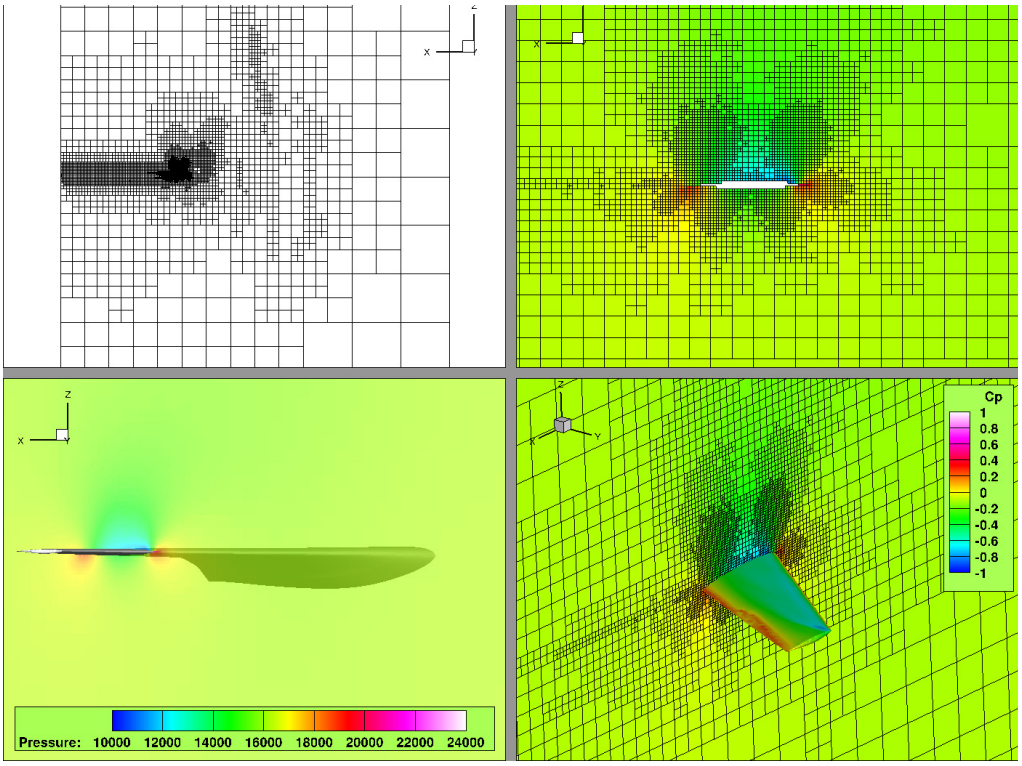

Figure 40: Flowfield mesh and pressure at 75% span and C_p on wing surface.

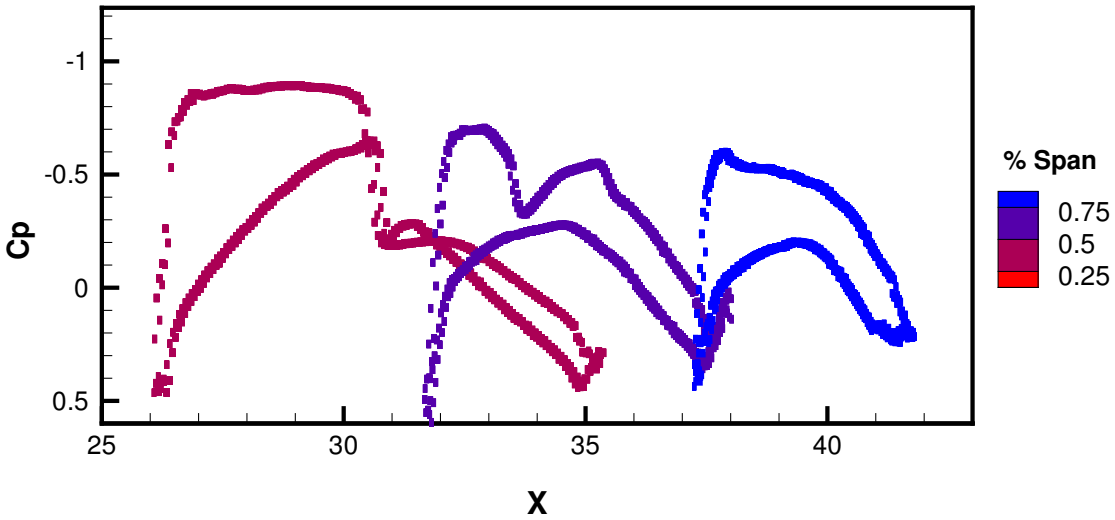

Figure 41: C_p for 25%, 50% and 75% span.

This load case represents the cruise mach number at the operating ceiling altitude. Thus we'd expect to see some transonic flow effects. The results indicate a normal shock forms inboard and results in a near discontinuous change in pressure, as can

be seen in Figure 41. The shock appears to dissipate towards the outboard of the wing. Figure 38 shows how NASCART-GT's mesh adaptation refines the mesh for better accuracy based on the shock's effects on the flowfield. C_p is only calculated at the surface of the body because it is zero in the far flowfield. The red regions in the flowfield indicate increased pressure near the leading and trailing edge stagnation points. Likewise, the C_p will be large and positive at the stagnation points because the pressure term in Equation 31 exceeds the freestream pressure and approaches the stagnation pressure.

The CFD results verify the supercritical nature of the wing design. The uCRM wing, based on the Boeing 777, utilizes supercritical airfoils to offset the effects of transonic flow caused by the cruise speeds. Figure 42 shows how such a design theoretically weakens the normal shock in order to keep the trailing edge flow separated and decrease drag in comparison to conventional airfoils. In Figure 38 the supersonic flow profile, indicated in the blue region, and the flat C_p distribution over the inboard top surface in Figure 41 both indicate supercritical airfoils are accurately modeled in the mesh and analyzed correctly in NASCART-GT.

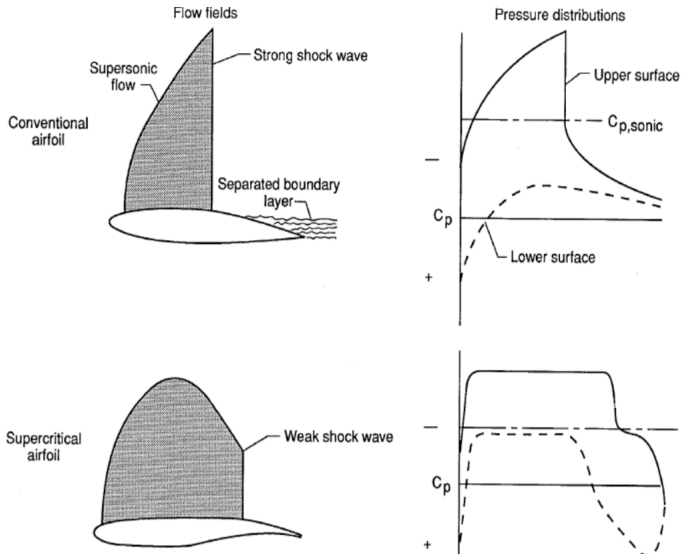

Figure 42: Comparison of transonic flow over a conventional NACA 64 airfoil with transonic flow over a supercritical airfoil using C_p variation (Chalia 2016).

Load Case 2: Mach 0.9, 23000 ft

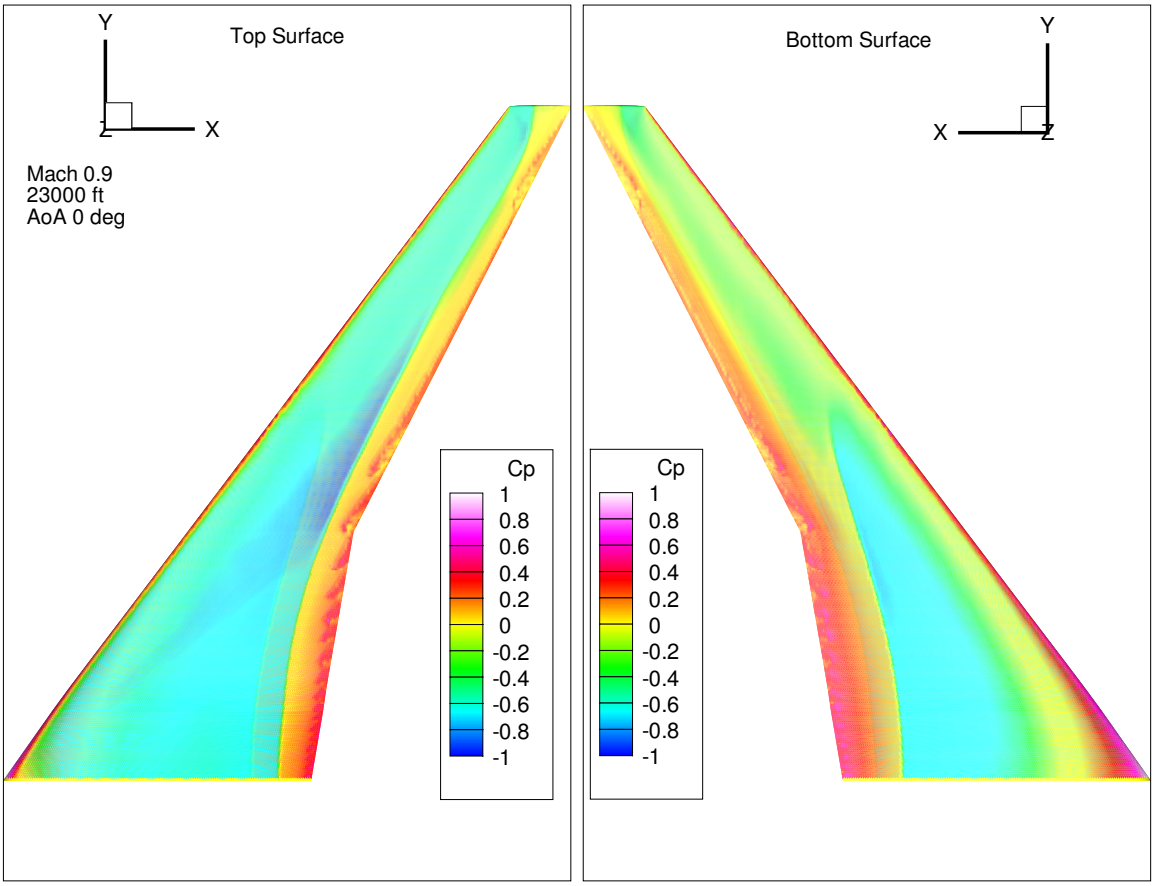

Figure 43: C_p distribution on top and bottom surfaces.

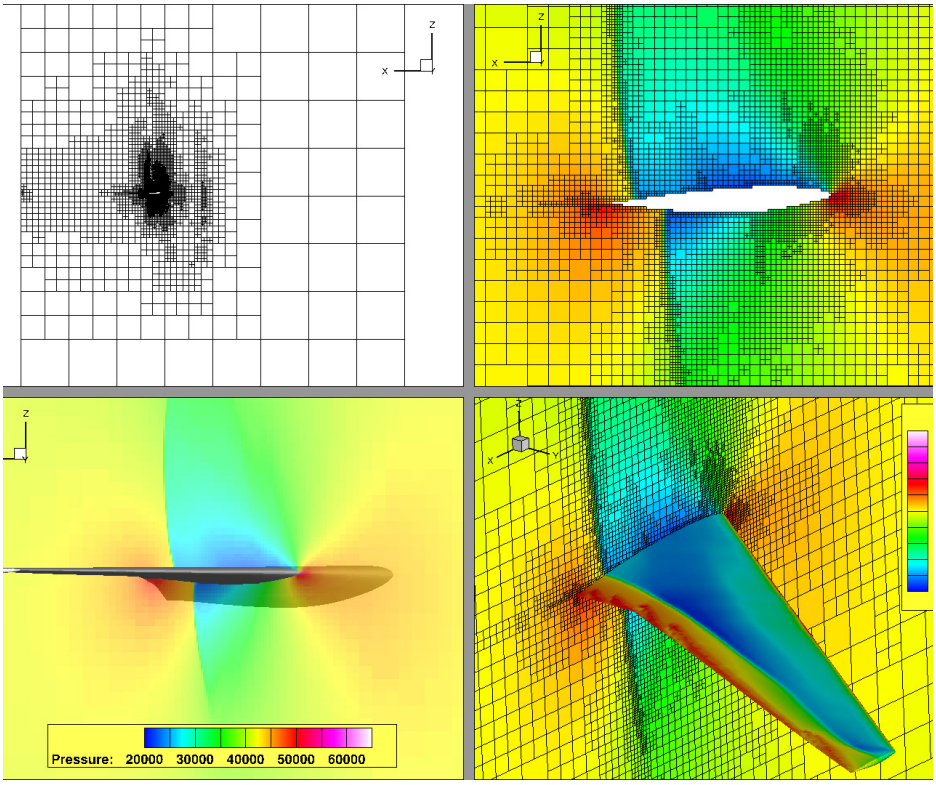

Figure 44: Flowfield mesh and pressure at 25% span and C_p on wing surface.

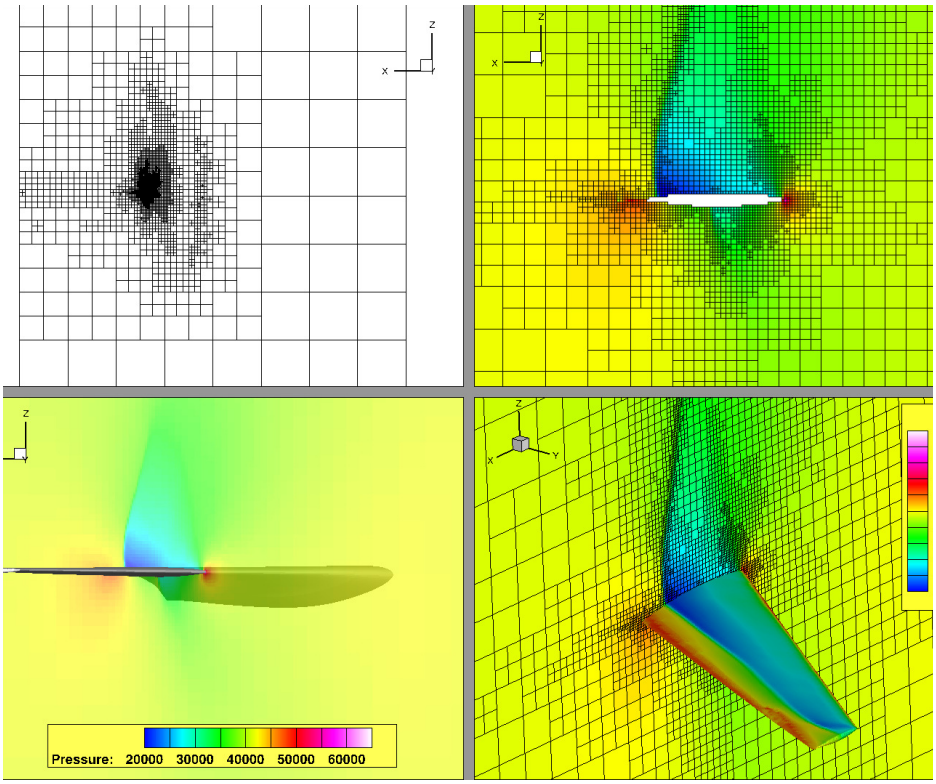

Figure 45: Flowfield mesh and pressure at 50% span and C_p on wing surface.

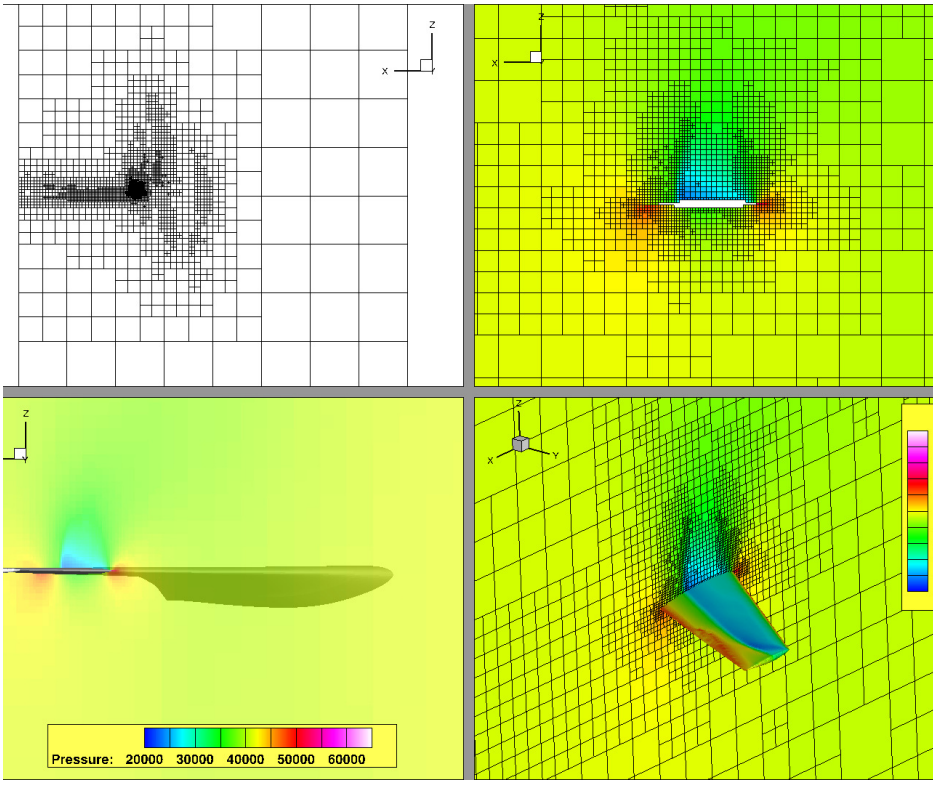

Figure 46: Flowfield mesh and pressure at 75% span and C_p on wing surface.

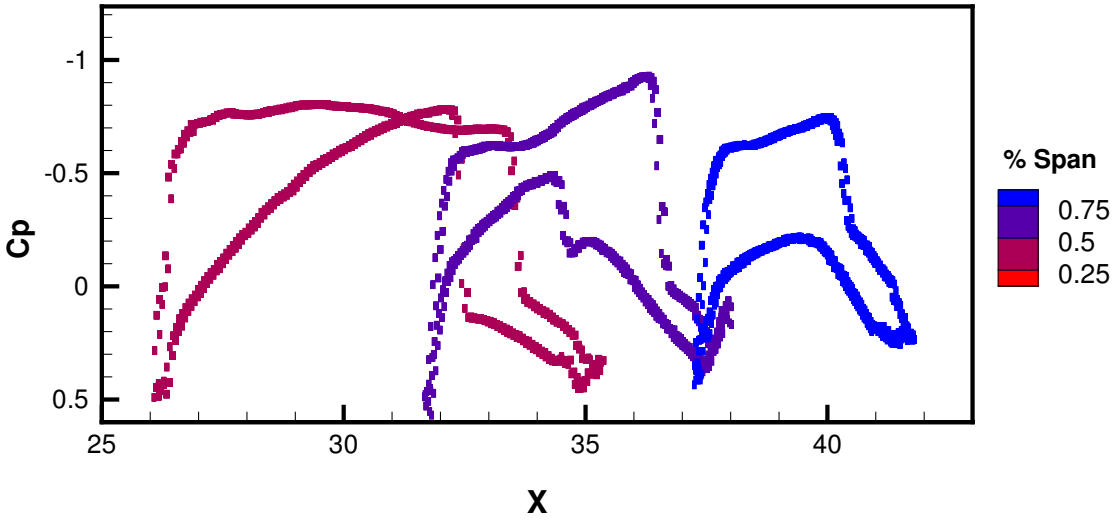

Figure 47: C_p for 25%, 50% and 75% span.

The second load case is at the highest Mach number but also at a relatively low altitude. In comparison with the first load case, the lower altitude causes the flowfield pressures to be much higher. Note that the pressure scales are not the same between

the load cases to better visualize the flow features within each, but the C_p scales are the same. The speed of sound is dependent on the temperature and it is relatively constant at the altitudes analyzed in these load cases. Thus the altitude variations have little affect on the the shock [45], but the higher Mach number in this load case affects the shock location and strength. The normal shock on both the top and bottom surfaces shifts towards the trailing edge and the supersonic region ahead of the shock becomes fuller as is expected in compressible flow theory and shown in Figure 48 [149]. The blue "shark fin" regions attached to the body indicate the decreased pressure due to supersonic flow. The strength of the normal shocks can be deduced from the change in C_p and as expected the second load case produces stronger shocks than the first. Also, in Load Case 1 the shocks on the top and bottom surfaces coalesce at the same chordwise location. In the second load case though the shocks have separated and the bottom surface shock is ahead of the top surface in agreement with theory (see Mach=0.9 case in Figure 48).

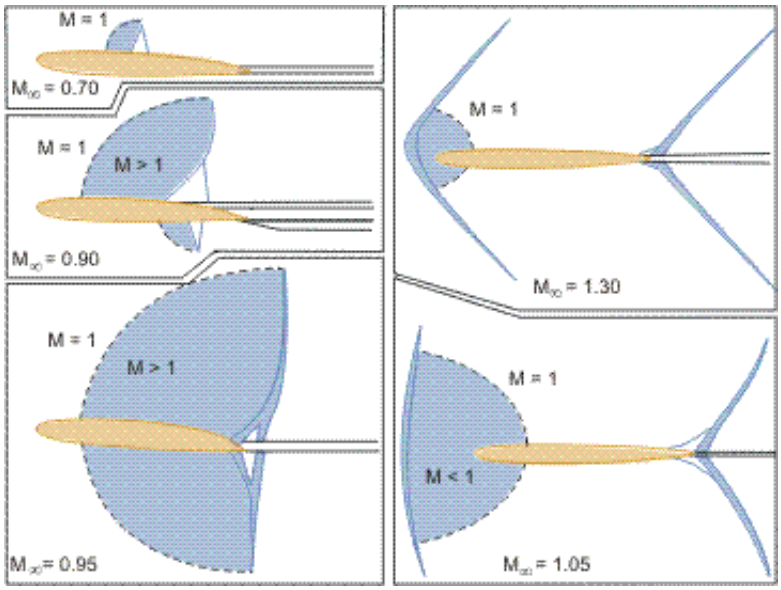

Figure 48: Shock formation on a transonic airfoil from Shapiro (1954).

Load Case 3: Mach 0.6, 20000 ft

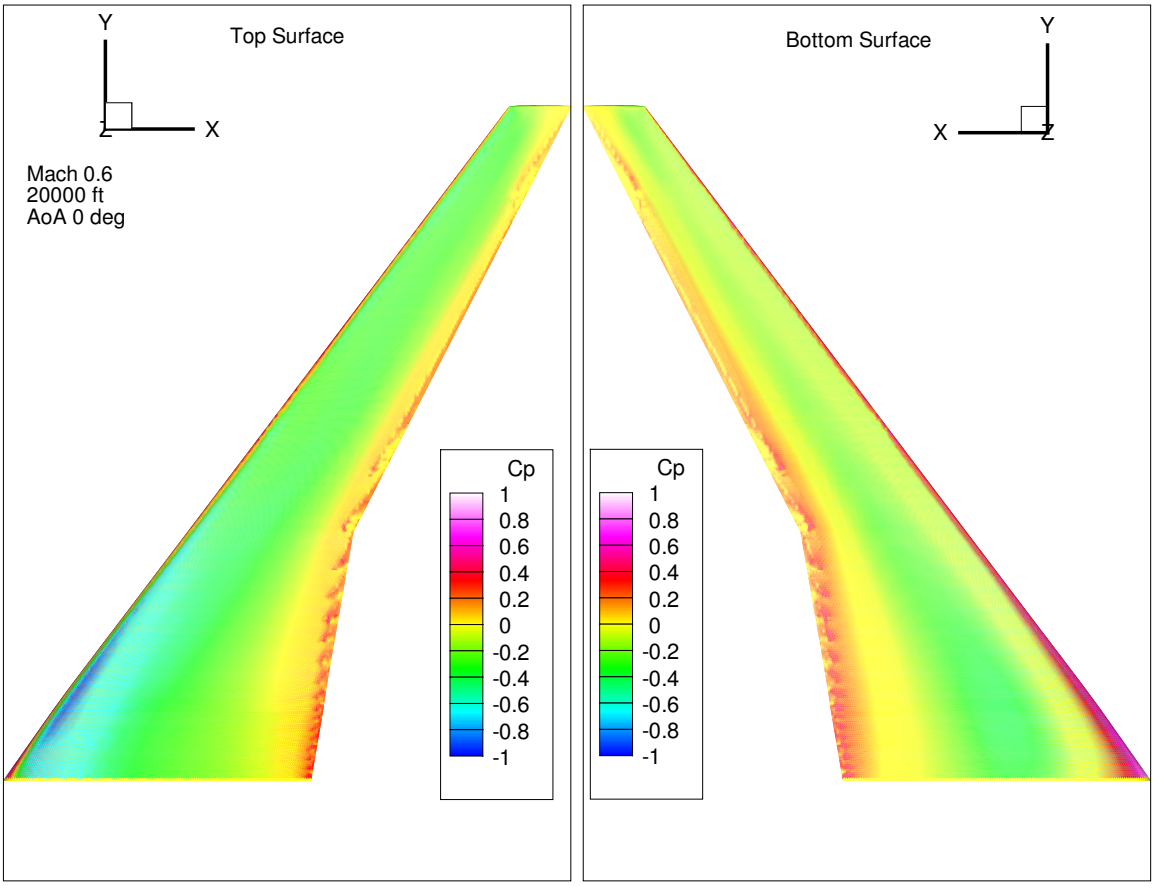

Figure 49: C_p distribution on top and bottom surfaces.

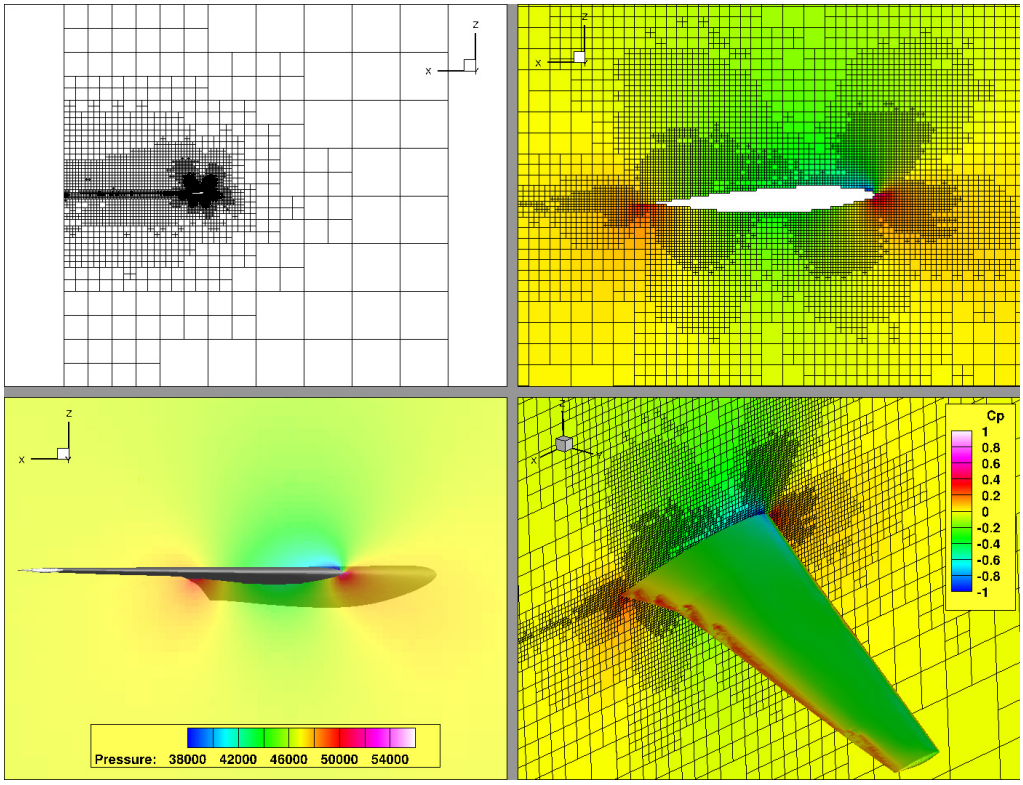

Figure 50: Flowfield mesh and pressure at 25% span and C_p on wing surface.

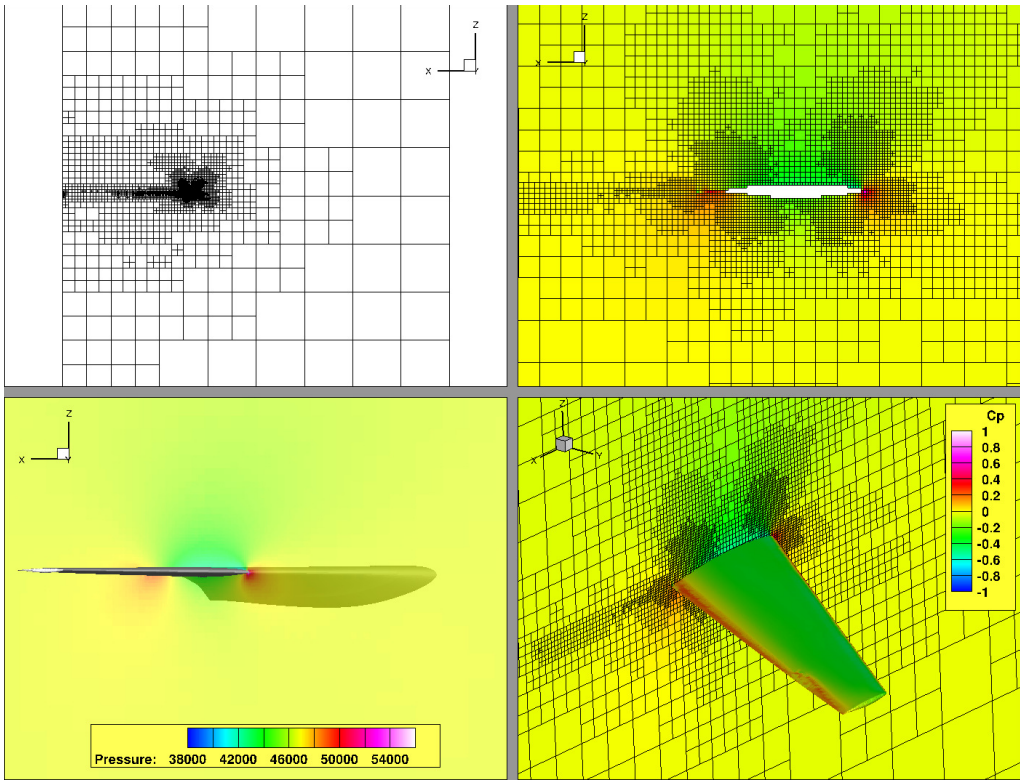

Figure 51: Flowfield mesh and pressure at 50% span and C_p on wing surface.

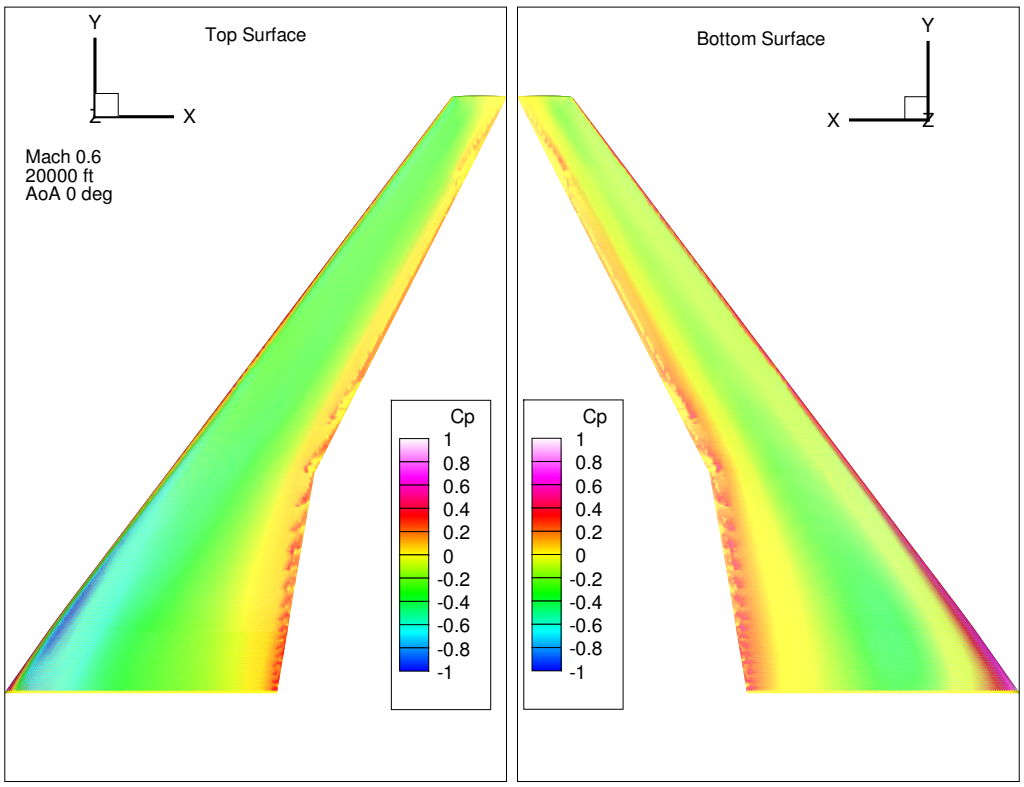

Figure 52: Flowfield mesh and pressure at 75% span and C_p on wing surface.

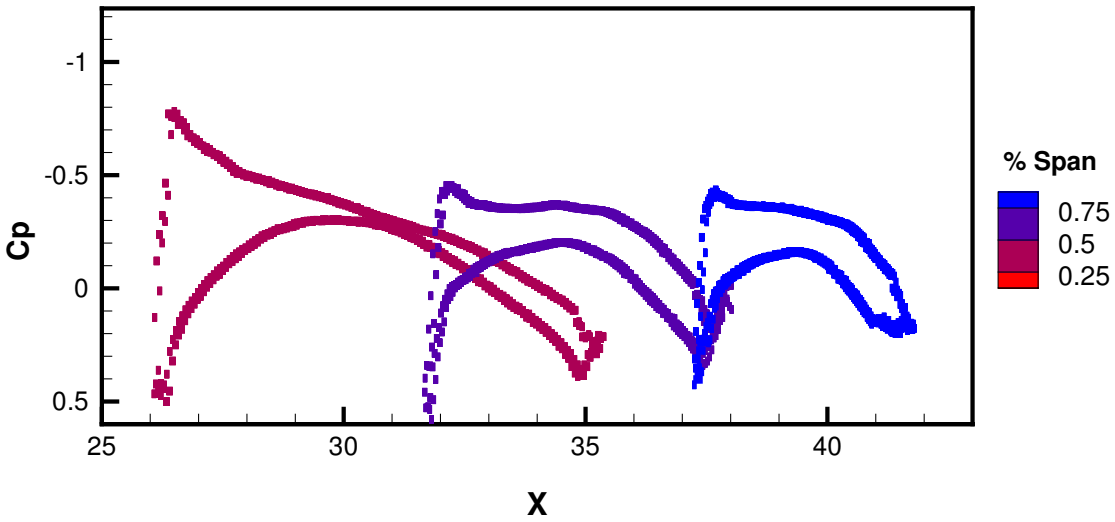

Figure 53: C_p for 25%, 50% and 75% span.

Load Case 3 has the lowest Mach number and altitude of all the load cases. The low Mach number is in the subsonic flow regime and reduces the compressibility effects so we don't expect to see any shocks. This will become more important later when

benchmarking the comparison between CFD to DLM. DLM cannot predict shocks so results from this load case should show the closest matching between the fidelity levels. As expected, there are no significant low pressure regions (blue) in the flowfield and there are no discontinuous changes in pressure in Figure 53.

It is interesting to note the difference in mesh adaptation when there are no shocks. Near the body the mesh is mostly refined only at the leading and trailing edges. This is expected because the geometry of the blunt leading edge and sharp trailing edge require higher resolution and the flow is more complex near these locations. In the far flowfield, the refinement is concentrated to the wake which is also much more complex due to vorticity and thus requires higher resolution. In comparison with the previous load cases, there is very little refinement ahead of the body. Compressibilty theory tells us that supersonic flow over a blunt body, such as the wing leading edge, will cause a separated bow shock in front of the body (see Mach=1.05 case in Figure 48). As such, NASCART-GT's mesh adaptation begins to refine ahead of the wing at the higher mach numbers.

Load Case 4: Mach 0.89, 43100 ft

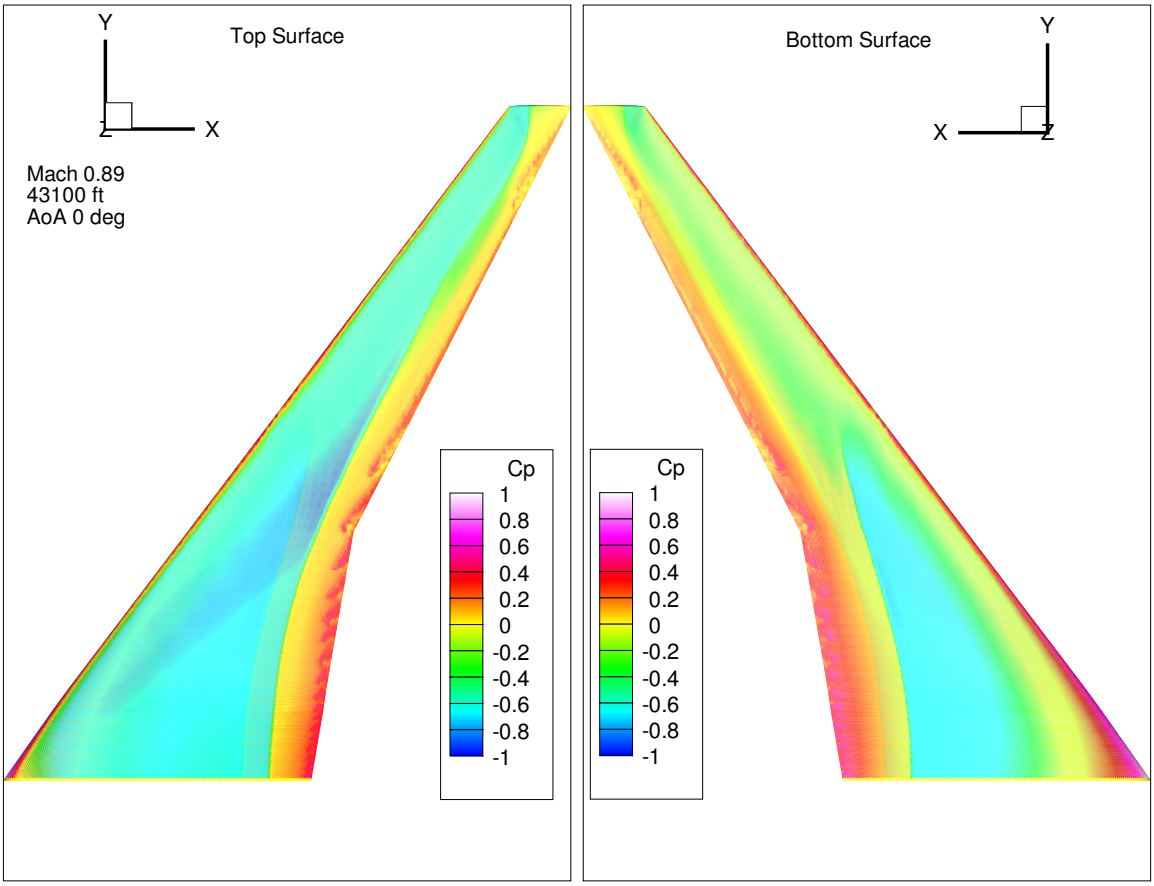

Figure 54: C_p distribution on top and bottom surfaces.

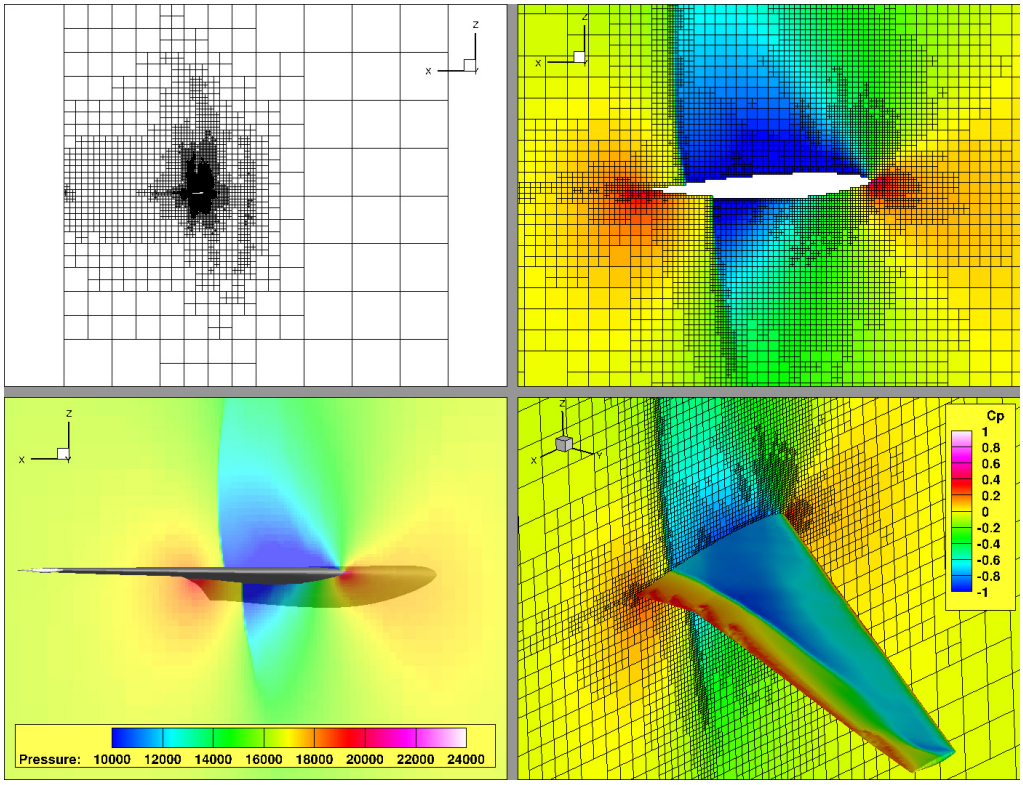

Figure 55: Flowfield mesh and pressure at 25% span and C_p on wing surface.

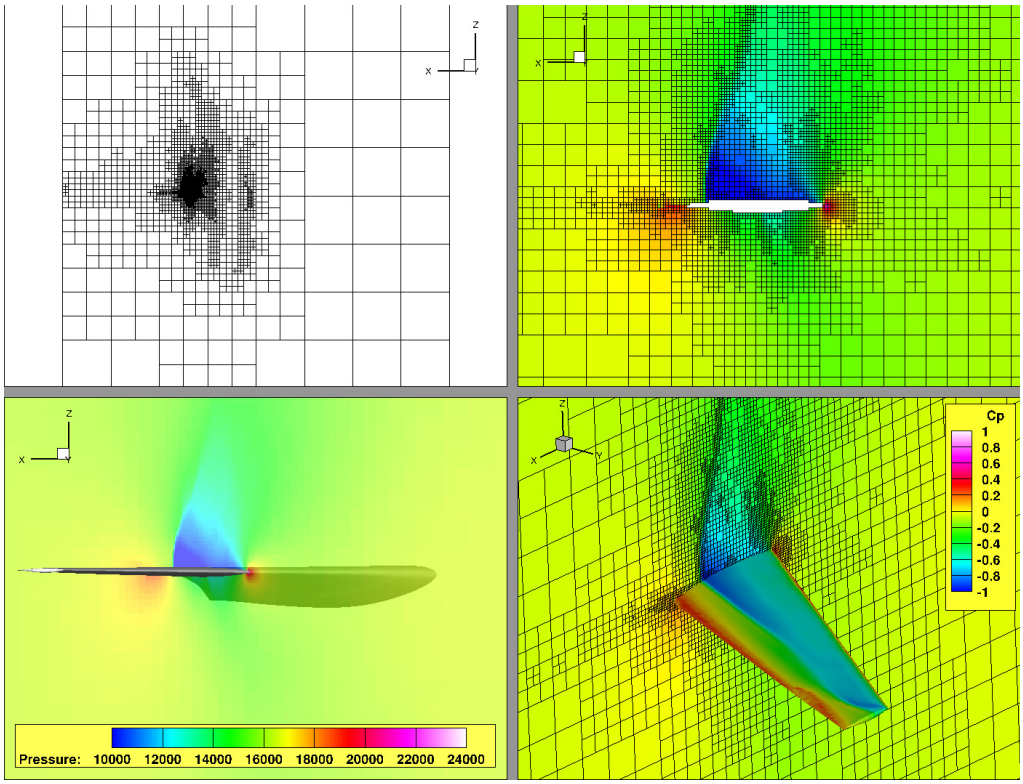

Figure 56: Flowfield mesh and pressure at 50% span and C_p on wing surface.

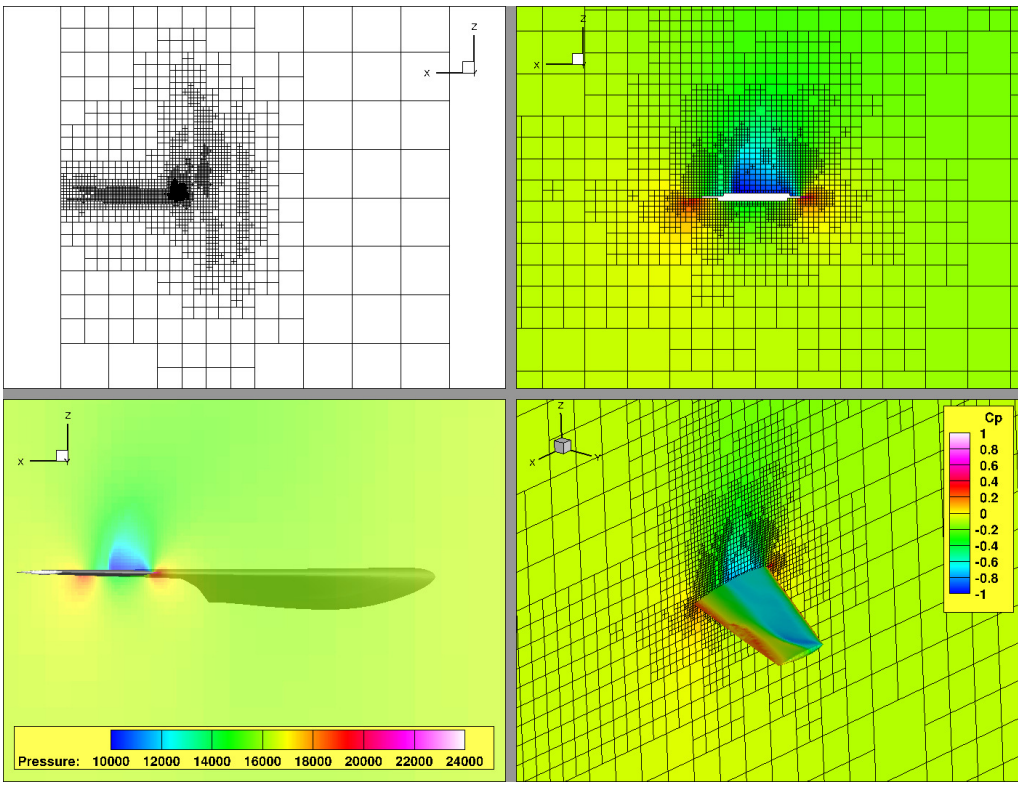

Figure 57: Flowfield mesh and pressure at 75% span and C_p on wing surface.

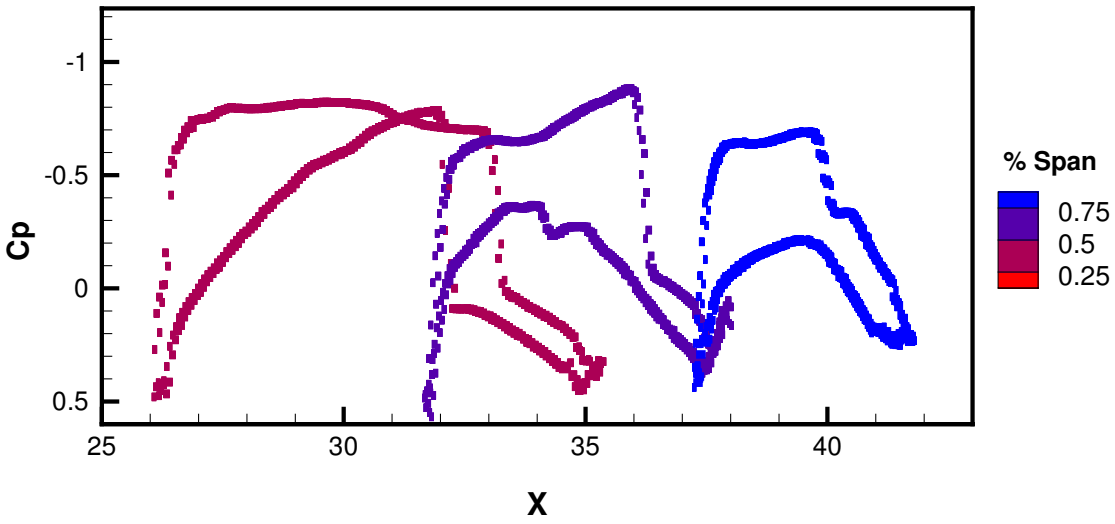

Figure 58: C_p at 25%, 50% and 75% span.

The fourth and final load case is at both a high Mach number and high altitude. The flow characteristics are very close to that of Load Case 2 which has a similar Mach number, but the pressure scales are much different due to the altitude difference. The

C_p distributions are almost identical as well, but keep in mind these results are at zero angle of attack. As will be seen later, when the angle of attack changes these two load cases will differ significantly.

Some key results were shown for the rigid CFD analysis in NASCART-GT at zero angle of attack. The resulting pressure for these cases will be used to define the $[FA2J]$ empirical adjustment matrix. The four load cases analyzed differ in Mach number and altitude and these effects can be seen in the flowfield and pressures on the wing body. Some expected flow characteristics in transonic flow over supercritical wings were verified in the results and thus helps validate the CFD modeling and analysis methods.

Looking ahead to the calculation of rigid $[W_{KK}]$, the flow features of most interest are shocks due to transonic flow. The discontinuous change in pressure can lead to quite extreme W_{KK} values so using the normal coefficient to smooth out these effects is justified. In the next section the rigid CFD results from NASCART-GT are compared against the DLM results from NASTRAN.

6.2.2.3 Comparison of Rigid CFD to Doublet-Lattice Method

The CFD results from the previous section are used to calculate C_n and eventually $[W_{KK}]$. In this section the CFD results are compared against the DLM results. As was discussed in Section 6.2.1.4 the C_p from NASCART-GT must first be transferred to the DLM mesh so it can be compared against the NASTRAN solution. Thus the transferred CFD results will be compared against the original CFD in this section to demonstrate the accuracy of the matching algorithm.

Load Case 1: Mach 0.85, 43100 ft, 2.5G

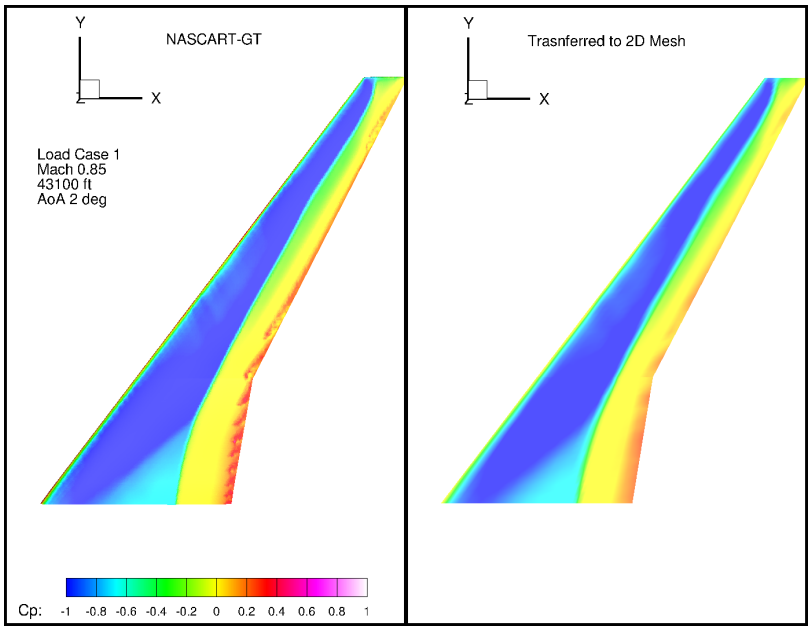

Figure 59: Top surface comparison of original and transferred CFD C_p for top surface.

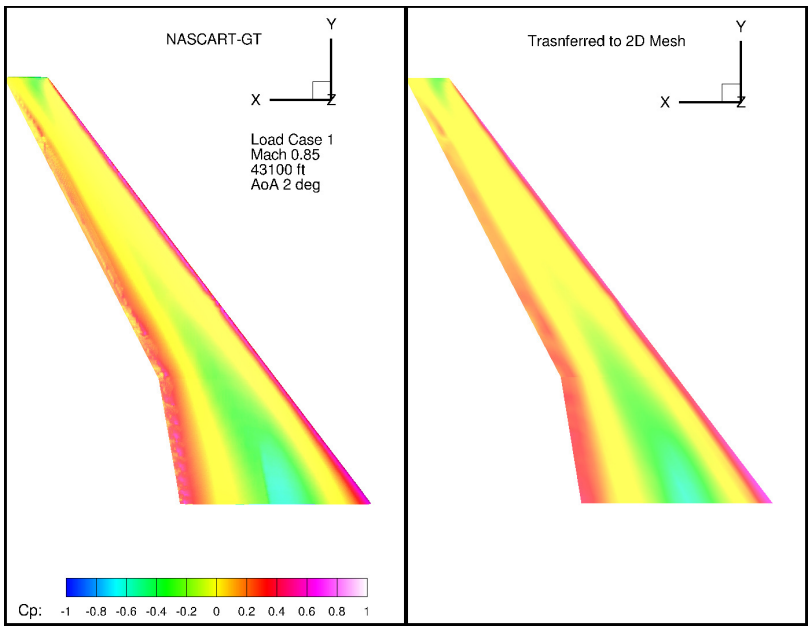

Figure 60: Bottom surface comparison of original and transferred CFD C_p for top surface.

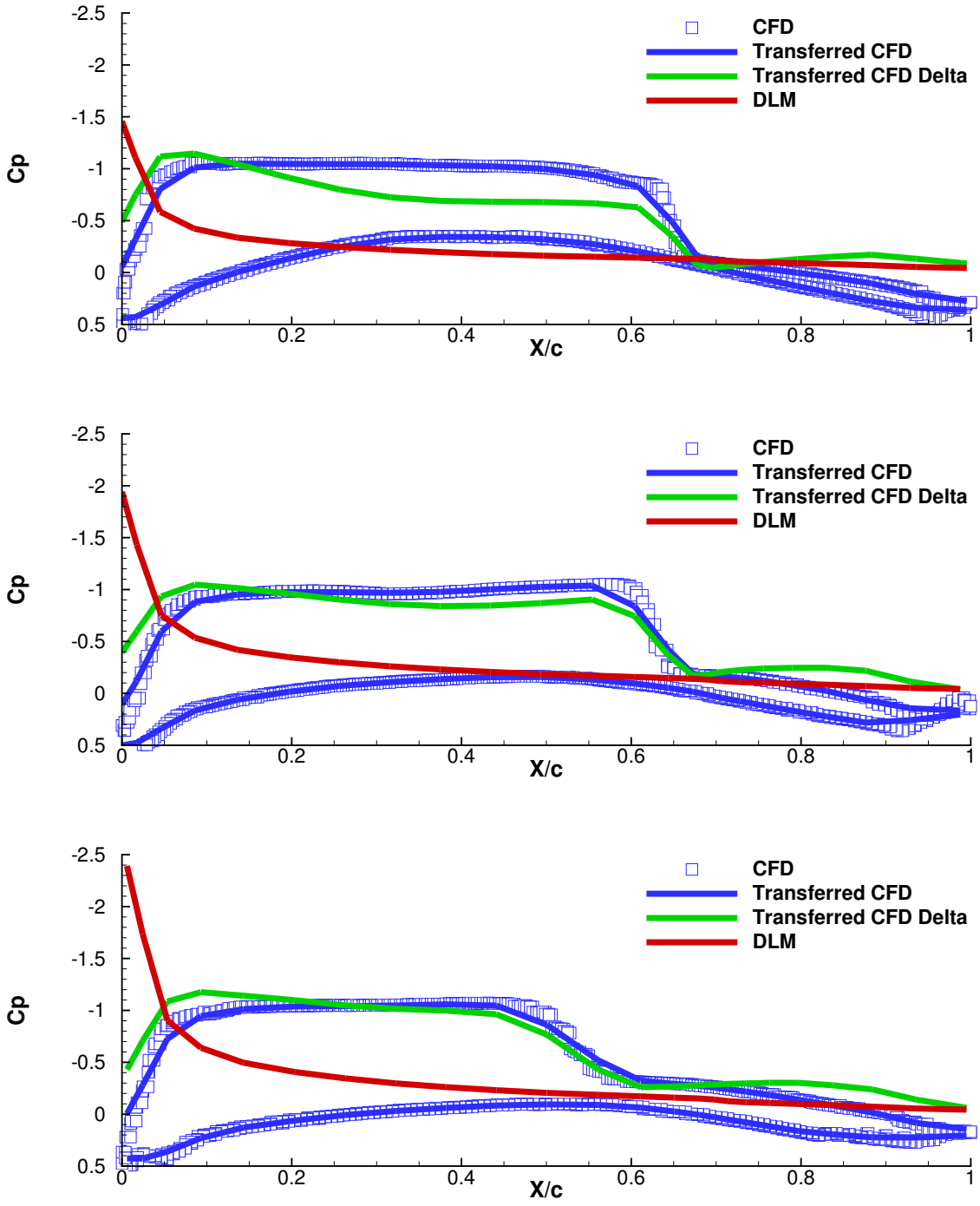

Figure 61: C_p comparison at 25% (top), 50% and 75% span for $\alpha = 2^o$.

Figures 59 and 60 show the accuracy of the matching algorithm to transfer C_p from the CFD mesh to the DLM mesh. Figure 61 compares the raw CFD results,

the transferred CFD results and the DLM results for three cross-sections of the wing. The CFD and transferred CFD results match very well and is further validation of the matching algorithm. As was discussed, the DLM mesh has no distinction between top and bottom surface so only the change in CFD C_p can be compared directly to DLM. The green line represents ΔC_p and is the difference between the top and bottom blue lines. Note that ΔC_p does not bisect the region between the blue lines because of the signage of C_p. In NASTRAN all uncorrected C_p values are positive and goes against the standard definition used in Equation 31. Typically $\Delta C_p < 0$, which indicates positive lift is being created. Thus in these results the negative of the DLM C_p is used for comparison.

The DLM results (red curves) are without any empirical adjustments. The difference between the red and green curves shows the error, and thus the epistemic uncertainty, in DLM. The epistemic uncertainty is greatest at the leading edge and ahead of the shock. In thin airfoil theory a singularity occurs in the calculation of circulation at a sharp leading edge [5]. The DLM results thus show an asymptotic-like increase in C_p while CFD better reflects a real flow around a blunt leading edge. In front of a normal shock the flow is supersonic and thus compressibility effects are greatest, but after the shock the flow becomes subsonic. DLM cannot account for nonlinear compressibility so there is much better agreement with CFD, and much less epistemic uncertainty, behind the shock.

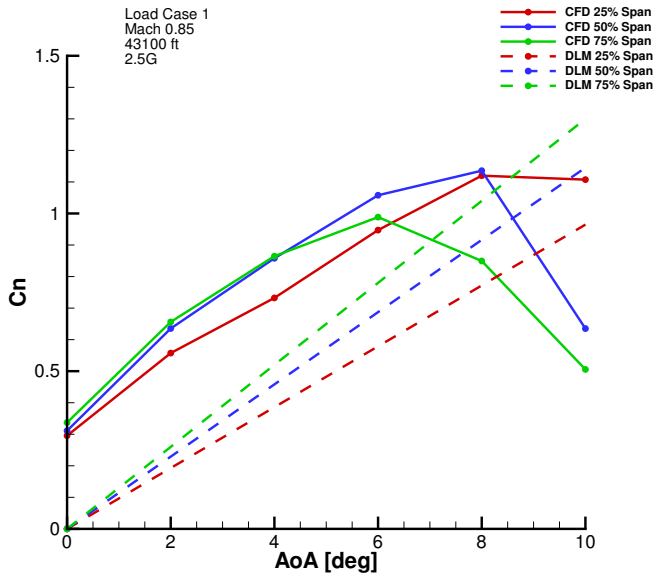

Figure 62: Comparison of normal force coefficient slope for CFD and DLM.

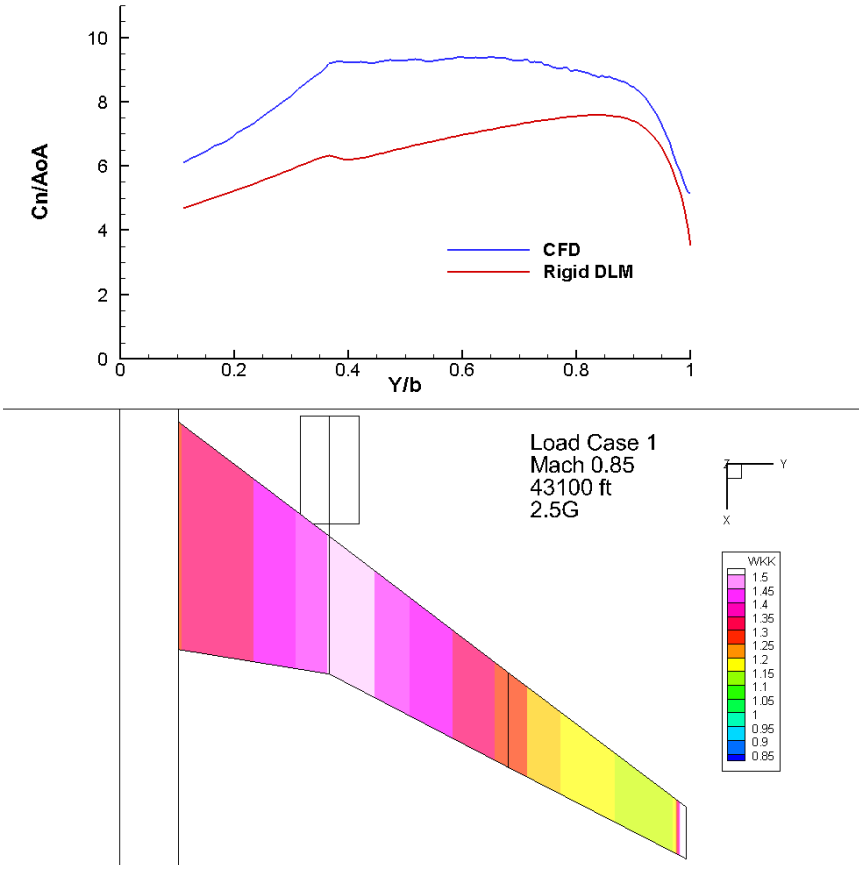

Figure 63: Top: $\Delta C_n/\Delta\alpha$ v.s. span for $\alpha = 0^o$ to 2^o. Bottom: distribution of $[W_{KK}]$ values on DLM wing mesh.

Figures 62 and 63 compare the transferred CFD results to DLM and the corresponding $[W_{KK}]$. Figure 62 shows the normal force coefficient slope. Recall that the $[W_{KK}]$ empirical adjustment assumes a linear slope, so it is beneficial to see if there are nonlinearities. Thus several angles of attack from 0^o to 10^o were run in CFD and plotted at three different span locations to show any nonlinearities. For Load Case 1 the lift curve is fairly linear up to 6^o for all spans locations. At higher angles the numerical viscosity causes separation and the nonlinear changes in the lift curve. More will be discussed later on the effects of numerical separation. These results verify that 2^o is within the linear range and a valid choice for defining $[W_{KK}]$. The relative slopes are most important on these plots, but it should be noted that the offset of the CFD and DLM lift curves is due to the assumption of zero lift at $\alpha = 0^o$ in DLM. This offset is exactly what $[FA2J]$ corrects for. The points on the CFD curves represent individual CFD runs which terminate at different iterations. Thus there are small variations which cause the slopes to not be perfectly linear. Nonlinearity due to numerical separation is much greater than that of numerical convergence so the two are easily distinguishable.

The top plot of Figure 63 shows the normal force coefficient slope as a function of span. For a given span location, the ratio of normal force coefficient slope values gives the W_{KK} coefficient. Thus the difference between the CFD and DLM curves is an indication of the magnitude of the W_{KK} coefficient shown in the bottom plot. The results shows there is greater agreement (W_{KK} closer to one) near the root and outboard of the wing. The largest discrepancy occurs at the wing tip where the circulation around the wing tips cause the dropoff in C_n and the large W_{KK} values.

Load Case 2: Mach 0.9, 23000 ft, 2.5G

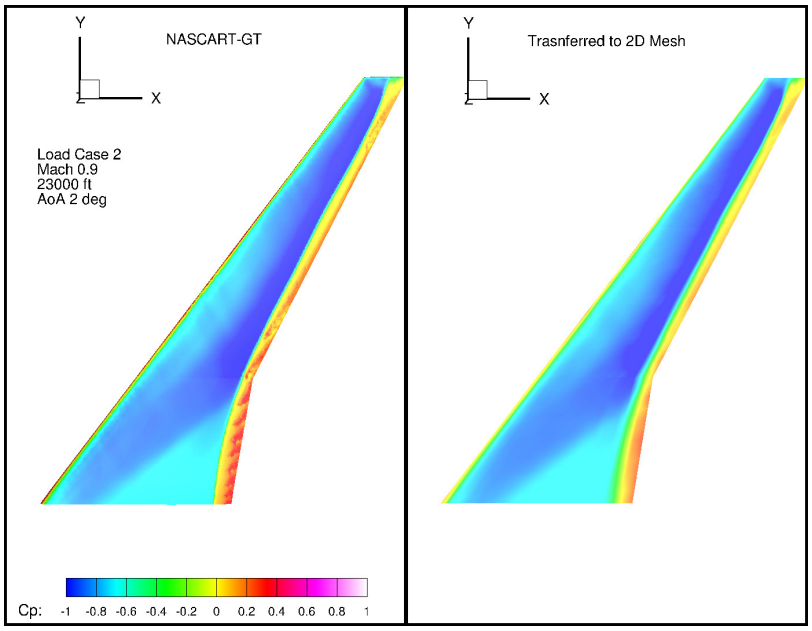

Figure 64: Top surface comparison of original and transferred CFD C_p for top surface.

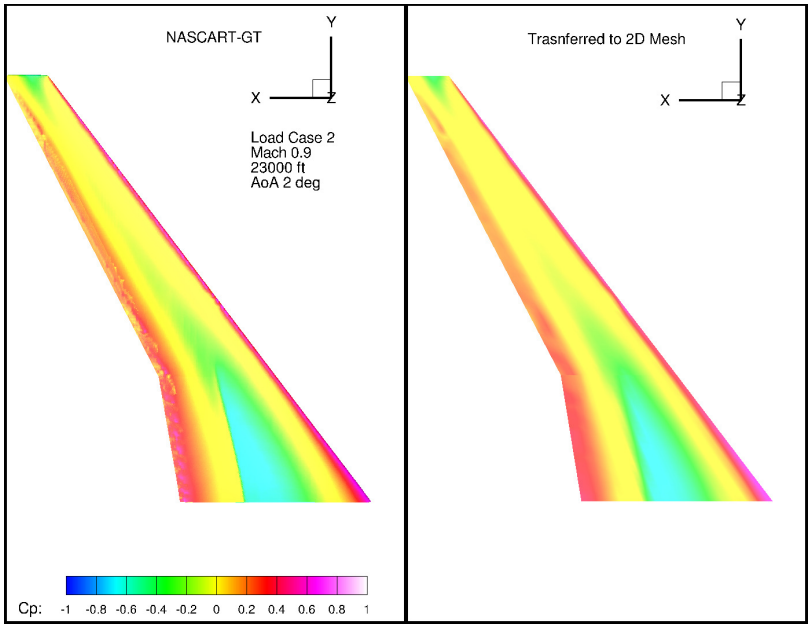

Figure 65: Bottom surface comparison of original and transferred CFD C_p for top surface.

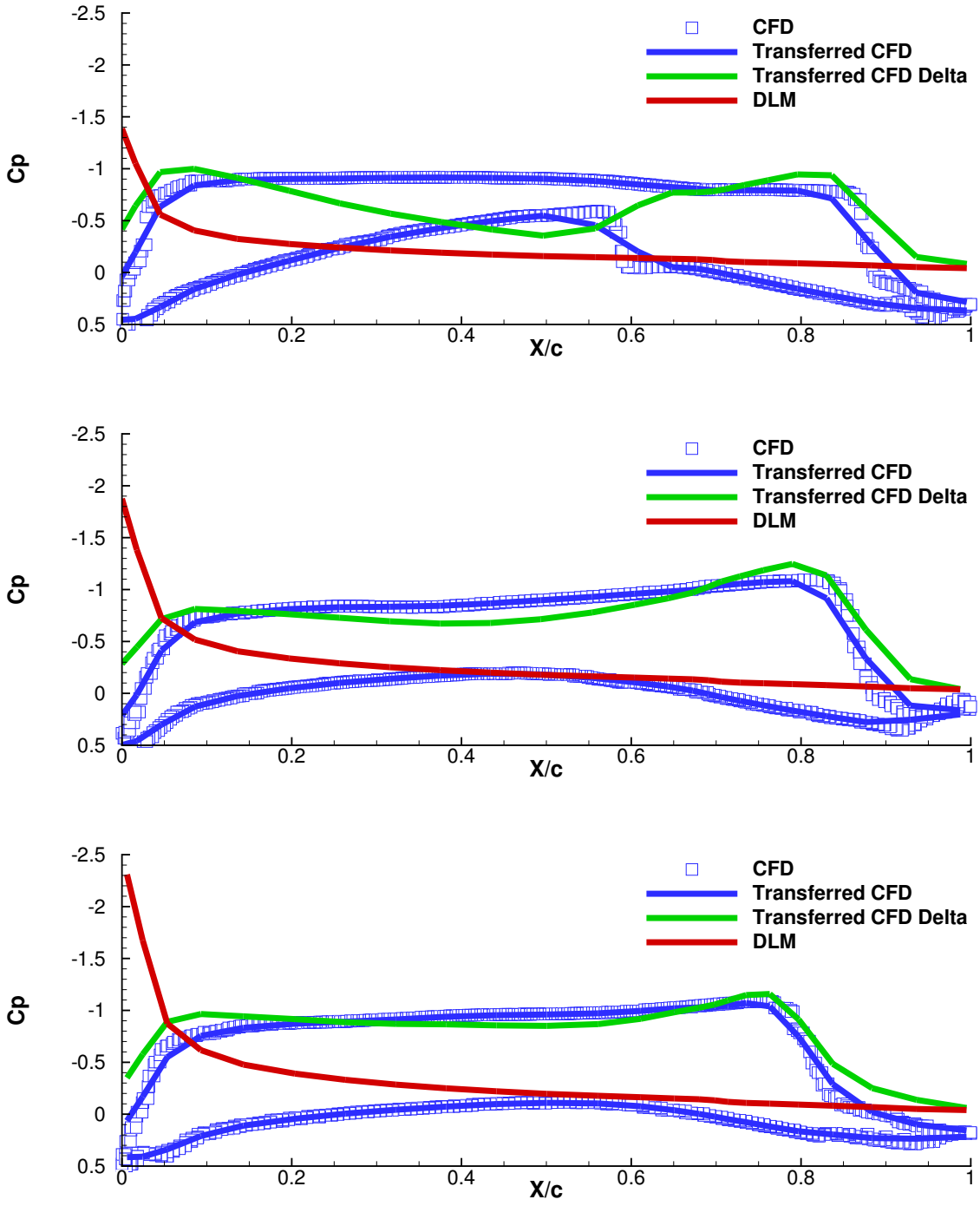

Figure 66: C_p comparison at 25%, 50% and 75% span for AoA = 2 deg.

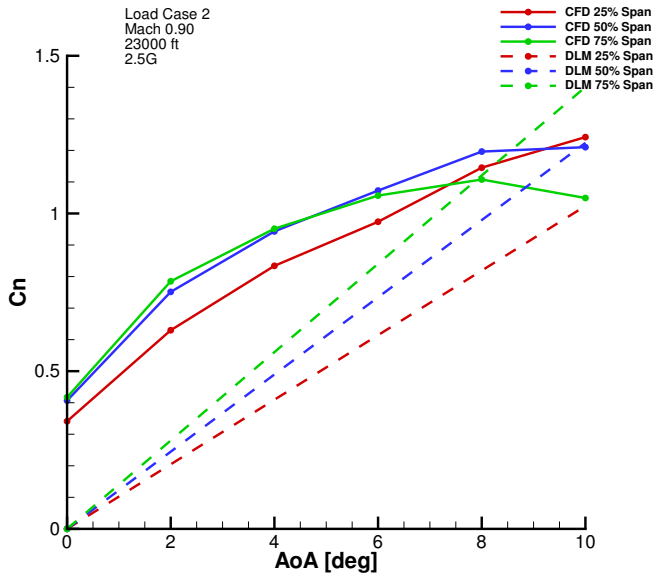

Figure 67: Comparison of normal force coefficient slope for CFD and DLM.

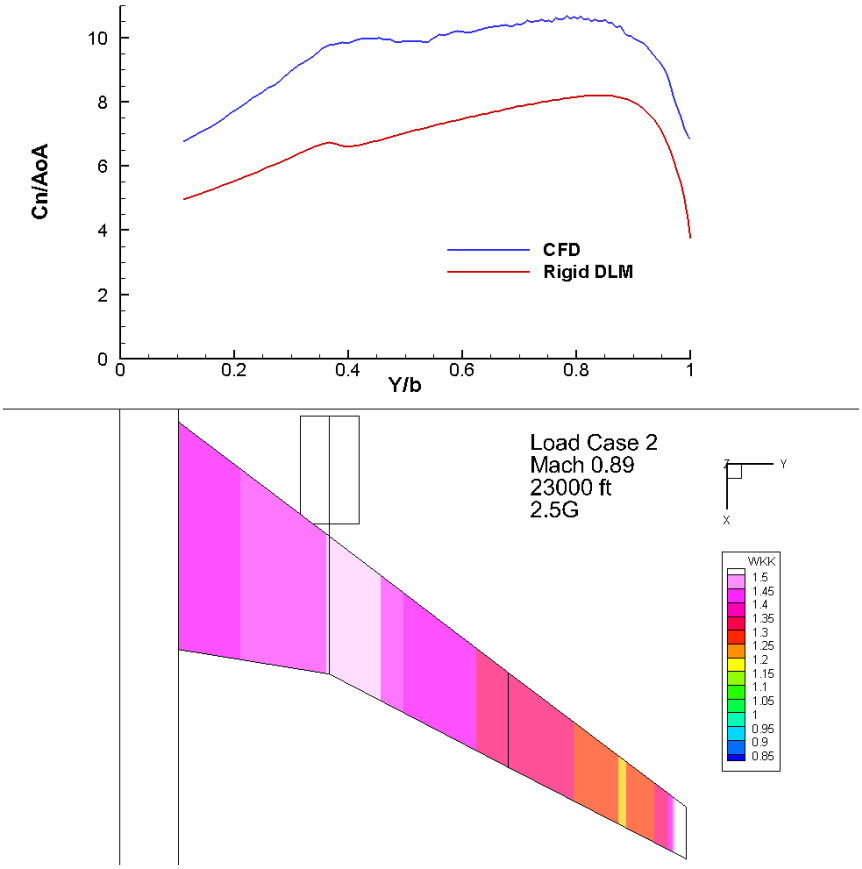

Figure 68: Top: $\Delta C_n/\Delta\alpha$ as a function of span. Bottom: distribution of $[W_{KK}]$ values on DLM wing mesh.

The C_p distributions in Figure 66 further show how the error is reduced after the normal shock (at the trailing edge) when the compressibility effects are less. For the 25% span there is also a weaker shock on the bottom surface at 60% chord which impacts the discrepancy between the CFD and DLM. The normal force coefficient slope in Figure 67 is linear at a higher angle of attack than Load Case 1, two degrees will still be used for defining the empirical adjustments for consistency. Also, this load case has larger W_{KK} values than the first. This is expected because the higher Mach number will cause more nonlinear compressibility effects, including stronger shocks, which leads to larger differences between CFD and DLM.

Load Case 3: Mach 0.6, 20000 ft, 2.5G

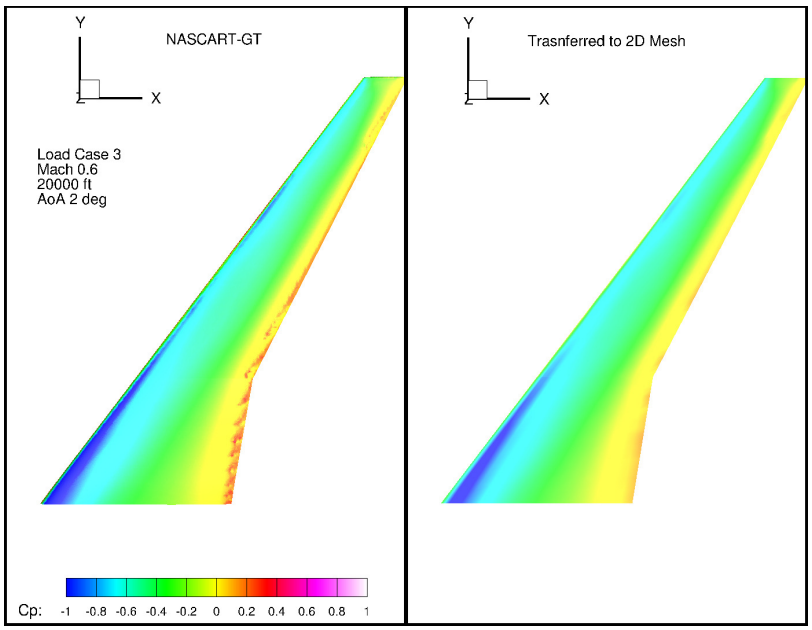

Figure 69: Top surface comparison of original and transferred CFD C_p for top surface.

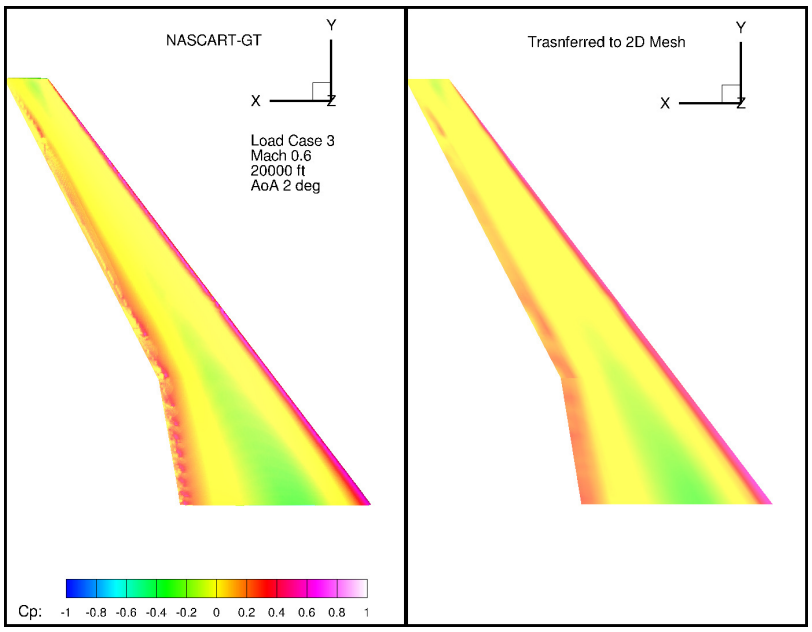

Figure 70: Bottom surface comparison of original and transferred CFD C_p for top surface.

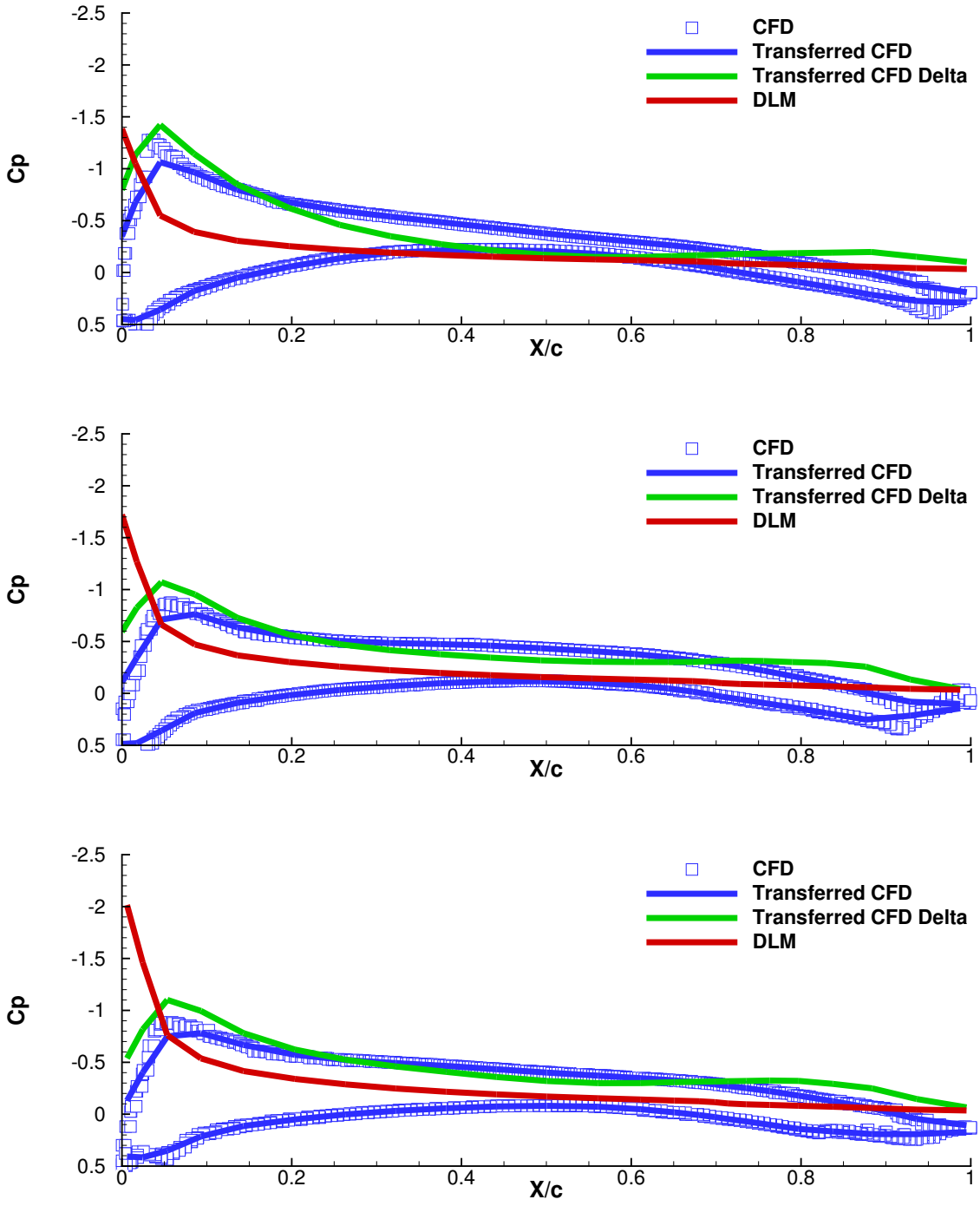

Figure 71: C_p comparison at 25%, 50% and 75% span for AoA = 2 deg.

The discrepancy between CFD and DLM is much less in this load case because of the low Mach Number and lack of shocks. The inboard results show the largest error

near the leading edge where the blunt leading edge of the 3D mesh is thickest and differs most from the flat plate assumption. Comparing these results to the other load cases shows the extent to which compressibility impacts the relative error between CFD and DLM. The remaining error in Load Case 3 can thus be attributed to 3D effects on the flow around the wing.

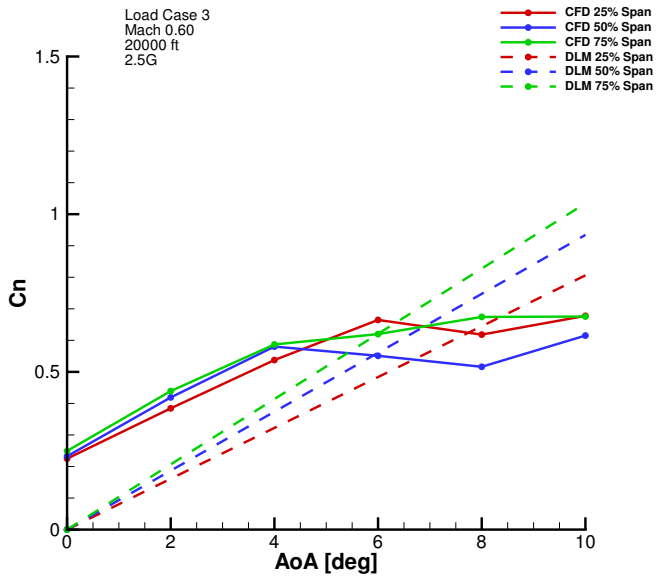

Figure 72: Comparison of normal force coefficient slope for CFD and DLM.

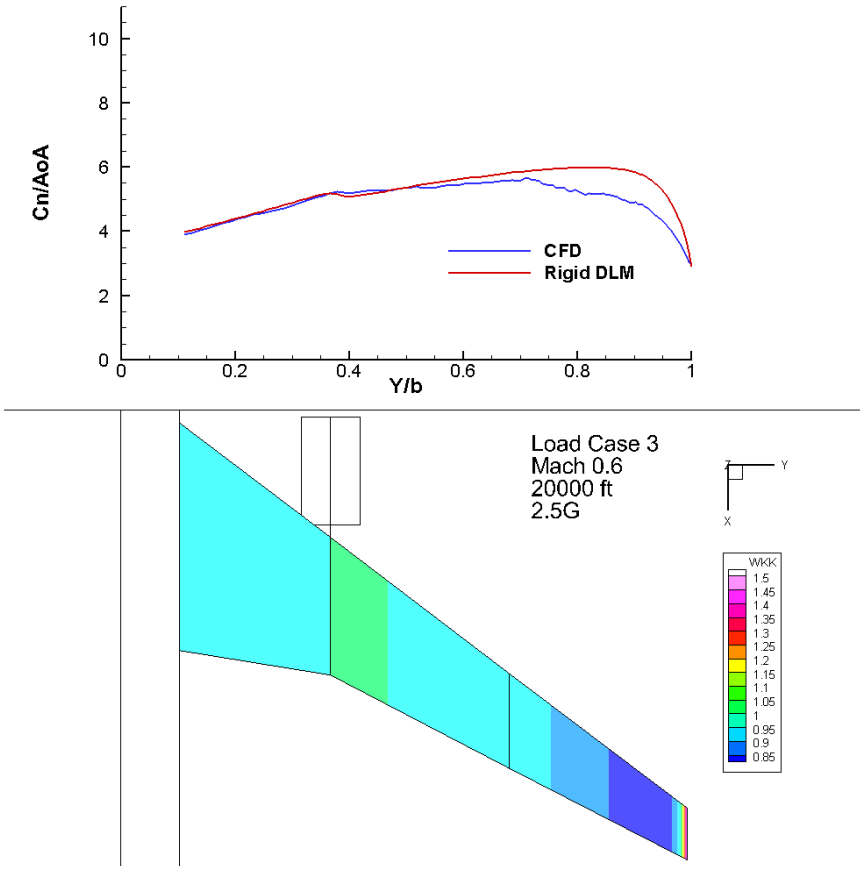

Figure 73: Top: $\Delta C_n/\Delta\alpha$ as a function of span. Bottom: distribution of $[W_{KK}]$ values on DLM wing mesh.

The linear region in the normal force coefficient slope lasts up to four degrees for Load Case 3. As expected, the $\Delta C_n/\Delta\alpha$ results show extremely close matching over the majority of the wing. As in the other load cases the largest adjustment occurs near the wing tip, but the DLM over-predicts the normal force coefficient slope unlike in the other cases. Thus W_{KK} adjustments are less than one in these areas, but they are very close to one for most of the inboard wing.

Load Case 4: Mach 0.89, 43100 ft, 2.5G

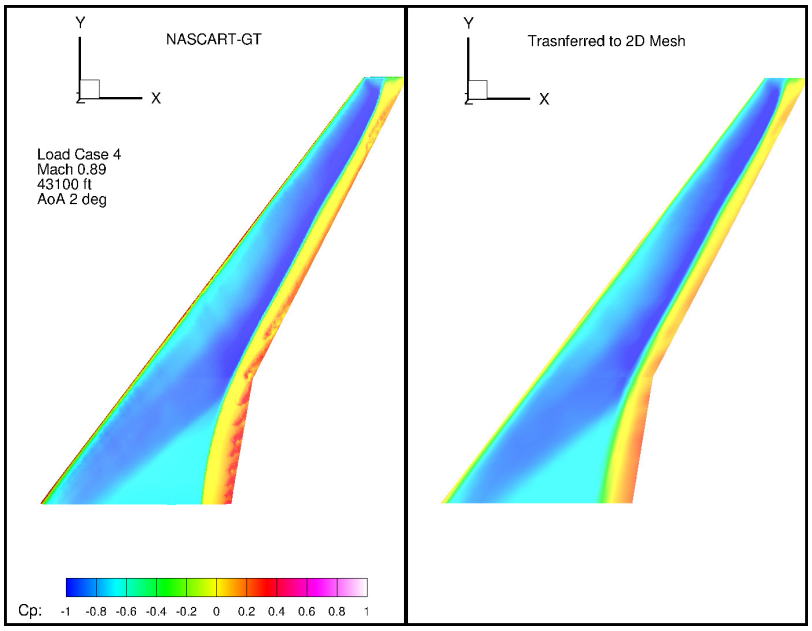

Figure 74: Top surface comparison of original and transferred CFD C_p for top surface.

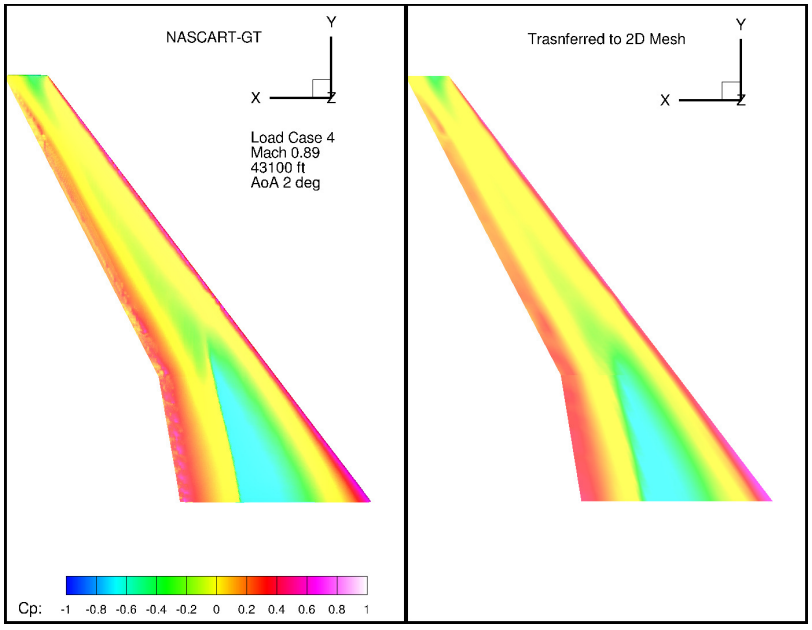

Figure 75: Bottom surface comparison of original and transferred CFD C_p for top surface.

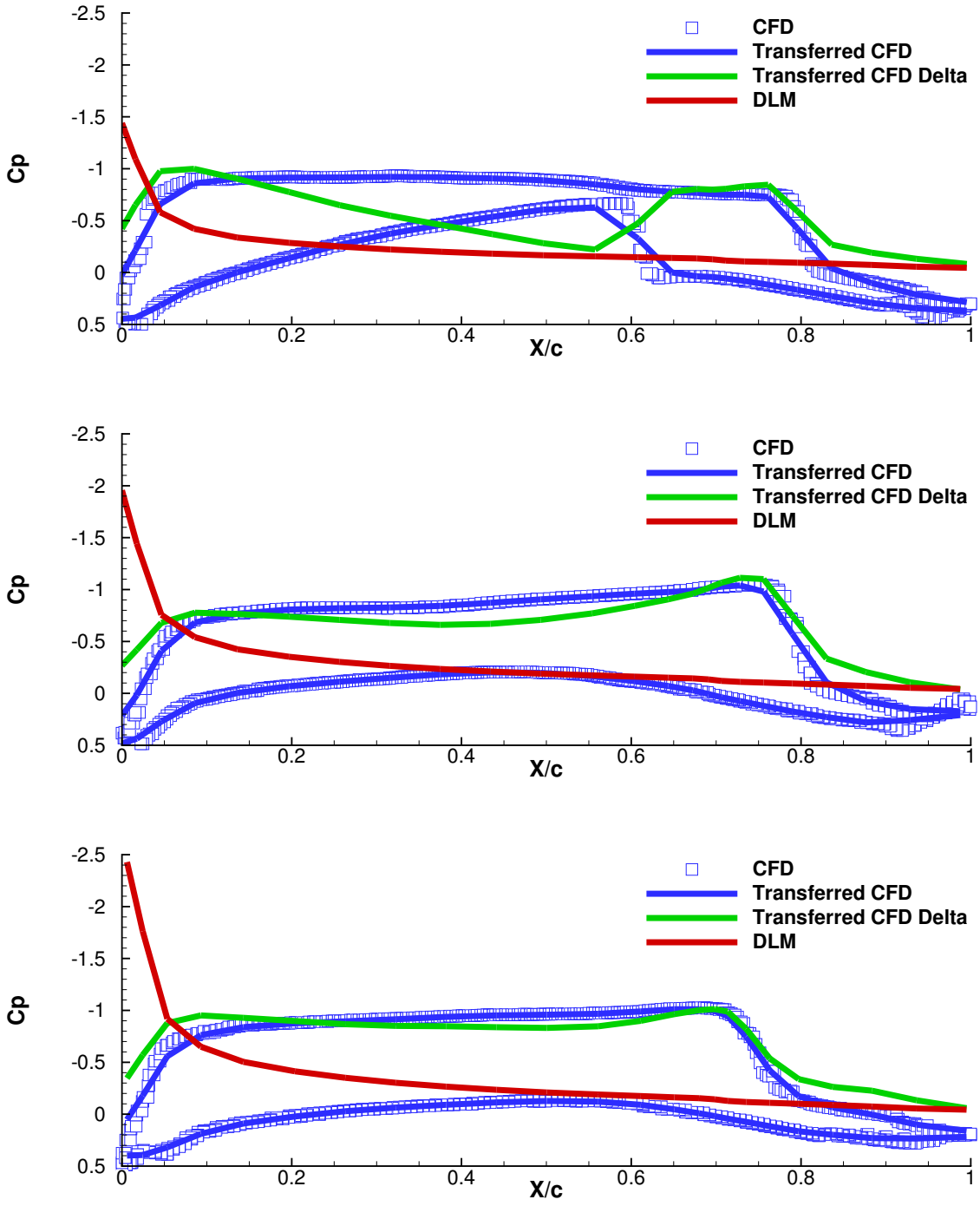

Figure 76: C_p comparison at 25%, 50% and 75% span for AoA = 2 deg.

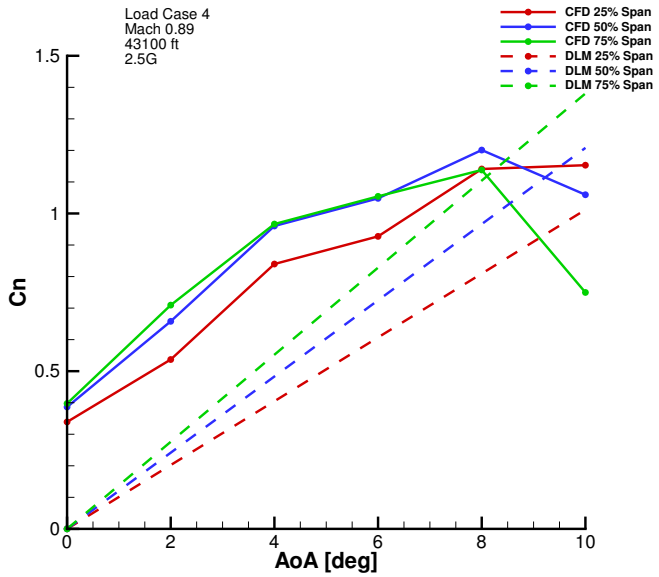

Figure 77: Comparison of normal force coefficient slope for CFD and DLM.

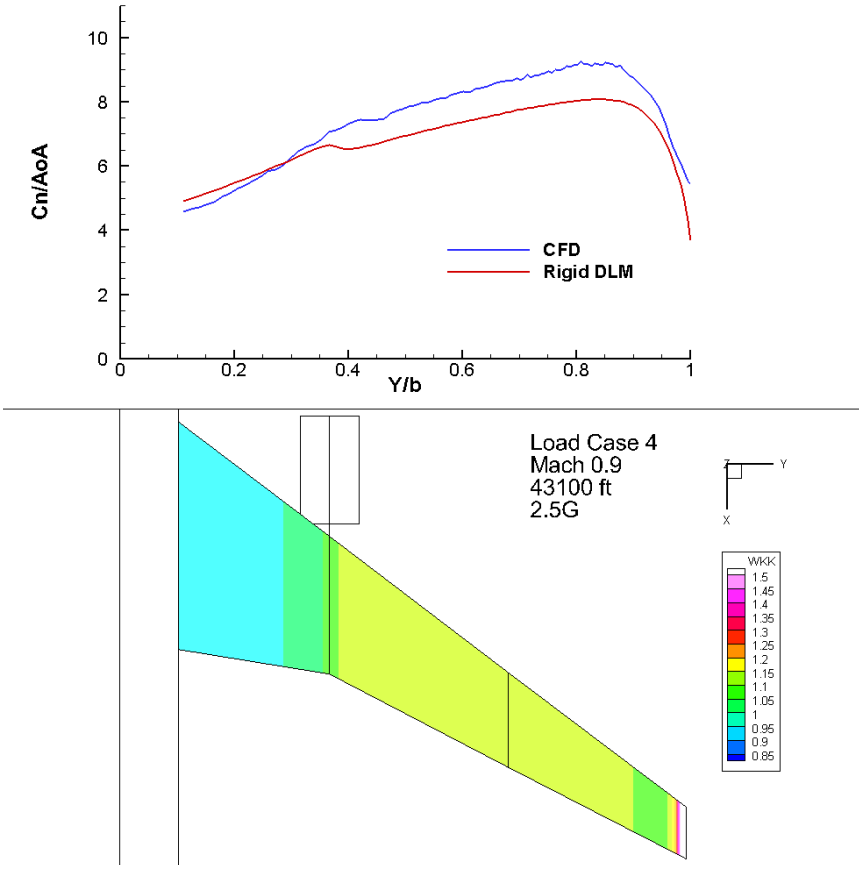

Figure 78: Top: $\Delta C_n/\Delta\alpha$ as a function of span. Bottom: distribution of $[W_{KK}]$ values on DLM wing mesh.

The high Mach number of Load Case 4 causes the C_p distributions in Figures 74 through 76 to be very similar to Load Case 2, but the error in the normal force coefficient slope is much less. The linear region also extends to $\alpha = 8_{\text{o}}$.

6.2.2.4 Rigid CFD Coupling Summary

The rigid CFD results were compared against the rigid DLM with fixed $\alpha = 1$ rad. The CFD C_p at $\alpha = 0$ is used to define $[FA2J]$ after the distribution is transferred to the DLM mesh. All the load cases showed very close matching between the original and transferred CFD validating the matching algorithm. Next the transferred CFD was compared against DLM and showed the largest contributor to error in this NASTRAN analysis comes from the inability to model nonlinear compressible flow effects. In all transonic cases the C_p for CFD and DLM were much closer after a normal shock where the flow velocity is significantly reduced and compressibility effects are negligible.

The C_n normal force coefficient slope was compared for both methods in order to define $[W_{KK}]$. The angle of attack was varied from zero to ten degrees to get visibility into nonlinearities in the slope. Although small variations in C_n occur due to numerical convergence in the CFD solutions the most significant nonlinearities are caused by separation at high angle of attack due to numerical viscosity. The point of separation occurs at different angles for each load case, but in all cases $\alpha = 0$ to 2^{o} falls in the linear range so this is used for defining $[W_{KK}]$.

A summary of the W_{KK} distribution for each load case is given in Table 7. The results show that Load Case 3 produces the least error in DLM when compared to CFD. This is expected because this load case is in the subsonic regime and essentially incompressible. The other W_{KK} values are within reasonable ranges and reflect the increase of compressibility with Mach number. In general these results reflect the

importance of shock prediction when defining epistemic uncertainty in DLM.

Table 7: Percentiles of Rigid W_{KK}

Load Case	*Mach*	*Altitude*	*Load Factor*	*25%*	*50%*	*75%*	*90%*
1	0.85	43100 ft	2.5G	1.0000	1.1910	1.3441	1.4290
2	0.9	23000 ft	2.5G	1.0000	1.3129	1.3816	1.4460
3	0.6	20000 ft	2.5G	0.8962	0.9802	1.0000	1.0000
4	0.89	43100 ft	2.5G	1.0000	1.1017	1.1270	1.1381

6.2.3 Flexible Coupling of CFD and Doublet-Lattice Method

6.2.3.1 Flexible CFD Coupling Process Overview

The flexible CFD coupling is intended to simulate the flight load survey after load cycles in order to validate the predicted loads and structural design for certification purposes. Thus the results discussed in this section were produced under the assumption that the structural stiffness (and loads) have converged, unlike the rigid results which use the initial stiffness values. The process for coupling flexible CFD to DLM is more involved than the rigid case because the CFD mesh must be deformed based on the results from NASTRAN. Figure 79 depicts the general steps of the process which are detailed here.

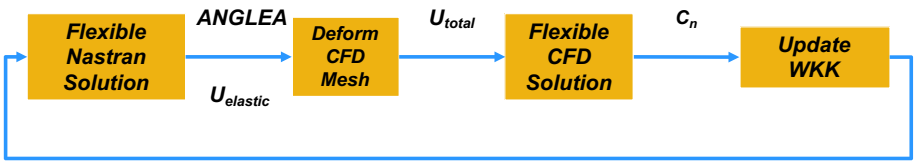

Figure 79: The flexible CFD coupling process.

The process begins with the NASTRAN solution from the conclusion of the simulated load cycles (iteration between NASTRAN and HyperSizer) with the rigid $[W_{KK}]$ and $[FA2J]$ corrections. The trimmed angle of attack $ANGLEA$ as well as deformations $U_{elastic}$ are outputted. The deformations of interest are the wing twist (about the span) and bending (about the fuselage) of the DLM mesh. These deformations are used to project the two dimensional deformation onto the three dimensional CFD mesh.

The translational displacement of each element centroid is extracted from the solution using Patran utilities. Patran is the post-processing graphical user interface for NASTRAN developed by MSC Software. The DLM mesh is segmented into twenty-three chordwise strips. The vertical displacement of the leading and trailing edge are used to calculate the twist angle of each strip. A smoothing spline function is fit to the spanwise twist distribution as shown in Figure 80. A similar process is carried out for the bending distribution based on the trailing edge of each strip.

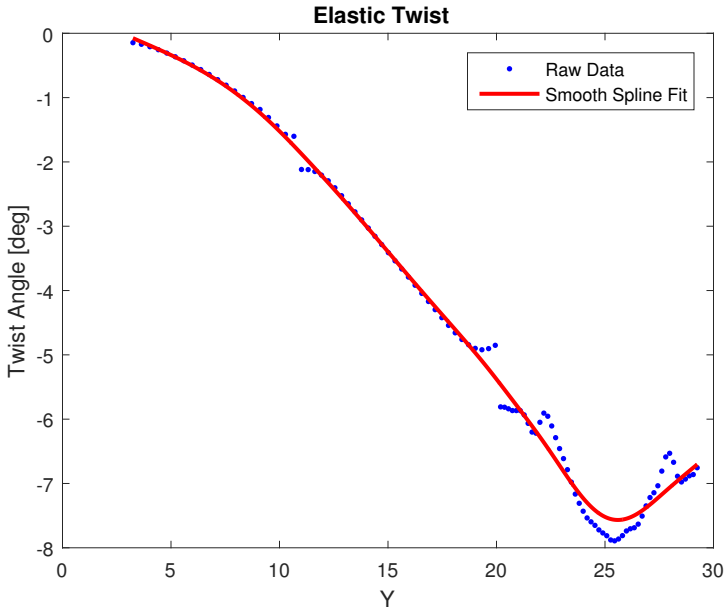

Figure 80: Example of twist spanwise distribution for Load Case 1

The 3D mesh is deformed by directly modifying the *stl* file (stereolithography)

which defines it. The following procedure is used to find the deformed z component of the vertices of each element in the CFD mesh. Given an element vertex with original coordinates (x,y,z):

Step 1: Find midpoint of corresponding strip, $x_{midpoint}$

Step 2: Calculate z-displacement of element vertex due to twist:

$$z_{twist} = |(x - x_{midpoint}) \tan(\theta_{twist})|$$

$$if\ \theta_{twist} < 0 \text{ or } \Delta x < 0$$

$$z_{twist} = -z_{twist}$$

$$elseif\ \theta_{twist} > 0 \text{ or } \Delta x > 0$$

$$z_{twist} = -z_{twist}$$

$$end$$

Step 3: Calculate total z-displacement

$$z_{total} = (z_{twist} + z_{bending}) + z$$

Only the z component is needed because the DLM mesh has only two degrees of freedom, vertical displacement and rotation about the span, which only results in translations in the z direction. NASCART-GT is then run using $U_{total} = \{U_{elastic}, ANGLEA\}$, in other words its run using the deformed mesh and rotated at an angle of attack equal to ANGLEA. The CFD results are used to calculate C_n using the procedures discussed in Section 6.2.1.3. In Equation 32, $\alpha_1 = \alpha_2 = ANGLEA$ and at $C_n(\alpha = 0)$ refers to the normal coefficient calculated in the rigid analysis. The matrix calculated using Equation 33 is actually the update coefficient matrix $[W_{KK_{Update}}]$ and the actual flexible empirical adjustment is found based on the previously found rigid empirical adjustment:

$$W_{KK_{Flexible}} = W_{KK_{Update}} * W_{KK_{Rigid}} \tag{35}$$

The next section discusses the load cycle results which precede the calculation of the flexible empirical adjustments.

6.2.3.2 Load Cycle Results with Empirical Adjustments

In an aeroelastic system the flexibility of a body will impact the aerodynamic loads which act upon it. Thus the wing twist and bending are important considerations. The elastic twist is of particular importance because it significantly influences aerodynamics by changing the angle of the flow a section sees (i.e. the angle of attack). Because of uncertainty, the initial stiffness is higher than the converged stiffness after the load cycles so the deformations are greater in the latter case. Figure 81 shows the results for elastic twist and wing bending before and after loads analysis. It should be noted that the twist angle is about the global Y axis and does not include the initial wing incidence built into the jig shape. In fact, this incidence is designed to achieve an overall twist (incidence + elastic) which creates favorable aerodynamics at the cruise condition.

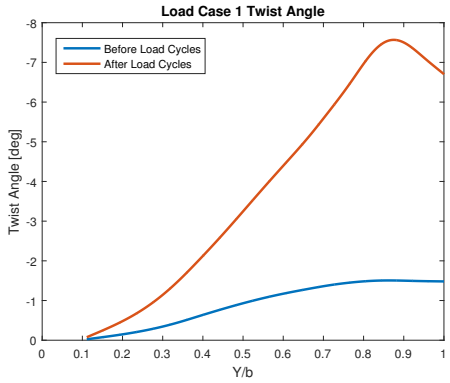

(a) Load Case 1 Elastic Twist, $\alpha = 6.36^o$

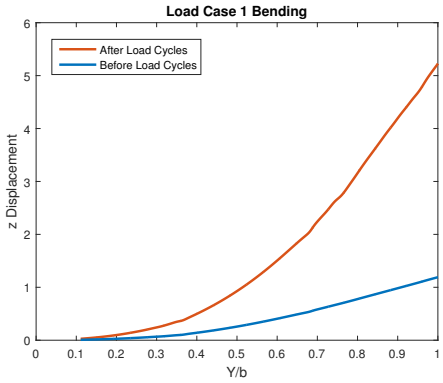

(b) Load Case 1 Bending

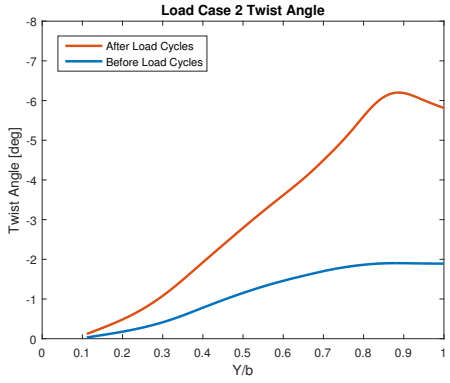

(c) Load Case 2 Elastic Twist, $\alpha = 3.60^o$

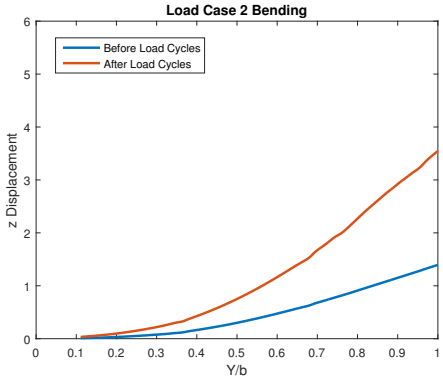

(d) Load Case 2 Bending

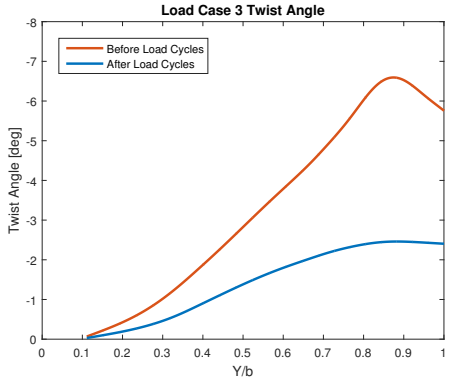

(e) Load Case 3 Elastic Twist, $\alpha = 5.16^o$

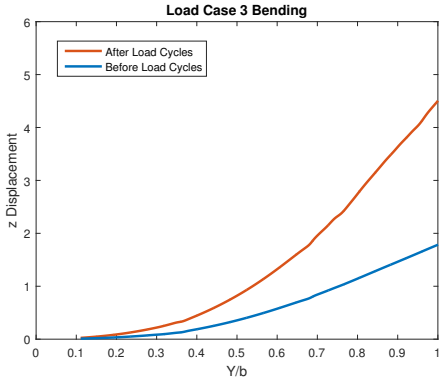

(f) Load Case 3 Bending

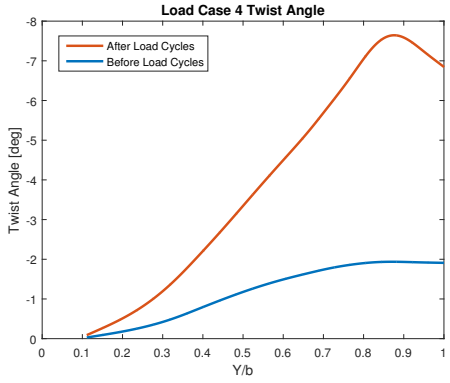

(g) Load Case 4 Elastic Twist, $\alpha = 5.37^o$

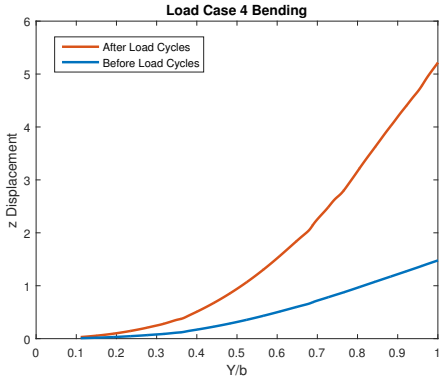

(h) Load Case 4 Bending

Figure 81: Effect of load cycles on twist and bending, 2.5G

The results further show how much softer the structure is after the stiffness has been reduced after load cycles. Keep in mind both the limited types of load cases (i.e. all symmetric) and failure modes used in this analysis contributes to this flexibility. Again, such limitations were incorporated to simplify the model and focus on the method.

In Figure 81 the angle of attack is listed to get a sense of the effective sectional angle of attack. For example, in Load Case 1 any portion of the span with negative twist greater than 6.36° will result in a negative effective angle of attack. Thus there will be some negative lift outboard of about the 75% span. Notice the majority of the twisted wing in Load Case 2 has negative effective angle of attack. Due to the taper, the majority of total wing lift is generate inboard so the impact of outboard twist is lessened.

Some negative effective angle of attack can be beneficial in this M&S environment because it helps prevent numerical separation. As has been discussed, high angles of attack can lead to separation due to numerical viscosity in inviscid CFD analysis. The twist angles reported in Figure 81 are all negative which indicates a reduction in the total angle of attack at a particular wing section. Thus the twist helps mitigate the possibility of separation.

On the other hand, if the effective angle of attack is too negative, it will cause numerical problems. The linear aeroelastic analysis used in this environment imply there are no large deformations in the structure that would require higher-fidelity nonlinear finite element solvers which are out of the scope of this work. Thus the flexible empirical adjustments assume a positive, linear normal force coefficient slope under deformation across the wing span. But if the model is flexible enough the twist can cause enough negative lift to lead to nonlinear and even infeasible W_{KK} values. In the next section we look at if and when nonlinearities due to separation occur or twist occur.

6.2.3.3 *Nonlinearities in Simulated Flight Load Survey*

Nonlinearities in the normal force coefficient slope due to flow separation must be avoided to maintain accurate empirical adjustments. In previous sections the concept of numerical viscosity was introduced in inviscid CFD analysis. The effect of angle of attack on flow separation is visualized in Figure 82 for Load Case 3. At $\alpha = 6^o$ the streamtraces around the wing show mostly attached laminar flow indicated by the smooth, parallel lines. On the contrary, at $\alpha = 10^o$ the flow is detached from the body and turbulent due to separation.

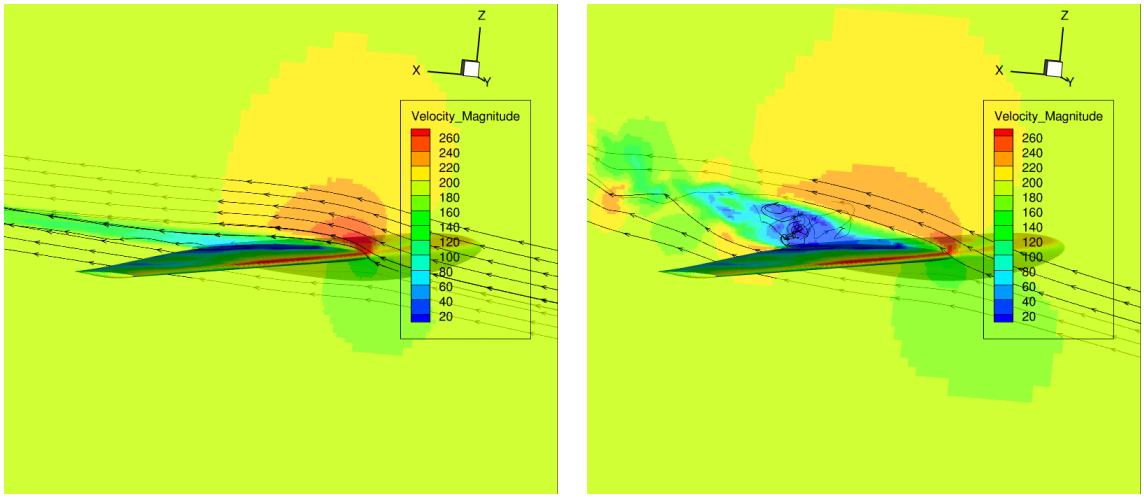

(a) $\alpha = 6^o$ (b) $\alpha = 10^o$

Figure 82: Example of flow separation caused by numerical viscosity at two angles of attack for Mach=0.6, 20,000 ft. Contour colors are intentionally banded (not continuous) to show contrast and flow features

Section 6.2.3.1 discussed the flexible CFD coupling process and how the trimmed angle of attack is used to define the flexible $[W_{KK}]$ adjustments. ANGLEA is determined in the NASTRAN solution to trim the aircraft and solve the equilibrium equations. If ANGLEA is large, numerical viscosity will cause separation. In order

to keep ANGLEA in the linear range of the normal force coefficient slope the vertical load factor input can be reduced from 2.5G. At a reduced load factor the weight force of the aircraft is less so less lift is required to maintain equilibrium, which in turn means a smaller angle of attack is required.

6.2.3.4 Comparison of Flexible CFD to Doublet-Lattice Method

The final structural design from loads analysis is tested for a range of load factors to determine when flow separation occurs and determine the highest load factor to be be used for the simulated flight test validation. The structure will still be designed to withstand the 2.5G critical load cases, so any reduced load factor will only affect the flight load survey. Comparison of the load factor sweep to *FA2J* shows the effect of the deformation and can be used to evaluate the small-deformation assumptions.

Load Case 1: Mach 0.85, 43100 ft

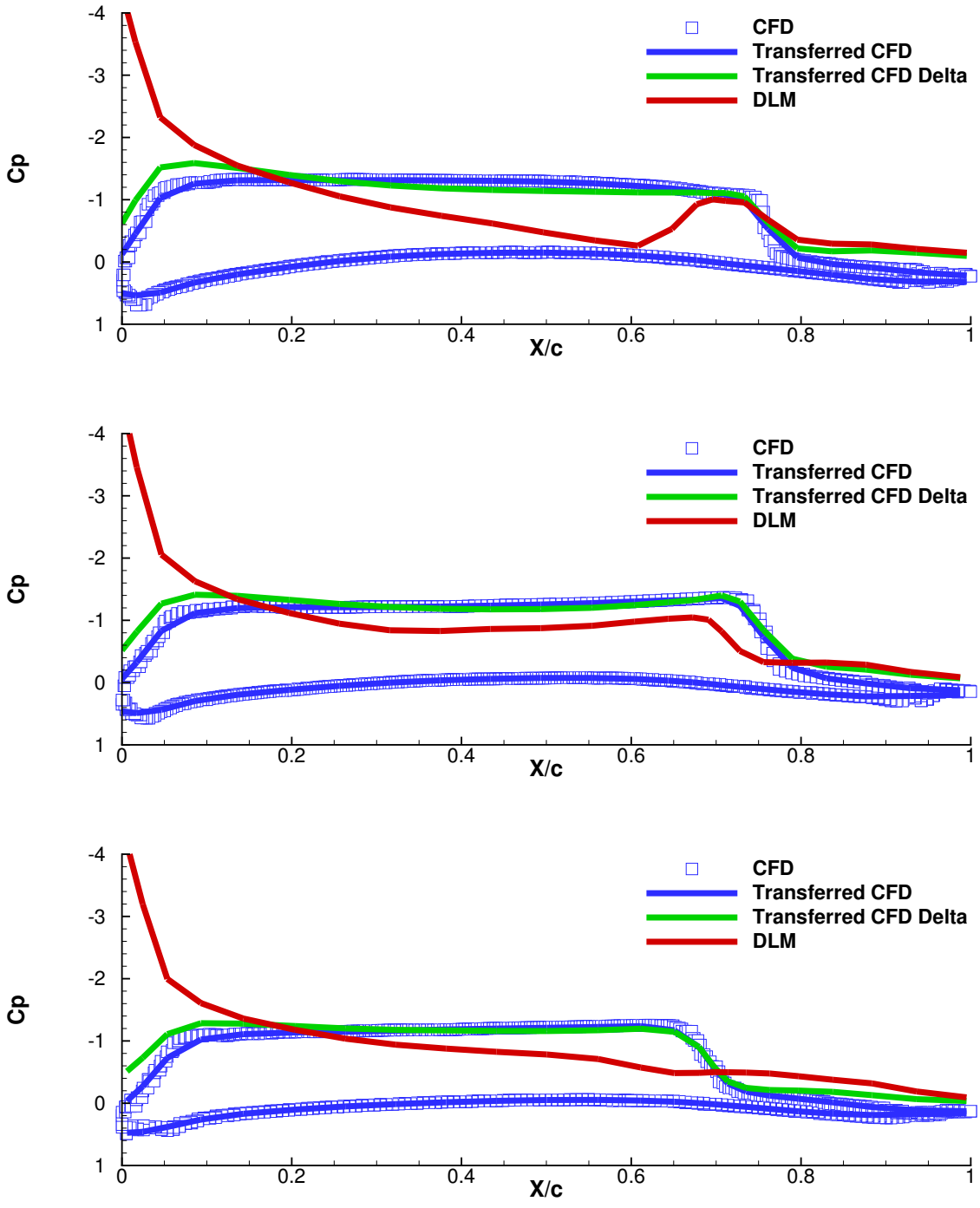

Figure 83: C_p comparison at 25% (top), 50% and 75% span, $\alpha = 6.36^o$, 1.5G.

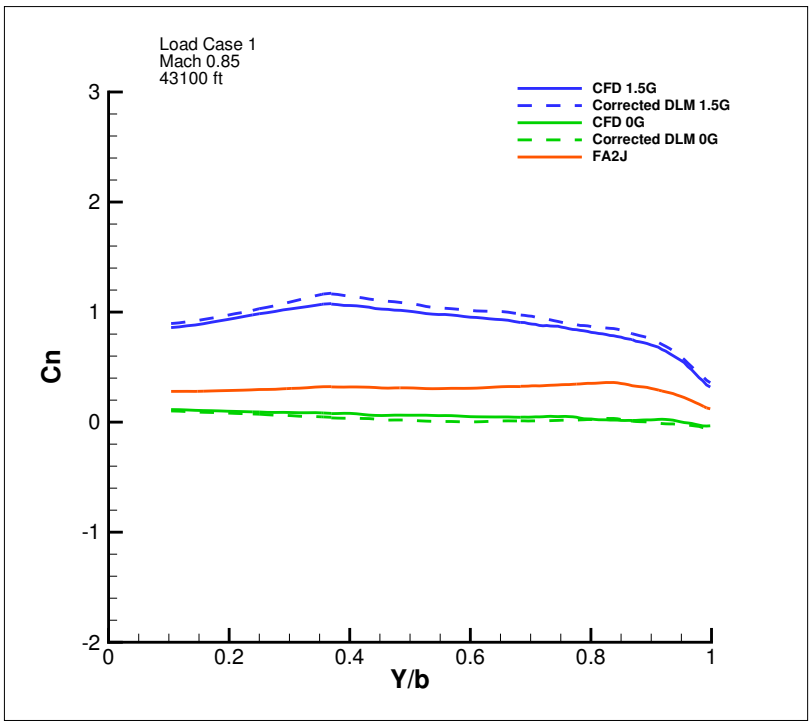

Figure 84: C_n comparison for 0G and 1.5G load factor

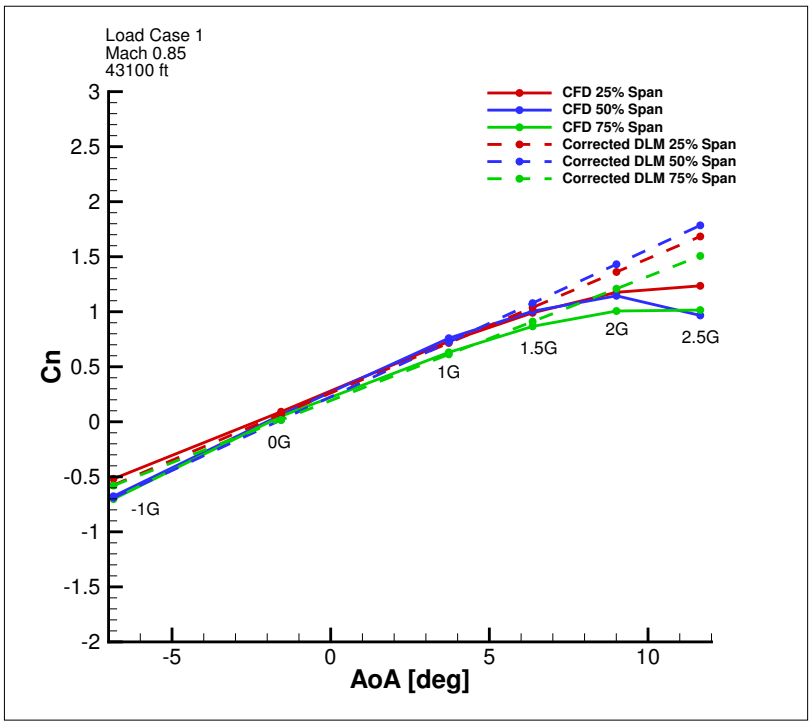

Figure 85: Load factor sweep.

In order to better explain the load factor sweep results, the C_p and C_n distributions are shown for each load case. The C_p and C_n are dimensionless so they can be compared and plotted on the same scale. Even though the NASTRAN solution includes the rigid $[W_{KK}]$ and $[FA2J]$, the corrections only affect the outputted forces and moments and not the pressure as shown in Equation 30. Thus the DLM results plotted in C_p vs X/c are uncorrected. A capability was added to MSC NASTRAN to output the corrected C_n which is utilized here. All DLM results in this section which include the empirical adjustment factors are labeled as such.

The flexible NASTRAN analysis allows for aeroelastic feedback and thus impacts the C_p distribution shown in Figure 83. In general the DLM C_p shows less error compared to CFD than in the rigid case even though the results are uncorrected. The elastic twist reduces the effective angle of attack at each section and subsequently reduces the airflow speed over the top surface. The lower speed results in less compressibility and thus better matching between DLM and CFD.

Figure 84 shows the C_n distribution as a function of the span for two load factors in the linear normal force coefficient slope range. The corrected DLM results closely match the CFD. This is expected because the CFD mesh is deformed based on the NASTRAN displacements. A vertical load factor of zero G's means there is no lift or weight acting on the structure so there should be very little deformation. Thus there is less error between DLM and CFD at load factors near 0 and this is apparent in the results. The orange line labled *FA2J* represents the C_n calculated at zero degrees angle of attack for the rigid (undeformed) case. Comparison of DLM and CFD at 1.5G to *FA2J* is an indication of the magnitude of the flexible W_{KK}. At a particular section the magnitude of W_{KK} is the distance between the solid blue and orange line divided by the distance between the dashed blue and orange line. Because there is very close matching between DLM and CFD at 1.5G the W_{KK} values should be very close to unity along the span.

It is clear in Figure 85 that separation occurs between 2G and 2.5G and so 1.5G will be the upper limit of the linear range. Relative to the rigid results, the separation occurs at a higher angle of attack because of the greater elastic twist. Comparison of the slopes between DLM and CFD is another indication of the flexible W_{KK}. The slopes are very similar between 0 and 1.5G which further shows that W_{KK} values will be close to one.

Load Case 2: Mach 0.9, 23000 ft

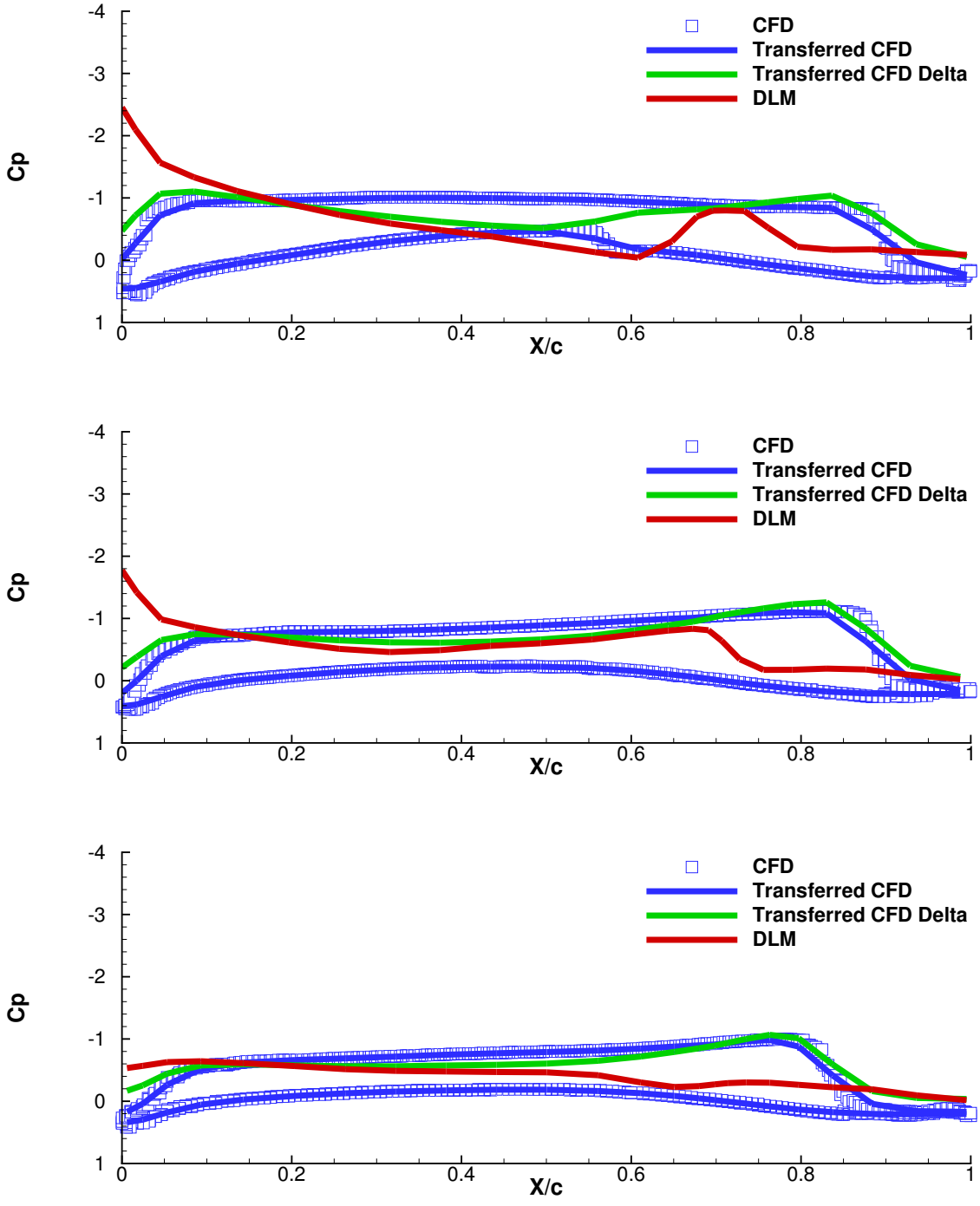

Figure 86: C_p comparison at 25% (top), 50% and 75% span $\alpha = 3.60^o$ and 2.5G. [UPDATE CFD DATA FOR CORRECT ALPHA]

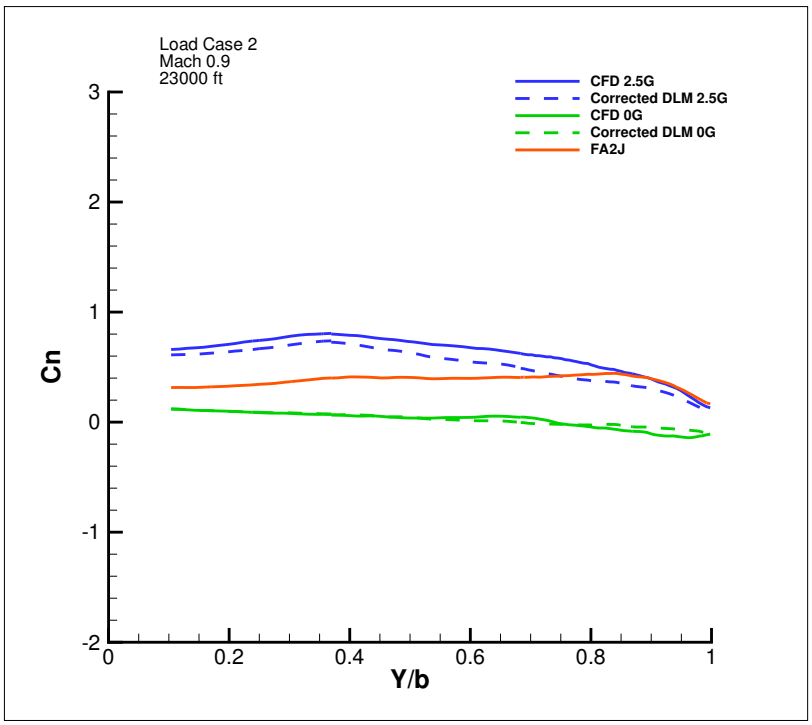

Figure 87: C_n comparison for 0G and 2.5G load factor

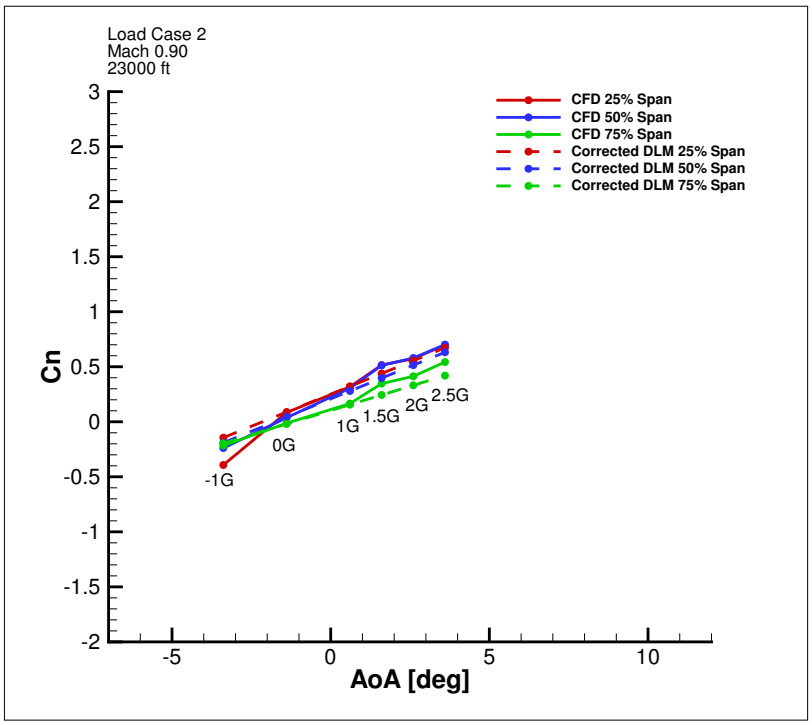

Figure 88: Load factor sweep.

The reduced error in flexible analysis is especially evident in Load Case 2 where the DLM and CFD match almost perfectly for significant parts of the chord in Figure 86. The trimmed solution for Load Case 2 has a relatively small angle of attack due to the combination of high Mach number and low altitude. This can be seen in Equation 36, where the speed and altitude reduce the C_l and requires a smaller α to trim. The lift cure slope thus remains linear up to the maximum of 2.5G, unlike in the other cases. Note, there are small nonlinearities due to convergence of the CFD solution but the general C_n trend increases linearly with α. In comparison, there is no distinct dropoff in C_n as in the other load cases.

$$C_l = \frac{L}{\frac{1}{2}\rho_\infty V_\infty^2} \tag{36}$$

The most significant result for Load Case 2 is in the intersection of the 1.5G and *FA2J* curves in Figure 87. The large negative twist due to flexibility in conjunction with the small positive angle of attack produces the same amount of lift as in the undeformed, zero-degree case on the outboard wing. This violates the linear assumptions of the empirical adjustments and would lead to highly inaccurate flexible W_{KK} values so this load case will be excluded from the flight load survey. Again, this does not violate the integrity of the study because the structure will still be sized for this load case. In addition, it will later be shown that this load case is not critical so excluding it does not significantly impact the evaluation of major rework in the flight load survey.

Despite this, these results are very beneficial by revealing that the structural model may be underestimating the stiffness. This insight can help improve the model or introduce other uncertainty sources into the current model. With larger deformations the linear static aeroelastic assumptions may result in larger epistemic uncertainty, making the proposed uncertainty quantification and management framework even

more important.

Load Case 3: Mach 0.6, 20000 ft

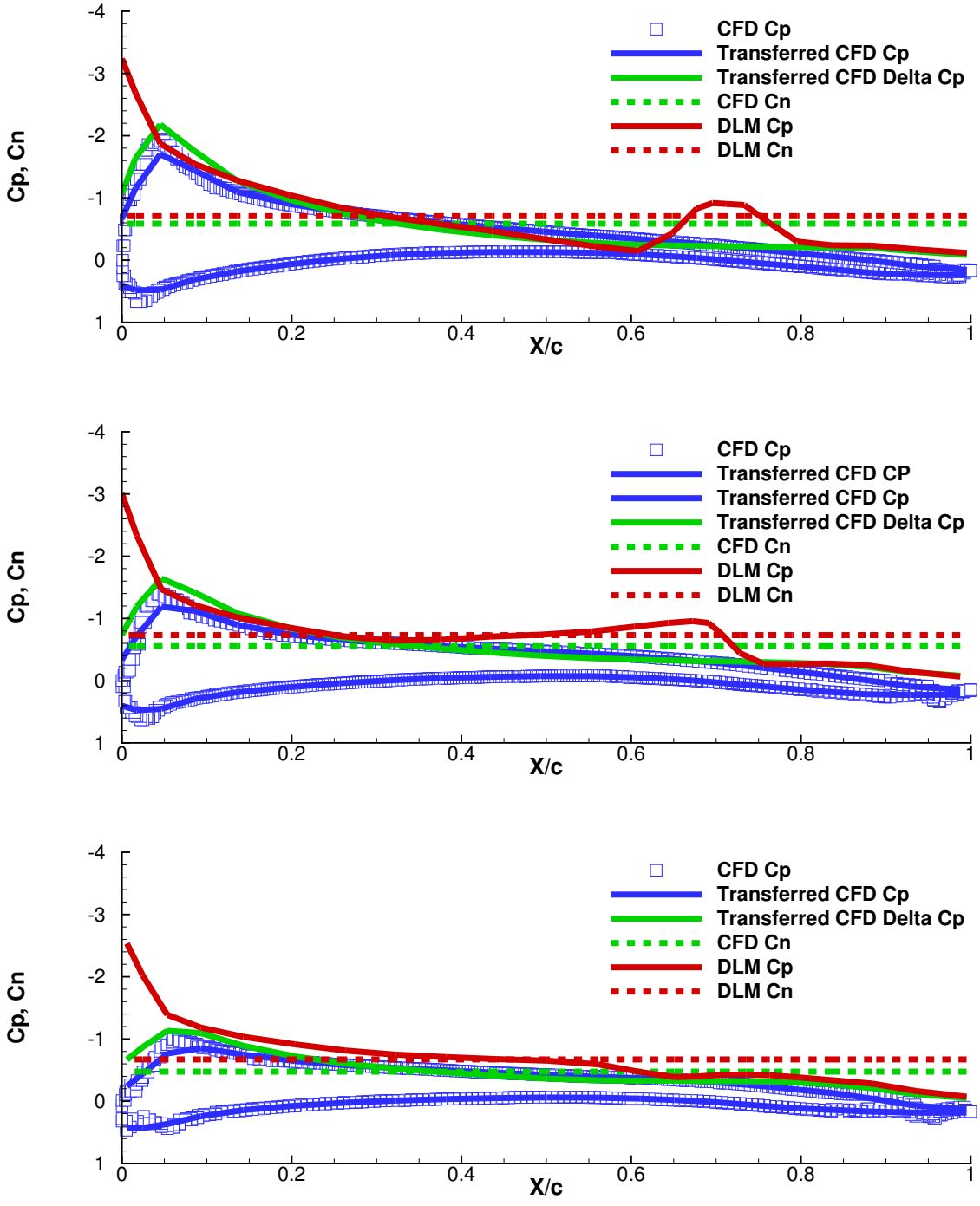

Figure 89: C_p comparison at 25% (top), 50% and 75% span $\alpha = 5.16^{\circ}$ and 1.5G.

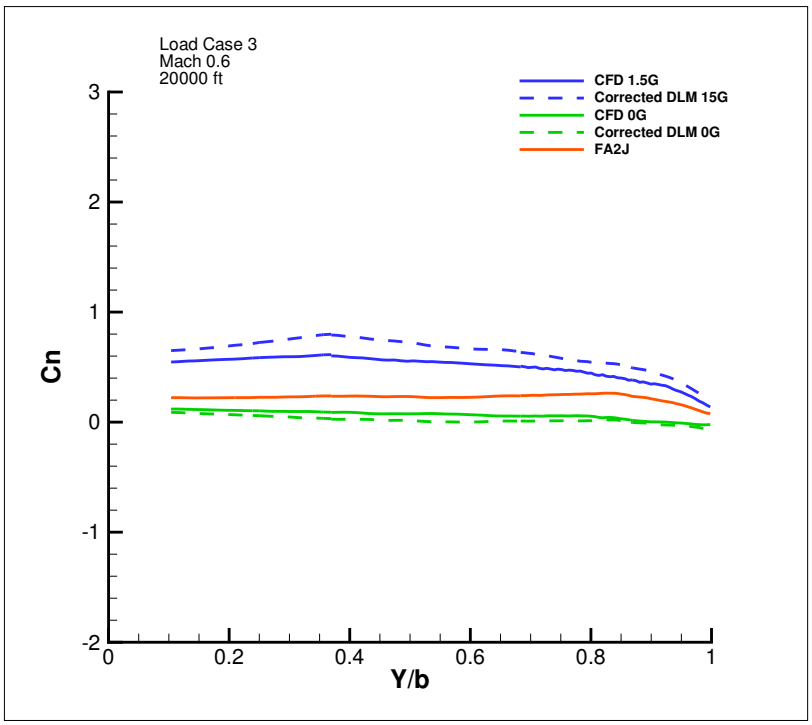

Figure 90: C_n comparison for 0G and 1.5G load factor

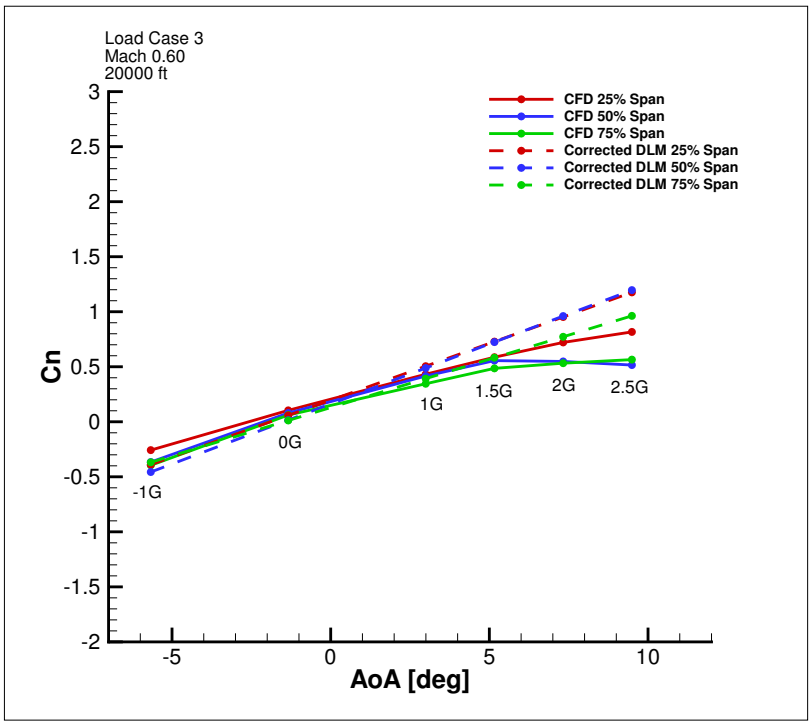

Figure 91: Load factor sweep for Load Case 3.

As the baseline case, Load Case 3 showed the least amount of error in the rigid analysis but the opposite is true when aeroelasticity is considered. To further explore the impact of this error, the resulting C_n is also plotted (dashed lines). Note, C_n is typically positive so the negative is plotted here to compare against C_p. In these figures, C_n is essentially a weighted average of the C_p over the chord. Comparing the DLM and CFD C_n shows the error results in DLM overpredicting the loads. This can be more clearly seen in Figure 90 which shows the C_n error over the span and is larger than the other cases. The rigid analysis was clearly dominated by nonlinear compressibility and thus Load Case 3 was the most accurate. In the more realistic scenario of flexible structures, the deformation plays more of a role on accuracy.

Load Case 4: Mach 0.89, 43100 ft

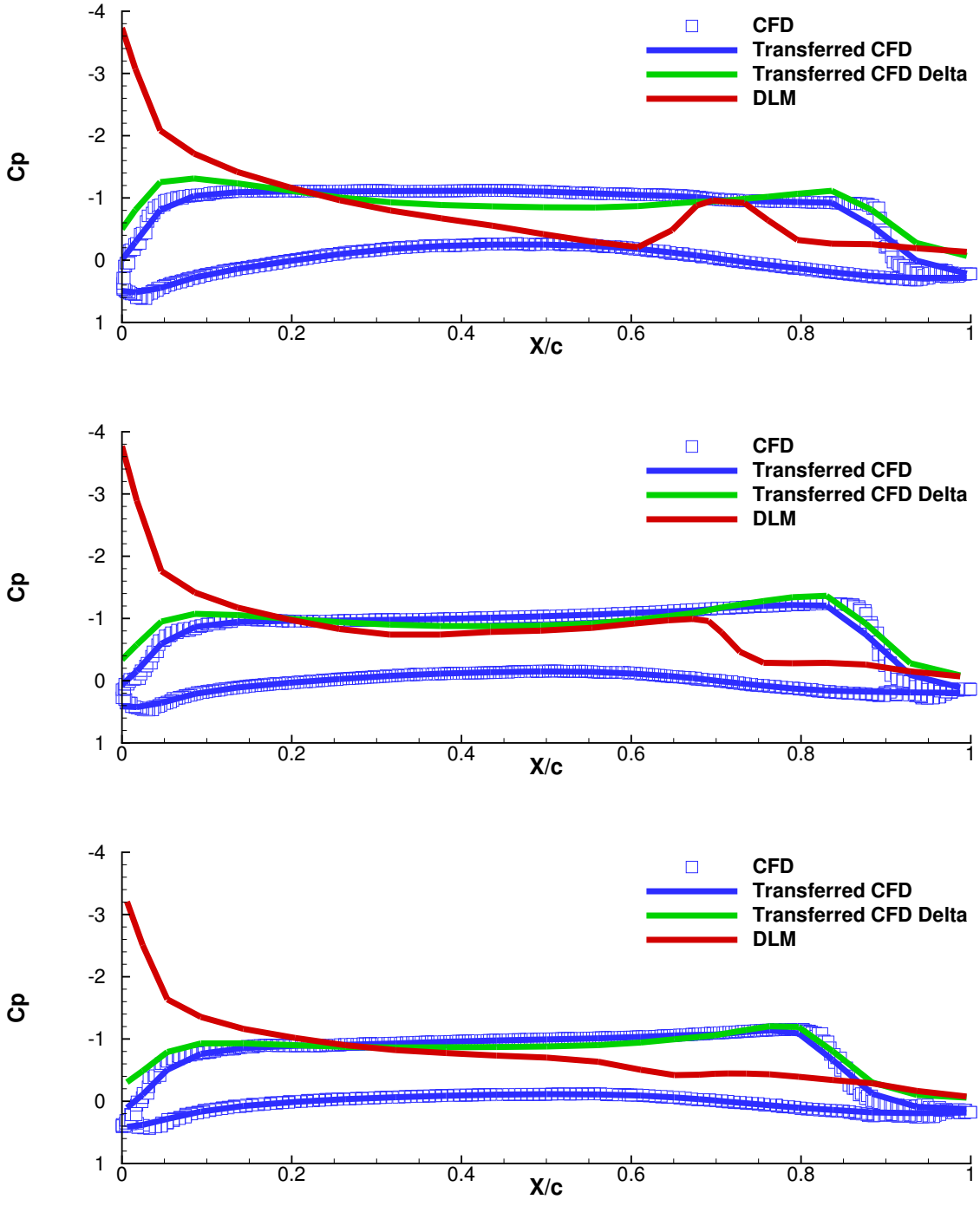

Figure 92: C_p comparison at 25% (top), 50% and 75% span $\alpha = 5.16^o$ and 1.5G. [UPDATE CFD DATA FOR CORRECT ALPHA]

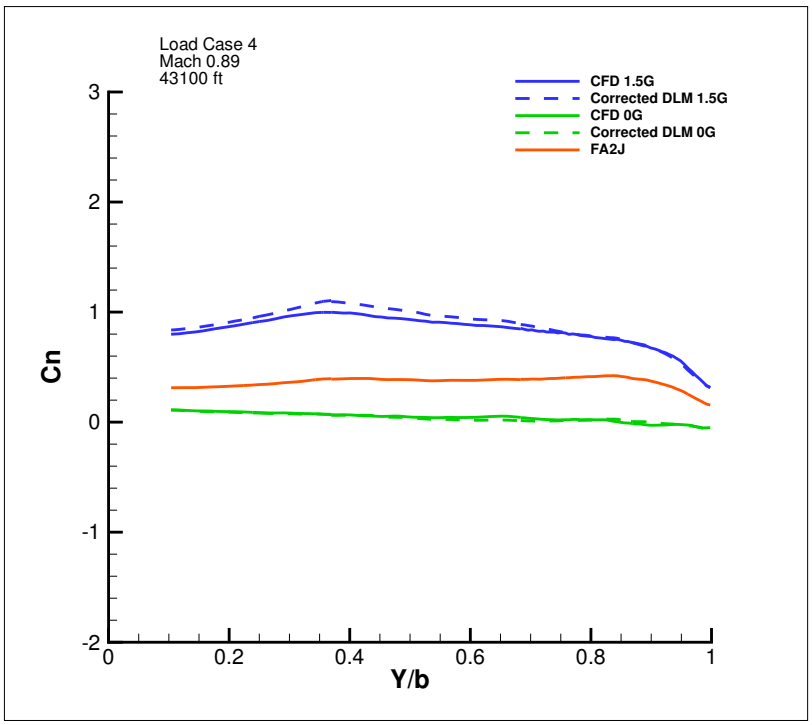

Figure 93: C_n comparison for 0G and 1.5G load factor

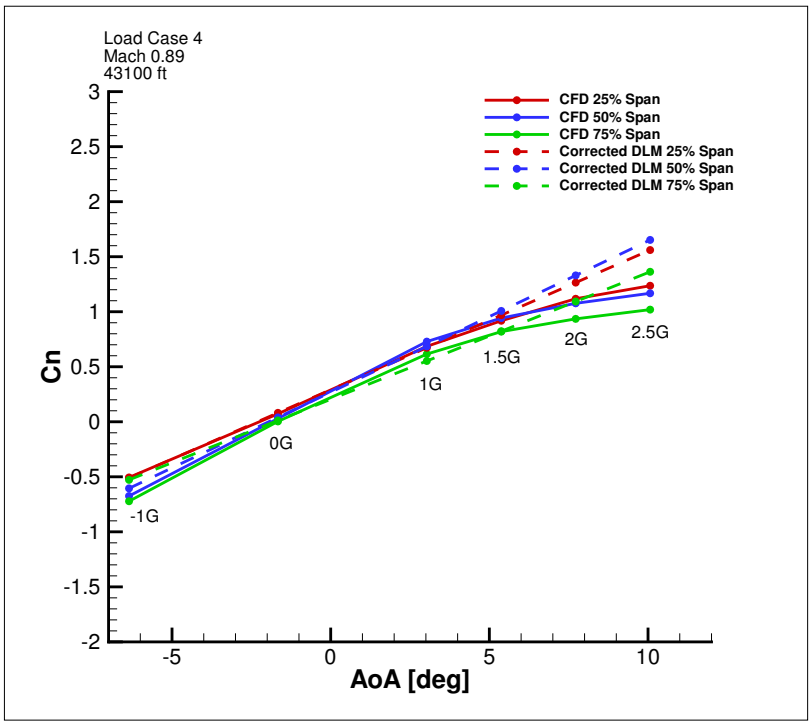

Figure 94: Load factor sweep for Load Case 4.

Similar to the rigid results, the C_p distribution resembles Load Case 2 but results in smaller error. Load Case 4 results in the most accurate DLM solution after correction with the rigid adjustments. There is a drop off in the C_n in the 2-2.5G region so 1.5G will be the upper limit.

6.2.3.5 Flexible CFD Coupling Summary

With the exception of Load Case 2, the normal force coefficient slopes for all cases appear to be linear up to 1.5G at all three span locations. The load factors for further consideration of the flight load survey are shown in Table 8 along with the corresponding trimmed angle of attack.

Table 8: Load factors for linear normal force coefficient slope

Load Case	***Mach***	***Altitude***	***Load Factor for Sizing***	***Load Factor for Flight Load Survey***	***Angle of Attack***
1	0.85	43100 ft	2.5G	1.5G	6.36°
2	0.9	23000 ft	2.5G	2.5G	3.60°
3	0.6	20000 ft	2.5G	1.5G	5.16°
4	0.89	43100 ft	2.5G	1.5G	5.37°

At this point it is clear that flexibility in the structure, and thus aeroelasticity, plays a more important role in some load cases more than others. The rigid adjustments correct for nonlinear compressibility and 3D flow effects but of course ignore deformation and aeroelstic effects. When the rigid adjustments were applied to NASTRAN the DLM was able to accurately predict the loads in Load Case 1 and 4 but not in 2 and 3. Looking at the bending and twist distributions reveal that there larger deformation in Load Case 1 and 4 most likely reduces the compressibility effects and

thus reduces the error. On the contrary, the deformation in Load Case 2 and 3 significantly increases the DLM error in comparison to the rigid case. This type of insight is helpful in analyzing the criticality of load cases in order to size the structure and characterize uncertainty.

As was mentioned, the linear elastic assumptions of this analysis must be maintained to accurately perform the flight load survey and evaluate major rework using this environment. It is not necessary to use all four load cases to do the flight test validation if a load case is more critical than the rest. Plotting the wing bending moment is one approach to determining which load cases are critical prior to structural design optimization. Figure 95 shows that Load Cases 1 and 4 envelope the bending moment for the other two cases and therefore are more critical. Given this result and the previous determination of reduced DLM error, Load Case 4 will be used to calculate the flexible $[W_{KK}]$ and perform the flight load survey. Both Load Cases 1 and 4 could be used, but to simplify the results, only the 4th case will be used because it is slightly more critical and results in less DLM error.

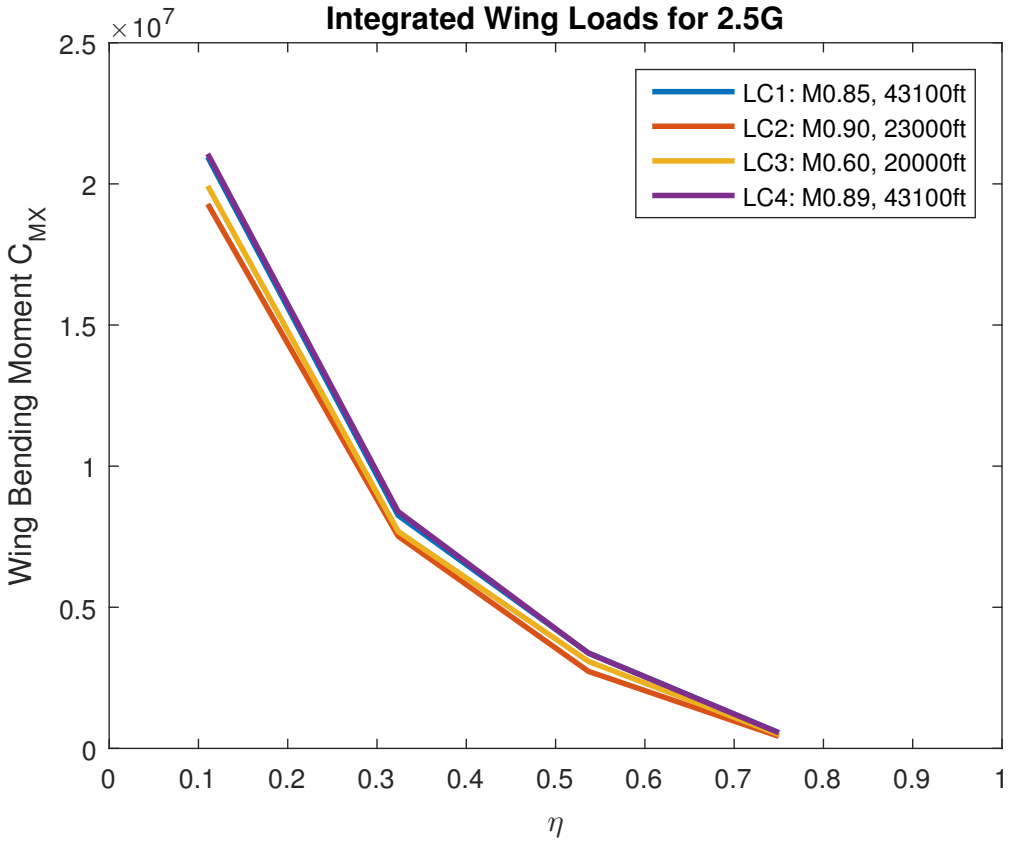

Figure 95: Integrated bending moment.

The flexible $[W_{KK}]$ defined by Load Case 4 and used for the flight load survey is summarized in Table 9. The other $[W_{KK}]$ types are listed for comparison. The fact that $W_{KK,rigid}$ and $W_{KK,flex}$ are calculated at different load factors has no consequence when comparing them because they are simply a ratio of the normal force coefficient slopes. The effect of applying $W_{KK,flex}$ to NASTRAN is shown in Figure 96.

Table 9: Percentiles of W_{KK} for Load Case 4; Mach 0.9, 43100 ft

Adjustment Factor	***Load Factor***	***25%***	***50%***	***75%***	***90%***
$W_{KK,rigid}$	2.5G	1.0000	1.1017	1.1270	1.1381
$W_{KK,update}$	1.5G	0.9188	1.0000	1.0013	1.0753
$W_{KK,flexible}$	1.5G	1.0000	1.0030	1.1302	1.1875

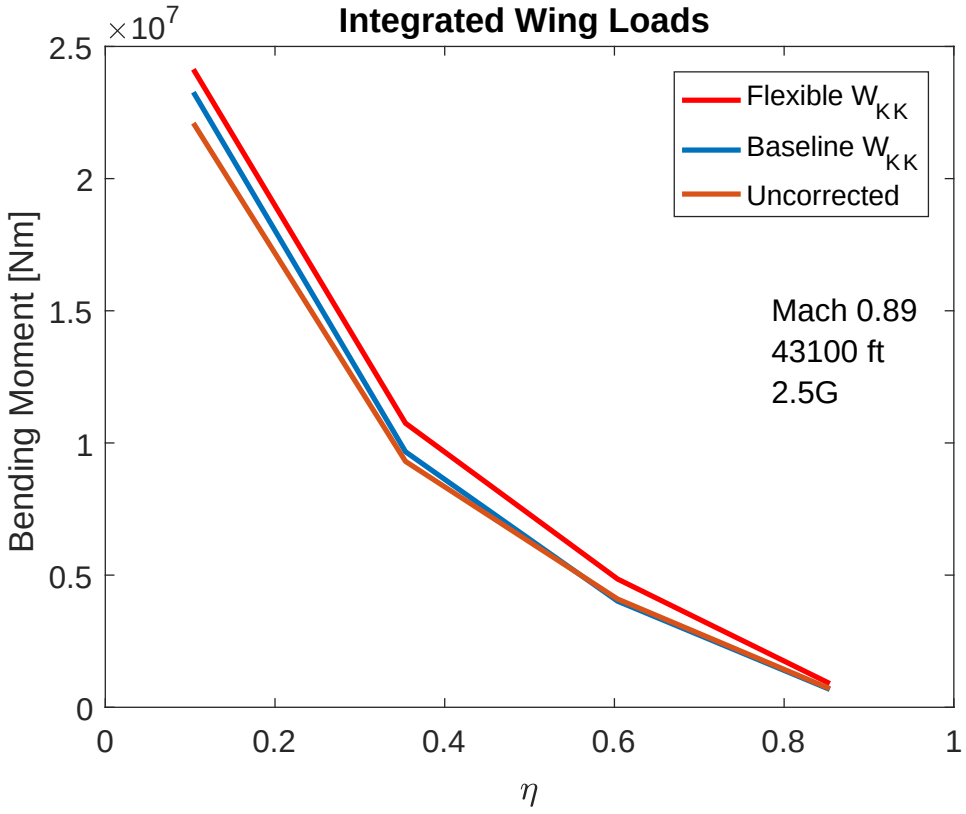

Figure 96: Integrated bending moment.

The results presented thus far represent a deterministic loads analysis and structural optimization because no uncertainty has been applied yet. By using the full values of $[W_{KK,rigid}]$ during the load cycles these results also capture the full effects of a simulated wind tunnel test. The bending moment curves in Figure 96 include the

baseline 10% structural margins, updated stiffness and final structural design after four load cycles.

The bending moment envelopes show that the rigid corrections reduce the error in comparison to the uncorrected case. More importantly, the results indicate the rigid corrections just slightly underpredict the loads. This can also be seen in the larger flexible W_{KK} values in Table 9. The load cases in this study represent critical cases and thus are extreme compared to normal operating conditions. If the structure were designed to withstand up to the rigid-corrected loads, there would be zero to slightly negative margins for loads experience during flight test. In an actual airplane development such results would indicate the structural design is unconservative and could cause a failure during the flight load survey and subsequently require significant rework to fix the design. This is due to a combination of the rigid assumptions in the wind tunnel calibration when predicting the loads and inadequate structural margins in the design. As mentioned in the background, such a failure at that stage of the development could cost millions of dollars due to redesign and testing efforts, delays, and damaged reputation.

The purpose of this thesis is to quantify and manage uncertainty to avoid this very scenario, but in a cost effective manner. To avoid rework the rigid adjustments should result in loads which exceed the flexible-corrected loads and margins which lead to a conservative design. Ideally, we would achieve this without a large weight penalty or exorbitant costs for minor rework.

The deterministic results presented thus far are the baseline to which the proposed framework will be evaluated to avoid major rework in the flight load survey. The baseline results assume a required margin of 10% for von Mises stress criterion and the highest fidelity aeroelastic analysis available to capture the full rigid corrections. For now on, the baseline loads with the flexible adjustments will be known as the *true loads*.

In subsequent sections uncertainty will be defined and included in the system and later the uncertainty management system will optimize the aerodynamic fidelity and required margins to minimize the probability of major rework. It is important to notice that even though a 10% structural margin was assumed in the baseline, this translated into a small negative margin in the bending moment. This emphasizes why both the aerodynamic fidelity and structural margins are optimized to avoid rework. The next section discusses how the epistemic uncertainty in the aerodynamics is defined based on the adjustment factors.

6.2.4 Epistemic Uncertainty

6.2.4.1 Defining Uncertainty

Section 3.3 detailed the various types of epistemic uncertainty and several statistical theories to model it. Probability theory was decided upon largely because it allows for Bayesian methods and easily integrates with aleatory uncertainty. The type of epistemic uncertainty is dependent on the source, and in this case the uncertainty in the empirical adjustment parameters represent model form error. [138] distinguishes between model parameter and model form error. The latter describes uncertainty due to using different forms of a model which represent different assumptions, for example the error associated with using the Euler instead of the Navier-Stokes equations. The assumption of the different forms can often be attributed to different fidelity levels. The NASTRAN empirical adjustments are intended to capture the effect for different aerodynamic model forms which are not captured in DLM but impact the lift curve slope in an assumed linear fashion. Thus the adjustment factors are parameters but capture model form error.

Model form error can be difficult to quantify and is often excluded from epistemic uncertainty studies [84]. Representing model form error with a parameter is compact and convenient, but to accurately capture the impact of fidelity each W_{KK} parameter

is represented by a known distribution family but unknown distribution parameters. A normal distribution is assumed for simplicity but the mean and standard deviation are not known. The various aerodynamic theories which are captured by the adjustment factor must reflect various levels of fidelity and uncertainty. Specifying the standard deviation of the normal distribution accomplishes this while the mean adjusts the lift curve slope based on the aerodynamic theory.

In the previous sections, CFD results were compared against DLM and the largest discrepancies were caused by nonlinear compressibility effects in the rigid case. Comparing the flexible CFD showed how the aeroelastic effects can sometimes be dominant. $[W_{KK}]$ attempts to capture these effects and so its uncertainty should also be based on them. When uncertainty is introduced, all previous discussions of the magnitude of rigid W_{KK} parameters refer to its mean value, while the standard deviation is naturally based on the error relative to the flexible parameters, which are treated as the true values.

The mean W_{KK} represent a linear adjustment to the lift curve slope so it is logical to assume a linear relationship also exists with the variation in the standard deviation. With this assumption the entire effect of fidelity can be represented by a scalar factor which will be referred to as the K-factor. The term comes from a similar use of a scalar factor to represent technology impact in the work of Kirby et al [74]. The K-factor varies between 0 and 1 to and symbolizes low and high fidelity respectively. In this context, the K-factor represents the analysis fidelity used in conjunction with wind tunnel calibration data. Thus the lower bound represents no calibration, i.e. $W_{KK} = 1.0$. The upper bound represents fully calibrated analysis, i.e. $W_{KK,rigid}$ and in between is partial calibration. Full calibration means an aerodynamic analysis has high enough fidelity to capture all the effects of the wind tunnel results while partial means only some of the effects can be applied to correct the aerodynamic loads. For example, NASTRAN is able to use wind tunnel data to calibrate the slope

and intercept of lift as a function of incidence, but a lower fidelity analysis may only be able to account for the intercept.

It is understood that this linearized view of fidelity may not always be applicable but it is a convenient form for modeling, simulation and optimization and works well with the linear empirical adjustment parameters in NASTRAN. Thus the K-factor will be used throughout the remainder of this thesis to represent aerodynamic fidelity. The relationship between the distribution parameters of W_{KK} and the K-factor are represented in Equations 37 through 39.

$$W_{KK} \sim N(\mu_{W_{KK}}, \sigma_{W_{KK}}) \tag{37}$$

$$\mu_{W_{KK}} = 1 - K + K * W_{KK,rigid} \tag{38}$$

$$\sigma_{W_{KK}} = (1 - K) * min(e_{uncorrected}, e_{rigid}) + K * max(e_{uncorrected}, e_{rigid}) \tag{39}$$

The min and max functions in Equation 39 are necessary because of the error terms, e, described in Figures 97 and 98, which show the uncorrected, rigid and flexible distribution of W_{KK} and associated errors for each strip along the span. The uncorrected adjustment is equivalent to $W_{KK} = 1.0$ and is plotted as a reference. Note, the mean value equation does not include the load margin, but will be included later in the uncertainty management optimization problem.

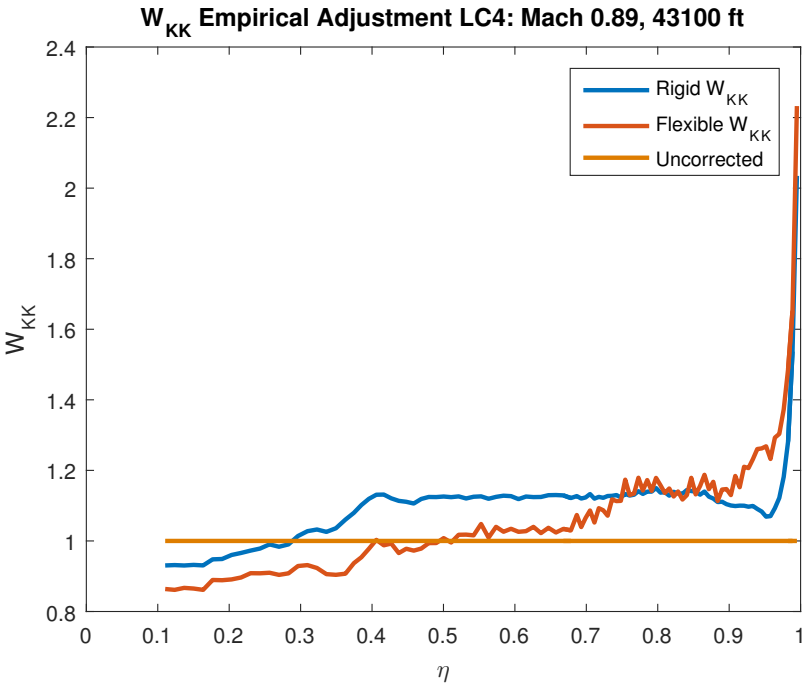

Figure 97: Rigid vs. flexible empirical adjustments.

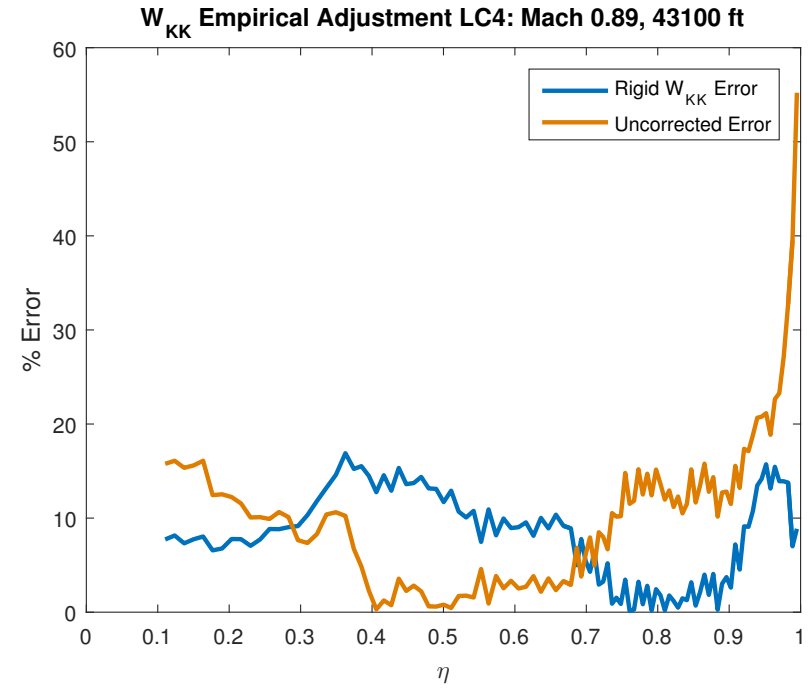

Figure 98: Error in empirical adjustments.

The discretization of the DLM grid and calcultion of W_{KK} per strip causes the

non-smooth distribution in both figures. Comparing the parameters of Figure 97 can be interpreted as visualizing three different fidelity levels; the uncorrected being the lowest level and flexible-corrected being the highest. The flexible data represents "truth data", so the uncorrected and rigid errors reported in Figure 98 are the discrepancy between the various fidelity levels in Figure 97.

It is assumed that the uncorrected error is always less than the rigid but in fact there is a portion near the center of the wing where the error is less. This simply means the magnitude of flexible W_{KK} is closer to 1.0 than the rigid in this region. These results can be attributed to the fact that the impact of fidelity is nonlinear in the middle region of the wing. We can circumvent this nonlinearity by utilizing Equation 39 for the standard deviation in terms of the errors. For example at the 50% span where the uncorrected error is nearly zero, the standard deviation for low fidelity, $K = 0$, will be equal to e_{rigid} and the high fidelity standard deviation will be $e_{uncorrected}$. This will allow the same linear scale to be applied to the distribution parameters of W_{KK} for all parts of the wing.

There 101 strips along the wing DLM mesh and thus 101 W_{KK} parameters. It will be difficult to fit reliable surrogate models with so many parameters, not to mention the additional aleatory parameters. The following section thus discusses dimensionality reduction efforts to reduce the number of uncertain parameters.

6.2.4.2 Reduction of Uncertain Parameters

Section 3.5.2 introduced sensitivity analysis and dimensionality reduction. Because of the specific goal of reducing the number of variables rather than simply determining their impact, dimensionality reduction was chosen. Once the reduced set of parameters is determined, sensitivity analysis will be done to include all uncertain variables to determine their effect on the response. Feature selection was deemed more

appropriate than feature extraction (also known as feature transformation) because each parameter represents a discrete strip on the wing and any transformation would eliminate the possibility of determining which specific strips significantly impacted the uncertainty in the probability of major rework.

Numerous feature selection algorithms exist and were briefly mentioned previously, three are available using MATLAB's Statistics and Machine Learning. One, based on sequential feature selection requires a user-supplied objective function to evaluate which features should be kept. The others two methods do not require a custom function be provided, so this option was not pursued. The other two are based off of RRELIEFF algorithm and Neighborhood Component Analysis (NCA) for regression. Both approaches utilize supervised learning which means each observation in the training set is "labeled", or attributed to a specific input, and a known output structure (in this case the bending moment response). Unsupervised learning is when the observations are unlabeled and the algorithm determines the hidden structure of the responses.

The first feature selection algorithm, is an improvement of RELIEF which uses a heuristic guidance algorithm and to handle incomplete data and multi-class data for classification problems [77]. RELIEFF has been modified further to handle regression, called RRELIEFF [127]. The benefits over other inductive learning techniques are it does not assume conditional independence of the attributes (inputs, features, etc.). The MATLAB implementation produces weights for each feature between 1 and -1, where large positive weights correspond to significant features.

The second feature selection approach, NCA, is an improvement of the popular K-Nearest Neighbor (KNN) classification algorithm. The algorithm uses a quadratic distance metric to determine the "nearest neighbor" and maximizes the expected leave-one-out classification error on the training data when used with a stochastic neighbor selection rule [67]. The algorithm has been for regression problems. Its

advantages are that it is non-parametric so it does not assume any form for the response distributions and or boundaries between them. In addition it is low rank so improves storage and search cost.

Both methods were implemented for the reduction of W_{KK} parameters. 500 samples of the parameters were drawn from a Latin Hypercube design and run in NASTRAN while keeping all other parameters fixed. A Latin Hypercube is a popular design of experiment for surrogate modeling and is a generalization of the Latin square, where only one sample is placed in each row and each column of a square grid representing the data [64]. The integrated bending moment was output for four locations on the wing at the wing root, 25%, 50%, and 75% span and at the 50% chord. The parameters are treated as uncertain inputs and the four loads are the responses. Then both feature selection algorithms were run on the data as shown in Figure 99 and 100.

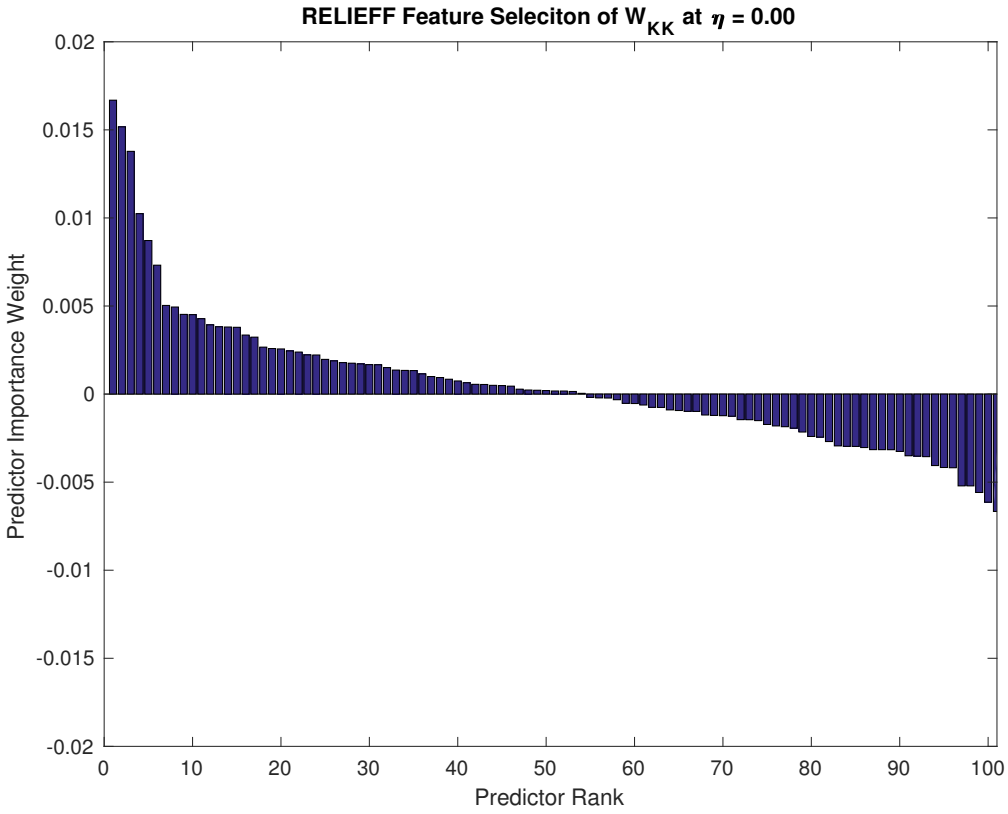

Figure 99: Feature selection using RRELIEFF

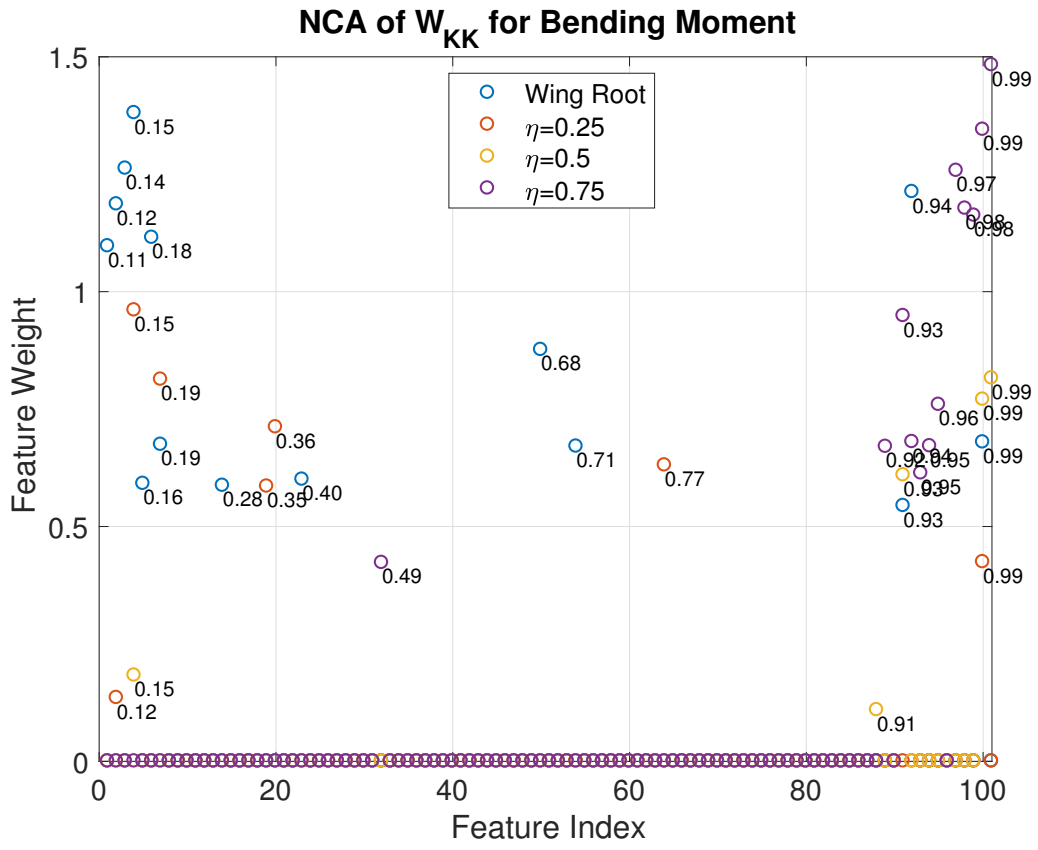

Figure 100: Feature selection using Neighborhood Component Analysis

Figure 99 gives the weights for the wing root bending moment. The algorithm was run for at all four locations. The weights determine the rank of features in terms of importance. Each feature index refers to a strip on the DLM mesh its associated W_{KK}. The algorithm is dependent on how many nearest neighbors the user selects to calculate per class. The number of neighbors must be between one and the number of observations, but either bound will produce unreliable or no important attributes respectively. This parameter was varied and determined that K gave good separation of features to determine a significant set. Figure 100 shows the selected features from NCA. All features close to zero are determined to be insignificant to the bending moment at a particular location. The features are color coded to show which bending moment they are important to. Note that there may be overlap for

significant features for the different responses but this is not shown in the figure. The values next to the dots refer to the η value (spanwise location) of the strip for the W_{KK} parameter. Similar to RRELIEFF, NCA is dependent on certain parameters to accurately select feature. λ is the regularization parameter which can be tuned to minimize the generalization error of NCA. The optimal λ was chosen for each bending moment response to do the final feature selection.

The bending moment is calculated internally in NASTRAN by integrating the loads from all wing structural grid points outboard of user-defined monitor points. Every W_{KK} parameter influences the aerodynamic load distribution and thus influences each bending moment response. But naturally, not all parameters will have the same impact on the responses. Thus the feature selection algorithms were run separately for each response and the aggregate of important parameters will be used. Any parameter which is deemed insignificant for all responses will be frozen for all future analysis. Table 10 shows the η value of selected features in NCA for each response compared against the highest ranking same number of features using RRELIEFF. The results for both methods are ordered in terms of importance. It should be noted that W_{KK} parameters with $\eta > 0.964$ are excluded from selection because the wing tip causes extreme and nonlinear behavior in W_{KK} due to the exacerbated geometric differences between CFD and DLM meshes.

Table 10: Comparison of Feature Selection Algorithms for Bending Moment Response

η	***NCA***	***RRELIEFF***
0.0	0.15, 0.14, 0.94, 0.12, 0.18, 0.11, 0.68, 0.19, 0.71, 0.40, 0.16, 0.28, 0.93	0.12, 0.14, 0.11, 0.15, 0.16, 0.93, 0.48, 0.57, 0.18, 0.19, 0.78, 0.20, 0.23
0.25	0.15, 0.19, 0.36, 0.77, 0.35, 0.12	0.36, 0.15, 0.35, 0.16, 0.24, 0.45
0.50	0.93, 0.15, 0.91	0.92, 0.96, 0.15
0.75	0.93, 0.96, 0.94, 0.952, 0.92, 0.946, 0.49	0.92, 0.952, 0.51, 0.88, 0.939, 0.946, 0.93

In general the two methods identify similar areas of the wing which are significant for each response even though the order of importance may vary somewhat and the exact same strips are not always selected. The ranking of features in RRELIEFF provides less information becuase there is no clear cutoff value for importance and assuming only negative weights are insignificant leads to too many selected features. In some responses such as the root bending moment there is a clear drop off of weights which can be used to screen out positive-weighted features, but in other responses there is no clear distinction. NCA on the other hand clearly distinguishes between significant and insignificant features and thus makes selection much easier. As was mentioned, the advantages of RRELIEFF is that it can handle correlated and incomplete data, but the correlation of W_{KK} is not explicitly considered in this work and the data is complete. Thus the NCA selected features will be used going forward and this choice is supported by agreement between the two methods despite the advantages of RRELIEFF.

The selected features are heavily distributed towards the wing root and tip. The W_{KK} parameters directly impacts the aerodynamic load of a particular strip so feature selection helps determines which parts of the wing are important to the structural loads. The extreme values at the tip may skew the results and lead to those parameters having more significance, but in general lift and drag are sensitive to the behavior of vortices and circulation at the tip so it is no surprise that these areas are significant. The significance of the root and tip can also be seen in the number of selected feature for each response. For example, the 50% span bending moment has the least number of important features and none of those features are close to the monitor point.

The set of uncertainty W_{KK} parameters has reduced from 101 to 22 using NCA feature selection. This is a much more reasonable number of parameters for fitting surrogate models and should improve their accuracy for a given sample size. To verify this, Gaussian Process Regression models, also known as Kriging models, were fit

to 500 Latin Hypercube samples of the full set and reduced set of W_{KK} values with epistemic uncertainty added. Kriging will be discussed in more detail in Section 6.3.1. The models were validated using resubstitution and cross-validation with 12.5% hold-out for testing data. The loss from both resubstitution and cross-validation reduced by 98.0% when using the reduced number of parameters. The feature selection was only done on Load Case 4 because it is the critical load case in terms of the bending moment and the only one used for the flight load survey. Thus the standard deviation for W_{KK} for the other load cases will be based on errors calculated for Load Case 4.

When all four load cases are considered the number of uncertain parameters increases to 88, which again is large. The component critical load case calculated in HyperSizer indicates that Load Case 1 and Load Case 4 are critical in 85% of the components. To reduce the problem size, all W_{KK} parameters will be fixed to their mean $W_{KK,rigid}$ values for Load Case 2 and 3 and the same insignificant parameters identified with NCA will be fixed for Load Case 1 and 4. A total of 55 parameters are included in the design of experiment (10 load case parameters and the required margin input), but problem dimensions will be reduced further after construction of the Bayesian network and global sensitivity analysis.

6.2.5 Conclusion

The epistemic uncertainty related to aerodynamic fidelity in the W_{KK} empirical adjustment parameters was defined. This uncertainty represents model form error based on its intended use in NASTRAN even though W_{KK} itself is a parameter. The uncertainty is assumed to be normal with unknown mean and standard deviation. A linear relationship is assumed for both distribution parameters which is specified by a scalar quantity call the K-factor with represents the aerodynamic fidelity level.

Previous work done by Bansal and Pitt (2013) [16] on flutter prediction under

uncertainty using NASTRAN's DLM and dynamic aeroelastic analysis served as a foundation for the epistemic uncertainty definitions used here. Based on this work and feedback from subject matter experts, the proposed uncertainty definition for the W_{KK} parameters was deemed acceptable. Therefore Hypothesis 1 is accepted. Defining uncertainty is somewhat subjective, so a measurable experiment to assess this hypothesis was not constructed. Some weaknesses of the uncertainty definition exist and could be improved in future work. Specifically, for regions near the middle of the wing span the uncorrected error was less than the rigid corrected error relative to the truth data. In order to maintain a linear representation of fidelity the min and max error terms were used to define the standard deviation. The linear definition of fidelity is largely dictated by the linear assumption of the W_{KK} parameters. In future work use of the direct grid import approach in NASTRAN could alleviate these linear assumption and allow a more sophisticated, and possibly nonlinear, definition of aerodynamic fidelity.

101 uncertain parameters poses a computational burden when fitting surrogate models and degrades their accuracy. Thus two feature selection algorithms were implement to determine the significant parameters and reduce the size of the problem. Both RRELIEFF and NCA were utilized and showed general agreement for the areas of the wing which were most important to the bending moment responses based on the selected set of significant W_{KK} parameters. NCA was chosen over RRELIEFF because it can better distinguish between significant and insignificant features. Twenty parameters were selected using NCA. Comparing Kriging models with the same sample size it was determined that the smaller parameter set reduced the model loss by 98%.

The feature selection results revealed that parameters near the root and tip were more significant than those in the middle of the wing span for Load Case 4. These results are beneficial for determining which parts of the wing to focus for uncertainty

reduction and possibly for design. In general, this experiment addresses the research gap related to data-driven estimation of epistemic uncertainty which is largely missing in the literature. It also provides a procedure and insight into the effort necessary to rigorously define epistemic uncertainty. This is important for transitioning UQ from research to practice in aerospace. Though significant effort was needed in this work to estimate the required error terms, much of this can probably be avoided with more sophisticated analysis methods.

The W_{KK} parameters with epistemic uncertainty will be incorporated into the Bayesian network along with aleatory uncertainty. The next section will discuss the design and construction of the Bayesian Network. Once fully assembled it will be used to propagate of all uncertainty sources through the loads analysis process and enable uncertainty quantification for the entire system. Global sensitivity analysis can then be done to determine the impact of the various uncertainty sources.

6.3 System Uncertainty Quantification: Bayesian Network

6.3.1 Surrogate Modeling

The Bayesian network for loads analysis requires surrogate modeling because of the complex and expensive analysis methods in the M&S environment. Surrogates are fitted to sampled data from the analyses. The method of choosing the samples is important for efficiently creating accurate surrogates. Instead of full factorial design in which every possible combination of variables are used to fit the surrogate model a structured design of experiment (DoE) can be used where only a fraction of the full set is analyzed. There are numerous DoE's which are tried and true in the statistic community. Some examples are fractional factorial designs, optimal designs, Latin squares, central composite, and space filling designs [176]. A Latin Hypercube Sampling (LHS) design is used to create the DoE for Kriging surrogate models, as was done for the W_{KK} parameter feature selection (see Section 6.2.4.2).

Gaussian Process Regression models, known as Kriging models, were originally developed for geostatistics to interpolate spatial data from only a few samples. The namesake comes from the 1951 Master's thesis of Danie Krige from South Africa [78] and the theory developed by Georges Matheron in France the 1960's [93]. According to MATLAB documentation (r2016b) Gaussian process regression (GPR) models are nonparametric kernel-based probabilistic models which can be trained from data to predict responses at unobserved inputs. A GPR model explains the response by introducing latent variables from a Gaussian process (GP) for each observation, and explicit basis functions which transform the original inputs into a p-dimensional feature space. A GP is a set of random variables, such that any finite number of them have a joint Gaussian distribution. The covariance function of the latent variables captures the smoothness of the response. The covariance function is usually parameterized by a set of kernel parameters or hyperparameters [161].

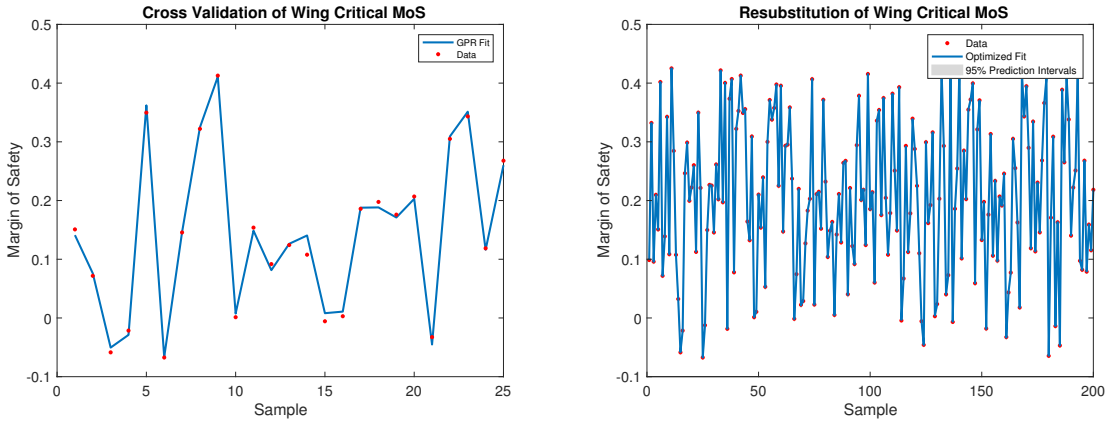

(a) Cross validation (b) Resubstitution

Figure 101: Validation of GPR models for wing critical margin of safety

200 Latin Hypercube samples were run in the M&S environment for one load cycle and used to fit Kriging surrogate models for global sensitivity analysis. The process of fitting was done in MATLAB's Statistics and Machine Learning Toolbox using a built-in Bayesian optimization to determine the optimal hyperparameters of the Kriging model for each response. Several methods are available to evaluate the quality of the fit including confidence intervals, cross validation loss and resubstitution loss (also called regression error). The cross validation and resubstitution loss are visualized in Figure 101.

Figure 101 shows the optimized GPR fits match pretty well to the data. For cross validation was done with a 12.5% training set. The Five K-fold loss is 9.34025e-05 and the resubstitution loss is 1.71535e-07. Kriging models were fit for the integrated bending moment at four span-wise locations and for the wing critical margin of safety. The margin of safety response is treated as the system response.

6.3.2 Experiment 1: Determine Impact of Uncertainty on Major Rework

The global sensitivity analysis method discussed in Section 3.5.2 is used to evaluate the impact of aleatory and epistemic uncertainty on the system. For GSA the system

response is the wing critical margin safety which is the minimum margin of safety of all the wing components. Sensitivity analysis was also done with respect to the bending moment responses because they will be used for calibration data for Bayesian inference on the W_{KK} parameters. The purpose of GSA is not only to identify significant uncertain parameters, but also to fix insignificant ones. Even though feature selection narrowed down the initial set of W_{KK} parameters from 404 (101 for each load case) to 44, the total amount of input variables for the DoE is large. Using GSA we can prioritize both the aleatory and epistemic uncertainty sources and reduce the require DoE sample size for the final surrogate models.

The epistemic uncertainty was defined in previous sections, but the aleatory uncertainty has yet to be defined. Normal distributions were assumed for all variables and the mean values are the nominal values used in the four load cases. The standard deviations for Mach number and altitude were assumed to be equal to 10% of the maximum nominal value. The load factor and fuel density standard deviations were determined from preliminary sensitivity studies. The aleatory uncertainty definitions are shown in Table 11.

Table 11: Aleatory Uncertainty Definition

Parameter	μ	σ
LC1 Mach	0.85	0.09
LC2 Mach	0.90	0.09
LC3 Mach	0.60	0.09
LC4 Mach	0.89	0.09
LC1 Altitude	43100 ft	4310 ft
LC2 Altitude	23000 ft	4310 ft
LC3 Altitude	20000 ft	4310 ft
LC4 Altitude	43100 ft	4310 ft
Load Factor	2.5G	0.01G
Fuel Density	100%	1%

Using the Equations 7 and 8 the sensitivities were calculated and are presented in Table 12, sorted by ascending total effects. As discussed, the total effects are better measures for fixing parameters than the first order, so they are prioritized. The W_{KK} parameters include Load Case 1 and Load Case 4 and are labeled as such. Also the last digit in the parameter name refers to the strip number starting from 1 at the root and ending at 101 at the tip. All parameters not listed are deemed insignificant for that response. To help interpret these results, the properties given by Saltelli et al [135] are repeated here:

- Whatever the strength of the interactions in the model, S_i indicates by how much one could reduce, on average, the output variance if X_i could be fixed; hence, it is a measure of main effect.
- By definition, S_{T_i} is greater than S_i, or equal to S_i in the case that X_i is

not involved in any interaction with other input factors. The difference $S_{T_i} - S_i$ is a measure of how much X_i is involved in interactions with any other input factor.

- $S_{T_i} = 0$ implies that X_i is noninfluential and can be fixed anywhere in its distribution without affecting the variance of the output.
- The sum of all S_i is equal to 1 for additive models and less than 1 for nonadditive models. The difference $1 - \Sigma_i S_i$ is an indicator of the presence of interactions in the model.
- The sum of all S_{T_i} is always greater than 1. It is equal to 1 if the model is perfectly additive.

Table 12: Wing Critical Margin of Safety Sensitivity Analysis

Input	***Total Effects***	***First Order***
W_{KK} LC1 64	0.4040	0.4023
W_{KK} LC4 14	0.1396	0.1396
W_{KK} LC4 50	0.1224	0.1226
W_{KK} LC4 3	0.0864	0.0860
W_{KK} LC1 2	0.0859	0.0862
W_{KK} LC1 88	0.0729	0.0733
LC2 23000 ft	0.0371	0.0361
2.5G Load Factor	0.0242	0.0235
W_{KK} LC1 3	0.0105	0.0099

The magnitude of the indices can be interpreted as the variables contribution to the response variance in percentages. For example, the W_{KK} parameter at the 64^{th}

strip for Load Case 1 contributes to 40.6% of the total variance in the wing critical margin of safety. All total effect indices are greater than their respective first order indicating that all listed variables have interactions. Only using the parameters in Table 12 for uncertainty quantification may result in too small a model to accurately predict the bending moment. So the sensitivity indices were calculated for the four bending moment responses and a minimum variance of 3% was used as cut-off for significance.

Table 13: Final Uncertain Parameters

Parameter	***Type***	***Parameter***	***Type***
LC1 Mach 0.85	Aleatory	W_{KK} *LC1 1*	Epistemic
LC2 Mach 0.90	Aleatory	W_{KK} *LC1 2*	Epistemic
LC3 Mach 0.60	Aleatory	W_{KK} *LC1 3*	Epistemic
LC4 Mach 0.89	Aleatory	W_{KK} *LC1 4*	Epistemic
LC1 43100 ft	Aleatory	W_{KK} *LC1 5*	Epistemic
LC2 23000 ft	Aleatory	W_{KK} *LC1 6*	Epistemic
LC3 20000 ft	Aleatory	W_{KK} *LC1 7*	Epistemic
LC4 43100 ft	Aleatory	W_{KK} *LC1 14*	Epistemic
2.5G Load Factor	Aleatory	W_{KK} *LC1 19*	Epistemic
Fuel Density	Aleatory	W_{KK} *LC1 20*	Epistemic
		W_{KK} *LC1 50*	Epistemic
		W_{KK} *LC1 64*	Epistemic
		W_{KK} *LC1 88*	Epistemic
		W_{KK} *LC1 89*	Epistemic
		W_{KK} *LC1 91*	Epistemic
		W_{KK} *LC1 93*	Epistemic
		W_{KK} *LC1 94*	Epistemic
		W_{KK} *LC1 95*	Epistemic
		W_{KK} *LC4 1*	Epistemic
		W_{KK} *LC4 3*	Epistemic
		W_{KK} *LC4 14*	Epistemic
		W_{KK} *LC1 50*	Epistemic

All parameters not listed in Table 13 are fixed. Fixing parameters is necessary

to make this problem computationally feasible with the available time and resources. But what impact does that have on uncertainty in the responses? The indices from global sensitivity analysis allow us to estimate the loss in accuracy by calculating the retained variance. The retained variance is shown in Table 14. The values listed under *All* are the retained variance considering both aleatory and epistemic parameters while *Epistemic* considers only epistemic parameters. Comparing the two indicates the impact of the epistemic uncertainty on the system. Given that only epistemic uncertainty is reducible, these results give an indication of the potential uncertainty reduction that can be achieved with the rework decision framework.

Table 14: Retained Variance after Fixing Insignificant Variables

Response	***All***	***Epistemic***
Wing Critical MoS	98.6%	92.5%
Root LC4 Bending Moment	99.1%	66.0 %
25% Span LC4 Bending Moment	86.5%	69.1 %
50% Span LC4 Bending Moment	99.2%	47.8 %
75% Span LC4 Bending Moment	97.1 %	58.2 %

6.3.3 Bayesian Network for Loads Analysis

After global sensitivity analysis and fixing insignificant parameters the Bayesian network for loads analysis can be constructed from the final Kriging surrogate models after four load cycles in the M&S environment. The network is visualized in Figure 102. There are 126 nodes in the network which would require a large number of surrogates. A surrogate model of the system response can be made directly instead of modeling each component's margin of safety individually. With this approximation the Bayesian network requires only 5 surrogate models which are a function of 31

parameters and the required margin design variable. As indicated in the Bayesian network, the K-factor and load margin design variables are captured through the W_{KK} parameters and are not treated as separate inputs in the DoE or surrogate models.

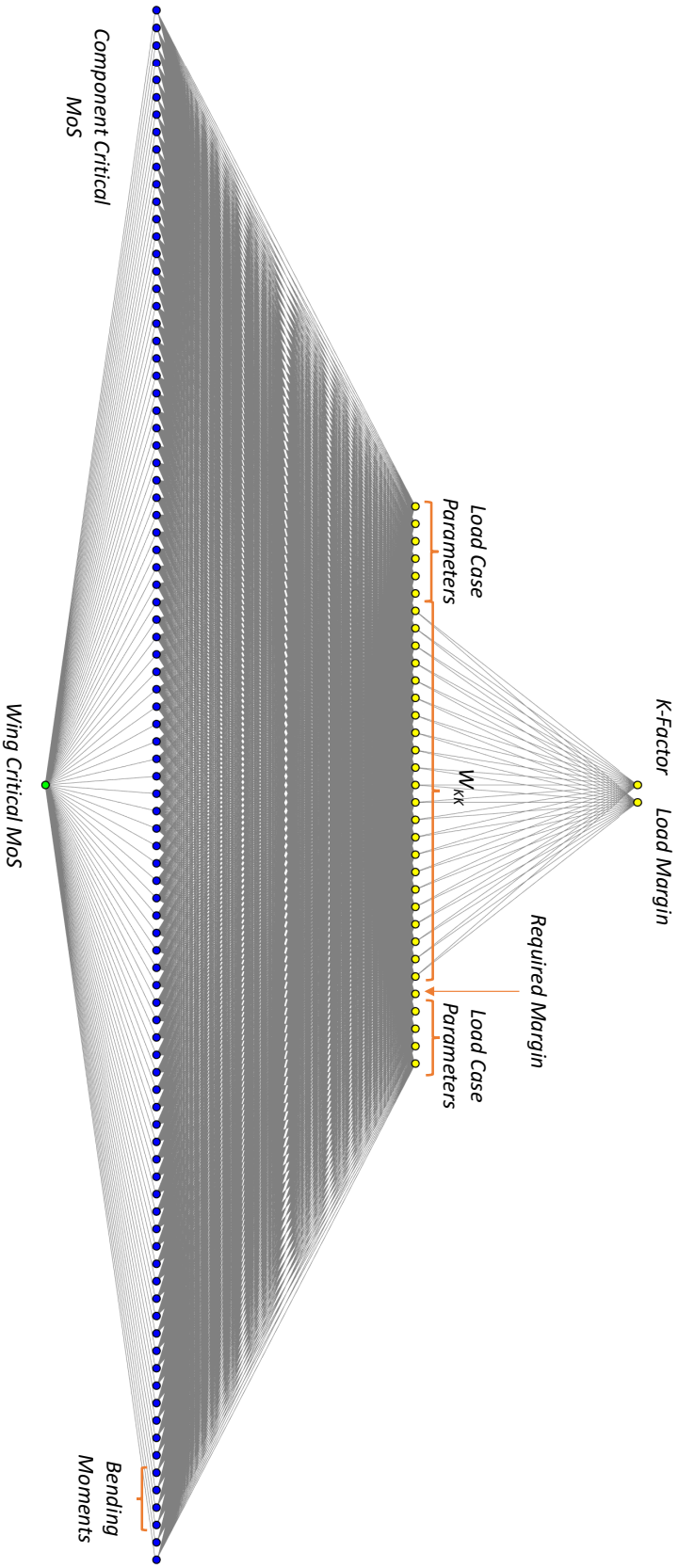

Figure 102: Bayesian network for loads analysis, circles represent nodes and grey lines show conditional dependence

6.3.4 Conclusion

The design of experiments and surrogate modeling methods for performing global sensitivity analysis and constructing the Bayesian network for loads analysis were discussed. Specifically, a 200 Latin Hyercube Sampling design was used for Kriging models for the wing critical margin of safety and bending moment responses. Results for global sensitivity analysis were presented. Insignificant uncertain parameters were identified and fixed with minimal losses to the system response variance. In the end 31 out of 54 parameters were retained, including all of the aleatory load case parameters. The impact of the W_{KK} parameters and epistemic uncertainty on the various responses was estimated.

Based on the findings, the epistemic uncertainty is significant to the wing critical margin of safety relative to the aleatory uncertainty. Therefore, Hypothesis 2 is accepted. But these results are highly dependent on the uncertainty definitions and their assumptions. Therefore this hypothesis can only be accepted for this problem and not generalized. A validated estimate of the aleatory uncertainty for the demonstration model could be done in future work to make a general claim about the significance of this epistemic uncertainty.

Nevertheless this experiment addresses on of the research gaps by taking steps towards finding a correlation between aerodynamic fidelity and design rework. The Bayesian network allows uncertainty propagation which is necessary for sensitivity analysis. The Bayesian network presented here serves as a unique approach to uncertainty quantification in loads analysis and is a contribution in itself.

With finalized set of parameters, the final five surrogate models are fitted and the Bayesian network for loads analysis constructed. The completed network will be used in the overall framework after the uncertainty management experiments which are discussed next.

6.4 Uncertainty Management: Resource Allocation Optimization

The resource allocation optimization problem for uncertainty management was introduced in the Proposed Approach, Chapter 4. In the following section the proposed optimization method is applied to a simple analytical problem and compared against other approaches. Afterwards the optimization will be applied to the modeling and simulation environment to carry out Experiments 3 and 4.

6.4.1 Experiment 2a: Multiobjective Resource Allocation

To help evaluate the performance of the proposed method, a simple problem was found in the literature based on the work from Sankararaman, et al. (2014) [139] which was used to formulate the test resource allocation optimization algorithm. The original problem is a mathematical example which is intended for illustrative purposes only. The corresponding Bayesian network is show in Figure 8. The problem consists of four independent quantities and three dependent. The numerical details are described in Table 15. Two types of experiment tests are simulated to update the θ parameters and reduce the uncertainty in the system response. The objective of the original problem is to determine the combination of both tests which minimizes the variance in Z.

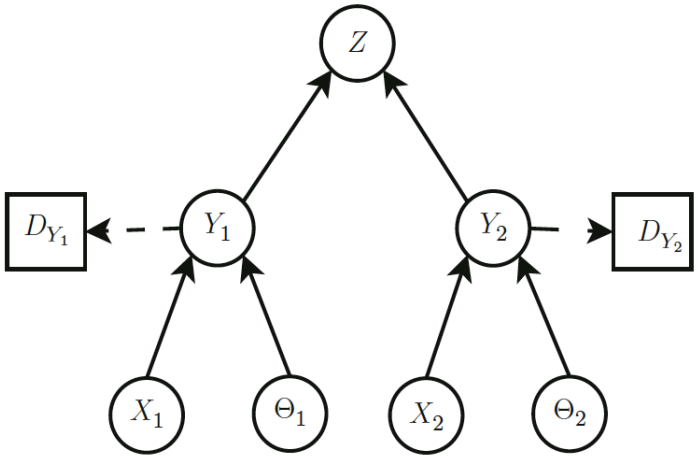

Figure 103: Bayesian network for illustrative problem [139]

Table 15: Numerical details of illustrative problem

Quantity	***Type***	***Description***
X_1 (input)	Independent	N(100,5)
Θ_1 (parameter)	Independent	N(50,10)
X_2 (input)	Independent	N(10,1)
Θ_2 (parameter)	Independent	N(15,4)
Y_1	Dependent	Model: $y_1 = x_1 + \theta_1$
Y_2	Dependent	Model: $y_2 = x_2 + \theta_2$
Z	System-level Response	Model: $z = y_1 - y_2$
Quantity to Measure	***Cost***	***No. of Tests***
Y_1	10	N_1
Y_2	5	N_2

The original problem has been modified to better represent the optimization problem which will be applied to the full modeling and simulation environment where both the mean and variance of the system response are included in the objective function.

Therefore the objective function for the illustrative problem is changed to a multiobjective one where the mean and variance of Z are minimized. For the multiobjective problem it is also necessary to include X_1 and X_2 into the design space, whereas before the design space only consisted of the number of each test to conduct. The the new optimization problem is posed as:

$$
\begin{aligned}
&\textit{Minimize}: && f(\ E[\mathrm{Var}(Z)],\ E[Z]\ ) \\
&\textit{s.t.}: && \textstyle\sum(C_i N_i) \leq 50, \\
& && 0 \leq X_1 \leq 100, \\
& && 0 \leq X_2 \leq 100
\end{aligned}
$$

where $E[\ ]$ is the expected value, $Var()$ is the variance, C_i is the cost of the ith test type and N_i is the number of ith test conducted.

The test resource allocation proposed by Sankararaman, et al. is intended to improve the design process by determining the combination of experimental tests which maximize the reduction in uncertainty. Therefore the minimization of the system response mean value can be thought of as the design problem which would occur after the optimal tests have been determined. This is referred to as a two-step procedure, where the first step minimizes the response variance and the second step optimizes for the mean response. This optimiation approach is suggested by Wu, et al (2009) and known as a location-dispersion modeling [176]. Wu, et al suggests the location (mean) be optimized first followed by the dispersion for minimization problems. In this problem it is assumed both the mean and variance of Z will be minimized. Therefore the "Two-Step" proposed optimization approach follows this suggestion. We can thus evaluate the performance of the proposed method against other methods using this illustrative problem modified for design purposes.

Three strategies for solving this problem were chosen to evaluate against the proposed two-step optimization. The first is a simple deterministic optimization which does not account for uncertainty and therefore does not employ any variance reduction. The second is a nondeterministic optimization which accounts for uncertainty in the optimization search but does not actively reduce the variance. The third method is that of Sankararaman (2014) where the optimal tests are first determined and then Z is minimized using the updated parameters found using the optimal test data. This is essentially a two-step approach with the dispersion optimized first, then the location.

The results are summarized in Table 16. The deterministic optimization utilizes a nonlinear constrained gradient-based optimization algorithm in MATLAB, *fmincon*. All other methods are nondeterministic in that they involve random inputs and parameters. Thus the objective function is non-smooth and therefore gradient-based methods like *fmincon* can easily get stuck in a local minimum. Thus the nondeterministic methods use a direct search algorithm in MATLAB, *patternsearch*.

Table 16: Results of illustrative problem

Problem Type	X_1	X_2	N_1	N_2	$E[Z]$	$E[Var(Z)]$
Deterministic	0.0	100.0	0	0	-65.00	142.00
Nondeterministic	0.0	100.0	0	0	-64.97	115.96
Sankararaman	0.0	100.0	2	6	-61.87	0.67
Two-Step	0.01	100.0	2	6	-64.81	0.71

The final solution for all the methods have similar mean responses but the variances are very different. A deterministic optimization by definition has no variance, so the reported variance is based on the propagated uncertainty at the initial X_1 and

X_2 and with no reduction efforts. The deterministic optimization search involves only the mean values of the inputs and parameters and the objective function is simply Z.

The nondeterministic optimization objective function is $E[Z]$ so there is no mechanism to directly reduce the variance even though the uncertainty in the inputs and parameters are considered. The probability distributions of X_1 and X_2 attribute to the uncertainty in Z so the optimal inputs will impact the variance. This can be seen in the variance reduction of 18% compared to deterministic optimization. This approach is akin to robust optimization techniques where the variance in a system is reduced by optimizing control factors instead of attempting to adjust noise factors directly which can be expensive [176].

The results between the Sankararaman and Two-Step methods are similar in terms of mean and variance, with the former having slightly better results for both objectives. As was mentioned, the way in which the Sankararaman resource allocation optimization was implemented into the design problem essentially makes it a two-step location dispersion model but in the reverse order [176]. Both methods utilize multiple stages to converge the solution as recommended by Sankararaman et al. [140]. Another important distinction in the proposed method is that within a given stage both the location and dispersion are minimized. In the Sankararaman method the location is minimized after all stages are complete and the dispersion converged. Although the final objective values are similar, there are computational advantages for the proposed method due to the aforementioned distinctions between the two methods.

The results of each stage of the optimization demonstrate how the mean and variance converge to the final solution and is shown in Figure 104. In the figure, Stage 0 refers to the initial conditions prior to any optimization. Therefore the mean response is the value of Z with the mean values of all inputs and parameters. In the Sankararaman method the mean fluctuates about the initial value but does not

reduce significantly. This shows that the number of tests does not have a significant impact on the mean of the system response. The sixth stage refers to the optimization of the location model to minimize $E[Z]$. In the dispersion model the Sankararaman method reduces the variance throughout the five stages by adjusting the number of tests. In the final stage only X_1 and X_2 are adjusted, but this still results in a further reduction of the variance.

It is clear that the proposed method converges at an earlier stage which can result in significant computational savings. This is primarily because all design variables are optimized within each stage so both the mean and variance reduce faster and converge by the second stage. Because of the integrated optimization approach, there is no need for a separate sixth stage to optimize X_1 and X_2 as in the Sankararaman method. Computational savings from less stages must be weighed against potential increases in cost from repeating the two-step optimization after each stage for a more complex problem.

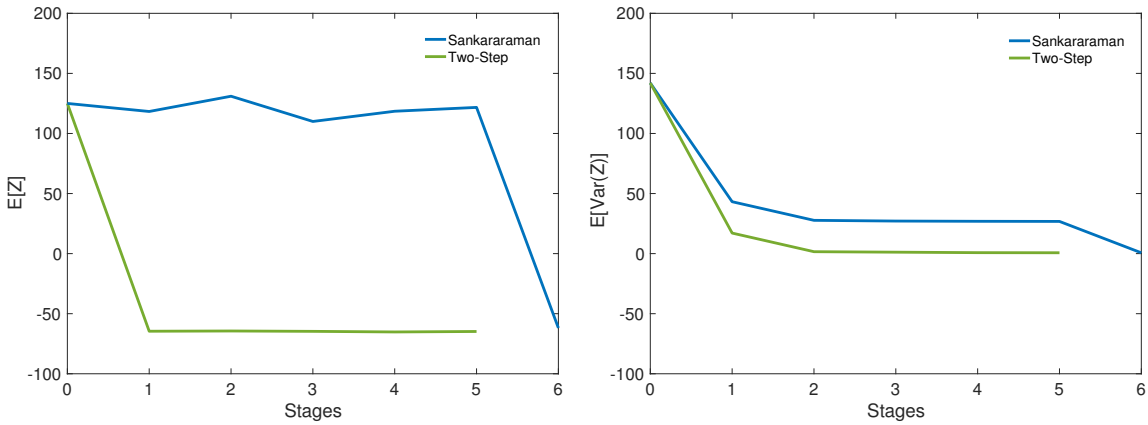

(a) Location Model, $E[Z]$ (b) Dispersion Model, $E[Var(Z)]$

Figure 104: Comparison of resource allocation optimization methods for illustrative problem.

The results from this simple problem illustrate the benefits of using Bayesian

methods in a resource allocation framework to reduce uncertainty compared to deterministic and robust optimization methods. The original method suggested by Sankararaman (2014) results in a 77.1% variance reduction by finding the optimal number of tests (based on published findings). Adjusting X_1 and X_2 further reduced the variance by 22.4% in the modified design problem. Similar reductions were seen in the proposed Two-Step optimization method but with significantly reduced computational costs in terms of required stages to converge the solution. All Bayesian-based optimization methods require significant computational expense due to the reverse and forward problems, so any computational savings make this approach much more attractive. Regardless, the additional expense can be justified by the reduction in uncertainty as shown in this problem.

This illustrative problem also reveals the importance of determining the variables which are location factors, dispersion factors and adjustment factors [176]. Location and dispersion factors significantly impact the mean and variance of the system-level response respectively. An adjustment factor is a location factor which does not significantly impact the dispersion model. In this problem X_1 and X_2 are location and dispersion factors and N_1 and N_2 are only dispersion factors so there are no adjustment factors. The absence of adjustment factors can make it more difficult to minimize both the mean and variance simultaneously because some factors will influence both objectives. This was not an important issue for the illustrative problem because there was no need to compromise either objective, but it may become relevant in full modeling and simulation environment and impact the optimization strategy and results.

6.4.2 Experiment 2b: Resource Allocation with Feedback Decoupling

Loads analysis is a highly coupled process and includes multiple feedback loops. In the M&S environment there is an inner feedback-coupling between aerodynamics and structures which is solved internally in the NASTRAN aeroelastic analysis. There is also a feedback loop between NASTRAN and HyperSizer which represents the load cycles. The computational expense of the resource allocation was commented on in the previous experiment, primarily due to Bayesian inference using Markov Chain Monte Carlo. Additional computational costs come with running the load cycles in the M&S environment to create the data to fit the required surrogate models. Breaking the feedback loop and decoupling the problem would require less iterations between NASTRAN and HyperSizer and decrease the overall expensive of the rework decision framework.

Approaches to decouple multidiscipline problems have long existed in the literature [154][22]. One such approach presented by Liang (2016) [85] was explored because it is derived from the LAMDA method developed by S. Sankararaman [137], who also extended the resource allocation methodology referenced in this work. The resource allocation methodology has been applied to feedback-coupled problems in the literature. Yet, to the authors knowledge, both methods have yet to be applied simultaneously to the same problem in the literature, but will done so in this experiment.

A detailed description of the decoupling method can be found in [83] and only a brief summary will be provided here by means of a simple example with two analyses, a design variable x and two coupling variables u_{12} and u_{21} between the analyses. The coupled and decoupled version of the problem along with the Bayesian network used for enforcing interdisciplinary compatibility are shown in Figure 105. For the original coupled problem, the coupling variables are passed between the analyses to calculate the responses A_1, and A_2 which are also dependent on x. If the coupling

variables converge then compatibility is enforce, i.e. $u_{21} = U_{21}$ and the iterations cease. Therefore we can define an error term $\epsilon_{21} = U_{21} - u_{21}$ and compatibility is enforced if $\epsilon_{21} = 0$.

The Bayesian inference problem can be posed to enforce this compatibility. The posterior distribution of $u_2 1$ could be calculated for some given data, D, based on Equation 4:

$$f''(u_{21}|D) \propto f(D|u_{21}) f'(u_{21}) \tag{40}$$

where f is the probability distribution function, f' is the prior distribution and f'' is the posterior distribution. We can assume the prior distribution is an uninformative uniform distribution and the posterior can be calculated given the compatibility condition:

$$f''(u_{21}|\epsilon_{21} = 0) \propto L(u_{21}) \tag{41}$$

where L is the likelihood function. The Bayesian network is used to carry out the inverse problem and update the distribution of $u_2 1$ to that which enforces compatibility, then carry out the forward problem to determine the system responses. With interdisciplinary compatibility satisfied the problem is decoupled and the responses from the Bayesian network represent the converged solution.

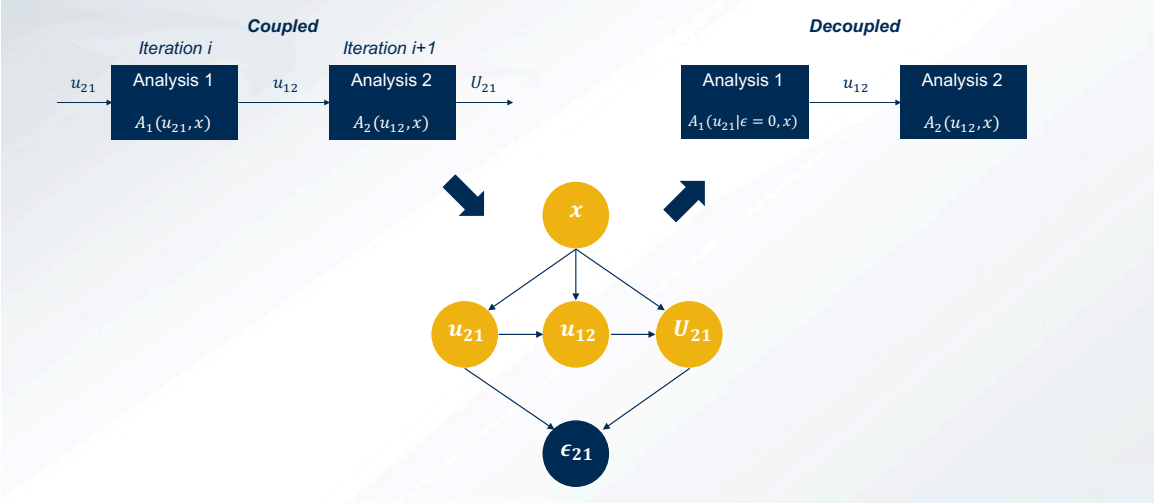

Figure 105: Example of feedback decoupling approach

An illustrative example is given here to demonstrate the use of resource allocation for a decoupled feedback problem. The problem is modified from the math problem presented by Liang et al (2016) [85]. It features two coupled analyses with coupling variables $u_{12}, v_{12}, u_{21}, v_{21}$. The subsystem responses g_1, g_2 are inputs to the system-level response $f = g_1 - g_2$. The problem is shown in Figure 106 and the robustness-based design optimization (RBDO) problem formulation is shown in Equation 6.4.2.

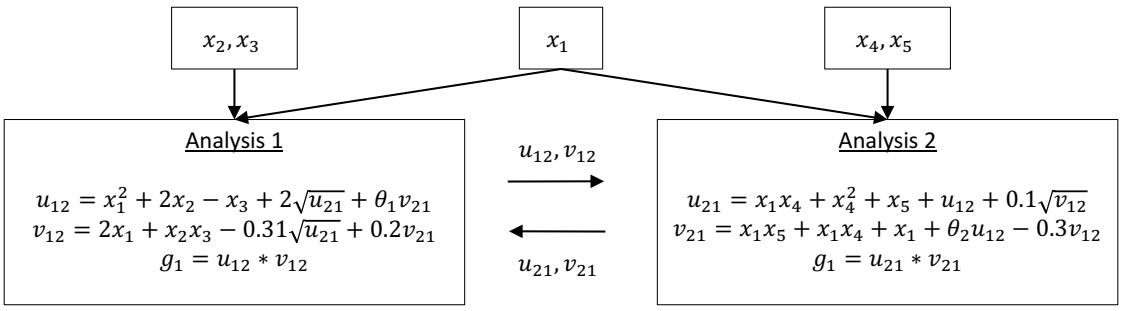

Figure 106: Illustrative problem for resource allocation with feedback coupling

$$
\begin{aligned}
&\underset{\mu_{x_i}}{min}\ \mu_f \\
&P(g_1 < 24.6) \geq 0.9,\ P(g_2 < 48.2) \geq 0.9 \\
&s.t. \qquad 0.8 \leq \mu_{x_i} \leq 1.2 \\
&P(x_i \leq 0.8) \leq 0.9,\ P(x_i \geq 1.2) \leq 0.9 \qquad i = 1, ..., 5 \\
&U_{12}(\boldsymbol{x}, u_{21}, v_{21}) - u_{12} = U_{21}(\boldsymbol{x}, u_{12}, v_{12}) - u_{21} = 0 \\
&V_{12}(\boldsymbol{x}, v_{21}, v_{21}) - u_{12} = V_{21}(\boldsymbol{x}, u_{12}, v_{12}) - v_{21} = 0
\end{aligned} \tag{42}
$$

The bounds of the design variables x_1 to x_5 are [0.82, 1.2] with an uncertainty defined by $N \sim (0, 0.02)$. To emulate the loads analysis problem the distribution type is known but the parameters are unknown for $\boldsymbol{\theta}$ and are specified based on different fidelity levels. Three levels are used in this problem and the epistemic uncertainty is assumed normal. The mean and variance of the uncertain parameters are defined in Table 17. The coefficients in the original problem are the "true" values of the parameters and the definitions for the mean and variance are derived from it.

Table 17: Uncertain Parameters for Illustrative Problem

Variable	***Level 1***	***Level 2***	***Level 3***	***True***
θ_1	$\mu = -0.11$, $\sigma = 0.0737$	$\mu = -0.165$, $\sigma = 0.03685$	$\mu = -0.198$, $\sigma = 0.018425$	-0.22
θ_2	$\mu = 0.075$, $\sigma = 0.05025$	$\mu = 0.1125$, $\sigma = 0.025125$	$\mu = 0.135$, $\sigma = 0.0125625$	0.15

The resource allocation methodology is applied first to update the parameters under a fixed budget. Then the RBDO decoupled problem is solved with compatibility of the coupling variables enforced. To solve the resource allocation optimization five stages are used with 10 budget each and a total budget of 50. The cost structure is intended to emulate the increased costs associated with higher fidelity analysis.

In addition to the fidelity level, a second variable is introduced; the number of test samples for updating. Each Level 1 sample has a cost of 2.5, 5 for Level 2 and 10 for Level 3. The final updated parameters are then used in the RBDO problem to minimize the mean of the system response. To assess the proposed method, RBDO was done with and without resource allocation. For the latter, the Level 1 values of $\boldsymbol{\theta}$ are assumed and no updating is performed. *patternsearch*, a global optimization algorithm in MATLAB was used to solve the integer problem. Note, *patternsearch* is not specifically intended for integer problems, but can solve them by modifying the mesh tolerance and scaling in the optimization options. The resource allocation results are shown in Figure 107 and the RBDO results are summarized in Table 18.

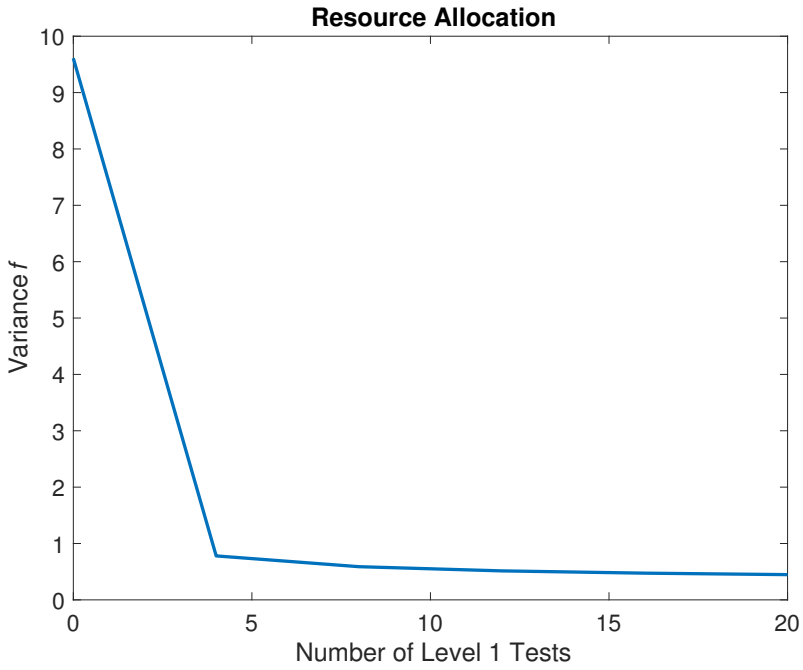

Figure 107: Results of resource allocation optimization

The optimal fidelity level and number of samples were consistently Level 1 and four samples respectively for each stage of the optimization. Thus the optimizer chose to exhaust the budget with maximum amount of low fidelity analyses. This means it was better able to reduce the variance by utilizing more data from the lowest fidelity

Table 18: Results for Illustrative Problem

	Variable	***No θ Update***	***θ Update***
Design Variables	x_1	1.0312	1.1230
	x_2	0.8281	0.8262
	x_3	0.8281	0.8262
	x_4	1.1250	1.1719
	x_5	1.1719	1.1738
Objective	μ_f	-21.09	-23.78
	σ_f	27.90	1.28
Constraints	$P(g_1 < 24.6)$	1.00	1.00
	$P(g_2 < 48.2)$	0.91	0.90
Compatibility Error	U_{21}	0.00%	-0.00%
	V_{21}	0.01%	-0.00%

than running fewer higher fidelity analyses. The purpose of including both analysis variables into the optimization was to see if this very situation would occur. Typically we assume higher fidelity is always better for uncertainty reduction, but when our resources are fixed uncertainty management principals may lead to different results. Of course, the simplistic definition of epistemic uncertainty and cost structure for this problem may lead to such results. Figure 107 shows similar results to the first illustrative problem where there is a large initial reduction in variance after the first stage and subsequently small reductions there afterwards to exhaust the budget.

The benefits of the parameter update can be seen with the 95.4% reduction with variance of the system response. The objective function improves as well with uncertainty reduction. In addition the subsystem response constraints and compatibility conditions are all satisfied. The published optimal system response using the true parameter values, i.e. no parameter uncertainty, is -26.60. Thus the error due to

epistemic uncertainty is 20.7% without updates and 10.6% with it. These errors are solely based on the prior probabilities of uncertainty in $\boldsymbol{\theta}$ but their relative value is important. The error in the system response is halved by using resource allocation to manage the uncertainty.

Finally it should be noted that the resource allocation and compatibility methods were decoupled. Thus $\boldsymbol{\theta}$ is updated after running the analysis for two iterations and without enforcing compatibility. The integration of both the parameter update and compatibility enforcement may lead to different, more accurate results. Additionally only the single objective function of variance in the system response was used for resource allocation, the multiobjective problem will be used in upcoming experiments. This experiment shows the resource allocation can be used in conjunction with decoupling, but the problem is not entirely represented of the loads analysis problem. In the following experiment the decoupling approach is tested on a math problem which is representative of the loads analysis problem.

6.4.3 Experiment 2c: Viability of Feedback Decoupling in Loads Analysis

The outer feedback-coupling between the structural design in HyperSizer and NASTRAN has been discussed. Changes in the structural design due to changing loads also changes the stiffness in the aeroelastic analysis. The stiffness impacts the deformation and in turn the aerodynamic loads, and so on. The coupling relationship is depicted in Figure 108. The sub-optimization of each component presents unique challenges to the normal iterative problem presented in the previous experiment. In this case, the coupling variables do not change solely due to the iterations between the analyses, they are also impact by the sup-optimization if a component is redesigned due to the critical margin of safety being less than the required margin. The component dimensions determined by the optimizer will influence the stiffness

coupling variables. This calls to question whether the previously discussed method for decoupling can enforce compatibility without substantial error.

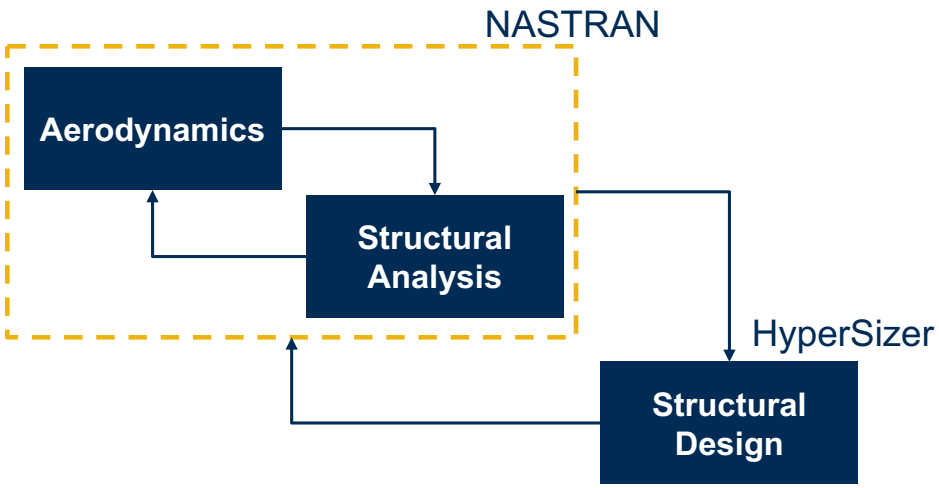

Figure 108: Feedback coupling schematic with inner and outer loops

To test the viability, the example problem from the previous experiment was modified to include a sub-optimization step on two design variables which occurs within each iteration if a constraint is violated. All other variable and parameters are the same. The sub-optimization is posed as the following:

$$\begin{aligned} \min_{x} \; & f = 1 - 10x_4^2 - x_5^2 \\ s.t. \quad & g_2 \geq c_2 \\ U_{12}(\boldsymbol{x}, u_{21}, v_{21}) - u_{12} &= U_{21}(\boldsymbol{x}, u_{12}, v_{12}) - u_{21} = 0 \\ V_{12}(\boldsymbol{x}, v_{21}, v_{21}) - u_{12} &= V_{21}(\boldsymbol{x}, u_{12}, v_{12}) - v_{21} = 0 \end{aligned} \tag{43}$$

where c_2 is a constant value included in the system optimization which is analogous to the required margin in the loads analysis problem. The sub-optimization is done in *Analysis 2* only, similar to the sub-optimization in the structures discipline. A Latin Hypercube design with 200 samples was constructed for the fidelity level of each analysis and the constraint minimum value c_2. The sample size is based on the

similar problem presented in [85]. The optimal solutions from Experiment 2b are used to fix the other design parameters, namely: $x_1 = 1.1230$, $x_2 = 0.8262$ and $x_3 = 0.8262$. In each sample the sub-optimization is completed and all coupling variable responses were recorded. Using this data Kriging surrogate models were constructed for the coupling variables, which include the effect of the optimized x_4 and x_5 variables. The same definitions for uncertain parameters θ shown in Table 17 are used.

Liang et al, states "...the training samples for the [Bayesian network] surrogate model only require a few iterations of the feedback-coupled analysis" [85]. The maximum number of iterations was varied to assess the error of decoupling compared to an iterative approach which includes the sub-optimization. The iterative approach is Monte-Carlo sampling outside of fixed-point iterations (SOFPI) as was done in Liang et al. To establish a baseline, SOFPI was run until the coupling variables converged and required twelve iterations and the final results are viewed as the "true" values. The results for the u_{12} coupling variable are shown in Figure 109.

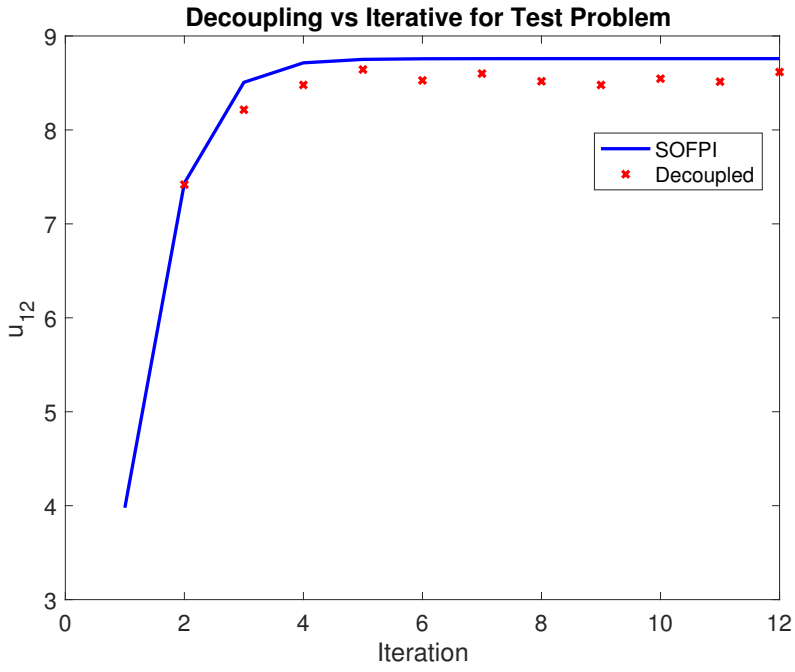

Figure 109: Results of u_{12} coupling variable for decoupling in test problem

where each of the decoupled points refer to the value of u_{12} after building the the Bayesian network with training data from the corresponding number of iterations and enforcing compatibility. The results indicate some error exists which theoretically should converge to the same as the iterative approach but seems to fluctuate around a relatively constant error. Similar results occurred for the other coupling variables. The "compatibility error" was also calculated during this experiment. For example, for u_{21} the compatibility error is equal to ϵ_{21}/U_{21}, where U_{21} is the final value after compatibility is enforced. Thus it was expected that the compatibility error would decrease with the number of iterations. The error for $u_2 1$ was fairly consistent around 9-10%, but fluctuated for $v_2 1$ and ranged from 1-30%.

Even though the errors in the coupling variables compared to the iterative approach are relatively small after three iterations, the inconsistency in the compatibility errors raise concerns. The simple test problems used in these experiments make it unclear how these errors will scale in the actual loads analysis. Therefore the LAMDA-based decoupling approach explored here will not be utilized in the final experiments. This decoupling approach will need to be explored further and on a more realistic problem before it can be confidently applied to loads analysis. The main concern is the ability to enforce compatibility with the sub-optimization which also influences the coupling variables in addition to the feedback effect. In the next section the insights gained from these three sub-experiments will be used to pose the final optimization problem utilized by the rework decision framework.

6.4.4 Objective Function for Loads Analysis

Three sub-experiments were conducted on a test problem to look at different aspects of the resource allocation methodology and how it could be implemented for loads analysis. The latter two experiments were focused on a potential method to

decouple one of the feedback loops and reduce the computational cost of constructing the Bayesian network for loads analysis. The results of the test problem indicated decoupling based on the LAMDA approach is suitable for normal iterative problems, but remains to be seen if it can be applied to loads analysis where sub-optimization occurs within the feedback loop. Nevertheless insight was drawn from all three sub-experiments to better formulate the resource allocation optimization problem for loads analysis, which is discussed in this section.

The need for a multiobjective optimization was presented in the motivation, and its implementation within the context of resource allocation was examined in Experiment 2a. Section 6.3 introduced the wing critical margin of safety as the system response, so the multiobjective function is dependent on its mean and variance. Therefore the mean margin of safety should be maximized and the variance should be minimized. There are two common approaches to multiobjective optimization; pose the multiobjective function as a single objective or use an algorithm specifically for multiobjective problems. Within the context of MATLAB (r2016b) both are possible with the various functions available in the Optimization Toolbox and Global Optimization Toolbox. The choice of optimizer is dependent on the problem, which will be discussed in more detail.

The inclusion of uncertainty in a probabilistic formulation dictates that the problem is nondeterministic. As has been discussed, this lends itself to non-gradient based methods. This significantly narrows the pool of available algorithms in the aforementioned toolboxes and focuses primarily on the Global Optimization Toolbox. The input variables in this optimization are the K-factor, load margin and structural required margin. The K-factor represents aerodynamic fidelity and specifically model form error. In the M&S environment the fidelity methods are separate analysis methods, so the K-factor variable is discrete. On the contrary the load margin and required margin are continuous variables. This is known as a *mixed integer*

problem [161]. Only one algorithm is available for global mixed integer optimization, the genetic algorithm (GA).

The concepts behind GA's were discussed in Section 3.5. The Global Optimization Toolbox has a single and multi-objective version of GA, but unfortunately the multiobjective version does not support mixed integer problems. A typical approach to formulating a multiobjective function as a single objective is to use a weighted sum [63]. The relative weights imply the users priority of the objectives. If the weights are equal, the optimizer should attempt to minimize each objective equally, therefore the terms in the weighted sum should be normalized so they are all of equal magnitude. Solutions to the single objective are Pareto optimum solutions to the multiobjective function. A Pareto optimum is an optimum point in the design space where no better point can be found to improve any of the individual objectives without causing any of the other objectives to be worse off [63].

The multiobjective optimization function used for loads analysis is shown in Equation 44.

$$\min_{x} \; f = W_{\sigma}\left(\frac{\sigma_R^2}{\sigma_{K=0}^2}\right) - W_{\mu}\left(\frac{\mu_{Current\ \ Approach}}{\mu_R}\right) \tag{44}$$

where f is the total objective function, R is the wing critical margin of safety, W are the individual objective weights and μ and σ^2 are the mean and variance of the wing critical margin of safety. $\sigma_{K=0}^2$ refers to the variance in the wing critical margin of safety for the lowest aerodynamic fidelity level (uncorrected) and is used as a normalizing constant to scale the objective function. Similarly $\mu_{Current\ \ Approach}$ is also a normalizing constant and is the mean wing critical margin of safety for the current approach. The "current approach" refers to deterministic loads analysis assuming K-factor of 0.25, zero load margin and required margin = 0. Analysis of the current approach will be used to evaluate the framework in the final experiment. Note

that in equation 44 f is minimized but the mean of R should be maximized so μ_R is in the denominator. The negative sign for the mean term is necessary because $\mu_{Current\ Approach}$ is a negative value and μ_R should be positive.

6.4.5 Cost Functions and Budget Constraint for Loads Analysis

The constraints for the original resource allocation method was a prescribed budget to perform experimental tests in order to decrease variance. Only the cost of each test, C_i was considered and therefore the total cost was $Total\ Cost = \Sigma C_i N_i \leq Budget$ where N_i is the number of each test conducted. As alluded to in Chapter 4, the cost functions used in rework decision framework will be more complicated and include the effects of performance (through weight), uncertainty, rework cost, and computational cost. Some of these cost functions were utilized in Experiments 2a-c in order gain insight into their implementation and impact on the optimization.

One of the most significant takeaways from the experiments in terms of the cost functions was that it can be difficult to assign values for the uncertainty and computational costs and thus makes it difficult to prescribe a reasonable budget which would lead to a feasible solution. All the costs are subjective but the uncertainty and computational costs are more abstract than the weight and a rework cost. Several formulations were evaluated for the cost functions during the experiments and in the end the uncertainty and computation costs are based off of the weight and rework respectively.

Historically in aerospace, correlations exist between the purchasing cost and performance with the total weight [70]. Therefore a penalty is assigned for each additional pound added by the optimization relative to the current approach. Kaufmann et al (2009) discusses how there are large variations in the literature as to the magnitude of the cost per unit weight, but an average of $250 per pound is used here based on

their findings [70]. The same amount is assumed as a savings if the optimized weight is less than the current approach. The weight is the total wing weight of the FEA strucutural model which includes the fuel and primary structure. The uncertainty cost is then tied to this weight penalty (or savings) by applying a coefficient. The logic is if the uncertainty is large than their is less confidence in estimating the wing weight so to account for this the weight cost should subsequently increase. This is of course a conservative view, but this is analogous to the standard approach of adding margins and safety factors to the structural design so it is deemed reasonable.

Previous work was discussed in Chapter 3 on balancing redesign and performance. In Matsumura et al 2013 [95] a ratio was used to relate the weight penalty to redesign costs. In the final design of experiments to build the Bayesian network (see Section 4.2) most of the cases resulted in only the rear spar requiring redesign during the four load cycles, meaning minor rework was limited to four components. Using the published weight cost to rework cost ratios along with four components requiring rework and the total cost relative to the budget a minimum rework cost of $9,000 per component was established. If the computational cost increases for using a higher fidelity aerodynamic analysis then this cost should also increase the rework cost. Therefore a coefficient for the computational cost was added to the rework.

The total cost function used for loads analysis in the rework decision framework is:

$$Total\ Cost = A_{computational} * C_{rework} + (1 \pm B_{uncertainty}) * C_{weight} \tag{45}$$

where C is the variable cost for rework per component and weight per pound, $A_{computational}$ is the computational cost coefficient and $B_{uncertainty}$ is the uncertainty cost coefficient. This form of the total cost function removes some of the subjectivity out of assigning the computational and uncertainty costs by making them coefficients

of the rework and weight costs. Similarly, basing the rework cost on the weight cost also reduces subjectivity given weight cost is a classically used cost driver in aerospace. Nevertheless this formulation is still subjective so variations in the coefficients and rework cost were used while the weight cost remained fixed at \$250/lb. These variations are depicted in Table 19.

Table 19: Cost Function Parameters

Parameter	***Min***	***Max***
C_{rework}	\$9,000.00	\$18,000.00
$A_{computational}$	1.0	1.75
$B_{uncertainty}$	0.0	1.25

$A_{computational}$ is proportional to the K-factor (fidelity level), e.g. $K = 0$ results in $A_{computational} = 1.0$. $B_{uncertainty}$ is also proportional to the K-factor but $K = 0$ results in $B_{uncertainty} = 1.25$. The $\pm$ for the uncertainty coefficient in Equation 6.4.5 is a plus if a weight penalty is applied and a minus if there are weight savings. This ensure that a maximum penalty or minimum savings occur if at the lowest fidelity level. The maximum value for rework cost was chosen based on the total cost relative to the weight costs. Increasing the rework cost essentially limits the amount of weight which can be added to the components in order to increase the wing critical margin of safety so care must be taken in choosing its maximum value to achieve a feasible solution (i.e. satisfying $\mu_R \geq 0$). The maximum value of the computational and uncertainty cost coefficients were chosen for similar considerations in addition to their impact on the rework and weight costs.

The budget allocation is the last aspect of the constraints applied to the optimization. The purpose of the budget is the same as in the original resource allocation method, to constrain the resources available to achieve an optimal solution. Here,

allocating a budget means there are limited financial resources available to cover the costs associated with performance, rework, uncertainty and computation when trying to reduce the risk of major rework. As with any constrained optimization, if the constraints are too restrictive no feasible solution can be found. An additional constraint was added to the problem such that the wing critical margin of safety had to be positive, mean a solution is only feasible if it is predicted that major rework would be avoided. Therefore enough budget had to be allocated to allow a feasible solution, but if too large the problem would be unconstrained. An unconstrained problem in this context is equivalent to uncertainty reduction rather than uncertainty management because no tradeoff is required and the user has unlimited resources to find the optimum solution. With these considerations the minimum budget is $150,000.00 and the maximum is $200,000.00.

Applying dollars to the costs and budget does not imply these are realistic cost estimates. As was discussed in Chapter 4, these magnitudes are meant to be interpreted in relative terms to reflect priority and appropriately constrain the problem. It is not necessary to use units at all for the costs and budget, but given the traditional practice of examining the costs of adding weight in aerospace, it seemed appropriate here to do so. The cost and budget formulation does allow for rigorous cost estimations to be made such that realistic financial impacts are assessed for choices of fidelity and margins is possible, but out of the scope of this thesis. Instead such cost estimations will be left to future work, but the methodology is provided here.

6.4.6 Uncertainty Management Optimization Problem

The insights drawn from Experiment 2 and the development of the objective function and constraints given the final optimization problem for uncertainty management in the rework decision framework based on resource allocation:

$$\min_{x} \; f(\boldsymbol{x}) = W_\sigma \left(\frac{\sigma_R^2}{\sigma_{K=0}^2} \right) - W_\mu \left(\frac{\mu_{Current\ \ Approach}}{\mu_R} \right)$$

$$s.t.\ A_{computational} * C_{rework} + (1 \pm B_{uncertainty}) * C_{weight} \leq Budget$$

$$\mu_R > 0 \tag{46}$$

$$\boldsymbol{x_l} \leq \boldsymbol{x} \leq \boldsymbol{x_u}$$

where $\boldsymbol{x}$ is the vector of design variables containing the K-factor, load margin and structural required margin and the l and u refer to the lower and upper bounds which are shown in Table 20. The K-factor and load margin are actually analysis variables but in the usual terminology of optimization problems $\boldsymbol{x}$ will be referred to as design variables.

Table 20: Design Variable Bounds

Variable	***Min***	***Max***	***levels***
K-factor	0.25	1.0	4
Load Margin	0.0%	25%	continuous
Required Margin	-10%	30%	continuous

The choice of minimum K-factor is based off the assumption that some correction from wind tunnel data is always used, as opposed to a K-factor of zero which means no calibration data is used. The bounds for the load margin were determined based on the fact that a 50% margin is customarily added for the ultimate load and how much additional load would be reasonably added based on the baseline and true bending moment results. The load margin is applied to the W_{KK} values and increases them by the indicate percentage. The increase is only added to the W_{KK} values identified from the sensitivity analysis discussed in Section 4.2.

The bounds for the structural required margin were determined based on observed results for the critical margin of safety of the von Mises yield criterion for ultimate load using the demonstration model. The structural margins are displayed in percentages. For example, a 10% margin for a particular component indicates the applied distortion energy to that component is 10% greater than the allowable distortion energy defined by the material stress allowables defined in Section 5.5.5. Due to the simplifying assumptions of the demonstration model, it should not be expected that these ranges for reflect the actual load or structural margin ranges used in a real commercial transport design.

Other important insights gained from Experiment 2 are related to the implementation of Bayesian inference using the slice sample MCMC method (see Section 3.4.2). The benefits of the slice sample method were discussed and one of the most important benefits is the fact that a "proposal distribution" isn't required to compute the posterior distribution, but this may also lead to more required samples and
or less accuracy. Several parameters are required for running the slice sample function and these can significantly influence the quality of the results [161]. Calculating the posterior distribution was straight forward for the test problems which only had a few parameters to update, but became much more difficult and computationally expensive when trying to update the twenty-two W_{KK} parameters. The suggested methods from the MATLAB documentation to assess the quality of the slice sample results and tune the parameters were utilized.

The expense of the slice sample approach made if infeasible to use within a heuristic optimization which requires numerous function calls, especially for large number of parameters in the loads analysis problem. Sankararaman et al suggests segregating the budget and completing the optimization in multiple stages [139] and this approach was used throughout Experiment 2. The multiobjective function and cost functions used for loads analysis make this approach impractical. Another suggested approach

to decreased computational burden of optimization is to construct a surrogate which relates the system response as a function of the design variables directly [141], then optimize using this surrogate model. This approach was implemented in the final experiments discussed in the next section.

A 200 sample Latin Hypercube design was used on the K-factor, load margin and required margin variables in order to build the surrogate used for optimization. Surrogates for the cost functions were also required and dependent on the design variables. Kriging models were used for all surrogates.

6.4.7 Conclusion

Experiment 22 is separated into three sub-experiments carried our on a simplified test problem to examine different aspects of the resource allocation methodology. Insights gained from these experiments helped formulate the optimization problem for uncertainty management used in the rework decision framework. Therefore Hypothesis 3 is accepted on basis that the core components of the resource allocation methodology presented in Sankararaman et al (2014) provides an appropriate foundation to reducing and managing uncertainty in loads analysis.

Modifications to the original method are necessary and were detailed. Specifically a multiobjective function is used to optimize the mean and variance of the wing critical margin of safety. Unique cost functions were developed and in conjunction with a prescribed budget allow tradeoffs between performance, rework cost, uncertainty and computational cost. To reduce the computational burden of the optimization a surrogate model was fit for the wing critical margin of safety as a function of the design variables and includes the affect of Bayesian inference. The most significant contribution for this experiment is the optimization formulation for uncertainty management to address rework in loads analysis. This formulation considers cost implications

which helps improve life cycle design as discussed in the motivation.

6.5 Framework to Support Rework Decisions

6.5.1 Experiment 3: Determine Impact of Cost Functions on Major Rework

A global sensitivity analysis method was previously discussed in Section 3.5.2 and was used in this experiment to determine the impact of the parameters for the cost functions defined using Equation 6.4.5. These parameters and their ranges are show in Table 19. In addition the sensitivity of the budget and objective function weights was assessed. The budget ranged from \$150,000.00 - \$200,000.00 and each objective weight ranged from 0.0 - 1.0. The results are shown in Pareto plots in Figures 110 - 112.

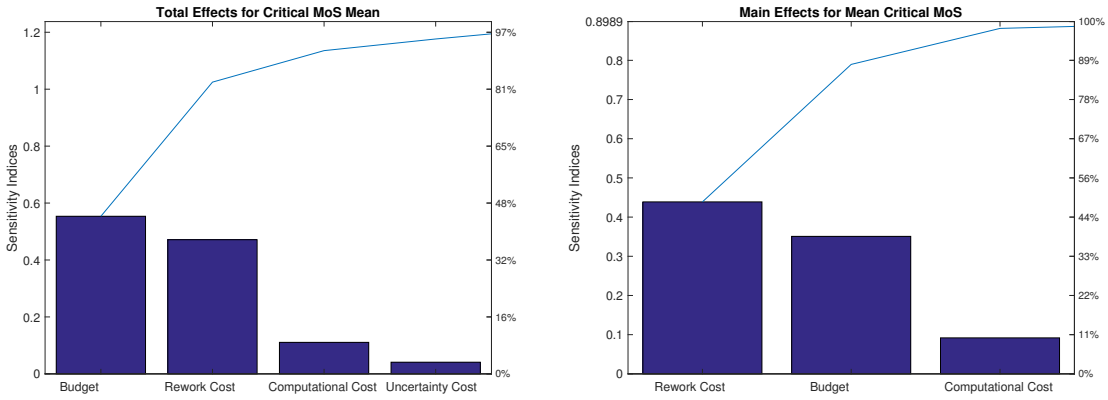

(a) Total effects

(b) Main effects

Figure 110: Sensitivity analysis of cost function parameters for wing critical margin of safety mean, μ_R

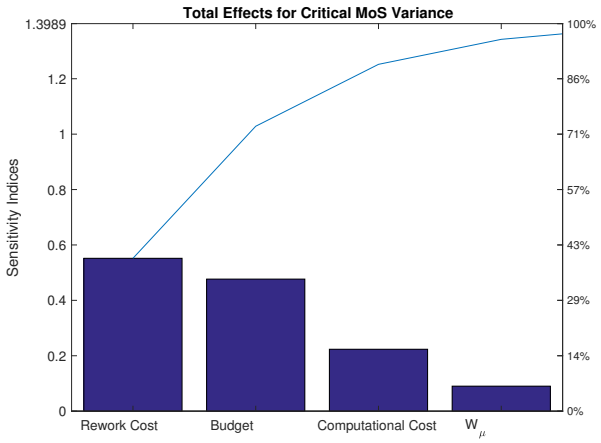

Figure 111: Total effects from sensitivity analysis of cost function parameters for wing critical margin of safety variance, σ_R^2

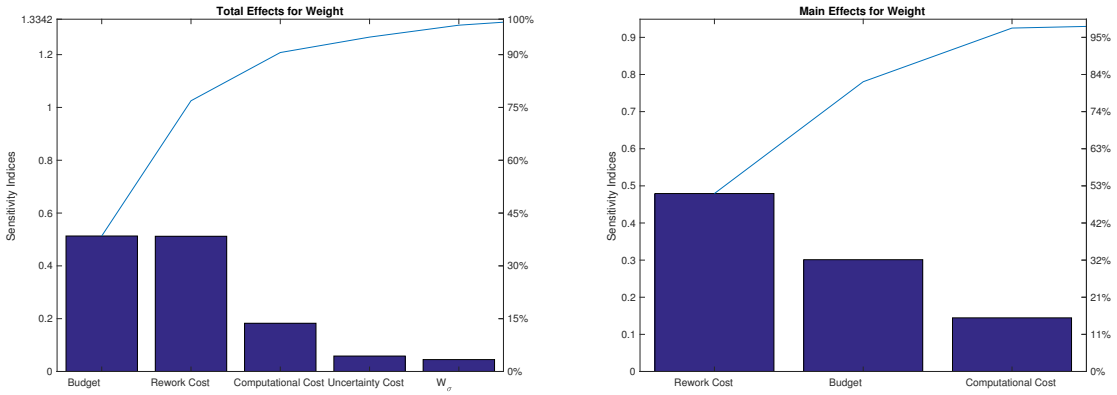

(a) Total effects

(b) Main effects

Figure 112: Sensitivity analysis of cost function parameters for wing weight

The Pareto plots show the total and main effect sensitivity indices on the right vertical and correspond to the bar heights. The cumulative variance for adding each variable as a percentage of the total variance is shown on the right vertical axis and corresponds to the blue line. The plots only show the variables accounting for at least 95% of the total variance, so all variables not listed can be treated as insignificant to the response. Recall, in the absence of numerical error the total effects would sum

to 1.0 or greater and the main effects would sum to one. Note, only the total effects for the response variance are shown because large numerical errors in the main effect calculations caused the indices to be inaccurate even though 10,000 samples from a Sobol sequence were used (see Section 3.5.2 for more details). The weight cost was kept fixed so no sensitivity analysis was done for it.

The results indicate the budget and rework cost are the most dominant effects for all of the responses. Comparison of the total and main effect magnitudes indicate there are important interaction effects for the budget and rework in the mean response and wing weight. Given the form of the cost function, the computational cost and uncertainty coefficients will likely have less impact than the rework and weight variable costs respectively. It is somewhat surprising that the objective weights are not more significant given they guide the optimization, but we will see later the objective function does play a major role in the results of the design scenarios. The computational cost coefficient directly influences the rework cost so it is understandable why it is consistently the third most significant parameter.

In terms of the rework decision framework, this information is useful in guiding how the decision maker to how to define the optimization problem. Given how sensitive the responses are to the rework cost and budget extra care should be taken in defining these. Even though no sensitivity analysis was done here for the weight cost it is very likely this is also a significant parameter to all of the responses. Besides the rework cost, weight cost and budget cost the sensitivity analysis shows how other parameters, albeit less important, impact the response which are of interest to the user. For example, if the decision maker is particularly concerned about minimizing the weight they should also focus on making sure the magnitudes of the computational cost coefficient are accurate. Most importantly, the sensitivity analysis shows how the design scenarios discussed in the next session should be defined.

6.5.2 Design Scenarios

In the problem formulation (Chapter 2) a need was established to use the rework decision framework in different scenarios which reflect the decision makers priorities at a given moment. It was also discussed that these priorities for the importance of performance, minor rework costs, uncertainty and computational costs will likely be determined by when in the development program one is or when external factors or events dictate a change in priority (e.g. the budget for the structural design team is expectantly cut due to new customer requirements). Seven "design scenarios" were created to reflect typical situations which might occur in a airplane development program.

The design scenarios are defined based on the cost function parameters, budget constraint and objective weights. The definition of each scenario is shown in Table 21 and will be discussed individually along with the results of the rework decision framework. The minimum value for the computational and uncertainty cost coefficients are set as 1.0 and 0.0 respectively for all the scenarios and so only the maximum value is scenario-dependent and influences the corresponding coefficient for each fidelity level. For example the nominal computational cost coefficient has values of [1.0000 1.1667 1.3333 1.5000]. If $K = 0.75$ $A_{computational} = 1.3333$ and it is assumed the rework cost increases by 33%. But if $A_{max} = 1.25$ then $A_{computational}$: [1.0000 1.0833 1.1667 1.2500] and only a 17% increase in rework cost if $K = 0.75$. The last column refers to the optimization constraint that the wing critical margin of safety must be positive. This constraint is applied to all scenarios except for the unconservative.

Table 21: Design Scenarios

Scenario	W_μ	W_σ	***Budget***	C_{rework}	A_{max}	B_{max}	$\mu_R \geq 0$
Nominal	1.0	1.0	\$150,000	\$9,000	1.5	1.0	*Yes*
Performance	*Minimize Weight*		\$150,000	\$9,000	1.5	1.0	*Yes*
Uncertainty	0.5	1.0	\$150,000	\$9,000	1.25	0.75	*Yes*
Budget	1.0	1.0	\$150,000	\$18,000	1.75	1.0	*Yes*
Schedule	1.0	1.0	\$200,000	\$18,000	1.75	1.0	*Yes*
Conservative	1.0	0.0	∞	\$9,000	1.25	0.75	*Yes*
Unconservative	1.0	1.0	\$150,000	\$9,000	1.25	1.25	*No*

6.5.2.1 Nominal Scenario

A "nominal" design scenario was created which established a baseline for all the other scenarios. Therefore all the parameter values used for this scenario are considered to be at the nominal level. This scenario will be used in Experiment 4 to evaluate the rework decision framework against the current approach so its results will be discussed in more detail then, but for reference the results of the optimization are shown in Table 22. The first three columns are the optimal design variables found at the optimization solution. The load margin is percent increase in each W_{KK} value which is intended to increase the aerodynamic loads. The required and critical margins are relative to the allowable distortion energy for the von Mises yield criterion. The weight penalty is the additional wing weight pounds relative to the current approach and the variance change is relative to the lowest aerodynamic fidelity level which is $\sigma^2_{K=0}$ in Equation 44. After detailing each scenario the aggregate results will be discussed.

Table 22: Nominal Scenario Results

Scenario	***K-factor***	***Load Margin***	***Required Margin***	***Wing Critical Margin***	***Variance Change***	***Weight Penalty***
Nominal	1.00	0.00%	25.81%	2.15%	-21.04%	384.00 lbs

6.5.2.2 Performance-Driven Scenario

The "performance-driven" scenario describes the situation when the decision maker is primarily focused on reducing weight over all other considerations. This is common in aerospace and can occur at any point in the development program, though there may be specific points when weight is being reduced to hit a specific performance metric. As such the objective function is changed to minimize weight as opposed to the multiobjective function in Equation 44. All other parameters are kept at their nominal values. The results are shown in Table 23.

The objective function clearly has an impact on the results. The weight objective minimizes the weight penalty relative to all other scenarios with feasible solutions. The absence of the multiobjective function results in the wing critical margin to be almost zero and is most likely only positive due to the constraint and the low K-factor setting is chosen which results in an increase in the variance. As was discussed in Section 6.4.6 the large number of parameters and the fact that the bending moment responses are influenced by design variables other than the K-factor (see Sec 6.3.2) means the variance may actually increase relative to the reference point which assumes the lowest fidelity level (uncorrected, $K = 0$) and zero load and required margin.

Table 23: Performance-Driven Scenario Results

Scenario	***K-factor***	***Load Margin***	***Required Margin***	***Wing Critical Margin***	***Variance Change***	***Weight Penalty***
Performance	0.25	24.96%	24.38%	0.06%	+6.85%	181.43 lbs

6.5.2.3 Uncertainty-Driven Scenario

The "uncertainty-driven" scenario is when the decision maker is primarily focused on decreasing the uncertainty in the system. This scenario may occur in situations where a high degree of accuracy is required for analysis and when a lot of confidence is needed in the major rework estimation. One such situation would be is major rework occurred after a flight or ground test failure and so the decision maker wants to be as certain as possible that no more failures will occur when repeating the test program.

To implement this scenario a larger weight is placed on the variance objective relative to the mean. Additionally the computational cost is decreased to encourage a higher fidelity level. The uncertainty cost is also decreased because it reduces the weight penalty and allows more room in the budget to reduce the uncertainty. The results are shown in Table 24. As expected the highest fidelity level is chosen and the uncertainty reduction is the largest relative to the other scenarios. The increase in weight relative to the nominal is most likely due to the decreased uncertainty cost. Even though the intention of decreasing B_{max} is to allow more room in the budget to increase the fidelity, the optimizer may choose to instead add more weight.

Table 24: Uncertainty-Driven Scenario Results

Scenario	***K-factor***	***Load Margin***	***Required Margin***	***Wing Critical Margin***	***Variance Change***	***Weight Penalty***
Uncertainty	1.00	0.00%	26.23%	2.57%	-22.84%	420.00 lbs

6.5.2.4 Budget-Driven Scenario

The "budget-driven" scenario is also common and occurs when a manager is focused on keeping costs low, perhaps due to budget cuts or increased costs in other areas. This scenarios is intended to emulate a focus on short-term costs related to design and not necessarily the cost of the aircraft which is typically driven by weight. Short-term costs would include labor, computational resources, small-scale testing, etc. for the various engineering groups (i.e. loads, stress, etc.) to design and develop the aircraft. Therefore the cost for redesign, i.e. minor rework, and computational costs are at a premium and is expressed in the larger parameter values. All other parameters are held at their nominal values. The results are shown in Table 25.

The optimizer was unable to find a feasible solution due to the constraints imposed by the budget-driven scenario. Specifically the positive critical margin constraint could not be satisfied. The increased rework costs and limited budget restricted the amount of weight which could be added to the structure to achieve a positive margin. This is evident in the relatively low weight penalty. The optimizer attempted to reduce costs by choosing the lowest fidelity level but it was not enough to reach a feasible solution. The K-factor setting was expected given the increase in computational cost and as a result the variance increases. The variance increase may also be a function of the infeasibility of the final solution. Given this is the only scenario which was unable to find a feasible solution, it speaks to how focusing on near-term

costs can have negative consequences for avoiding rework and life cycle design.

Table 25: Budget-Driven Scenario Results

Scenario	***K-factor***	***Load Margin***	***Required Margin***	***Wing Critical Margin***	***Variance Change***	***Weight Penalty***
Budget	0.25	24.96%	23.83%	-0.73%	+14.06%	156.00 lbs

6.5.2.5 Schedule-Driven Scenario

The "schedule-driven" scenario is when a manager is under additional pressure to complete a design activity by a certain deadline. For example, a previous load cycle had setbacks and caused delays therefore in the manager must ensure his/her team completes the current load cycle within a tighter schedule. When time is of the essence a technical leader may make different design and/or analysis decisions such as using a lower fidelity analysis method because it is quicker.

The budget was increase for this scenario because a manager is most likely willing to spend more for near-term costs in order to meet a deadline. The rework and computational costs are at a premium because of additional time to redesign and use high fidelity methods. All other parameters are at their nominal values. The results are shown in Table 26. Despite the increased costs for redesign, the budget allows for a feasible solution to be found, unlike the budget-driven scenario. The lowest fidelity level is chosen to reduce the costs for minor rework and as such the variance barely decreases. Relative to the nominal case, the lower wing critical margin is accompanied by a lower weight penalty. These results exemplify the saying "time is money" and so sometimes takes a larger budget to meet a tight schedule.

Table 26: Schedule-Driven Scenario Results

Scenario	***K-factor***	***Load Margin***	***Required Margin***	***Wing Critical Margin***	***Variance Change***	***Weight Penalty***
Schedule	0.25	2.03%	24.29%	1.63%	-0.01%	256.00 lbs

6.5.2.6 Conservative Design Scenario

The "conservative design scenario" is less of a specific situation and instead conveys a mindset towards design. A decision maker with this mindset is extremely risk adverse, even at the sacrifice of performance. Additionally they rely on traditional methods of design and is skeptical of modern approaches such as uncertainty quantification. This represents an extreme scenario and is included to test the extremes of the rework decision framework. It is not common in aerospace to disregard weight but there may be specific types of aircraft or custom built derivatives which require a conservative mindset to ensure safety. One such example could be designing VIP transport, e.g. Air Force One, where safety is paramount to performance as required by the customer.

In this scenario the variance objective weight is set to zero indicating that the only objective is to maximize the mean wing critical margin of safety. Maximizing the critical margin undoubtedly means adding a significant amount of weight so the budget constraint is lifted for this scenario. The computational cost is decreased because a conservative decision maker will most likely want the best analysis tools available regardless of the cost or schedule. The uncertainty cost is also reduced to lessened given the lack of consideration of the variance objective.

As expected, the critical margin and weight penalty shown in Table 27 are the largest of any scenario. Maximizing the critical margin would indeed minimize the risk

of rework but doing so without regard to uncertainty can clearly degrade performance which some may regard as unnecessary for typical safety standards. Naturally the required margin is at its maximum value to achieve such a relatively large critical margin. Even though the K-factor is at the second to highest level there is still a large variance increase. This is primarily due to the lack of variance reduction in the objective function and also indicates that the required margin has a strong influence on the variance.

Table 27: Conservative Design Scenario Results

Scenario	***K-factor***	***Load Margin***	***Required Margin***	***Wing Critical Margin***	***Variance Change***	***Weight Penalty***
Conservative	0.75	0.00%	30.00%	7.00%	+20.40%	713.48 lbs

6.5.2.7 Unconservative Design Scenario

The last design scenario is at the other extreme of the conservative mindset. A decision maker who is unconservative is willing to take risks and will sacrifice structural integrity (within reason) in order to achieve better performance. Although not common in commercial transports this is alto common in the design of unmanned aerial vehicles. The exponential growth of UAV's has undoubtedly changed the way traditional aerospace manufacturers approach design. The removal of a pilot significantly lowers the minimum required safety standards, although new regulations could change this. Additionally, for some applications expensive payloads or the airframe itself can lead to more of a conservative approach to designing UAV's.

The most significant implementation for the unconservative scenario is relaxing of the positive critical margin constraint. The mean value is still included in the objective function so not too much risk is taken on. In addition the computational

cost is decreased and the uncertainty cost increased because higher fidelity tools should be encouraged to reduce uncertainty as much as possible given the relaxed constraint. Unlike the conservative scenario, the multiobjective function leads to the same K-factor level but results in variance reduction because of the combination of load and structural margin which impact the bending moment responses used for Bayesian inference.

Table 28 summarizes the results. Even though the constraint is relaxed the critical margin is essentially zero, which is what the minimum critical margin should be during the flight load survey. Thus this scenario is actually not very extreme and may be viewed as a compromise between the performance and conservative scenarios. This is evident in the second lowest weight penalty (for feasible solutions) which increases performance. Another interpretation of these results is that adding the positive margin constraint added additional conservatism to the other scenarios while here the approximately zero critical margin was maintained with the multiobjective function alone and allowed a different solution to be found which previously would have been deemed infeasible.

Table 28: Unconservative Design Scenario Results

Scenario	***K-factor***	***Load Margin***	***Required Margin***	***Wing Critical Margin***	***Variance Change***	***Weight Penalty***
Unconservative	0.75	19.86%	24.83%	-3.7e-6%	-6.04%	226.29 lbs

6.5.2.8 Discussion of Design Scenarios

The final results of all seven scenarios are summarized in Table 29 which include the optimal solution of the K-factor, load margin and structural required margin inputs and the optimal responses based on the constrained problem described in Table

21. The important responses are also visualized in Figures 113 - 115 to compare the results of the seven scenarios.

Table 29: Summary of Results from all Design Scenarios

Scenario	***K-factor***	***Load Margin***	***Required Margin***	***Wing Critical Margin***	***Variance Change***	***Weight Penalty***
Nominal	1.00	0.00%	25.81%	2.15%	-21.04%	384.00 lbs
Performance	0.25	24.96%	24.38%	0.06%	+6.85%	181.43 lbs
Uncertainty	1.00	0.00%	26.23%	2.57%	-22.84%	420.00 lbs
Budget	0.25	24.96%	23.83%	-0.73%	+14.06%	156.00 lbs
Schedule	0.25	2.03%	24.29%	1.63%	-0.01%	256.00 lbs
Conservative	0.75	0.00%	30.00%	7.00%	+20.40%	713.48 lbs
Unconservative	0.75	19.86%	24.83%	-3.7e-6%	-6.04%	226.29 lbs

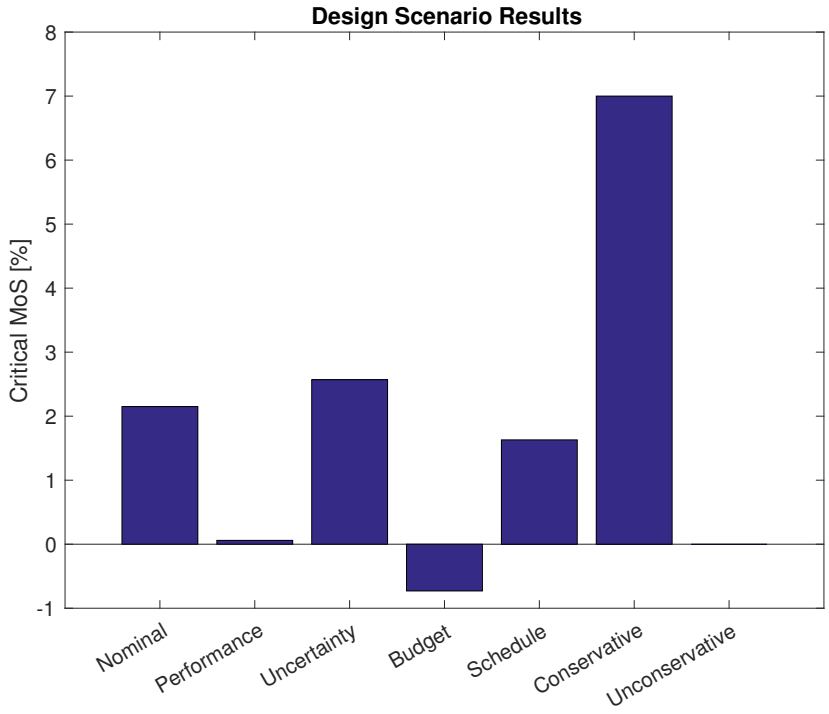

Figure 113: Comparison of wing critical margin of safety mean for design scenarios, ~ 0.0 for unconservative

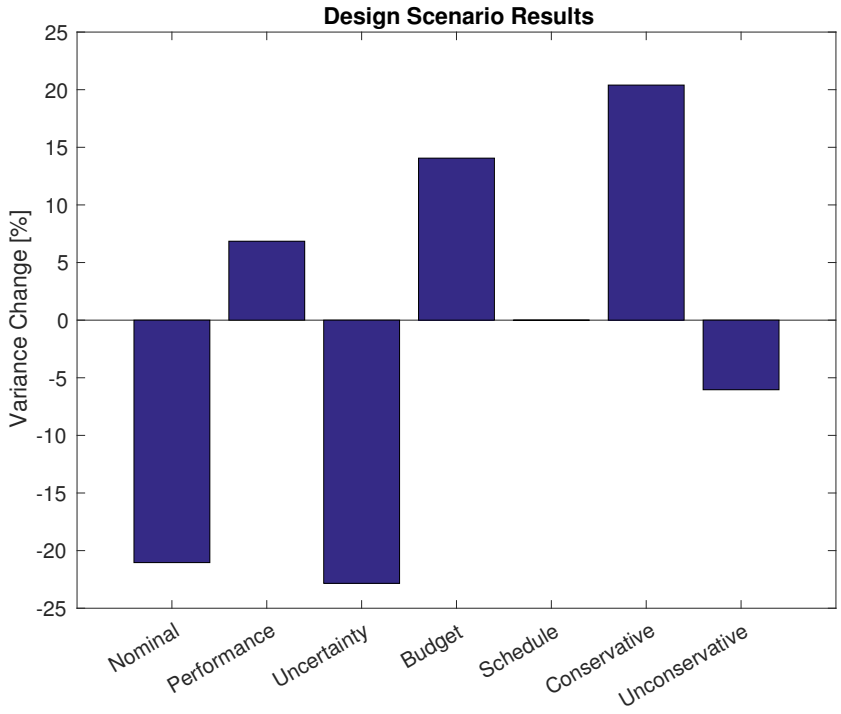

Figure 114: Comparison of wing critical margin of safety variance for design scenarios, ~ 0.0 for schedule-driven

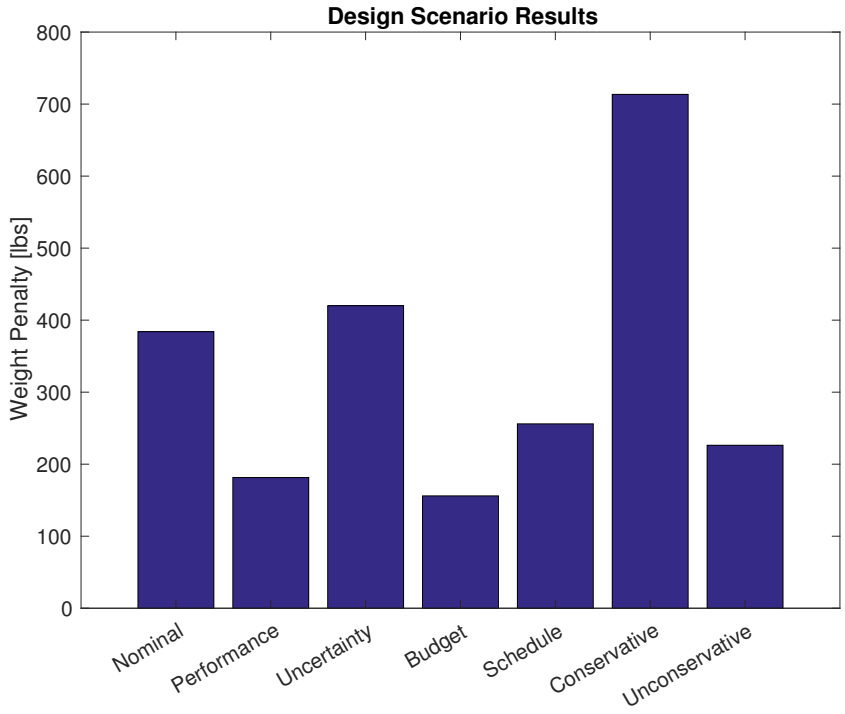

Figure 115: Comparison of wing weight for design scenarios

The ability to examine different scenarios which reflect priorities for performance, redesign, uncertainty and computational cost is one of the most important benefits of the proposed rework decision framework. This capability is possible because of how the optimization problem for uncertainty management was posed from Experiment 2. Although the parameter values used in Experiment 3 may seem subjective, this subjectivity adds flexibility for the decision maker to express different priorities. Additionally, the results from each of the scenarios fit the expected trends which justifies the definitions and helps validate the framework.

Looking at all the scenarios allows us to more closely examine the effects of the optimum K-factor, load margin and structural required margin. As had been alluded to, the variance of the wing critical margin of safety is heavily influenced by the margins. This was somewhat surprising given the only intentional mechanism for

variance reduction is in the aerodynamic fidelity. These results indicate the relationship between uncertainty for major rework is more complicated than just the fidelity. Just as in robust design optimization the uncertainty in the response can be reduced by adjusting design variables which may only indirectly impact uncertainty [176]. In this problem the load and required margin affect the bending moment responses used in Bayesian inference to update the W_{KK} parameters. Therefore all three design variables will have an impact on the uncertainty in the system.

It is clear that additional weight is needed to achieve a positive margin and avoid major rework. The lowest optimal required margin of all the scenarios was 23.83% (though this solution was infeasible). It should be noted that the critical margin of safety almost always came from the same upper skin panel. Thus it would not be recommended to apply this margin to every component because this would unnecessarily add weight. But the assumption in this model is that the structural required margin is applied uniformly to all components.

In terms of realistic aerospace structural designs 24% is a large margin, especially given a 1.5 safety factor is already assumed. But the magnitude is less important given the simplifications of the demonstration model compared to reality. The more important observation is how the structural margin is the dominant design variable for avoiding major rework and reducing structural design risk. This comes at no surprise but being able to quantify the importance of the structural margin is very beneficial from a design perspective. In this work a uniform, deterministic margin was applied to all the components and fixed throughout the load cycles. Future work and improvements to the decision framework could shed new light onto how probabilistic-based margins which are individually defined by component can lead to reduced risk but at a lower weight. Additionally, the margins could be varied throughout the load cycles to potentially reduce overall costs.

It is difficult to determine a clear trend for how the load margin impacts the

responses with this limited data set. The load margin adds conservativism to the loads analysis but has a different affect on the critical margin of safety than the required margin which is a constraint on the structural design. As in the other design variables, the genetic algorithm tends towards the extreme values. It would appear that there are important interaction affects between the load margin and other variables which the optimization is able to exploit to find an optimal solution. This finding in itself is important because it can guide future work to focus on the load margin in order to decipher how exactly it influences the responses of interest.

The seven design scenarios defined in this experiment are able to showcase various aspects of the rework decision framework by allowing the optimizer to exploit the design variables and achieve different solutions. The diversity of the final results indicate that beneficial information is provided to improve decisions related to analysis and design. The user of the rework decision framework can use each scenario as it occurs in the development program and of course create their own scenarios. But some observations can be drawn fro looking at these scenarios in aggregate.

The best balance of performance and uncertainty is the unconservative design scenario. In terms of the total wing weight the unconservative design increases the weight by 0.5%, but is able to achieve a 12% reduction in uncertainty compared to the performance scenario. This is primarily due to the relaxation of the positive margin constraint which these results indicate should be relaxed for all scenarios because it adds unnecessary conservativism given the multiobjective function. Focusing too much on near-term costs can jeopardize life cycle design and increase major rework risk as shown in the budget-driven scenario. Similarly, if decisions are driven by schedule, one should be prepared to invest more up front to cover near-term costs in order to meet an imposing deadline.

Of course these insights are predicated to the assumptions used in this model, but nevertheless preview they type of beneficial analyses and capabilities of the rework

decision framework. The rework decision framework was able to demonstrate expected trends in the design scenarios which help validate it. The framework can now be evaluated against the current approach to loads analysis in the final experiment.

6.5.3 Baseline: Current Approach to Loads Analysis

A baseline is established based on the current approach to loads analysis which was discussed in the Motivation and Problem Formulation Chapters. To recap, the major limitations identified in the current approach is a lack of uncertainty quantification, solely relying on expensive experiments for uncertainty reduction and a reactive approach to major and minor rework. Ultimately it is the stance of this thesis that these limitations have led to increased design risk and specifically increased risk for major rework when the structural design of novel concepts fail to meet requirements during flight and ground tests. The baseline model attempts to capture these limitations and is used to evaluate the rework decision framework in Experiment 4. The baseline is discussed in this section.

The lack of uncertainty quantification and management means the baseline model is deterministic and no Bayesian methods will be employed for uncertainty reduction. Without UQ, there is no way to directly compare the uncertainty management efforts of the framework against the baseline. Contrary to the colloquial saying, in this case what you don't know *can* hurt you. The inability to quantify the uncertainty in the system reduces the confidence that the empirically-based margins which may have worked for previous designs will be enough to avoid major rework in new concepts, or that there won't be undue additional weight which will degrade performance.

The baseline model assumes a K-factor of 0.25 which is equivalent to using a low-fidelity aerodynamic analysis in conjunction with rigid wind tunnel calibration throughout the load cycles. This is viewed as the current approach due to the fact

that linearized aerodynamics such as NASTRAN's Doublet Lattice Method are used to design even modern commercial transports based on subject matter experts. The model also assumes no load margin is applied and a structural required margin of zero for the von Mises yield criterion is applied to all components. Additional insight from subject matter experts claim the load margin is typically added if empirical data or preliminary studies indicate the loads analysis will underpredicts the "true" loads anticipated during the flight load survey. The baseline model is assumed to be a new concept where such data does not exist and thus no load margin is applied. The required margin is set to zero because a 1.5 safety factor is assumed for ultimate loads and every effort is made to save weight when finalizing the design at the certification load cycle.

The deterministic baseline model is run in the M&S environment for four load cycles in order to produce the finalized design. As stated previously, the structural components are only redesigned if the critical margin of safety falls below the required margins. A minimum gauge thickness of 0.35mm is assumed for all components. After completing the load cycles the wing critical margin of safety is 9.0% and the final wing weight is 15,893 lbs. Due to the required margin and minimum thickness no redesign is necessary and thus no minor rework occurs during the load cycles. More details on this will be discussed in the next section.

The final bending moment is depicted in Figure 116. The blue line represents the baseline including a K-factor of 0.25 and the red line is the simulated flight load survey, i.e. the truth data. The uncorrected loads ($K = 0$) are also shown in brown as a reference. From a loads perspective, the analysis underpredicts the true loads and thus increases the risk of major rework. This risk is confirmed after the true loads are applied to final design and the margin of safety decreases below the required level in one of the upper skin panels. The final wing critical margin is -8.02% and is classified as major rework. A more detailed analysis on this component will be discussed in the

next section.

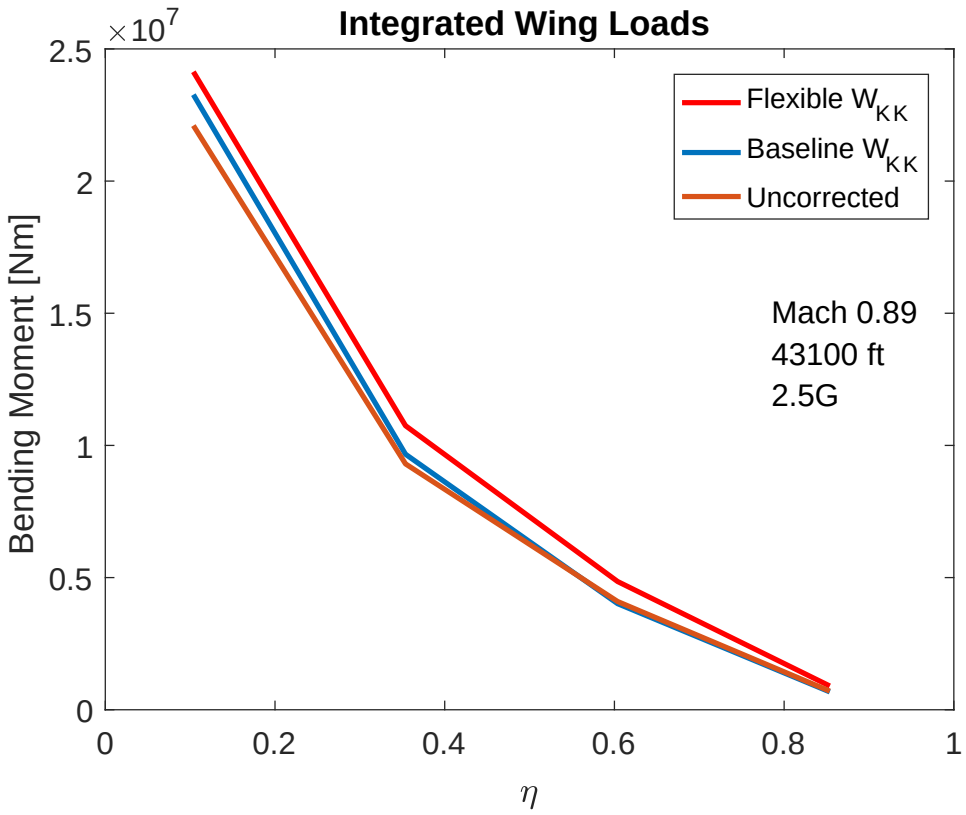

Figure 116: Integrated wing bending moment for baseline model

The deterministic baseline which represents the current approach to loads analysis results in major rework. The lack of uncertainty considerations make it more difficult to predict how the analysis fidelity and margin choices will impact structural failures during the test phase for new concepts. Without these predictions, the ensuing major rework to fix the wing skin and repeat the flight load survey can not be planned for in advance and proactively avoided. The baseline results exemplify this reactive approach, albeit for a simplified model. The final experiment can now be conducted to compare the proposed framework against the baseline.

6.5.4 Experiment 4: Evaluate Framework to Support Rework Decisions

The rework decision framework has the capability to evaluate different design scenarios which were discussed in Experiment 3. The results from the nominal scenario will represent the rework decision framework and be used to compare against the baseline model results from the previous section. The input assumptions for the nominal scenario are repeated here in Table 30. A comparison of the results from the two approaches is shown in Table 31.

Table 30: Nominal Design Scenario Inputs

Scenario	W_μ	W_σ	***Budget***	C_{rework}	A_{max}	B_{max}	$\mu_R \geq 0$
Nominal	1.0	1.0	$150,000	$9,000	1.5	1.0	*Yes*

Table 31: Comparison of Rework Decision Framework against Current Approach

	K-factor	***Load Margin***	***Required Margin***	***Wing Critical Margin***	***Variance Change***	***Wing Weight***
Current Approach	0.25	0.00%	0.00%	-8.02%	N/A	15893 lbs
Framework	1.00	0.00%	25.81%	2.15%	-21.04%	16277 lbs

In order to avoid major rework, the framework estimates a structural margin of 25.81% is needed during the load cycles and results in a critical margin of 2.15% during the flight load survey. In order to satisfy the required margin the wing weight is increased by 2.4%. In the framework uncertainty quantification is done on a model which assumes no corrections and zero load and required margin. The uncertainty is then reduced by resource allocation optimization using the multiobjective function previously discussed and results in a 21% reduction in the uncertainty. "N/A"

stands for not applicable in Table 31 because the current approach does not employ uncertainty quantification or management.

The optimization solution in the rework decision framework is based on Bayesian network and thus is based on surrogate models. To analyze the results further and compare to the baseline, the optimal design variables for the nominal scenario were used in the full M&S environment for four load cycles. The resulting distribution of the critical margin of safety for both approaches is shown in Figure 117.

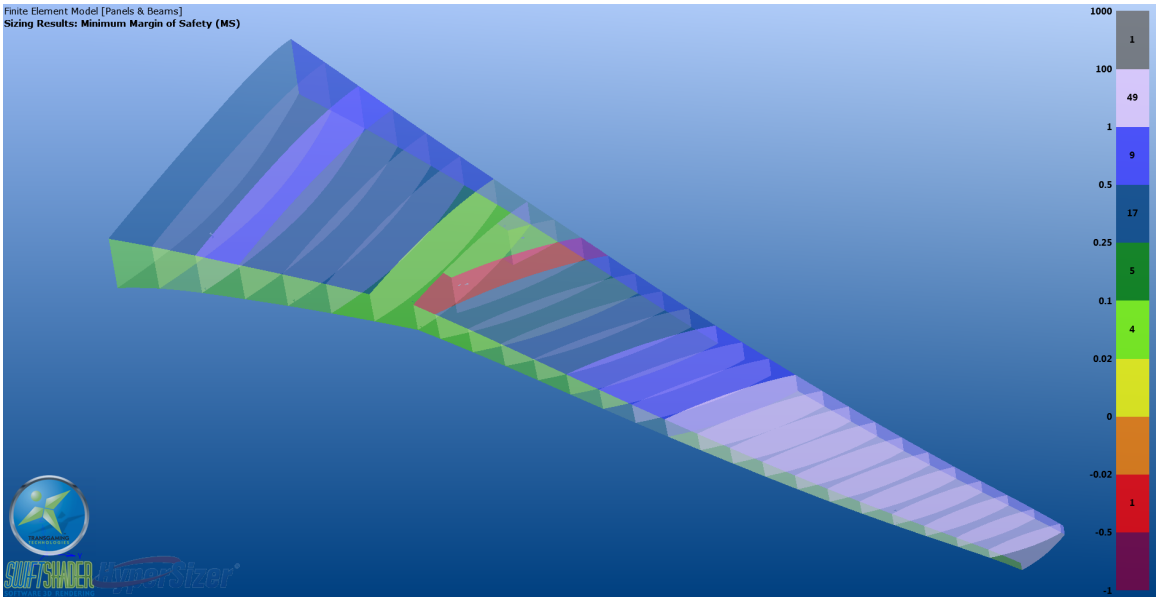

(a) Current approach

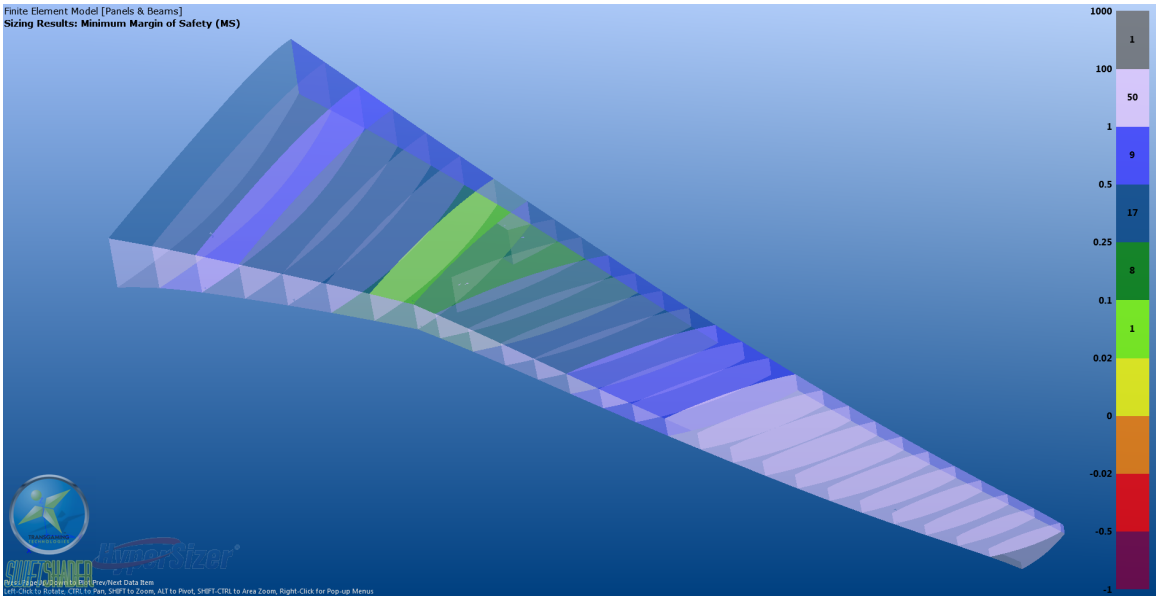

(b) Rework decision framework

Figure 117: Distribution of component critical margin of safety during flight load survey

The margin of safety (MoS) is expressed in terms of HyperSizer's definition (see

Equation 27) but can be converted to normal percentages relative to the distortion energy allowables used throughout this thesis using the following equation:

$$Distortion\ Energy\ Margin = \left(1 - \frac{1}{MoS + 1}\right) * 100 \tag{47}$$

The colorbar represents the magnitude of the margin and components with orange or red indicates failure during the flight load survey and major rework. The numbers printed inside the color ranges indicates the number of components within that margin range. The distribution is very similar for both approaches with the exception of a few components. Two components stand out, the upper skin panel which results in major rework and the rear spar. These two components will be examined further to compare minor and major rework in the two approaches.

The baseline results showed no minor rework occurred during the load cycles. For the framework, the rear spar required redesign after each load cycle. The internal load and margin of safety results are shown for both approaches in Figure 118. The load plots show the internal moments per unit length as a function of the load cycles.

When the original NASTRAN model is imported into HyperSizer the initial stiffness and material definitions are updated as a preliminary step prior to the first load cycle. These results are not shown in these plots, but there are significant changes to the stiffness in this first step. For the baseline case the minimum gauge thickness is large enough where all the components are able to achieve positive critical margins after the first load cycle. The loads change very little, if at all, during the subsequent load cycles because none of the wing components are redesigned. If redesign does not occur, the stiffness in the wing is constant and there is essentially no feedback effect between NASTRAN and HyperSizer. If the loads and stiffness are constant the margins of safety will not change either. After completing the load cycles the true loads are applied in the simulated flight load survey. The internal loads of the baseline rear

spar increase and cause the margin of safety to decrease, but still remains positive indicating major rework would not be needed for this component.

A different picture is painted for the rear spar in the framework results. Here a larger required margin is applied to all the components. The internal rear spar loads increase after the first load cycle and cause the critical margin to decrease below the required level and necessitates the rear spar to be redesigned, i.e. minor rework. Each time the rear spar is redesigned HyperSizer attempts to minimize the weight so the new margin is as close to the required level as possible. But the feedback between HyperSizer and NASTRAN causes further increases in the load and subsequently more minor rework. As was mentioned before, in an actual airplane development program four load cycles is usually enough to converge the loads and stiffness. In the demonstration model the maximum number of cycles was thus limited to four. If more cycles were permitted, the loads would eventually converge and no more rework would be required. Unlike in the baseline, the flight load survey causes the internal loads to decrease so the final margin for the rear spar is well above the required minimum. It should be noted, even though the required margin is fixed at 25.81% throughout the load cycles, major rework is always defined with respect to zero margins.

The flight load survey caused the rear spar internal loads to increase in the baseline but decrease for the framework. Thus it is clear the load paths are different in the different approaches and thus can affect the same component in distinct ways. The HyperSizer optimization for each component modifies the load paths such that the entire wing structure satisfies all the selected failure analyses at minimum weight.

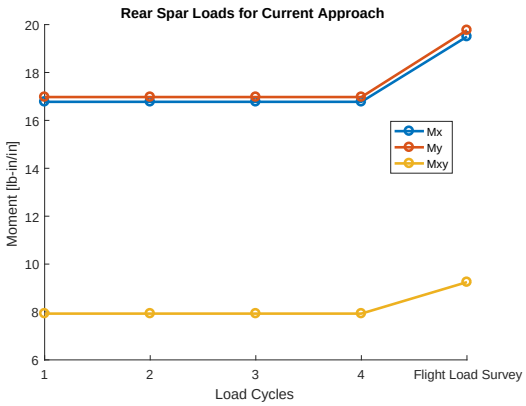

(a) Loads for current approach

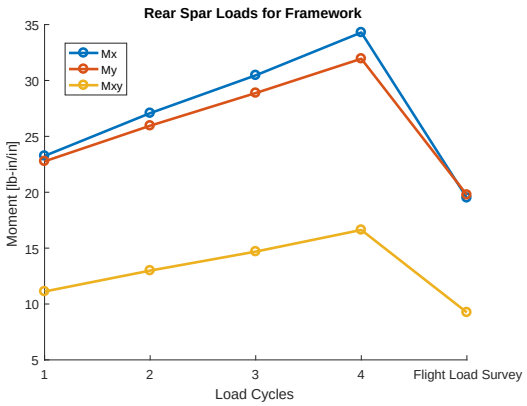

(b) Loads for rework decision framework

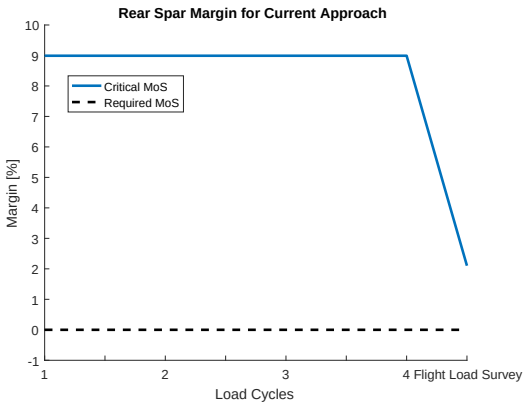

(c) Critical margin for current approach

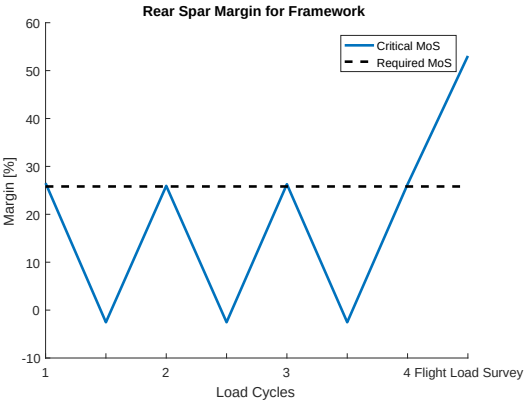

(d) Critical margin for rework decision framework

Figure 118: Comparison of methods for rear spar

The internal moments were chosen as an example to visualize how the changing loads impact the critical margin, though other load components follow similar trends. It should be reiterated that all margins are only based on the von Mises stress criterion discussed in the HyperSizer model's failure analysis in Section 5.5.5. This criterion is only dependent on stress and thus the sizing of each component is only depended on the applied stress and the material stress allowables. All components in this model consist of single-sheet unstiffened panels. In reality the rear spar would have upper

and lower flanges and a shear web, but these features were not included in this model. Therefore the structural model is quite simplified compared to reality and the results of the rear spar reflect this, particularly in how the loads and stiffness do not converge. After each cycle when the rear spar is redesigned it becomes stiffer and the load path adjusts so more load passes through it. Therefore the loads and stiffness for this component may not converge. Again, this is not a realistic scenario and reflects the assumptions of the simplified model.

A similar analysis was done on the upper skin panel which caused major rework for the baseline case, the results are shown in Figure 119. For the baseline, the panel loads and margin remain constant throughout the load cycles followed by an increase in the loads for the flight load survey, just as in the rear spar. The difference is the final critical margin actually decrease below zero. For the framework results there are very small but finite changes in both the internal loads and margin throughout the load cycles. These small changes are a direct result of the rear spar changes previously discussed. The entire load distribution changes as a result of minor rework in a single component and impacts all other components, although the impact is small in this case. The panel margin is able to maintain a healthy margin above the required level but reduces as the flight load survey increases the internal loads. A positive margin is still maintained though, so major rework is avoided.

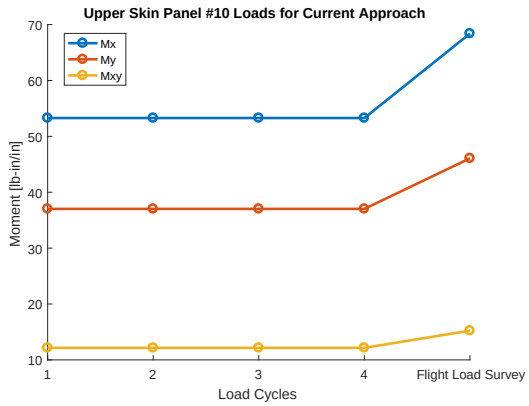

(a) Loads for current approach

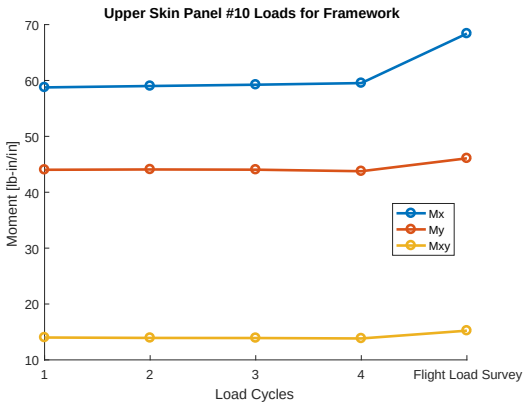

(b) Loads for rework decision framework

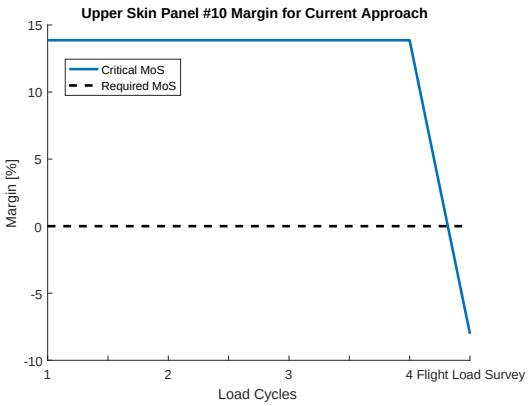

(c) Critical margin for current approach

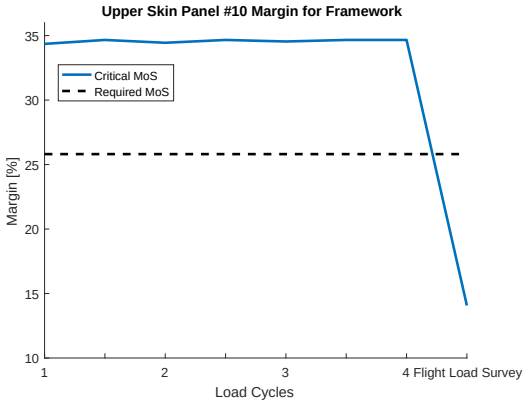

(d) Critical margin for rework decision framework

Figure 119: Comparison of methods for upper skin panel #10

As was mentioned, a load margin can be applied to correct analysis loads which underpredict the true loads. In order to assure a fair comparison of the current approach to the rework decision framework, a 10% load margin was applied to the baseline. By only looking at the bending moment a 10% increase in the W_{KK} correction factors should be sufficient to account for the unconservative analysis loads. After the load margin was applied to the baseline model for four load cycles the wing critical margin remained at -8.02% for the flight load survey so major rework still

occurred. The failure occurred in the same upper skin panel. The increase in loads reduced the margins in all the components but not enough to warrant any redesign. Therefore the structure essentially remained the same as the baseline case and when the true loads were applied, the resulting margin was also the same. Even with the additional load margin, the rework decision framework was able to avoid major rework compared to the current approach.

6.5.5 Conclusion

The final rework decision framework was developed based off the M&S environment discussed in the experimental setup and the results of Experiments 1 and 2. The framework was then used to perform sensitivity analysis on parameters related to the objective function and constrains of the optimization problem. The results of Experiment 3 indicated the rework cost and budget were the dominant parameters impacting the wing critical margin of safety mean and variance, as well as the wing total weight. Naturally the weight variable cost is also another significant parameter though it was kept fixed in these experiments.

Seven design scenarios were defined and evaluated using the framework based on the aforementioned objective and constraint parameters. The scenarios reflect different situations which may influence a decision makers' priorities for trading performance, rework, uncertainty and computational cost. The results for each scenario was discussed and several expected trends were observed which further validated the framework. The optimal design variables indicate the structural margin is the most dominant variable. Additionally, the response variance, i.e. the uncertainty, is not just dependent on the fidelity level but the combination of all three design variables. Overall the unconservative design scenario resulted in the best balance of performance

and design risk reduction. The budget-driven scenario resulted in an infeasible solution which highlights how focusing on near-term costs can jeopardize the life cycle design and increase the risk of major rework.

After validating the performance of the framework with the design scenarios, it was compared against the current approach. A baseline model was discussed which represents the current approach and its limitations. The rework decision framework was able to avoid major rework while the baseline could not. The framework is also able to quantify and reduce uncertainty while the baseline cannot. Although the simplified structural model is not representative of reality, both the framework and the baseline used the same assumptions so a fair comparison was made when evaluating major rework.

The ability to perform optimization and evaluate different tradeoffs via design scenarios provides the decision maker with more information in order to make choices related to fidelity and margins. Thus Hypothesis 4 is accepted to address Research Question 4. Furthermore Experiments 3 and 4 helped address the research gap by developing proactive rework strategies during the design phase. Strategies can be developed for any number of design scenarios and are not limited to the ones evaluated here. The major contribution of these final experiments is an original, comprehensive framework to improve decision making in aerospace structural design which has been tested against the current approach to loads analysis.

6.6 Discussion, Recommendations & Thesis Statement

The experimental plan has been completed to address all the research questions and validate the secondary hypotheses. In this final section the aggregate of the results as a whole will briefly be discussed along with key assumptions leading to these results and recommendations based on the data developed throughout the experimental plan.

6.6.1 Modeling & Simulation Environment

The modeling and simulation environment constructed for this work is an integrated, multidiscipline, MATLAB-based environment which involves CFD via NASCART-GT from the Georgia Institute of Technology; aeroelastic and finite-element analysis via MSC NASTRAN (2014) and structural design via Collier Research Corporation's HyperSizer (2016). Some of the key assumptions for the current environment are inviscid CFD analysis and linear, static aeroelastic analysis and linearized aerodynamic with NASTRAN's Doublet Lattice Method.

For viscous flow, other CFD programs may need to be explored due to the computational expense of analyzing a viscous 3D model in NASCART-GT. Nonlinear and/or dynamic aeroelastic analysis would involve different solution sequences in NASTRAN and most likely required modification and refinement of the model. For nonlinear aerodynamics, the direct grid import method should be utilized in NASTRAN to bypass the Doublet Lattice Method. This would also eliminate the use of the empirical adjustment factors which define the epistemic uncertainty in this work, so naturally substantial modifications to the framework would be necessary, though it would allow more advanced characterizations of aerodynamic fidelity as opposed to the linear assumptions used here.

The iterations between NASTRAN and HyperSizer took a considerable amount of time with the resources available. For example, running 500 cases for four load

cycles took over a week to complete. Each case requires a NASTRAN run after each iteration, but thankfully a computing cluster was available to run several NASTRAN jobs simultaneously. The biggest bottleneck by far was HyperSizer sizing optimization for each of the 86 components multiple times within a cycle. No paralellization was possible given HyperSizer requires Windows and the cluster runs on Linux. Significant savings could be realized if a Windows-based cluster were available.

The number of iterations was always assumed to be fixed at four to simulate the four load cycles in a development program. As was seen in the final experiment, some components (particularly the rear spar) did not always converge within four iterations. An alternative is to let the iterations persist until convergence. It was also assumed that each component is only redesigned if its critical margins falls below the required level. Alternative the components could be redesigned after each iteration which would undoubtedly decrease the total weight, but then the definition of minor rework would need to be modified. The recommendation is to use which methods align best with what is done in reality.

Nevertheless, the M&S environment as it stands offers a foundation to further develop and advance the rework decision framework. Many of the analyses in this environment can be substituted with others (with some effort) and can be used for various aeroelastic design problems, even those non-related to rework.

6.6.2 Demonstration Model

The demonstration model used to develop and evaluate the rework decision framework is based on the *undeformed* Common Research Model (uCRM) developed out of the University of Michigan. The specific model utilized in this thesis was provided by the Boeing Company. Many aspects of the NASTRAN model were untouched to

maintain its integrity but other aspects took significant effort to adapt to the M&S environment. Most of the key assumptions for the model are dependent on the analysis assumptions previously discussed. The load cases defined in NASTRAN were limited to steady symmetric cases and it is recommended these be expanded to include a diverse set of load case types and potentially additional load case parameters. The HyperSizer model was significantly limited in terms of materials, component types and failure methods and it is highly recommended that HyperSizer's full capabilities be utilized for any future work. Specifically the assumptions are all components were considered to be aluminum unstiffened single sheet panels with only the von Mises stress criterion failure mode considered.

6.6.3 Epistemic Uncertainty

Defining the epistemic uncertainty using data-driven approaches took considerable effort but was important to address a gap in the literature. Typically epistemic uncertainty research focuses on theory and settles for assumptions and generalizations when it comes to demonstrating these theories on complex problems. Even though defining the uncertainty based on Gaussian noise and the linearized normal coefficient curve slope error is relatively simplistic compared to some of the advanced theory available, this limitation is more than compensated by the efforts made to quantify this error and not just assume an arbitrary distribution parameter value. The procedures for defining the epistemic uncertainty is well-documented in this thesis and can serve as guide for applying more advanced epistemic uncertainty methods and close the gap between UQ research and practice.

The key assumption for the epistemic uncertainty definition is use of the scalar K-factor to define the aerodynamic fidelity levels. The K-factor approach assumes

a linear variation in fidelity, but is limited by the linear empirical adjustment parameters of NASTRAN and specifically the linear assumption of the lift curve slope for the W_{KK} corrections. Additionally the uncertainty is only applied to the W_{KK} parameters identified as significant, all other parameters are fixed at their rigid W_{KK} values. Another assumption is that all W_{KK} parameters are treated as independent, when most likely significant correlations exist. An alternative approach would be to define the error relative to the significant parameters but apply uncertainty to all W_{KK} parameters in some type of uniform way. This would allow the full extent of the epistemic uncertainty to be captured in the environment. It is recommended this latter approach be pursued to see how significant the fidelity is compared to the margins.

6.6.4 Bayesian Network and Sensitivity Analysis

The development of the Bayesian network to quantify and reduce epistemic uncertainty through Bayesian inference is a critical component to the rework decision framework. The Bayesian network can be an indispensable tool for uncertainty quantification in loads analysis and structural design. Surrogate modeling is highly recommended for computational efficiency, but caution should be taken to ensure quality surrogates are constructed, especially for complex systems such as the environment used in this thesis. The Bayesian network used in this thesis is essentially a coupling of surrogate models and MCMC functions for inference in MATLAB. Professionally developed software is available to specifically carry out all the leg work for Bayesian networks in an integrated environment and it is recommended that these be explored as opposed to the "do-it-yourself" approach taken here. Some of these programs are MATLAB-based while some are not. All were avoided though in this work due to a lack of time to learn new software so consequently the effort required is unclear.

Uncertainty propagation for sensitivity analysis is one of the most important uses

of the Bayesian network. The global sensitivity analysis (GSA) method implemented in this work required a large sample size to avoid numerical errors [135]. This may be due to the quality of the surrogate models used in conjunction with the Bayesian network. Still it may be beneficial to explore other approaches suggested by Saltelli et al or other authors.

A combination of feature selection using machine learning and GSA were employed at different times to narrow down the large pool of parameters into a reasonable amount for the computational resources available. If given more time or more resources, a single analysis would be done using one method with all parameters from all load cases (over 400 in total) using a very large sample size (at least 2000). This would be preferred to doing it in multiple steps in order to capture the most significant parameters but it would have been very difficult to run so many cases in this environment. With the current computational resources 2000 cases could take several weeks to complete. An alternative way to reduce the problem size could be to redefine how the empirical adjustments are applied. For example they could be constant for an area of the wing as opposed to each strip.

The GSA results from Experiment 1 identified significant aleatory and epistemic uncertainty parameters for the system and subsystem responses. A key assumption is the standard deviation for the Gaussian distribution defining each aleatory parameter. The focus of this thesis was primarily on the epistemic uncertainty so it is recommended that more effort be made to also rigorously define the aleatory sources with data. Several epistemic uncertainty parameters were identified as significant by GSA. Based on the results the wing root and tip W_{KK} parameters have the largest epistemic uncertainty in terms of bending moment. This may be because of the largest moment occurs towards the cantilevered root. The tip may be significant because of wing tip vortices but these results may be skewed by the large discretization error which seems to increase the W_{KK} magnitude at the tip. It is recommended future

work focus on defining and reducing epistemic uncertainty on these areas of the wing.

The sensitivity analysis was only done on Load Case 4 and it was assumed the other load cases had the same significant parameters, but this should be verified in future work. The bending moment response used for the sensitivity analysis only included four spanwise locations and were always set at the mid-chord. A more refined bending moment distribution may reveal other results from sensitivity analysis.

6.6.5 Rework Decision Framework

The insight from building and testing the rework decision framework on a simple problem for the literature was very beneficial for formulating and solving the final optimization problem on the full system. It is thus recommended a similar approach be taken for any future developments of the framework. A lot of Experiment 2 was focused on implementing the decoupling approach of Liang et al [85] and even though in the end it wasn't utilized it was also beneficial. Of course the actual load cycles in a development program should not be modified, but from a modeling perspective decoupling would substantially decrease the computational burden.

One useful insight from this work was potentially enforcing compatibility through Bayesian inference in order to model variations in the design variable through the load cycles. For example, instead of assuming the required margin is fixed at a given value, it could be large in the beginning cycles and gradually decreased to zero at the final. These variations complicate the design of experiments because surrogates would be needed for each iteration, but these surrogates would be disjointed. The methods of Liang et al could potentially solve this problem by linking the surrogates through Bayesian methods. Unfortunately there was not enough time to pursue this further in this work, but it is recommended this approach be explored to see if it is viable.

An assumption is that the load margin should only be applied to the significant W_{KK} parameters, if it were applied to all the parameters uniformly the impact of the margin may be more significant. As just alluded to, the structural required margins are assumed to be fixed throughout the cycles and uniformly applied to all components. During the flight load survey the required margin is always set to zero to define major rework. It is recommended that the design variables, especially the fidelity and required margin, be allow to change during the load cycles.

MATLAB's genetic algorithm was the only suitable choice for the optimization problem with the available Toolboxes. The GA offered a lot of flexibility and performed well on the surrogates. The required function evaluation of GA's made it intractable to use with the slice sample method for Bayesian inference, which is why the additional surrogate relating the responses directly to the design variables was necessary. Other optimization algorithms exist for MATLAB from third-party developers which may be applied to this problem. Again, caution must be taken to produce high quality surrogate model to ensure the errors do not grow too large. The Bayesian network enables error terms such as surrogate modeling error to be treated as additional parameters and updated. Although this was not pursued here it is highly recommended given the reliance of surrogates to make the framework computationally feasible.

The question of scalability is an important one for advancing and implementing the rework decision framework. It is of the authors' opinion the environment and overarching framework can be scaled to more realistic models and even more advanced analyses, but high-performance computing and parallelization is highly recommended. High quality surrogate modeling is another prerequisite for scaling to minimize errors because it is not recommended to run the optimization on the full M&S environment.

6.6.6 Final Recommendations for Reducing Major Rework Risk

In light of all the assumptions previously discussed, the results of the experimental plan reveal some general strategies for reducing design and rework risk for this particular model which may be extrapolated to future work.

1. ***Epistemic Uncertainty***

   Focus epistemic uncertainty reduction efforts for the wing root and tips because sensitivity analysis reveals these areas are more significant to the integrated bending moment responses considered. By itself, the K-factor representing aerodynamic fidelity was not the most significant driver for the wing critical margin uncertainty, but in conjunction with the load and structural margins significant uncertainty reduction was possible. Therefore it is recommended that higher-fidelity aerodynamic methods such as CFD be incorporated into loads analysis for commercial transport aircraft to calibrate the linear DLM in NASTRAN.

2. ***Load Margin***

   A clear trend could not be established for how the load margin alone impacted major rework risk with these results, but it is clear by the optimal load margins chosen by the optimizer in the various design scenarios that it plays an important role. More data is needed to define clear trends for the main effects and interaction effects of the load margin relative to the other variables. Therefore it is recommended that the load margin continue to be used as a design variable along with the required margin to reduce rework risk.

3. ***Structural Margins***

The structural required margin is the dominant factor in reducing major rework risk. It is recommended a minimum structural margin of 24% is needed for the upper skin panel #10 to avoid major rework based on the seven design scenarios analyzed and the baseline model (see Tables 29 and 31). This margin was determined as part of the optimal solution found by the Genetic Algorithm when solving the constrained multiobjective problem discussed in Section 6.4.6. The rear spar consistently was the only component to require minor rework (i.e. redesign during the load cycles) so other component types (such as I-beam) should be considered. The scenarios also emphasize that fidelity and load margin are important in balancing the weight and uncertainty, but the required margin is the primary way to achieving positive margins in the flight load survey. It must be reiterated that structural model used here is very simplified and assumes all components are single-sheet unstiffened panels made of aluminum, all components have the same structural required margin and the only failure analysis considered is von Mises yield criterion for ultimate load. Therefore the magnitude of the margins and weight are not representative of a realistic commercial transport wing

4. ***Design Scenarios for Proactive Rework Planning***

   The optimization problem formulation allows the design scenarios to play an important role in reducing design risk in a cost effective manner. It is recommended these cost considerations be taken into account when making decisions to avoid major rework. Therefore it is recommended the user of this framework to analyze various scenarios to develop proactive strategies for both major and minor rework and assess the cost implications of such strategies.

6.6.7 Thesis Statement

The culmination of the experimental plan and results validate the primary hypothesis made in the problem formulation. This overarching hypothesis is thus the thesis statement for this work:

> ***Thesis Statement:*** *For a given design scenario, the proposed framework involving uncertainty quantification and management has lead to improved decisions regarding rework and performance compared to the current approach*

CHAPTER VII

CONCLUSION

7.1 Summary

Cost overruns and schedule delays have plagued almost all major aerospace development programs and have resulted in billions of dollars lost. Design rework has attributed to these problems and one approach to mitigating this risk is reducing uncertainty. Failure to meet requirements during flight or ground tests results in one of the most significant and costly rework efforts. This type of rework is referred to as *major* rework and the main purpose of this thesis is to reduce this risk by improving design and analysis decisions impacting the loads analysis process.

Loads analysis is a crucial part of the design process for aerospace vehicles. Its main objective is to determine the worst-case loading conditions which will realistically be experienced in normal and abnormal flight operations. These conditions are called critical loads. With this information, a structure is designed and optimized to withstand such loads and certify the design. Observing the current approach to loads analysis has revealed some shortcomings related to uncertainty and the allocation of load and structural margins. The fields of uncertainty quantification and uncertainty management were chosen to address these limitations and a framework was proposed to support decisions for rework in loads analysis.

Key aspects of the framework include utilizing a Bayesian network for modeling the loads process as well as propagating various uncertainty sources to the system response. Bayesian-based resource allocation optimization is another key aspect and used to reduce and manage uncertainty. Finally, the goal of the framework is to determine the optimal tradeoffs between aerodynamic fidelity and margin allocation to

minimize the risk of major rework while considering their respective cost implications with finite resources. Assigning costs related to fidelity and margins are intended to reflect the users' prioritization for redesign costs, uncertainty, computational cost and performance degradation through weight penalties.

The demonstration model is the undeformed Common Research Model (uCRM) wing, which is representative of a transonic wide-body commercial transport. The modeling and simulation environment is multidisciplinary and anchored in three software programs to perform various analyses: NASCART-GT for computational fluid dynamics; NASTRAN for doublet-lattice method aerodynamics, structural analysis and aeroelastic analysis; and HyperSizer for failure analysis and structural optimization.

The experimental plan includes four experiments which have facilitated the contributions of this work to the research community. The final rework decision framework was evaluated against seven design scenarios to explore a potential decision makers' varying priorities as well as a baseline model representative of the current, deterministic approach to loads analysis and rework. Key findings reveal the structural required margins are the dominant factor in reducing the risk of rework but the aerodynamic fidelity and load margin are important for balancing performance and uncertainty when considering financial implications within a finite budget.

A recap of the research development is given in the following section and followed by the major contributions from the experimental plan.

7.2 Research Development

The following is a brief summary of the research development for this thesis.

- ***Experimental Setup***

Addressed the research gap for modeling load cycles in aerospace structural design

- ***Epistemic Uncertainty***
  - **Research Question 1:** What are the appropriate methods for defining the prior probabilities of uncertain nodes in the Bayesian Network?
    * Assume Gaussian distribution for lift-curve slope correction factor uncertainty
    * Base mean value on fidelity level using K-factors
    * Base standard deviation on error relative to simulated truth data
  - Addressed the research gap for rigorous, data-driven estimation of epistemic uncertainty

- ***Experiment 1:*** *Determine Impact Of Uncertainty On Major Rework*
  - **Research Question 2:** How important is epistemic uncertainty to major rework relative to other sources?
    * They are significant to major rework relative to aleatory sources
    * Like all uncertainty, their significance is highly dependent on assumptions
  - Addressed the research gap for determining if correlations exist between aerodynamic fidelity and design rework

- ***Experiment 2:*** *Evaluate Uncertainty Management Optimization Approaches*

  - **Research Question 3:** How should the optimization problem be posed to effectively reduce and manage uncertainty in the loads analysis process?
    * Modified resource allocation methodology
    * Multi-objective function
    * Optimization on surrogate model instead of multi-stage approach
    * Unique cost constraints related to weight, rework, fidelity level and computational cost

- ***Experiment 3:*** *Determine Impact of Cost Functions On Major Rework*
- ***Experiment 4:*** *Evaluate Framework to Support Rework Decisions*
  - **Research Question 4:** For a given design scenario, what is the appropriate method to improve rework decisions regarding major rework in loads analysis?
    * For a given set of costs, optimizing the aerodynamic fidelity, load margin and structural margin improves rework decisions regarding major rework
  - Addressed the research gap for developing proactive rework strategies during the design phase

- ***Primary Hypothesis:*** *For a given design scenario, the proposed framework involving uncertainty quantification and management will lead to improved decisions regarding rework and performance compared to the current approach*

  - Accepted based on experimental plan, observations and results
  - Forms thesis statement

- ***Research Objective:*** *Develop a methodology for loads analysis to quantify and manage uncertainty related to aerodynamics and load case parameters in order to improve decision making for rework by optimizing fidelity, load margins and structural margins for new concepts*
  - Accomplished with rework decision framework utilizing unique resource allocation optimization and Bayesian network in conjunction with loads analysis M&S environment

7.3 Contributions

7.3.1 Integrated M&S Environment

The modeling and simulation environment for the loads analysis process is an important contribution. A great deal of effort was necessary to integrate the CFD, FEA and structural design programs together in MATLAB. Such an environment could be used as a testbed for more advanced studies in loads analysis and structural design. All the software programs utilized are capable of being scaled up to handle sophisticated, highly detailed models. Observations from the literature reveal that not a lot of aerospace research has been focused on modeling the load cycles in a development program so this is a relatively unique capability and particularly valuable for life cycle design.

The environment developed here was intended for commercial transport aircraft but is flexible enough to include other aerospace and even non-aerospace models. Many engineering systems experience aeroelastic loads from fluid (including liquid)

and are feedback coupled. Some examples of systems which could utilize this environment are unmanned airacft, military aircraft, rotorcraft, hypersonic vehicles, general aviation, rockets, missiles, propulsion systems, wind turbines, automobiles, watercraft, submarines, etc.

7.3.2 Epistemic Uncertainty Quantification

One of the identified research gaps was that many epistemic uncertainty studies in the literature do not use data-drive approaches for defining the sources of uncertainty for complex problems. Even studies which have developed advanced methods of quantifying episetmic uncertainty in various forms and from various types of data rarely demonstrate their techniques on realistic engineering problems and instead use simplified or even analytical problems. As detailed in Section 6.2, extensive work went into coupling both rigid and flexible CFD to NASTRAN in order to define the mean and standard deviation of the episemic uncertainty representation for each W_{KK} parameter.

Accurately defining epistemic uncertainty is one of the most significant challenges for UQ and also one of the major barriers of its wide-spread use in industry. This work defies the status quo and estimates this uncertainty with data rather than solely relying on subjective opinion or assumptions. Perhaps this work can serve as an example for bridging the gap between academic research and application.

The approach to defining aerodynamic epistemic uncertainty can also be beneficial, especially for NASTRAN users who rely on empirical adjustment factors and external aerodynamic data for calibration. According to industry experts, this is common practice in commercial transport design programs so this effort could serve as a starting point for uncertainty quantification. Especially given the fact that the demonstration model and modeling and simulation environment are fairly complex

and therefore give a more realistic picture of potential implementation.

Although the specific form of the W_{KK} matrix is specific to NASTRAN, it represents a correction to the lifting force slope which could be utilized in many aerodynamic analyses outside of NASTRAN. In closing, the epistemic uncertainty quantification work of this thesis contributed to filling a relevant gap in the literature which benefits the aerospace community, both academic and industrial.

7.3.3 Bayesian Network for Loads Analysis

Bayesian methods in general have been applied to aerodynamic, structural design and aeroelasticity individually but rarely to loads analysis and modeling the load cycles in a development program. Due to the complexity of loads analysis and the many interactions between loads, stress and design groups there are many potential uncertainty sources. Bayesian networks are especially suited for modeling many uncertain quantities and complex relationships through conditional dependence.

The sensitivity analysis and dimensionality reduction efforts related to Experiment 1 are examples of how large problems can become computationally feasible and enable the use of Bayesian networks for realistic problems. The results of Experiments 1, 3 and 4 demonstrate the effectiveness of using Bayesian networks and Bayesian methods in general to loads analysis, which could improve future efforts.

7.3.4 Uncertainty Management System for Loads Analysis

The results of Experiment 2 helped form the resource allocation optimization problem utilized in the rework decision framework. Carrying out the sub-experiments served as important test-beds for modifying the original method and using Bayesian inference in loads analysis.

Some contributions arose from these experiments which were not directly related

to the framework but still are important to the broader research community. The resource allocation method developed by Sankararaman (2012) and the Bayesian-based feedback decoupling approach of Liang (2016) are two powerful methods for MDAO. As was noted, both approaches had yet to be applied simultaneously to a problem. Experiment 2 filled this gap and demonstrates the effectiveness. The computational expense of the Bayesian inference in resource allocation can be offset by decoupling feedback systems. Even though the latter also uses Bayesian inference, Experiment 2 shows the computational effort is much smaller compared to the multiple realizations of the parameter update required by resource allocation. Thus this experiment can serve as an example for improving future design efforts by utilizing both approaches.

Enforcing compatibility with the methods suggested by Liang et al ultimately were not used in the final implementation of the rework decision framework. Yet, it is still possible they can be applied with future work to evaluate errors associated with the sub-optimization which occurs during the load cycles. As was alluded to in the discussion, this method of enforcing compatibility has the potential to enable modeling variations in the fidelity and margins during the load cycles.

7.3.5 Rework Decision Framework

The final experiments determined the sensitivity of the objective and constraint function parameters with respect to the important system responses. The rework cost and budget allocations were the dominant parameters so care should be taken in defining them. Seven design scenarios were developed and used in the framework to determine important trends. The framework was able to exhibit expected trends in analyzing the design scenarios which helped validate the problem formulation was appropriate.

Some of the key insights gained was the necessity of appropriately setting the

required margin to avoid rework. The K-factor and load margin had less impact on the ability to achieve a positive critical margin during the flight load survey but had a large impact on the cost functions and the ability to balance performance and uncertainty within the allocated budget.

Finally the rework decision framework was evaluated against a baseline model which represents the current approach to load analysis. In the end the framework was able to avoid major rework while providing more information on the system uncertainty and cost implications of the optimal design variables compared to the current approach.

The contributions of this thesis are encapsulated in the rework decision framework and summarized below:

1. Potential M&S testbed for future studies in aeroelastic loads analysis
2. Viable Bayesian network for uncertainty reduction and propagation in loads analysis
3. Unique Bayesian-based approach for uncertainty management in loads analysis which considers cost implications
4. Original, comprehensive framework to improve decision making in aerospace structural design and proactively address rework

7.4 Limitations and Future Work

7.4.1 Aerodynamic Modeling

Aerodynamic fidelity is an important focus of this thesis. With only two analysis methods to choose from (CFD and NASTRAN DLM) the definition of fidelity was somewhat restricted. A mid-fidelity analysis such as AVL (Athena Vortex Lattice) and a viscous CFD solver could have expanded the fidelity range to test its impact

on rework.

The W_{KK} empirical adjustments only allow for linear lifting force curve slope which in turn linearizes the calibration data. As was discussed, another method of supplementing NASTRAN with high fidelity data is the direct grid import method. This bypasses DLM and allows for nonlinear aerodynamics. This option was not explored due to the required remodeling effort, but this is an option which should be explored for future work. The linearization also called for a linear K-factor approach to simulating fidelity. The results for the W_{KK} error for the uncorrected and corrected compared to the truth data revealed there are nonlinearities which could not be captured by the K-factor. Using the direct grid import would circumvent this and allow for a nonlinear K-factor, or other measure, for fidelity.

In the current framework, the simulated high fidelity data to update the W_{KK} parameters were only from rigid CFD analysis. Future work could expand this and test the effects of updating the parameters with flexible CFD data during the load cycles.

Thirty-eight symmetric steady load cases were downselected to four critical cases in this work. In reality thousands of load cases of all different types are required in a development program which may lead to hundreds of critical cases. Therefore future studies must expand the load case design of experiment and include unsteady, asymmetric, gust and other important load case types. Naturally with this expansion more load case parameters would be necessary. For such studies it will again be critical to perform sensitivity analysis to reduce the problem size.

7.4.2 Uncertainty Definition

The epistemic uncertainty in the W_{KK} parameters was modeled as Gaussian with mean and standard deviation distribution parameters based on the rigid W_{KK} nominal values and relative errors. Due to an increased focus in the field of uncertainty quantification, there are advanced methods for defining distributions specifically for epsitemic uncertainty. Epistemic uncertainty in this thesis only represented model form error, but there are other types including data uncertainty, numerical error, etc and methods exist for defining and mitigating these types as well. Such approaches could be used here while maintaining a probability-based definition so Bayesian methods can still be applied.

Although this study focused much more on epistemic uncertainty than aleatory, global sensitivity analysis showed these sources were still significant. More effort could be made to define the aleatory uncertainty distributions for the load case parameters so they reflect realistic operational conditions. Also, other pertinent sources of aleatory uncertainty could be included such as material properties.

7.4.3 Structural Design

The structural design model used in this framework does not take advantage of the true strengths of HyperSizer. These choices were made to simplify the initial development but future work should use more advanced and realistic models to better estimate rework. Such changes would include a design of experiments for the structural optimizer which includes multiple component concepts (e.g. stiffened, sandwich, bonded, etc.), failure methods and materials. The DoE should not be uniform as was done here and instead should vary for the component types. For example, several stiffened panel concepts may be appropriate for the skins but not for the spars. In particular it would be remiss not to use HyperSizer's advanced composite modeling for

any future work, especially given the growth in composites in the aerospace industry. Such advanced modeling could be utilized with the same existing M&S environment and requires very little effort to implement into HyperSizer.

The structural margins and safety factors in this thesis were defined in the classical context, i.e. they were deterministic. This was largely due to simplifying the model and wanting to develop a framework which could easily be used under normal industry practices. There is a growing body of research on probabilistic and reliability-based approaches to defining margins or even alternative approaches. Such advanced approaches could be integrated into this framework but would likely required creating custom functions in HyperSizer or running Monte Carlo simulations of HyperSizer. One advantage of this approach would be to set custom required margins for each component, rather than assuming the same for the entire system as was done here.

7.4.4 Variations Between Load Cycles

The M&S environment developed in this thesis has the potential to include many important aspects of a real development program but were excluded from the initial development of the framework for simplification purposes. One of the most important aspects is modeling the variations in the system as the load cycles progress. In this thesis, the only changes which occurred in the system between load cycles was the loads, stiffness and component dimensions. In reality, the models in the initial load cycle are not the same ones used in the certification load cycle. The number of load cases and resolution of internal structure increases significantly throughout the load cycles. Additionally, as time progresses new information is gained, customer requirements may change, new high-level design decisions by upper management, market changes, etc. can impact the design.

Most of these variations can be captured within this M&S environment and accounted for in this framework to optimize the analysis fidelity and margins and support more realistic rework decisions. Naturally modeling such variations would significantly increase the problem size and require optimization after each load cycle. As shown in this thesis, surrogate modeling is an essential part to making this framework computationally feasible. Having discrete system changes between cycles means the approaches for DoE sampling to fit surrogates would most likely be highly inaccurate. The aforementioned Bayesian-based feedback decoupling method developed by Liang [83] potentially could be modified to enforce compatibility between surrogate models of different cycles and drastically decrease the number of samples needed. This approach was deemed out of scope for this thesis but should be explored for future work to test its validity. If true, it could serve as a key enabler for life cycle modeling and design.

7.4.5 Future Work Prioritization

Some key limitations of this thesis were discussed along with recommendations to overcome them in the future. Naturally not all of these recommendations are weighed equally and not all can feasibly be explored simultaneously. Thus the author's opinion on the prioritization of future work is given, here starting with the biggest priority:

1. ***Increase Load Case and Structural Design Resolution***

   Adding more load cases and implementing an advance HyperSizer model requires no significant change to the integrated M&S environment but results in substantial increases in the fidelity of the rework assessment.

2. ***Include Variations Between Load Cycles***

   An essential part of accurately modeling the loads process is to account

for internal and external changes in the system which naturally occur in all airplane development program as load cycles progress. This is a key enabler to life cycle design.

3. ***Improve Simulation of Aerodynamic Fidelity***

   Accurately simulating the effects of aerodynamic fidelity is a cornerstone of this thesis and requires new analysis methods be introduced representing various fidelity levels. Directly importing an external aero grid into NASTRAN and circumventing DLM is an important enabler for capturing nonlinear effects of fidelity on aerodynamic loads. Modeling other types of epistemic uncertainty (data, numerical, etc.) would also be an important improvement.

4. ***Improve aleatory uncertainty estimations***

   The sensitivity studies done in this thesis are ultimately based on the uncertainty definitions assumed. More effort should be made to realistically define the aleatory uncertainty in order to see how important they are relative to the epistemic sources.

7.5 Concluding Remarks

The rework decision framework developed in this thesis is an important first step to improving loads analysis and in general life cycle design. Bayesian-based methods have been shown to be viable approaches for modeling and mitigating uncertainty for advanced aerospace systems. I hope this work serves as a foundation for future work to address rework and uncertainty in design. Aerospace development programs continue to be plagued by cost overruns and delays and even reducing a small amount could produce significant savings and enhance the overall life cycle of aerospace systems.

APPENDIX A

NASCART-GT INPUT FILE

```
$ NASCART-GT Input File
$ All lines beginning with '$' or completely empty will be ignored


$ Case name
CASE_NAME uCRM LC 1 AoA 1.164607e+01 Iteration 0
$----------- Freestream conditions -----------$
$
$ Freestream velocity specified as either Mach number of velocity in
m/s (Do not specify both)
FREESTREAM_MACH_NUMBER 0.85

$ Freestream pressure in Pa
FREESTREAM_PRESSURE 16227.0

$ Freestream temperature in K
FREESTREAM_TEMPERATURE 216.6500

$ Angle of Attack in degrees (adjust orientation of freestream flow)
ANGLE_OF_ATTACK 0.0

$ Side slip angle in degrees (adjust orientation of freestream flow)
SIDE_SLIP_ANGLE 11.646072

$---------- Surface Boundary Conditions ----------$
$
$ Velocity boundary condition (SLIP for inviscid, NO_SLIP for viscous)
VELOCITY_BC SLIP

$ Thermal boundary condition (ISOTHERMAL, ADIABATIC)
THERMAL_BC ADIABATIC

$ Isothermal wall temperature in K
ISOTHERMAL_TEMPERATURE 300.0

$---------- Grid ----------$
$
$ Problem dimension (1D, 2D, 3D)
DIMENSION 3D

$ Axisymmetric (YES, NO)
AXISYMMETRIC NO

$ Minimum/Maximum values for grid
XMIN -100.0
XMAX 100.0
YMIN 0.0
YMAX 200.0
ZMIN -100.0
ZMAX 100.0
```

```
$ Root grid dimension (typically leave as 1, unless there's a specific
reason to change)
ROOT_CELLS_X 1
ROOT_CELLS_Y 1
ROOT_CELLS_Z 1

$ Domain boundary conditions (RIEMANN_INVARIANTS, FREESTREAM,
SUPERSONIC_OUTLET, SYMMETRY)
$ RIEMANN_INVARIANTS: farfield condition capable of handling both
subsonic and supersonic
$ FREESTREAM: Can be used where freestream flow enters domain only if
supersonic
$ SUPERSONIC_OUTLET: Can be used where freestream flow exits domain
only if supersonic
$ SYMMETRY: Applies symmetry condition
XMIN_BC RIEMANN_INVARIANTS
XMAX_BC RIEMANN_INVARIANTS
YMIN_BC SYMMETRY
YMAX_BC RIEMANN_INVARIANTS
ZMIN_BC RIEMANN_INVARIANTS
ZMAX_BC RIEMANN_INVARIANTS

$ Initial refinement level (results in an initial mesh of 2^n x 2^n x
2^n for each root cell)
INITIAL_REFINEMENT_LEVEL 3

$---------- Geoemtry Configuration ----------$
$
$ Geometry configuration file name (name of file containing input
geometry information)
$ If no geometry is to be used, then specify NONE
GEOMETRY_CONFIG_FILE geometryConfiguration.input
$GEOMETRY_CONFIG_FILE NONE

$---------- Gas Properties ----------$
$
$ Chemistry Model (CPG_AIR, CPG_USER_DEFINED, REACTING)
THERMOCHEMICAL_MODEL CPG_AIR

$ Location of mixture model (only for REACTING or CPG_USER_DEFINED)
MIXTURE_MODEL_PATH NONE

$ Temperature model (only for REACTING), (ONE_TEMPERATURE,
TWO_TEMPERATURE)
TEMPERATURE_MODEL ONE_TEMPERATURE

$---------- Simulation Parameters ----------$
$
$ Simulation type (NAVIER_STOKES (includes Euler), BODY_ONLY)
```

```
SIMULATION NAVIER_STOKES

$ Initiate simulation from restart file (YES,NO)
RESTART NO

$ Use a restart file (<name of restart file>)
RESTART_FILE restart_previous.output

$ Number of iterations
NUMBER_OF_ITERATIONS 10000

$ Simulation time (use large number to ignore this convergence
criterion)
SIMULATION_TIME 1.0E10

$ Convergence criteria: normalized RMS error of all conserved
variables
RMS_CONVERGENCE 1.0e-8

$ Time integration scheme (EXPLICIT_EULER, HANCOCK_PC, RK4, TVD_RK3,
SSP_RK45, SSP_RK34, SSP_RK35, SSP_RK410, LUSSOR)
TIME_SCHEME TVD_RK3

$ Local vs. global time-stepping (LOCAL, GLOBAL)
TIME_STEP_APPROACH GLOBAL

$ Choose time step based on CFL number (YES, NO)
CFL_DRIVEN YES

$ Starting CFL number (requires CFL_DRIVEN = YES)
CFL_START 1.0

$ Ending CFL number for linear ramping (requires CFL_DRIVEN = YES)
CFL_END 1.0

$ Iteration number to begin CFL ramping (requires CFL_DRIVEN = YES)
CFL_START_ITERATION 100

$ Iteration number to end CFL ramping (requires CFL_DRIVEN = YES)
CFL_END_ITERATION 1000

$ Specified constant time step (requires CFL_DRIVEN = NO)
TIME_STEP 5.0E-6

$ Inviscid flux scheme (ROE, AUSMPW+, HLLC, M-AUSMPW+, AUSM+up2)
INVISCID_FLUX_SCHEME ROE

$ Extrapolation for invscid flux scheme (UPWIND_1, MUSCL_2, MUSCL_3,
NASCART_MUSCL_2, NASCART_MUSCL_3, WENO_3, WENO_5, MLP_3, MLP_5)
EXTRAPOLATION_SCHEME WENO_3
```

```
$ Extrapolation limiter (NONE, MINMOD, SUPERBEE, SWEBY, VAN_LEER),
(only for MUSCL_2, MUSCL_3)
LIMITER NONE

$ Viscous case (YES, NO)
VISCOUS NO

$ Viscous flux scheme, VISCOUS must be set to YES
(CENTRAL_DIFFERENCE_2)
VISCOUS_FLUX_SCHEME CENTRAL_DIFFERENCE_2

$ Turbulence (YES, NO)
$ (Not supported yet)
TURBULENCE NO

$ Turbulence formulation, TURBULENCE must be set to YES (RANS, LES,
RANS_LES, PANS)
TURBULENCE_FORMULATION RANS

$ RANS model (K_OMEGA, K_EPSILON, SST)
RANS_MODEL K_OMEGA

$ Point interpolation method (NEAREST_POINT, DISTANCE_WEIGHTED,
LEAST_SQUARES)
POINT_INTERPOLATION DISTANCE_WEIGHTED

$---------- Solution-based grid adaption ----------$
$
$ Apation frequency (a value of "0" is equivalent to turning off
solution adaption)
ADAPTION_FREQUENCY 500

$ Iteration at which to start solution adaption
ADAPTION_START 500

$ Iteration at which to stop solution adaption
ADAPTION_STOP 8000

$ Solution adaption normalized gradient parameters
$ The numerical value represents a scale factor with
$ respect to the mean gradient throughout the flowfield
$ The MIN parameter specifies where the mesh should be coarsened
$ The MAX parameter specifies where the mesh should be refined
$ Negative values for MIN will ensure that that parameter will not
coarsen the mesh
$ Very large values for MAX will ensure that that parameter will not
refine the mesh
MIN_DIVERGENCE 0.3
MAX_DIVERGENCE 0.8
```

```
MIN_VORTICITY -0.5
MAX_VORTICITY 1.0e10
MIN_PRESSURE_GRADIENT -0.5
MAX_PRESSURE_GRADIENT 1.0e10
MIN_TEMPERATURE_GRADIENT -0.5
MAX_TEMPERATURE_GRADIENT 1.0e10
MIN_MACH_GRADIENT -0.5
MAX_MACH_GRADIENT 1.0e10

$ Solution adaption bounds - only allows solution adaption within the
specified box
$ For no restrictions, bounds must be greater than computational
domain
XMIN_ADAPTION -1.0E10
XMAX_ADAPTION 1.0E10
YMIN_ADAPTION -1.0E10
YMAX_ADAPTION 1.0E10
ZMIN_ADAPTION -1.0E10
ZMAX_ADAPTION 1.0E10

$---------- Aerodynamic Reference Quantities ----------$
$

$ Reference length to be used for computing moment coefficient
AERO_REFERENCE_LENGTH 7.224

$ Area to be used for computing lift, drag, and moment coefficients
AERO_REFERENCE_AREA 812.542

$ Center about which to calculate aerodynamic moment
AERO_MOMENT_CENTER_X 0.25
AERO_MOMENT_CENTER_Y 0.0
AERO_MOMENT_CENTER_Z 0.0

$---------- Output Options ----------$
$
$ Location of visual output data (NODE_CENTERED, CELL_CENTERED)
VISUALIZATION_LOCATION CELL_CENTERED

$ Frequency to write out visualization output data
VISUALIZATION_FREQUENCY 100

$---------- Parallel computing options ----------$
$
$ Number of CPU nodes to partition grid (NOT IMPLEMENTED YET, will use
MPI)
NUMBER_OF_CPU_NODES 1

$ Options for threads (ALL, SINGLE, USER_DEFINED)
$ Use ALL if computational resources provide multi-core option
```

```
$ ALL will use all available threads on single compute node, but
$ will not distribute across multi-node setup
$ Uses OpenMP
THREAD_OPTION ALL

$ Threads per node (specify number of threads if THREAD_OPTION =
USER_DEFINED)
THREADS_PER_NODE 1
```

REFERENCES

[1] "Boeings 787: trials, tribulations, and restoring the dream," *Reinforced Plastics*, p. 6, Novembe/December 2009 2009.

[2] "Skylon assessment report," tn, European Space Agency, 06/05/2011 2011.

[3] "Easy meshing with structured accuracy: Overset grids in pointwise," 2012.

[4] "Part 25 - airworthiness standards: Transport category airplanes," 2015.

[5] Abbot, I. H. and Von Doenhoff, A. E., *Theory of Wing Sections*. New York: Dover Publications Inc., 1959.

[6] Acar, E., "Reliability-based design of representative wing and tail system together with structural tests," *Journal of Aircraft*, vol. 48, no. 6, pp. 2130–2144, 2011.

[7] Ainsworth, J., "Composit design & analysis," in *The Composites and Advanced Materials Expo*, (Hampton, VA), Collier Reserch Corporation.

[8] Anderson, E. J. and Ferris, M. C., "A direct search algorithm for optimization with noisy function evaluations," *SIAM Journal on optimization*, vol. 11, no. 3, pp. 837–857, 2001.

[9] Anderson, J. D., *Fundamentals of Aerodynamics*. McGraw-Hill Education, 5 ed., 2010.

[10] Andres, S. P., Juan, J. A., Francisco, P., Matthew, F. B., and Michael, S. E., "Multi-fidelity uncertainty quantification: Application to a vertical axis wind turbine under an extreme gust," 2014.

[11] Arundachawat, P., Roy, R., Al-Ashaab, A., and Shehab, E., "Design rework prediction in concurrent design environment: Current trends and future research directions," in *19th CIRP Design Conference*.

[12] Arundachawat, P., *The Development Of Methods To Estimate And Reduce Design Rework*. Thesis, 2012.

[13] Asmussen, S. and Glynn, P. W., *Stochastic Simulation: Algorithms and Analysis*. Stochastic Modelling and Applied Probability, Springer-Verlag New York, 1 ed., 2007.

[14] Baals, D. D. and Corliss, W. R., "Wind tunnels of nasa."

[15] Baldelli, D. H., Chen, P. C., and Panza, J., "Unified aeroelastic and flight dynamic formulation via rational function approximations," *Journal of Aircraft*, vol. 43, no. 3, pp. 763–772, 2006.

[16] Bansal, P. and Pitt, D. M., "Stochastic variations in aerodynamic influence coefficients (aics): Effects on flutter prediction of a generic wing," April 8-11 2013.

[17] Barton, R. R. and Ivey Jr, J. S., "Nelder-mead simplex modifications for simulation optimization," *Management Science*, vol. 42, no. 7, pp. 954–973, 1996.

[18] Batchelor, *An introduction to fluid dynamics*. Cambridge University Press, 1973.

[19] Bayes, T. and Price, R., "An essay towards solving a problem in the doctrine of chances," *Philosophical Transactions of the Royal Society of London*, vol. 53, pp. 370–418, 1763.

[20] Beyer, H.-G. and Sendhoff, B., "Robust optimization a comprehensive survey," *Computer Methods in Applied Mechanics and Engineering*, vol. 196, no. 33-34, pp. 3190–3218, 2007.

[21] Bower, A. F., *Applied Solid Mechanics*. CRC Press, 1 ed., 2009.

[22] Brevault, L., Balesdent, M., and Brend, N., "Decoupled multidisciplinary design optimization formulation for interdisciplinary coupling satisfaction under uncertainty," *AIAA Journal*, vol. 54, no. 1, 2016.

[23] Carlsson, M. and Kuttenkeuler, J., "Design and testing of a blended wing body aeroelastic wind-tunnel model," *Journal of Aircraft*, vol. 40, no. 1, pp. 211–213, 2003.

[24] Caticha, A. and Preuss, R., "Maximum entropy and bayesian data analysis: Entropic prior distributions," *Phys Rev E Stat Nonlin Soft Matter Phys*, vol. 70, no. 4 Pt 2, p. 046127, 2004.

[25] Cavagna, L., Ricci, S., and Travaglini, L., "Aeroelastic analysis and optimization at conceptual design level using neocass suite," 4-7 April, 2011 2011.

[26] ChanHoon, C., SangJoon, S., and Taehyoun, K., "A new robust aeroelastic analysis including aerodynamic uncertainty from varying mach numbers," 2008.

[27] Chen, W., Jin, R., and Sudjianto, A., "Analytical variance-based global sensitivity analysis in simulation-based design under uncertainty," *Journal of Mechanical Design*, vol. 127, no. 5, p. 875, 2005.

[28] Chen, X., Zha, G.-C., and Yang, M.-T., "Numerical simulation of 3-d wing flutter with fully coupled fluidstructural interaction," *Computers & Fluids*, vol. 36, no. 5, pp. 856–867, 2007.

[29] Chris, P., Muhammad, H., and Philip, B., "Gust loads with uncertainty due to imprecise gust velocity spectra," 2007.

[30] Christine V. Jutte, B. K. S., "Aeroelastic tailoring of transport aircraft wings: State-of-the-art and potential enabling technologies," 2014.

[31] Clarke, C. and Carswell, B., *Principles of Astrophysical Fluid Dynamics*. Cambridge University Press.

[32] Collopy, P. D. and Hollingsworth, P. M., "Value-driven design," *Journal of Aircraft*, vol. 48, no. 3, pp. 749–759, 2011.

[33] Company, T. B., "Boeing current market outlook 2014," report, 2014.

[34] Coppe, A., Haftka, R. T., Kim, N. H., and Yuan, F.-G., "Uncertainty reduction of damage growth properties using structural health monitoring," *Journal of Aircraft*, vol. 47, no. 6, pp. 2030–2038, 2012.

[35] Corporation, C. R., "Hypersizer support documentation," 2015.

[36] Corporation, M. S., "Msc nastran aeroelastic user's guide," 2004.

[37] Dagum, Paul; Galper, A., "Dynamic network models for forecasting," in *Eighth Conference on Uncertainty in Artificial Intelligence*, pp. 41–48, AUAI Press.

[38] d'Alembert, J. l. R., "Essai d'une nouvelle thorie de la rsistance des fluides," 1752.

[39] Dawson, B., Fixson, S. K., and Whitney, D., "Orchestrating coordination: Reducing rework in complex product development," Report 4, 2012.

[40] Denning, S., "What went wrong at boeing," *Strategy & Leadership*, vol. 41, no. 3, pp. 36–41, 2013.

[41] Diamanti, K. and Soutis, C., "Structural health monitoring techniques for aircraft composite structures," *Progress in Aerospace Sciences*, vol. 46, no. 8, pp. 342–352, 2010.

[42] Dimitrios, I. P. and Costas, P., "Uncertainty propagation for robust aerodynamic shape optimization," 2014.

[43] Ding, C., He, X., Zha, H., and Simon, H., "Adaptive dimension reduction for clustering high dimensional data," in *International Conference on Data Mining*, pp. 147–154, IEEE.

[44] Dym, C. L. and Williams, H. E., *Analytical Estimates of Structural Behavior*. CRC Press, 2012.

[45] Everest, F., *The Master Handbook of Accoustics*. New York: McGraw-Hill, 2001.

[46] Eymard, R., Gallout, T., and Herbin, R., *Finite volume methods*, vol. Volume 7, pp. 713–1018. Elsevier, 2000.

[47] Fischer, D. E., Anderson, J., and Ram, R., "2013 commercial aerospace industry perspective," report, Strategy&, 2012.

[48] Fisher, R. A., "On the mathematical foundations of theoretical statistics," *Philosophical Transactions of the Royal Society of London. Series A, Containing Papers of a Mathematical or Physical Character*, vol. 222, no. 594-604, pp. 309–368, 1922.

[49] Flow Science, I., ""what are artificial and numerical viscosities?"," 2016.

[50] Frank, C. P. ., Ataniany, M. F., Pinon-Fischerz, O. J., and Mavris, D. N., "A conceptual design framework for performance, life-cycle cost, and safety evaluation of suborbital vehicles," 2016.

[51] Fujikubo, M., "Structural analysis for the design of vlfs," *Marine Structures*, vol. 18, no. 2, pp. 201–226, 2005.

[52] Garrick, L. E., "Aeroelasticity-frontiers and beyond," *Journal of Aircraft*, vol. 13, no. 9, pp. 641–657, 1976.

[53] Gates, D., "Boeing 787 may not fly this year," July 22, 2009 2009.

[54] Gates, D., "Boeing 787 wing flaw extends inside plane," July, 30, 2009 2009.

[55] Gates, D., "Boeing celebrates 787 delivery as programs costs top $32 billion," September 24, 2011 2011.

[56] Giesing, J. P., Kalman, T. P., and Rodden, W. P. Report AFFDL-TR-71-5, Air Force Flight Dynamics Laboratory, 1971-1972.

[57] Gikhman, I. I. and Skorokhod, A. V., *Introduction to the Theory of Random Processes*. Courier Corporation, 1969.

[58] Goldstein, E., "Wind tunnels: Don't count them out," *Aerospace America*, vol. 48, no. 4, pp. 38 %@ 0740–722X, 2010.

[59] Guyon, I. and Elisseeff, A., "An introduction to variable and feature selection," *Journal of Machine Learning Research*, vol. 3, pp. 1157–1182, 2003.

[60] Hamed, K. and Jonathan, E. C., "Propagation of structural uncertainty to worst case gust loads predictions," 2013.

[61] Helton, J. C., "Conceptual and computational basis for the quantification of margins and uncertainty," Report SAND2009-3055, Sandia National Laboratories, 2009.

[62] Humphrey, D. G. and Wilson, J. R., "A revised simplex search procedure for stochastic simulation response surface optimization," *INFORMS Journal on Computing*, vol. 12, no. 4, pp. 272–283, 2000.

[63] Hwang, C. L. and Masud, A., *Multiple Objective Decision Making - Methods and Applications*. Lecture Notes in Economics and Mathematical Systems, Springer-Verlag Berlin Heidelberg, 1979.

[64] Iman, R., Helton, J., and Campbell, J., "An approach to sensitivity analysis of computer models, part 1. introduction, input variable selection and preliminary variable assessment," *Journal of Quality Technology*, vol. 13, no. 3, pp. 174–183, 1981.

[65] Jaehun, L., Maenghyo, C., Heung Soo, K., and Jun-Sik, K., "Layup optimization of laminated composite patches considering uncertainty of material properties," 2010.

[66] James, L., Hemsch, M. I., and Joseph, M., "Uncertainty in computational aerodynamics," 2003.

[67] J.Goldberger, S.Roweis, G.Hinton, and R.Salakhutdinov, "Neighbourhood components analysis," *Advances in Neural Information Processing Systems*, vol. 17, pp. 513–520, 2005.

[68] Jones, H., "Common cause failures and ultra reliability," 15 - 19 July 2012.

[69] Kameyama, M. and Fukunaga, H., "Laminate design of composite plate wings for aeroelastic characteristics using real-coded distributed genetic algorithms," 20 - 22 September 2004.

[70] Kaufmann, M., Zenkert, D., and Wennhage, P., "Integrated cost/weight optimization of aircraft structures," *Structural and Multidisciplinary Optimization*, vol. 41, no. 2, pp. 325–334, 2009.

[71] Kenway, G. K. W., Martins, J. R. R. A., and Kennedy, G. J., "Aerostructural optimization of the common research model configuration," 16-20 June 2014.

[72] Keum, W. L. and Sahjendra, N. S., "Multi-input higher-order sliding mode control of aeroelastic systems with uncertainties and gust load," 2014.

[73] King, J. M. C., "The airbus 380 and boeing 787: A role in the recovery of the airline transport market," *Journal of Air Transport Management*, vol. 13, no. 1, pp. 16–22, 2007.

[74] Kirby, M. and Mavris, D., *An approach for the intelligent assessment of future technology portfolios*. Aerospace Sciences Meetings, American Institute of Aeronautics and Astronautics, 2002.

[75] Kohavi, R. and Provost, F., "Glossary of terms," *Machine Learning*, vol. 30, no. 2-3, pp. 271–274, 1998.

[76] Komahan, B., Markus, P. R., and Raymond, M. K., "Robust optimization of a wing under structural and material uncertainties," 2008/09/01 2015.

[77] Kononenko, I., Simec, E., and Sikonja, M. R., "Overcoming the myopia of inductive learning algorithms with relieff," *Applied Intelligence*, vol. 7, pp. 39–55, 1997.

[78] Krige, D. G., *A statistical approach to some mine valuations and allied problems at the Witwatersrand*. Thesis, 1951.

[79] Kroo, I., "Aircraft design: Synthesis and analysis."

[80] Larsen, C. E. and Raju, I. S., "Moving aerospace structural design practice to a load and resistance factor approach," January 4-8 2016.

[81] Lee, J. J., Lukachko, S. P., Waitz, I. A., and Schafer, A., "Historical and future trends in aircraft performance, cost, and emissions," *Annual Review of Energy and the Environment*, vol. 26, no. 1, pp. 167–200, 2001.

[82] Li, C. and Mahadevan, S., "Variance reduction estimation in bayesian inference," 2017.

[83] Liang, C., *Multidisciplinary Analysis and Optimization under Uncertainty*. Thesis, 2016.

[84] Liang, C. and Mahadevan, S., "Bayesian sensitivity analysis and uncertainty integration for robust optimization," *Journal of Aerospace Information Systems*, vol. 12, no. 1, pp. 189–203, 2015.

[85] Liang, C. and Mahadevan, S., "Multidisciplinary optimization under uncertainty using bayesian network," *SAE International Journal of Materials and Manufacturing*, vol. 9, no. 2, 2016.

[86] Lissaman, P. B. S., "Low-reynolds-number airfoils," *Annual Review of Fluid Mechanics*, vol. 15, p. 17, 1983.

[87] Lomax, T. L., *Structural Loads Analysis for Commercial Transport Aircraft*. AIAA Education Series, American Institute of Aeronautics and Astronautics, 1996.

[88] Lyonnet, M., Deleglise, B., and Lesant, Y., "Application of pressure sensitive paint technique in the s1ma onera wind tunnel," 14-17 January 2002.

[89] Lyu, Z., Kenway, G. K. W., and Martins, J. R. R. A., "Aerodynamic shape optimization investigations of the common research model wing benchmark," *AIAA Journal*, vol. 53, no. 4, pp. 968–985, 2015.

[90] Malone, P. and Smoker, R., "Increasing development cost estimate accuracy of complex systems using advanced tools," 2012.

[91] Markov, A., "Rasprostranenie zakona bol'shih chisel na velichiny, zavisyaschie drug ot druga," *Izvestiya Fiziko-matematicheskogo obschestva pri Kazanskom universitete*, p. 135156, 1906.

[92] Maskew, B., "Program vsaero theory document: A computer program for calculating nonlinear aerodynamic characteristics of arbitrary configurations," 1987.

[93] Matheron, G., "Principles of geostatistics," *Economic Geology*, vol. 58, p. 12461266, 1963.

[94] Matsumura, T. and Haftka, R. T., "Reliability based design optimization modeling future redesign with different epistemic uncertainty treatments," *Journal of Mechanical Design*, vol. 135, no. 9, p. 091006, 2013.

[95] Matsumura, T., Haftka, R. T., and Kim, N. H., "Conservativeness in failure probability estimate: Redesign risk vs. performance," 2013.

[96] Matsumura, T., Haftka, R. T., and Sankar, B. V., "Reliability estimation including redesign following future test for an integrated thermal protection system," 2011.

[97] Matthew, R., Ramana, G., and Raymond, K., "Quantification of modeling uncertainty in aeroelastic design," 2010.

[98] Matthies, H. G. and Steindorf, J., "Partitioned strong coupling algorithms for fluidstructure interaction," *Computers & Structures*, vol. 81, no. 811, pp. 805–812, 2003.

[99] Mohammad, R. and Masoud, R.-R., "Modeling and uncertainty quantification of nanofiber enhanced polymer composite materials with functionally graded interphase properties," 2011.

[100] Mukhopadhyay, V., "Historical perspective on analysis and control of aeroelastic responses," *Journal of Guidance, Control, and Dynamics*, vol. 26, no. 5, pp. 673–684, 2003.

[101] Mullur, A., Hajela, P., and Bahei-El-Din, Y., "Uncertainty management in design optimization of coupled systems," 2006.

[102] Murphy, B., OCallaghan, J., Fox, M., Ilcewicz, L., and Starnes, J. H., "Overview of the structures investigation for the american airlines flight 587 investigation," 18 - 21 April 2005.

[103] Murua, J., Palacios, R., and Graham, J. M. R., "Applications of the unsteady vortex-lattice method in aircraft aeroelasticity and flight dynamics," *Progress in Aerospace Sciences*, vol. 55, pp. 46–72, 2012.

[104] Murugan, S., Harursampath, D., and Ganguli, R., "Material uncertainty propagation in helicopter nonlinear aeroelastic response and vibratory analysis," *AIAA Journal*, vol. 46, no. 9, pp. 2332–2344, 1966.

[105] Nastran, M. S. C., "Quick reference guide," report, 2014.

[106] Navier, C. L. M. H., *Memoire sur les lois du mouvement des fluides*, pp. 389–440. 1827.

[107] Neal, R. M., "Slice sampling," *The Annals of Statistics*, vol. 31, no. 3, pp. 705–767, 2003.

[108] Nelder, J. A. and Mead, R., "A simplex method for function minimization," *The computer journal*, vol. 7, no. 4, pp. 308–313, 1965.

[109] Niu, M. C.-Y., *Airframe stress analysis and sizing*, vol. 2. Conmilit Press Hong Kong, 1997.

[110] Opgenoord, M. M. J. and Willcox, K. E., "Sensitivity analysis methods for uncertainty budgeting in system design," *AIAA Journal*, vol. 54, no. 10, 2016.

[111] Ostergaard, M. G., Ibbotson, A. R., Roux, O. L., and Prior, A. M., "Virtual testing of aircraft structures," *CEAS Aeronautical Journal*, vol. 1, no. 1-4, pp. 83–103, 2011.

[112] Ostrower, J., "Understanding the 787 structural reinforcement (update1)," 2009.

[113] Pae, P., "Airbus giant-jet gamble okd in challenge to boeing; aerospace: Eu rebuffs clinton warning that subsidies for project could lead to a trade war," December 20, 2000 2000.

[114] Patankar, S. V., *Numerical Heat Transfer and Fluid FLow*. Hemisphere Publishing Corporation, 1980.

[115] Patrick, M., Keenan, C., Dmitry, P., Yiying, T., and Mathieu, D., "Energy-preserving integrators for fluid animation," *ACM Trans. Graph. %@ 0730-0301*, vol. 28, no. 3, pp. 1–8, 2009.

[116] Pearl, J., "Bayesian networks: A model of self-activated memory for evidential reasoning," 15-17th August 1985.

[117] Peoples, R. and Willcox, K., "Value-based multidisciplinary optimization for commercial aircraft design and business risk assessment," *Journal of Aircraft*, vol. 43, no. 4, p. 9, 2006.

[118] Platanitis, G. and Strganac, T. W., "Suppression of control reversal using leading- and trailing-edge control surfaces," *Journal of Guidance, Control, and Dynamics*, vol. 28, no. 3, pp. 452–460, 2005.

[119] Price, N. B., Balesdent, M., Defoort, S., Le Riche, R., Kim, N. H., and Haftka, R. T., "Simulating future test and redesign considering epistemic model uncertainty," 2016.

[120] Price, N. B., Matsumura, T., Haftka, R. T., and Kim, N. H., "Deciding how conservative a designer should be: Simulating future tests and redesign," 2014.

[121] Pudil, P. and Novoviov, J., *Novel Methods for Feature Subset Selection with Respect to Problem Knowledge*, vol. 453 of *The Springer International Series in Engineering and Computer Science*, book section 7, pp. 101–116. Springer US, 1998.

[122] Rebane, G.; Pearl, J., "The recovery of causal poly-trees from statistical data," in *3rd Workshop on Uncertainty in AI*, p. 222228.

[123] Reddy, J. N., *An Introduction to the Finite Element Method*. McGraw-Hill Higher Education, 2006.

[124] Rediess, H. and Melton, H., "Integrated flight test environment - a concept for integration of simulation with flight test," 1994.

[125] Ricketts, R., "Experimental aeroelasticity - history, status and future in brief," 2-4 April 1990.

[126] Robbins, H. and Sutton, M., "A stochastic approximation method," *The Annals of Mathematical Statistics*, vol. 22, no. 3, pp. 400–407, 1951.

[127] Robnik-Sikonja, M. and Kononenko, I., "An adaptation of relief for attribute estimation in regression," in *Machine Learning: Proceedings of the Fourteenth International Conference*, pp. 296–304.

[128] Rodden, E. A. and P., W., "A doublet lattice method for calculating lift distributions on oscillating surfaces in subsonic flows," January 22-24, 1968 1968.

[129] Rodden, W. P. and Revell, J. D., "The status of unsteady aerodynamic influence coefficients," *Institute of the Aeronautical Sciences*, vol. Fairchild Fund Paper No. FF-33, 1962.

[130] Rosenblatt, M., "Remarks on some nonparametric estimates of a density function," *The Annals of Statistics*, vol. 27, pp. 832–837, 1956.

[131] Roweis, S. T. and Saul, L. K., "Nonlinear dimensionality reduction by locally linear embedding," *Science*, vol. 290, no. 5500, pp. 2323–6, 2000.

[132] Rswarbrick, "Yield surfaces," 2009.

[133] Ruffin, S., O'Brien, D., Smith, M., Hariharan, N., Lee, J.-D., and Sankar, L., "Comparison of rotor-airframe interaction utilizing overset and unstructured grid techniques," 5 - 8 January 2004.

[134] Ruffin, S. M., "Nascart-gt: A viscous solution- adaptive cartesian grid flow solver," report, Georgia Institute of Technology School of Aerospace Engineering.

[135] Saltelli, A., Ratto, M., Andres, T., and Campolongo, F., *Global Sensitivity Analysis: The Primer*. New York: John Wiley & Sons, 2008.

[136] Samuel, A. L., "Some studies in machine learning using the game of checkers," *IBM Journal of Research and Development*, 1959.

[137] Sankararaman, S., *Uncertainty Quantification And Integration In Engineering Systems*. Thesis, 2012.

[138] Sankararaman, S., Ling, Y., Shantz, C., and Mahadevan, S., "Inference of equivalent initial flaw size under multiple sources of uncertainty," *International Journal of Fatigue*, vol. 33, no. 2, pp. 75–89, 2011.

[139] Sankararaman, S. and Mahadevan, S., *Bayesian Methodology for Uncertainty Quantification in Complex Engineering Systems*, pp. 117–146. 2014.

[140] Sankararaman, S., Mahadevan, S., McLemore, K., Bradford, S., Liang, C., and Peterson, L., "Test resource allocation for uncertainty quantification of multi-level and coupled systems," 2011.

[141] Sankararaman, S., McLemore, K., Mahadevan, S., Bradford, S. C., and Peterson, L. D., "Test resource allocation in hierarchical systems using bayesian networks," *AIAA Journal*, vol. 51, no. 3, pp. 537–550, 2013.

[142] Schmitt, V. and Charpin, F., "Pressure distributions on the onera-m6-wing at transonic mach numbers," Report AR 138, AGARD, May 1979.

[143] Schweikhard, W., "Flight test made easy – doing simple flight tests simply," 1983.

[144] Schwenn, R. E., Brink, H., Mebane, C. T., Seales, S. C., and Wintfeld, J. R., "Defense acquisitions: Assessments of selected weapon programs," 2009.

[145] Scott, L. P. and Dimitri, N. M., *Robust Design of Aeroelastically Tailored Composite Plates Using a New Formulation of Anti-Optimization and Optimization*. AIAA SciTech, American Institute of Aeronautics and Astronautics, 2015.

[146] Shafer, G., *A Mathematical Theory of Evidence*. Princeton University PRess, 1976.

[147] Shafer, G., "Dempster-shafer theory," report, 2002.

[148] Shams, R., "Dollar-euro exchange rate 1999-2004 -dollar and euro as international currencies," Report 1616-4814, Hamburg Institute of International Economics (HWWA), 2005.

[149] Shapiro, A. H., *The Dynamics of Thermodynamics of Compressible Fluid Flow*, vol. II. The Ronald Press Company, 1954.

[150] Shirk, M. H., Hertz, T. J., and Weisshaar, T. A., "Aeroelastic tailoring - theory, practice, and promise," *Journal of Aircraft*, vol. 23, no. 1, pp. 6–18, 1986.

[151] Simpson, T. W., Poplinski, J. D., Koch, P. N., and Allen, J. K., "Metamodels for computer-based engineering design: Survey and recommendations," *Engineering with Computers*, vol. 17, no. 2, pp. 129–150, 2001.

[152] Smith, J. E. and Heath, L. S., "Identifying influences on model uncertainty: An application using a forest carbon budget model," *Environmental Management*, vol. 27, no. 2, pp. 253–267, 2001.

[153] Smith, S. B. and Nelson, D. W., "Determination of the aerodynamic characteristics of the mission adaptive wing," *Journal of Aircraft*, vol. 27, no. 11, 1990.

[154] Sobieszczanski-Sobieski, J., "optimization by decomposition: A step from hierarchic to non-hierarchic systems," Report TR-CP-3031, NASA, 1988.

[155] Soutis, C., "Fibre reinforced composites in aircraft construction," *Progress in Aerospace Sciences*, vol. 41, no. 2, pp. 143–151, 2005.

[156] Struk, P., Oeftering, R., Easton, J., and Anderson, E., "Semi-automated diagnosis, repair, and rework of spacecraft electronics," 2008.

[157] Stults, I. C., *A Multi-Fidelity Analysis Selection Method Using A Constrained Discrete Optimization Formulation*. Thesis, 2009.

[158] Swiler, L., Paez, T., Mayes, R., and Eldred, M., *Epistemic Uncertainty in the Calculation of Margins*. Structures, Structural Dynamics, and Materials and Co-located Conferences, American Institute of Aeronautics and Astronautics, 2009.

[159] Tang, C. S. and Zimmerman, J. D., "Managing new product development and supply chain risks: The boeing 787 case," *Supply Chain Forum*, vol. 10, no. 2, pp. 74–86, 2009.

[160] Tartaruga, I., Sartor, P., Cooper, J. E., Coggon, S., and Lemmens, Y., "Efficient prediction and uncertainty propagation of correlated loads," 5-9 Januray, 2015 2015.

[161] The Mathworks, I., "Matlab: On-line documentation."

[162] Thompson, J. F. and Weatherill, N. P., "Structured and unstructured grid generation," *Critical reviews in biomedical engineering*, vol. 20, no. 1-2, pp. 73–120, 1992.

[163] Tibshirani, R., "Regression shrinkage and selection via the lasso," *Journal of the Royal Statistical Society*, vol. 58, no. 1, pp. 267–288, 1996.

[164] Tu, S.-Z. and Ruffin, S., "Solution adaptive, unstructured cartesian-grid methodology for chemically reacting flow," 24-26 June 2002.

[165] Unay, E., *Load Analysis Of An Aircraft Using Simplified Aerodynamic And Structural Models*. Masters, 2015.

[166] Unkown, "Center of gravity limits," Unkown.

[167] Urbina, A., Mahadevan, S., and Paez, T., *Resource Allocation Using Quantification of Margins and Uncertainty*. Structures, Structural Dynamics, and Materials and Co-located Conferences, American Institute of Aeronautics and Astronautics, 2010.

[168] Urbina, A., Mahadevan, S., and Paez, T. L., "Quantification of margins and uncertainties of complex systems in the presence of aleatoric and epistemic uncertainty," *Reliability Engineering & System Safety*, vol. 96, no. 9, pp. 1114–1125, 2011.

[169] Van Zyl, L. H. and Mathews, E. H., "Aeroelastic analysis of t-tails using an enhanced doublet lattice method," *Journal of Aircraft*, vol. 48, no. 3, pp. 823–831, 2011.

[170] Vassberg, J., Dehaan, M., Rivers, M., and Wahls, R., "Development of a common research model for applied cfd validation studies," 18-21 August 2008 2008.

[171] Villanueva, D., Haftka, R. T., and Sankar, B. V., "Accounting for future redesign to balance performance and development costs," *Reliability Engineering & System Safety*, vol. 124, pp. 56–67, 2014.

[172] Villanueva, D., Haftka, R. T., and Sankar, B. V., "Including the effect of a future test and redesign in reliability calculations," *AIAA Journal*, vol. 49, no. 12, pp. 2760–2769, 2011.

[173] von Mises, R., "Mechanik der festen krper im plastisch deformablen zustand," *Nachr. Ges. Wiss. Gottingen*, vol. 1, pp. 582–592, 1913.

[174] Whitley, D., "A genetic algorithm tutorial," *Statistics and Computing*, vol. 4, no. 2, pp. 65–85, 1994.

[175] Wooseok, J., Anthony, W., Peter, G., Wei, N., Evan, P., Pavana, P., and Ravi, R., "Computational modeling of failure in composite structures including uncertainties in material and geometrical properties," 2011.

[176] Wu, C. F. J. and Hamada, M. S., *Experiments: Planning, Analysis, and Optimization*. Wiley, 2 ed., 2009.

[177] Xiao, Z., Wan, Z., and Yang, C., "Robust structural design optimization of flexible backswept wings," 12 - 15 April 2010.

[178] Yates, E. C., "Agard standard aeroelastic configurations for dynamic response," report, National Aeronautics and Space Administration, Auguts 1987.

[179] Yiming Yang, J. O. P., "A comparative study on feature selection in text categorization," in *Proceedings of the Fourteenth International Conference on Machine Learning*, pp. 412–420, Morgan Kaufmann Publishers.

[180] Zadeh, L. A., "Fuzzy sets," *Information and Control*, vol. 8, no. 3, pp. 338–353, 1965.